The Use of Twisted Nematic Displays in the Evaluation of Chirality and its Effects at the Molecular Level

Xiang Jia

PhD

University of York

Chemistry

December 2014

Abstract

The work in this thesis can be divided into three areas: chirality and structure of dopants, host dependency and investigation of reaction pathways in the search for chiral induction.

The 'reverse-twist disclination' method first reported by Raynes was used to determine the helical twisting power (HTP) of a selection of chiral materials dissolved in achiral nematic liquid crystal hosts: E7, PCH7, BL036 and ZLI559. The chiral materials studied include oxazoline and lactate derived chiral dopants, commercial liquid crystal chiral dopants and thalidomide.

One of the most notable outcomes is that the overall shape of the molecular structure of a chiral dopant dictates the magnitude of HTP values, whereby a propellar-like molecular shape consistently provides high HTP values. Additionally, the technique used was found to be very sensitive to differences in the optical purity of the dopant. Host dependency was found for all chiral dopants suggesting that HTP should not be considered as an intrinsic property of a chiral material but rather a property that results from a combination of host and dopant.

It had been reported in the literature that the Mitsunobu reaction can, for racemic secondary alcohols, give non-racemic products, a remarkable result that implies that mirror symmetry can be broken on a macroscopic scale. The effect of various different reaction conditions upon the optical purity of 1-methylheptyl esters was studied. The resulting materials were analysed *via* the reverse-twist disclination method and occasionally the Mitsunobu reaction was found to produce a product that was indeed optically active. Without exception, the Steglich reaction was only found to preserve mirror symmetry and produce non-chiral products.

Contents

List of Figures

List of Tables

Acknowledgements

Author's Declaration

The research presented in this thesis is, to the best of my knowledge, original except where due references has been made to other authors and/or co-workers.

The work contained in this thesis has not been previously submitted for award at this or any other institution.

Xiang Jia

Chapter 1.   Introduction

The background to this thesis is concerned with chirality and broken symmetries at the molecular level. In the gas phase the bulk properties are dependent on molecular structure, whereas in condensed phases there can be transmission of chiral information from one molecule to the next, which may result in chiral ensembles, for example helical macrostructures.[1] In the research presented, the transmission of information imparted from a chiral dopant to quasi-liquid phases, known as nematic liquid crystals, is investigated. The transmission takes the form of the creation of a helical structure, where the helical handedness and the pitch of the helix are related to the chemical structure of the dopant.

The basis of the majority of the experimental work in this thesis is therefore quite simple. It involves using a twisted nematic device, *i.e.* those that are used in liquid crystal displays, where the orientational directions of the liquid crystal on the upper and lower surfaces are orthogonal to one another.[2,3] For an achiral material, this gives a quarter helical structure of the nematic phase, where the left-handed and right-handed helical structures have the same energy. Disclination lines, which occur in the regions where domains of opposing handedness meet, can therefore be observed by optical microscopy.[4] However, the addition of a chiral dopant breaks the energetic degeneracy of the two helical states and causes the disclination lines to bend. In this case, the radius of curvature of the disclination line is directly related to the pitch of the helix.[5,6]

Investigation of these disclination lines allow a multitude of molecular properties to be investigated, from sensing chirality to determining enantiopurity.[6] This method also provides sensitivities on the order of milligrams of dopant per kilogram of host liquid crystal, thereby making measurements at the extremes of

enantiopurity from racemic to optically pure forms of the dopant possible. Such work may be of fundamental relevance as, for example, a method for determining spatial configuration, or of practical/commercial importance as a tool for determining the purity of pharmaceuticals.[7]

1.1 Chemical Isomers

The dopants used in this work are optically active and therefore have at least two different structural forms, or isomers.[8] The dopants used are carbon based, with multiple carbon atoms in their chemical structures. For the simple situation of a hydrocarbon with four carbon atoms, there are at least two bonded arrangements of the atoms thereby giving two isomers. Increasing the number of carbon atoms in the hydrocarbon quickly increases the number of isomers. For example, for a hydrocarbon with 30 carbon atoms there are over four billion isomers (see Figure 1.1). Some of the isomers will be chiral and, in a mixture with a nematic liquid crystal, these chiral isomers will have different influences on the nematic host.[9,10]

Isomers can be divided into two groups; *structural isomers*, which can be subdivided into *functional* and *positional isomers*, and *stereoisomers*, which can be divided into *geometric* isomers and *optical isomers*.[8] This thesis will focus on optical isomers and their properties.

Isomers

Compounds with the same molecular formulae, but differing in one or
more of their physical or chemical properties

Alkanes

C_1, C_2, C_3	1 isomer
C_4	2 isomers
C_8	18 isomers
C_{15}	4,347 isomers
C_{30}	4,111,846,763 isomers

Isomers

Structural Isomers   Stereoisomers

| Functional Group Isomers | Positional Isomers | cis/trans isomers geometrical Isomers | Optical Isomers |
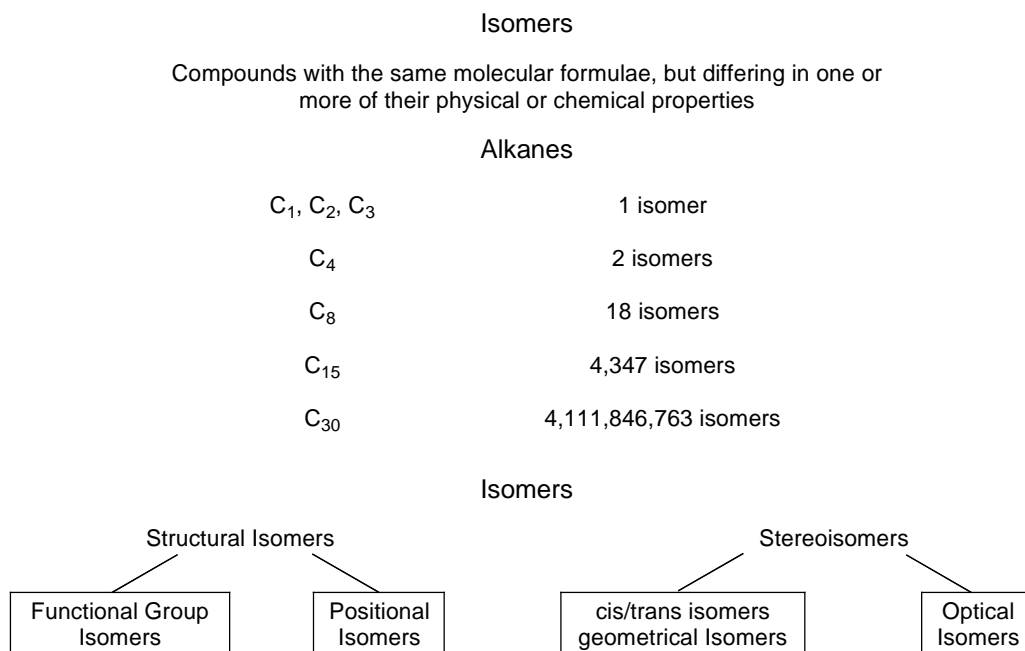
Figure 1.1: Relationship between chemical structure and isomers.

1.2 Symmetry and Molecular Structure

In order to define the shape and structure of a molecule four factors need to be considered; its constitution, configuration, chirality and conformation.[8]

• The constitution of a compound specifies the atoms that are present in a molecule, and the types of bonds used for direct interatomic bonding.

• Configuration can be described by two terms, relative and absolute. Relative configuration specifies the relative spatial arrangements of the bonds and atoms that make up the molecule, ignoring the spatial arrangements that may occur on rotation about single bonds. Absolute configuration specifies the actual spatial arrangement of atoms and bonds within a given structure.

• The conformations that a molecule may possess describe the different spatial arrangements of atoms that may arise by rotation about single bonds within the structure.

• Chirality, which will be discussed in more detail in later sections, is a property associated with three-dimensional forms that are not superimposable with respect to their mirror images.

Constitution, configuration and chirality are static properties, which specify the shape of a molecule in three-dimensional space; however, it must be remembered that the dynamics of molecular movement can have a major influence on the structure, with many conformations being possible.

1.3 Molecular Chirality

In the early nineteenth century Biot, discovered that certain biological substances cause a rotation of plane-polarized light, *i.e* they are optically active.[11] At this time the cause of such behaviour could not be defined in chemical terms because the shape, structure and physical properties of molecules themselves were not understood. Biot's discovery raised two important questions, firstly, what was the physical nature of light, which makes the phenomenon of optical activity possible, and secondly, why do some materials show this property whereas others do not?

In 1822 Fresnel put forward a transverse wave theory of light that accounted for several of the phenomena associated with plane-polarized light.[12] He showed that linearly polarized light could be resolved into two circularly polarized components that rotate in opposite directions (a right-circularly polarized and a left-circularly polarized ray), and that the direction of linear polarization rotates if the two circularly-polarized rays travel through a medium at different velocities. Fresnel suggested that the concept of optical rotation of plane-polarized light was equivalent to "circular double refraction"; a theory that forms the basis of more complex understandings of this effect. Fresnel later reasoned that certain substances are optically active due to a particular constitution of the refracting

medium or of its constituent molecules. He suggested that a helical arrangement of the molecules in a medium could present contrasting properties for opposing helical twist senses.[13] This concept was foreign to chemistry as nothing was known about the geometrical arrangement of molecules in matter, even though helices were recognised to exist in nature, *e.g.*, snail shells and whirlpools. However, in the case of quartz crystals Fresnel's idea turned out to be correct, but this shed little light on the concept of molecular optical activity (in the liquid or gaseous phases).

The first step in the understanding of optical activity in discrete molecules was taken when Pasteur discovered that for some substances, the occurrence of dissymmetric crystals was correlated with the existence of optical rotatory power in solution. His studies of sodium ammonium tartrate led to the discovery that two crystal forms occur in this material, which are mirror images of each other.[14] When the two forms were separated and dissolved in a solvent, each gave a rotation of plane polarized light, but in opposite directions. From this discovery Pasteur concluded that the similarity of the two crystal forms implied a similarity of the constituent molecules. However, the opposite rotations of plane-polarized light observed, when each form was dissolved in a solvent, indicated that the molecules were not identical, but were mirror images of each other. The constituent molecules were therefore termed asymmetric, or chiral, a term first used by Kelvin in a series of lectures at John Hopkins University.[15]

However, twenty years before Kelvin first coined the word 'chiral' van't Hoff, and Le Bel, both published papers proposing a tetrahedral arrangement of atoms bonded to carbon as the basis for molecular chirality.[16,17] They argued that such a structure would be asymmetric if the four atoms attached to carbon were different, and would be symmetric if any two were identical. This theory, although giving an exact correlation with the observed optical activity data available at the time, was

not immediately accepted, and indeed became the subject of some ridicule, with a particularly scathing attack coming from Kolbe. In this attack he stated that there was a fundamental lack of general and chemical knowledge which led to, quote *"the spread of the weed of the apparently scholarly and clever, but actually trivial and stupid, natural philosophy, which was displaced fifty years ago by exact natural science, but which is now brought forth again, out of the store-room harbouring the errors of the human mind, by pseudo scientists who try to smuggle it, like a fashionably dressed and freshly rouged prostitute, into good society, where it does not belong".*[18] However, in 1878 van't Hoff was appointed as a Professor at the University of Amsterdam, and in 1901 he received the Nobel Prize for his work on the structure of carbon containing compounds.

A greater understanding of the exact mechanism of the optical rotatory power of chiral organic molecules was now being sought by a number of scientists. The reasons why an asymmetric tetrahedral molecule should be optically active required a mathematical treatment of an extremely complex physical problem, namely the interaction of four different atoms at the corners of a tetrahedron with a beam of incident light. The theories of Born,[19] Oseen,[20] and Gray[21] suggested that the rotations of plane polarized light given by molecules that were mirror images of one another would be equal, but opposite, and that the rotation would be zero if the molecule were symmetric. The theories were based on the idea that the sum of the induced dipoles in asymmetric molecules, in the presence of circularly polarized light, were dependent on the polarization direction, and this would be the case even after these induced dipoles are averaged over all random orientations of the molecules in a liquid or a gas. This is illustrated in Figure 2 for one of the simplest optically active organic materials bromochlorofluoromethane. In Figure 1.2 the molecule is imagined to be located inside each of the circularly polarized light beams shown above it. The atoms are polarized at some instant in time by the electric field of the light wave, shown by the arrows in each beam. The arrows on

the atoms show the direction and strength of the induced dipoles associated with each individual atom (assuming C-H is zero). The total induced dipole associated with the whole molecule is different for each polarization direction (of the light wave), as shown by the calculated values that are given in units of 10^{-6} Debye, for field strength of 1 electrostatic unit.[22] The resulting difference in the refractive index of the two waves produces optical rotation.
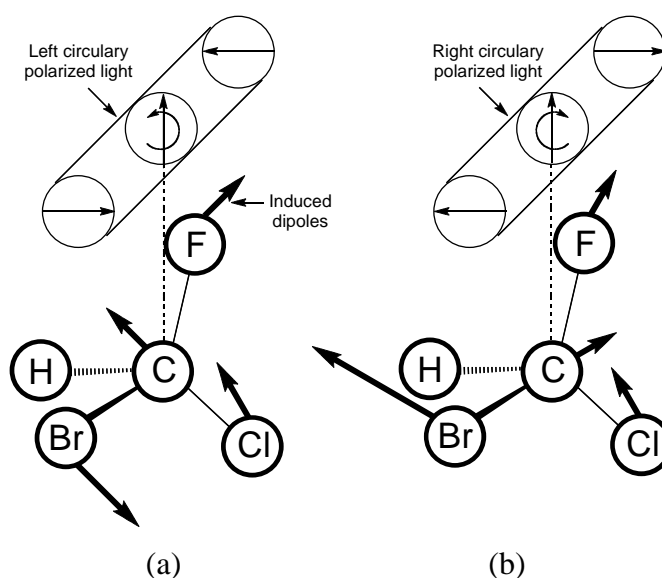
Figure 1.2: Interaction between a chiral molecule and (a) a left-hand circularly polarized light ray and (b) a right-hand circularly polarized light ray that constitute together plane polarized light. The total dipole of (a) is 5.32 and of (b) is 4.98.

An important discovery by Cotton in 1895 found that optically active compounds of tartaric acid that contained copper and chromium (which gave them colour) showed an unequal absorption of right- and left-circularly polarized light in the wavelength region where the absorption occurred.[23] This effect, which came to be known as "circular dichroism", was soon understood to arise in a similar way to the optical rotation of plane-polarized light given by some asymmetric materials. If a material is chiral, it's the amount of left- and right-circularly polarized light, which are themselves chiral, that it absorbs will be different. This difference (left-minus right-circularly polarized rays) acts as a measure of circular dichroism.[24] Due to their common origins, circular dichroism and optical rotatory power offer

7

similar information about the structure of a material. Circular dichroism, however, is concentrated more on the light absorbing entities, *i.e.* the chromophores, within a molecular structure.

The classification of molecules that are optically active needs a number of terms. Firstly, any molecule that possesses a tetrahedral carbon atom with four different groups attached to it is said to be *asymmetric*, or *chiral* in nature, and the atom at the centre is the location of the *stereogenic centre*.[8] The two-mirror image forms that may exist are known as *enantiomers*, with each one giving an equal, but opposite rotation of plane-polarized light. A 50-50 % mixture of the two enantiomers is known as a racemic mixture and is optically inactive. However, if one enantiomer is in excess, known as the *enantiomeric excess* or *ee* (more details in section 1.4), then the mixture will be optically active. Each enantiomer is usually labelled according to the absolute configuration of its stereogenic centre. The labelling system most commonly used was first introduced by Cahn, Ingold, and Prelog in the 1950's.[25,26] The system operates by first prioritising each atom (or group) that is attached to the asymmetric carbon atom in terms of atomic number (called the *priority rule*). The tetrahedron is then viewed with the lowest priority group (or atom) set to the rear. A path is then traced between the remaining three groups (or atoms) from the highest to the lowest priority (called the *sequence rule*). If a clockwise direction is transcribed then the stereogenic centre is classified as *Rectus* or Right (R). If, however, an anticlockwise path is taken then the chiral centre is classified as being *Sinister* or Left (S), see Figure 1.3.

Absolute Spatial Configuration - R and S
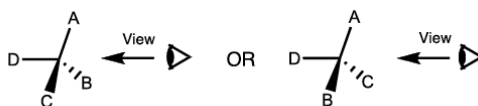
View stereogenic (chiral) centre and place the lowest priority group, in this case, D, to the rear.

Conversion Rule

The groups A, B, C, D are arranged in ascending atomic number (1 to 4) with the group of the lowest value pointing back into the plane of the page. The priority count will then be either clockwise, *rectus*, or anticlockwise, *sinister*, when viewed from the opposite side to D.
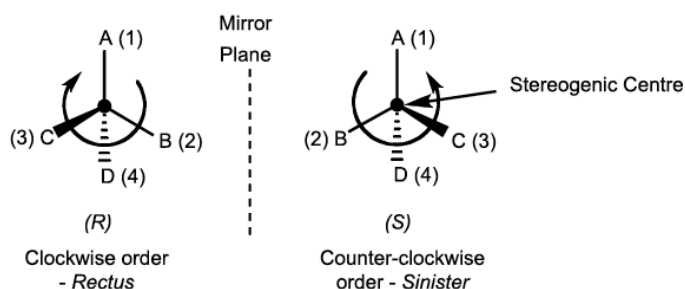
(a)
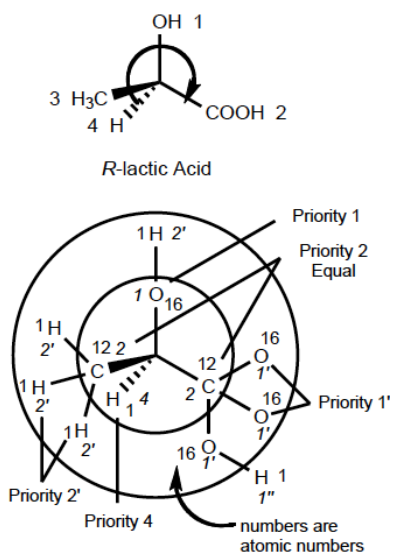
Group Priority: An ordering of functional groups based on their atomic number (heaviest isotope first:

$I > Br > Cl > SO_2R > SOR > SR > SH > F > OCOR > OR > OH > NO_2 > NO > NHCOR > NR_2 > NHR > NH_2 > CX_3$ (X = halogen) $> COX > CO_2R > CO_2H > CONH_2 > COR > CR_2OH > CH(OH)R > CH_2OH > C≡CR > C≡CH > C(R)=CR_2 > C_6H_5 > CH_2 > CR_3 > CHR_2 > CH_2R > CH_3 > D > H >$ electron pair.
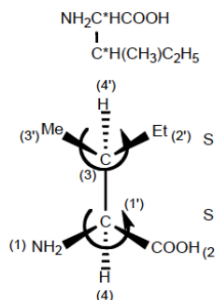
(b)

Figure 1.3: The Cahn, Ingold, and Prelog labelling system for stereogenic centres. (a) The priority and sequence rules, (b) examples the rules applied to *R*-lactic acid and 2*S*, 3*S*-isolucine.[25,26]

The directions of rotation of plane-polarized light given by either enantiomer is classified as being either positive (+) in the case of a clockwise rotation, or negative (⁻) in the case of an anticlockwise rotation. No obvious correlation,

however, exists between the configurations of enantiomers, or between the (R) and (S) designation and the direction of rotation.[27]

If a molecule has two or more chiral centres, then the material may be diastereomeric. This is illustrated in Figure 1.4, giving aldotetrose as an example.
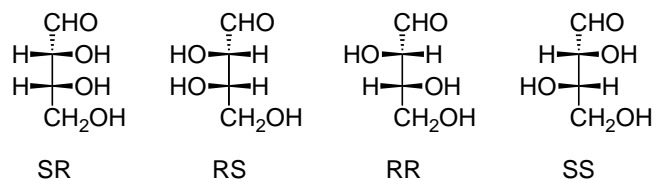
Figure 1.4: Diastereoisomers of aldotetrose.

A molecule which has two asymmetric centres that have an (R,S) configuration, *i.e.*, one chiral centre is labelled as (S), whereas the other is (R), is the diastereoisomer of a molecule that has an (R,R) configuration. Similarly, a molecule with an (S,S) configuration is the diastereoisomer of a molecule with an (R,S) configuration. A molecule with an (R,S) configuration, however, is the enantiomer of another with an (S,R) configuration, this relationship is also true for molecules with (S,S) and (R,R) configurations. Classical theory dictates that the physical properties of enantiomers are the same, whereas those of diastereoisomers may differ.[8]

Molecules that have mirror symmetry and contain two identical, but oppositely labelled stereogenic centres are non-chiral. They are termed *meso* compounds. They possess an additional plane of symmetry and are found to be optically inactive. An example of a *meso* compound (*meso*-2,3-dibromobutane) is illustrated in Figure 1.5.

stereogenic centres   *meso*-form

Mirror Plane - therefore Achiral
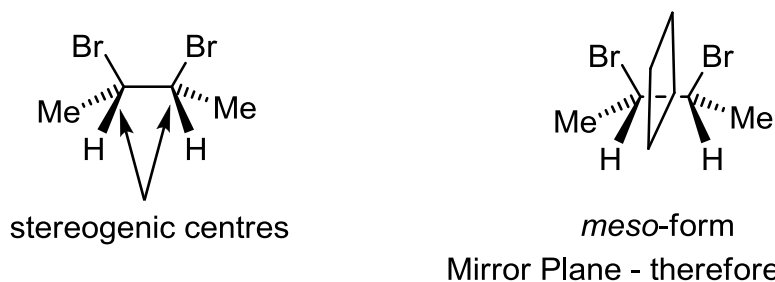
Figure 1.5: Structure of a meso-compound (meso-2,3-dibromobutane) showing the mirror plane.

Another interesting situation arises when a molecule that does not possess an asymmetric carbon atom is optically active. An example of this is helicene, which is optically active because it does not have a mirror plane as a consequence of its helical structure (the rings are twisted out of plane giving rise to a left- or right-handed helical structure). The structure of helicene is illustrated in Figure 1.6.[28]

Helicene has an extra symmetry element in comparison to an asymmetric carbon atom, a simple two-fold axis of rotation, and so is considered as dissymmetric and not asymmetric. Thus, the maximum symmetry element allowable for chirality is a rotational axis; if, however, mirror symmetry is introduced then the system becomes achiral. In fact, a more general way to classify chirality in relation to symmetry elements can be made; a molecule can only be chiral if it lacks an axis of improper rotation (S_n), *i.e.* an axis that leaves a given object unchanged upon rotation about an followed by reflection in a plane perpendicular to the axis of rotation.[1] Therefore, a chiral molecule or object obviously cannot possess a mirror plane or a centre of inversion, but can exhibit rotational symmetry (a C_n axis) as in the case of helicene.[1,8,27,28]

11
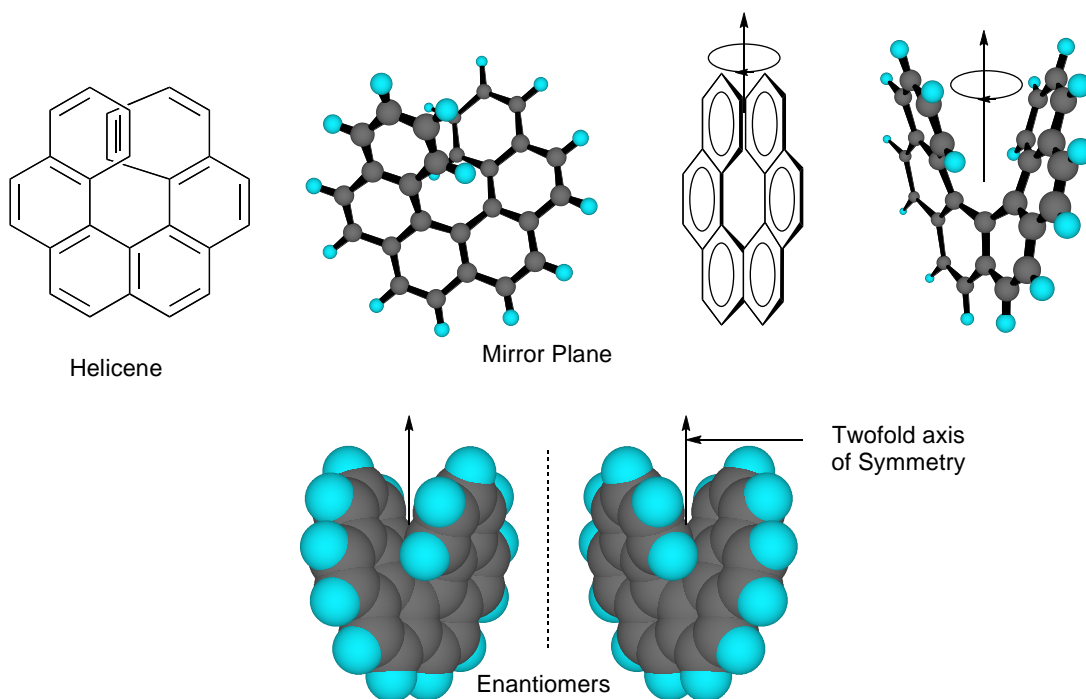
Figure 1.6: Helicene, a chiral dissymmetric molecule, with a two-fold axis of rotation.[28]

There are a number of symmetry operations involving structures with stereogenic centres and which may or may not exhibit optical activity. Figure 1.7 shows a number of compounds based on a cyclobutane scaffold that are attached to the 2-position of butyl aliphatic chains. The 2-butyl chains are chiral and thus the symmetry operations for the various susbtitutions of the cyclobutane motif can be explored as show in the figure 1.7. Achiral, and hence non-optically active compounds are obtained where there is a mirror plane, a centre of inversion, or an improper axis of rotation, as shown in the upper part of the figure. However, as with helicene, materials that have simple axes of rotation, such as two-fold axes are chiral. This type of study allows for the analysis of symmetry operations that produce chiral compounds and those that do not as shown in Table 1.1.[1,8,27]
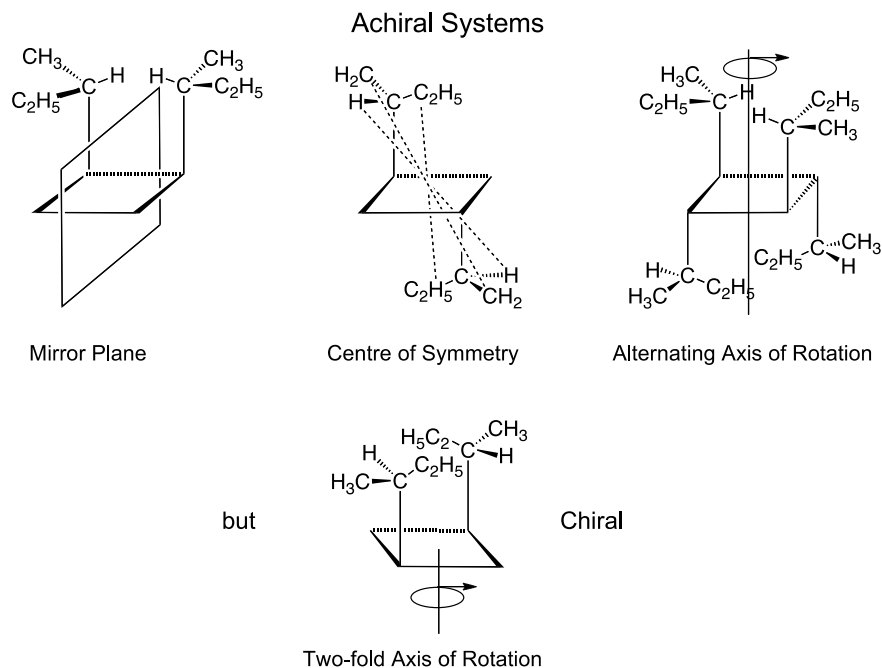
Figure 1.7: Using similar molecular constitutions, symmetry operations are shown to affect the formation of chiral or achiral compounds.

Term	Improper Rotational Axis	Rotational Axis	Optical Activity
Symmetric	Present	May or may not be present	Inactive
Dissymmetric	Absent	May or may not be present	Usually active
Asymmetric	Absent	Absent	Usually active

Table 1.1: Symmetry operations in relation to the formation of symmetric, dissymmetric and asymmetric materials.[1,8,27].

At this stage it should be mentioned that carbon is not the only atom that can be a stereogenic centre. Silicon and germanium, from the same group in the periodic table, also form tetrahedral compounds and therefore have the ability to display optical activity,[29] see Figure 1.8. In certain instances a chiral nitrogen or sulphur atom may also be used, with a lone pair of electrons taking the place of an atom or group in the asymmetric structure.[30]

13
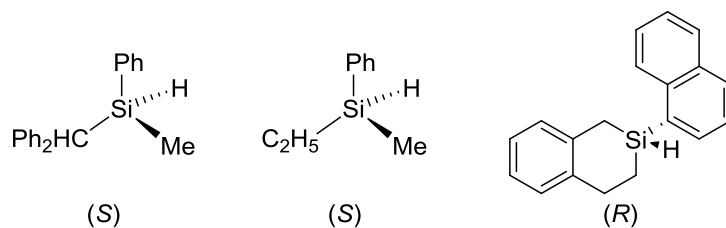
Single enantiomers of a small number of organosilica compounds, with a silica atom at the stereogenic center have been isolated.
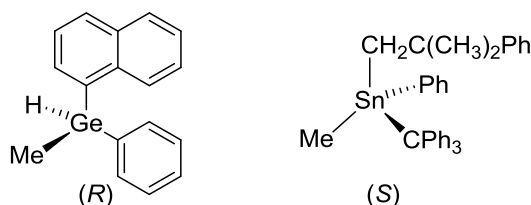
Tetraorganotin compounds with a stereogenic geranium and tin atom have been obtained as single enantiomers by resolution, asymmetric synthesis, or for the materials shown above, by chiral chromatographic separation of enantiomers on cellulose acetate.

Figure 1.8: Optically active materials with asymmetric atoms, which are not carbon.[28]

1.4 Chirality and Enantiomeric Excess

In this discussion it has so far been presumed that the molecules in each example are of one hand, *i.e.* they are defined as right-handed (*R*) or left-handed (*S*) by application of Cahn, Ingold, Prelog rules.[25,26] However, this is often not the case and the majority of chiral materials are composed of a unequal mixture of left-handed and right-handed molecules (enantiomers). The proportion of left-handed to right-handed enantiomers in a given mixture is called the enantiomeric excess (*ee*). The percentage enantiomeric excess is be defined in equation (1).[8,31]

$$\% \ ee = \frac{\text{no. of moles of enantiomer A} - \text{no. of moles of enantiomer B}}{\text{no. of moles of both enantiomers}} \quad (1)$$

For materials that possess one chiral centre with spatial configuration (*R*) or (*S*) the enantiomeric excess is given by equation (2):

$$ee = \frac{[R] - [S]}{[R] + [S]} \times 100 \quad \text{or} \quad \frac{[S] - [R]}{[R] + [S]} \times 100 \quad (2)$$

The optical purity (OP) can therefore be calculated in accordance with equation (3):

OP = 100*(specific rotation of sample)/(specific rotation of pure enantiomer)(3)

Experimental measurements of enantiopurity can be achieved using NMR with chiral shift reagents,[32] chiral gas chromatography, chiral high pressure liquid chromatography, or polarimetry. However, these methods are not generally applicable to all varieties of materials and their accuracies are often no better than +/- 2%.

Probably the most common way of determining the optical purity, and hence the enantiomeric excess, is through the use of polarimetry. This technique involves passing monochromatic plane polarized light, usually produced by a sodium lamp, through a cylinder, 10 cm long, of a mixture of a specimen material in a suitable solvent. The plane of the polarized light is rotated through an angle α, which is determined *via* the rotation of a polarizer (analyzer) at the exit port of the cell, as shown in Figure 1.9. The optical rotation α is standardised by the concentration, the length of the tube, the wavelength of the light, and the temperature at which the measurement is conducted. This gives the specific rotation, which is a standard for any particular chiral material.

However, what is not often realised is that specific rotations for various materials are not actually 100% *ee*, simply because it is too difficult to obtain materials with

absolute optical purity. Thus, optical purity values given for commercial products are often not very accurate or useful.[7,31]
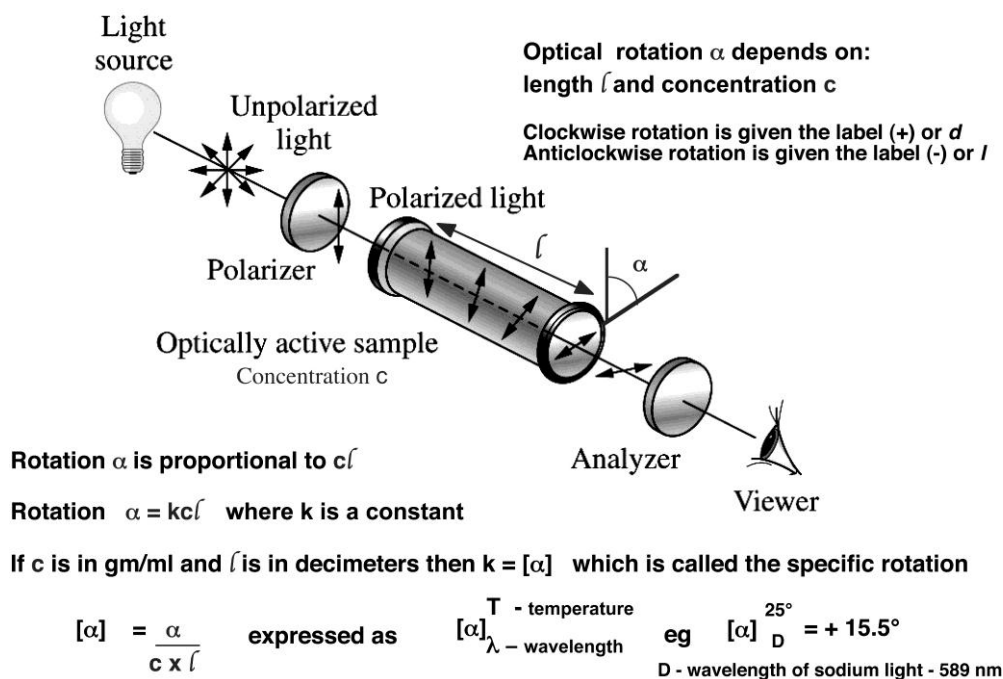
Figure 1.9: The structure of a polarimeter and the relations between the optical rotation and the specific rotation.[28]

1.5 Chirality in Anisotropic Soft Materials

The types of molecules that form calamitic liquid-crystalline phases usually possess an extended rod-like structure.[33-35] Chirality can be built into the mesogenic system by the inclusion of an asymmetric carbon atom. This functionality may be incorporated into any part of the molecule, but because of synthetic considerations it is most often placed in either one, or both of the terminal aliphatic chains that are often part of the molecular structure.[36] The effects of chirality in mesogenic systems will be discussed in greater detail later in this Section. However, the properties that occur as a result of chirality can be quantified in terms of the pitch length of optically active phases, the thermal stability of liquid-crystalline phases that are known to depend on a high degree of molecular chirality for their existence, *e.g.*, blue phases[37] and Twist Grain

16

Boundary phases,[38-41] and the value of the spontaneous polarization in ferroelectric phases.[42]

In order to induce a high level of chirality into the system the enantiomeric excess (*ee*) must be high, that is to say that the minority enantiomer must be present only in very small amounts. This can be accomplished using synthetic routes and reagents to specifically achieve this purpose, or by utilising biological materials with high optical purity. The position of the stereogenic centre within the molecular structure in relation to the core of the mesogen also has a major effect on the degree of chirality induced into the system, as do the substituents located at the stereogenic centre itself.[1,27]

For example, the dipoles associated with, and the size and steric shape of the substituents located at the stereogenic centre, can have huge effects on the chirality of the system.[27,42] In some cases, a large resultant dipole can enhance the HTP, as can a bulky group associated with the stereogenic centre.[43] The second effect is thought to be due to a restriction in rotational freedom of the stereogenic centre about the long axis.[44] Thereby increasing polarity and steric interactive effects. This effect can also be observed if the chiral group is placed very close to the core structure, or in some instances when lateral substituents located at the core structure are extended in length. In at least one example the linking group associated with the chiral moiety was selected so that it would hydrogen bond with a lateral group attached to the core, thereby reducing the rotational freedom of the chiral centre completely (see Figure 1.10).[45]
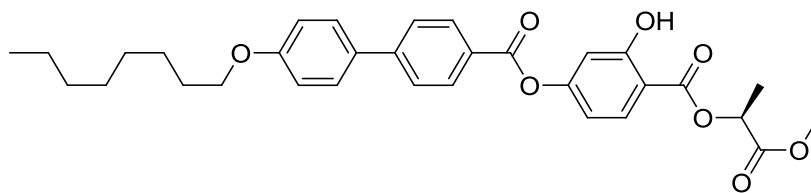
Figure 1.10: Rotationally trapped stereogenic centre in a typical rod-like chiral mesogen.[45]

Rotational freedom can also be reduced by extending the terminal aliphatic chain on the peripheral side of the stereogenic centre, although it must be remembered that this may also cause a dilution effect (for example, on the spontaneous polarization of a SmC* phase, see Section 1.9) as well.[46] These points are summarised in Figure 1.11.
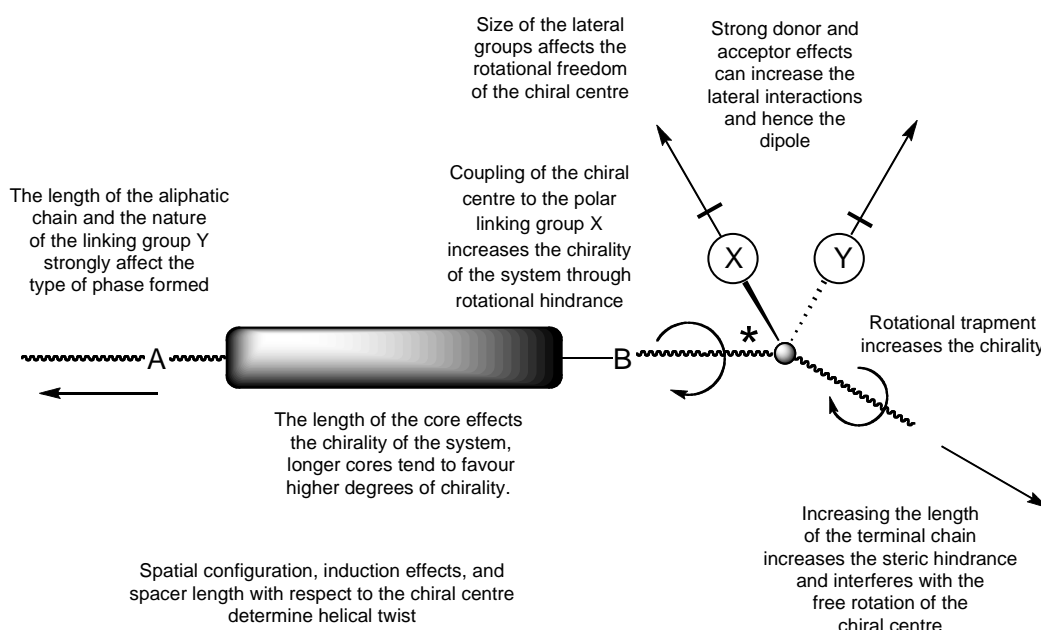
Figure 1.11: Chirality in rod-shaped molecules of calamitic liquid crystals. Figure reproduced, with permission of the author, from reference 47.

1.6 Anisotropic Phases

1.6.1   The Nematic Phase

The nematic phase is the least ordered of the commonly observed mesophases and can be described as a one-dimensional elastic fluid.[35] The molecules are not positionally ordered but as they diffuse throughout the sample the long axes of the rod-shaped molecules tend to align statistically parallel to a preferred direction, known as the director, $\hat{n}$ (see figure 1.12).[48,49]   In the bulk nematic phase there are as many molecules pointing in one direction relative to the director as there are in the opposite direction, the phase therefore has rotational and mirror symmetry relative to $\hat{n}$, and the directions $\hat{n}$ and $-\hat{n}$ are equivalent.[1,50]

The degree to which the long axes of the molecules within the nematic phase are aligned with the director, averaged over time and space, is given by equation (4).

$$S = 1/2 \langle 3\cos^2 \theta - 1 \rangle \quad (4)$$
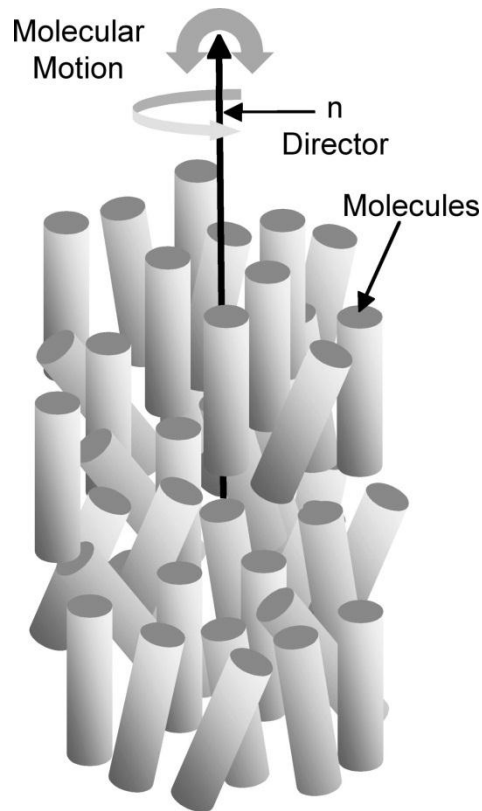
Figure 1.12: A diagrammatic representation of the nematic phase.

In equation (4) θ is the angle between the long axis of an individual molecule and the director, and the angular brackets indicate that an average value of a large number of molecules has been calculated.[51] If all the long molecular axes of the molecules are perfectly aligned along the director then $S = 1$, and if there is no orientational order (isotropic liquid), then $S = 0$. The value of the order parameter for nematic phases is typically between 0.4 and 0.7.

1.6.2 The Chiral Nematic Phase

In the chiral nematic phase the local ordering of the constituent molecules is similar to that of the nematic phase, and the molecules still align their long molecular axes statistically parallel to the director, however, the molecular chirality causes a gradual rotation of the director throughout the bulk phase which

gives rise to a helical macrostructure (see Figure 1.13).[1,27] The helical axis is at a right angle to the orientation of the molecules and the local director, and the distance in which the director rotates through 360° is defined as the pitch length, p. However, since as the directions $\hat{n}$ and $-\hat{n}$ are equivalent the helical structure of the chiral nematic phase repeats every 180°, and the periodicity of the structure corresponds to p/2. The director can rotate to form a left- or right-handed helix and as in the nematic phase there is no positional ordering of the molecules.

Helical Axis

Spiraling
Orientational
Ordering of
Molecules

Molecules

Half Pitch
Length
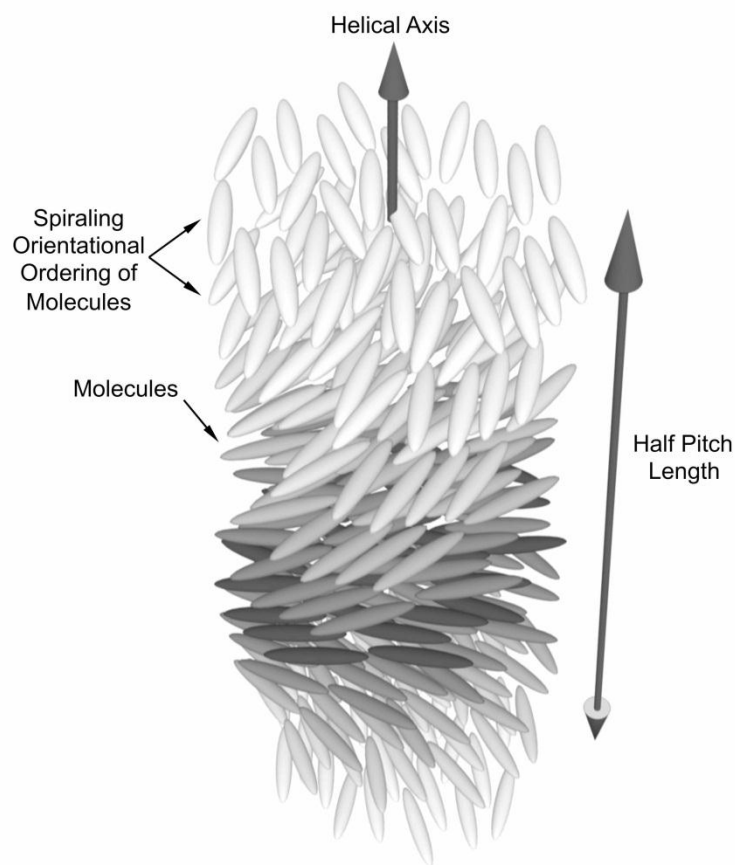
Figure 1.13: A diagrammatic representation of the chiral nematic phase.[1]

The pitch length of the helix is temperature dependent, and it usually decreases with increasing temperature and varies from about 0.1×10^{-6} m to almost infinity.[27] The displacement angle is the angle between the directors of adjacent molecules along the helical axis, and as the mesophase is heated the displacement angle

widens as the molecules have more thermal energy, and consequently the pitch length shortens. As the mesophase is cooled the displacement angle narrows and this lengthens the pitch of the helix, and as the transition to a smectic A* phase is approached the pitch rapidly unwinds and becomes almost infinite in length.[52] However, exceptions do occur and the pitch length of the chiral nematic phase of cholesteryl-2-(2-ethoxyethoxy)ethyl carbonate has been shown to *increase* with increasing temperature.[53]
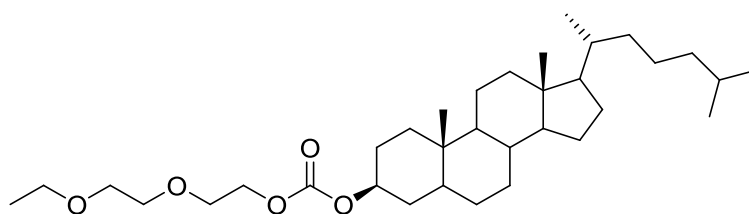
Figure 1.14: The structure of cholesteryl ethyl carbonate.[53]

The chiral nematic phase is often referred to as the cholesteric phase for historical reasons, as the first compounds known to possess this phase were derivatives of cholesterol, and it was once thought that this mesophase was different to the nematic phase. However, other steroids and many non-steroidal chiral compounds also exhibit the chiral nematic phase, and Saeva[54] showed that the addition of a chiral dopant to a nematic material leads to the formation of the chiral nematic phase. Leclerq *et al.*[55] have shown that a racemic mixture of (−)- and (+)-4'-(2-methylhexyl)biphenyl-4-carboxylic acid exhibits the nematic phase, whereas optically active mixtures exhibit chiral nematic phases, and as the excess of one of the enantiomers is further increased there is a continuous enhancement of the optical properties which characterise the chiral nematic phase. It therefore seems more reasonable to name the phase the chiral nematic phase, as it is now known that it is the chiral version of the nematic phase.

1.7 Determination of Helical Pitch Length

The helical pitch length of a chiral liquid crystal, provided it is in the micron regime, can be determined as a function of temperature by measuring the distance between dechiralisation lines in the polarizing microscope using a microfurnace to control the temperature.[56] In this situation is important to remember observed optical repeat distance is half the pitch length for a chiral nematic phase, but either half or the full pitch for a chiral smectic phase depending on the surface alignment treatment used and the direction of the alignment buffing.[57]

However, the most common way of determining the pitch length and hence the helical twisting power of a chiral material, be it liquid-crystalline or not, is to dissolve the material in a suitable liquid crystal host, and determine the pitch as a function of temperature and concentration using the Grandjean-Cano Wedge method.[58] Typically such studies are done at room temperature so that comparisons can be made between materials.

The definition of the helical twisting power (HTP) β is given by the equation (5):

$$\beta = 1/P*C*ee \qquad\qquad (5)$$

where c_w is the weight concentration of chiral dopant and r defines its enantiopurity, ee. Depending on the material concerned, the sign of β_M can be either positive (right-handed helix) or negative (left-handed helix). Two pure enantiomers of the same material should have the same magnitude of β_M, but opposite signs.[4,5,59]

23

1.7.1 The Grandjean-Cano Wedge Method of Determining Helical Pitch

In the chiral nematic phase the adjacent molecules have a very small tendency to twist with respect to one another as they pack side by side.[60] This packing cannot be satisfied over all space, and so the system becomes frustrated, with the consequence that defects are formed.

In the chiral nematic phase the formation of the helix can only be satisfied in one direction, and because the pitch is often quite small it cannot be easily evaluated by microscopy, unless as stated above, the helix lies parallel to the specimen substrate and is greater than about approximately a micron in length.

In order to measure pitch lengths over a wider length scale the Grandjean-Cano Wedge was developed.[58] In this method the chiral nematic liquid crystal is placed in the gap between two glass surfaces which are pinned along one edge and have a spacer of known thickness at the other edge, thereby giving a wedge opening between the glass pieces of a few degrees (α), see Figure 1.15, for an empty cell.
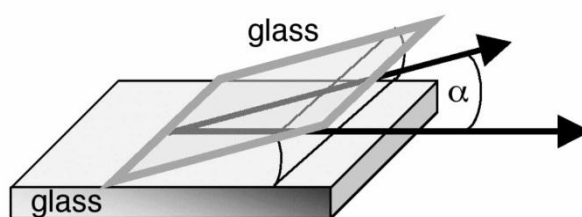
Figure 1.15: Unfilled Grandjean-Cano Wedge where the angle α is only a few degrees in size.

The surfaces of the glass have to be coated to give a planar arrangement of the molecules. Usually a rubbed polymer of nylon is used to give such an alignment so that the phase forms a helical macrostructure perpendicular to the glass.

The material to be investigated is then dissolved in an achiral liquid crystal host. Typically materials that exhibit a nematic phase at room temperature, such as E7, are used as the host. The weight percentage, and hence the molar proportion, is measured, and the mixture is inserted into the wedge cell. Disclination lines are formed between the regions of half a twist, a full twist, one and a half twist *etc.* as shown in the cell in Figure 1.16, and in a photomicrograph in Figure 1.17. The distance between the disclination lines, d, is measured, and the distance multiplied by tanα gives an integer multiplied by the half pitch length, p.

$$2d \tan \alpha = p \qquad (6)$$
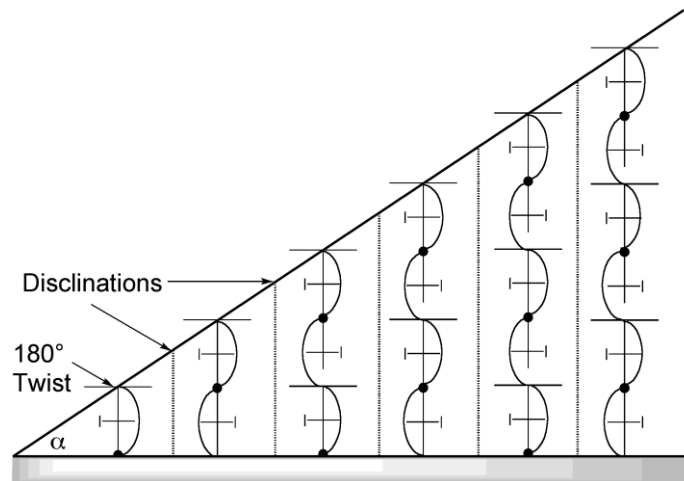
Figure 1.16: The Grandjean-Cano Wedge showing the disclination lines and multiples of the half-pitch perpendicular to the aligning surface.
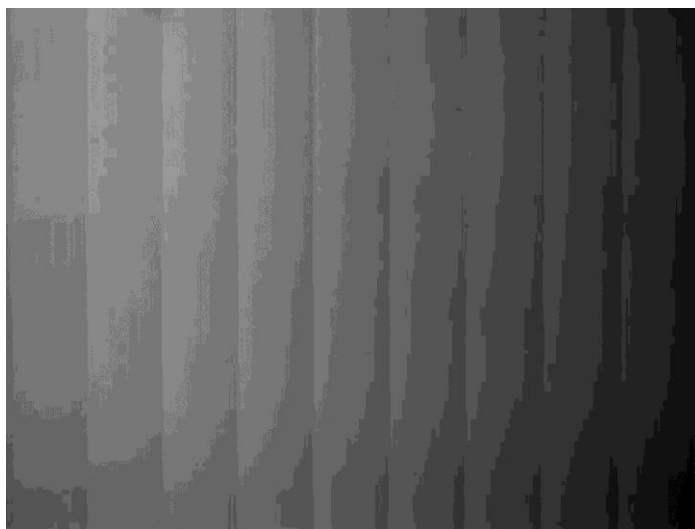
Figure 1.17: Dechiralisation lines formed in a Grandjean-Cano Wedge for a nematic phase (x100).

It should be noted, however, that although the Grandjean-Cano wedge is an effective method for the measurement of a range of pitch lengths, it is impractical to use this method to measure long pitch lengths (>1 mm). For instance, in a Cano wedge cell with an opening angle of 15°, if the pitch length is 1 mm, then the measurement would require at least 10 kg of nematic host and the Grandjean-Cano wedge would need to be approximately 20 m^{2}.[4,61]

1.7.2 The TN-Polarimeter

A new technique for the accurate measurement of very long pitches of chiral nematic liquid crystals has been reported recently, which employs the use of twisted nematic cells found in watch displays.[4,5,61] Accurately constructed twisted nematic (TN) cells are readily available from LCD device manufacturers, and the ones used in the study were obtained from Merck. TN cells are generally constructed from ITO coated glass where the inner surfaces of the cells are coated with polyimide, which is unidirectionally buffed.[2,3] The inner buffed surfaces are arranged so that the buffed directions are perpendicular to one another and, crucially, particles to control the cell spacing are also included prior to assembly.

When an achiral liquid crystal mixture is introduced into the cell the nematic phase spontaneously forms a quarter-helix on passing from one surface to the other, as shown in Figure 1.18. In this arrangement the plane of plane polarized light is rotated through 90 ° when it traverses the helical structure.[2,62] As noted previously, for the 90 ° orientation of the two glass surfaces, two degenerate helical domains, associated with left- and right-handed quarter helices, are formed. The two domains are separated by disclination line defects, which can be observed by transmitted polarized-light optical microscopy, as shown in Figure 1.18.
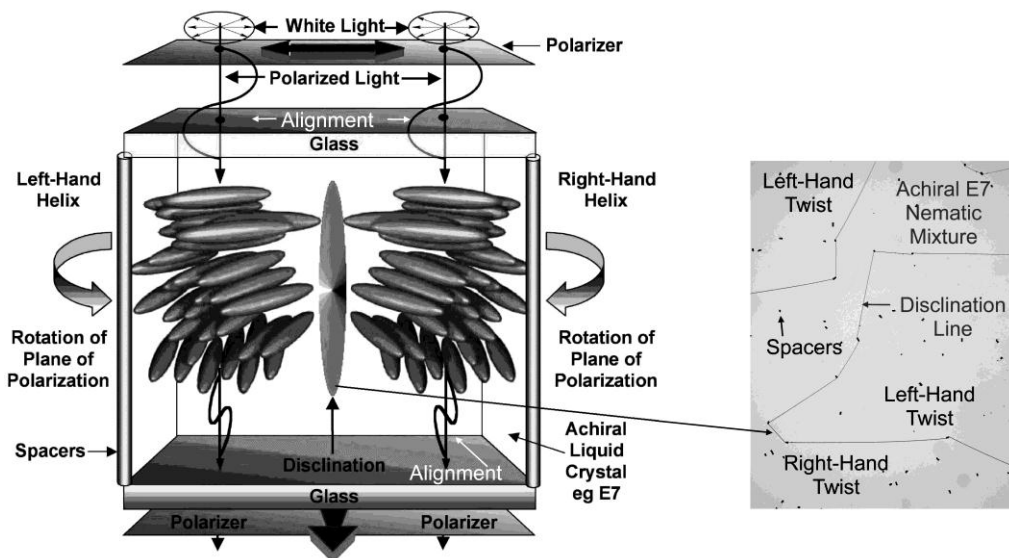
Figure 1.18: A TN device filled with an achiral liquid crystal showing degenerate twists to the left and the right separated by disclination lines (left). A photomicrograph (right) of the cell showing the disclination lines and polystyrene spacers (x100).[6]

If an achiral mixture of a target dopant, such as 4′-(2-methylbutyl)-4-cyanobiphenyl (racemic CB15), solvated in a commercial liquid crystal mixture, for example E7, is placed into a conventional twisted nematic cell, then twist domains of opposite handedness are formed. However, if the dopant is chiral, e.g., commercially available *S*-4′-(2-methylbutyl)-4-cyanobiphenyl (CB15, Merck), one domain will predominate, see Figure 1.19 (bottom right).[4,5]

If the twisted nematic cell is heated so that the mixture forms a liquid, and is then cooled back into the nematic phase, then disclination lines will form rapidly. As the mixture is cooled to room temperature the domains for the achiral dopant will stabilise and become pinned by the spacers in the cell which are used to maintain the distance of the cell-gap, whereas those for a chiral mixture will rapidly coalesce and disappear, see Figure 1.19 as a whole. Furthermore, although not discussed here, the rate that the disclinations disappear is also related to the concentration, HTP and enantiomeric excess of the dopant.[63]
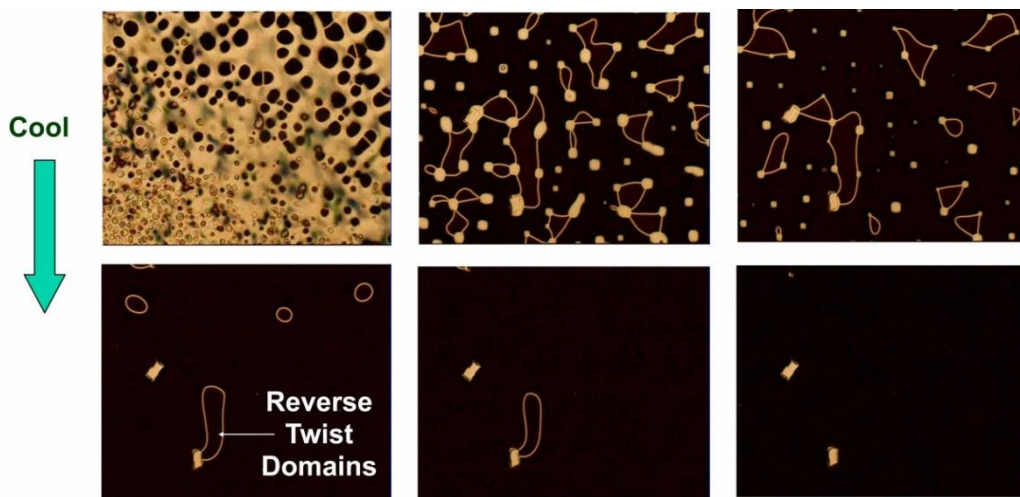
Figure 1.19: The formation of disclination loops pinned to the spacers produced when a doped chiral nematic phase forms on cooling from the isotropic liquid (x100).

For smaller concentrations, HTP or enantiomeric excess of the dopant, the chirality is too weak to induce a single domain. However although it is weak, the chirality is still strong enough to induce a slight energy imbalance between the two domains, resulting in a bowing of the disclination lines, see Figure 1.20. Equating the energy imbalance of the two domains with the energy per unit length of the disclination results in a simple relationship between the pitch P of the chiral nematic liquid crystal and the radius of curvature of the line R:[4,5,61]

$$P = 2R \qquad (6)$$

28
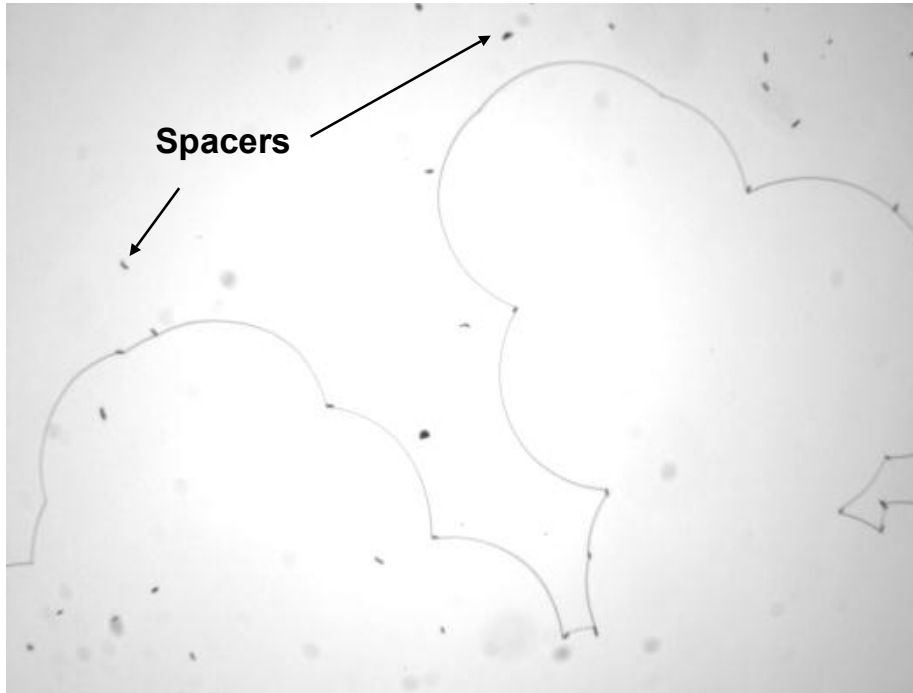
Figure 1.20: Curved disclination lines for a doped chiral nematic phase of weak HTP or low dopant concentrations (x100).

Using this method it is possible to measure pitch lengths in excess of 10 mm, corresponding to less than 0.001 wt% of a nominally optically pure chiral dopant. Moreover, only a small amount of the host/dopant mixture ($\approx$ 5 mg), which corresponds to 5 x 10^{-5} mg of the dopant, is required to fill the cell, *i.e.* orders of magnitude less than required by conventional, and less sensitive, methods.

1.8 Types of Materials used in Pitch Measurements

1.8.1   Nematic Hosts

Since the discovery of liquid crystals a wide variety of materials have been synthesised and characterised, many of these for potential use in display devices.[64,65] Nematic liquid crystals are the most important type of materials for displays, and in order to be useful they must possess certain values of a variety of physical properties including viscosity, dielectric anisotropy and the temperature

range of the nematic phase.[65] Nematic hosts can be either a single component system or, more commonly, possess multiple components. Formulation of mixtures allows physical properties to be tuned to fit device specifications, such as wide nematic phase range or low threshold voltage.[66] A typical single component nematic host that has been used in experiments designed to measure the chiral induction properties of dopant materials is PCH7, which is a 4-cyanophenylcyclohexane-based liquid crystal, with the structure shown in Figure 1.21.[67]

For a target material that has a high helical twisting power, or has a high enantiomeric excess, quantitative measurements of the *ee* can be made at low concentrations of the target in the host liquid crystal using the standardised value of the HTP of the nominally optically pure chiral material and measurement of the pitch. Similarly, quantitative measurements of targets of low optical purity can also be achieved by the same method.
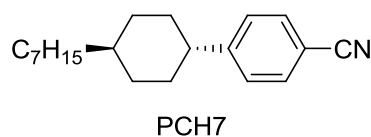
<center>PCH7</center>

Figure 1.21: Chemical structure of 4'-pentylcyclohexyl-4-cyanobenzene, PCH7, Phase transitions: Cryst 30 N 60 °C Iso Liq.[67]

In the case of multiple components nematic host, E7 has been employed as the host in the measurement of the properties of dopant/host mixtures. The eutectic mixture E7, which was designed by E. P. Raynes, was the first commercially useful nematic host mixture.[68] It has a wider nematic temperature range in comparison to PCH7.[67] This is because it is the eutectic mixture of four components, three of them are based on biphenyl liquid crystal, while the fourth one is based on terphenyl liquid crystal (5CT), as shown in Figure 1.22.[69]
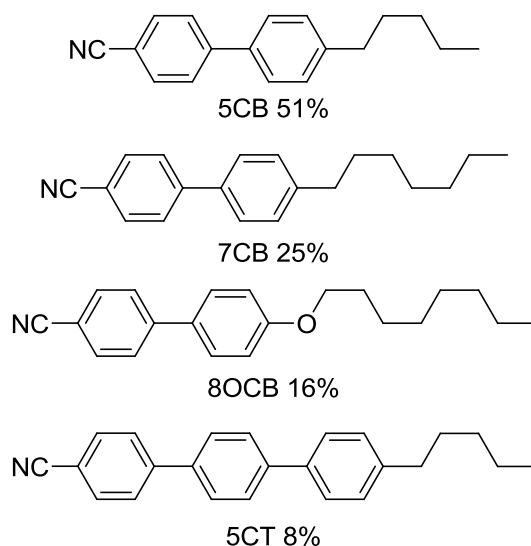
Figure 1.22: The Chemical structures of E7, Phase transitions: Cryst -10 N 60 °C Iso Liq.[69]

Of course, E7 and PCH7 are just two examples of nematic liquid-crystalline hosts and in practice many different host systems can, and have, been used in experiments designed to measure the chiral induction properties of a given dopant material. However, for practical reasons, materials that exhibit a room-temperature nematic phase are commonly used.

1.8.2   Dopant Types

As noted previously, when a guest chiral material, called the dopant, is introduced into a nematic host, the interaction between the dopant and nematic host results in a phenomena called the helical twist.[70] The strength of this effect induced by the dopant in the nematic host is expressed as the helical twisting power, given in equation (7):

$$\beta = 1/ P_{Cee} \qquad (7)$$

where β is helical twisting power the unit is μm^{-1}, P is the helical pitch length in microns (μm), C is the concentration of the dopant (percentage by weight), and *ee* is the enantiomeric excess (optical purity) of the dopant.

Through this equation, the helical twisting power is related to the pitch length, concentration and the optical purity of the dopant. As the concentration is an inherent property of the dopant itself, the pitch length and the enantiomeric excess are the only parameters that can be explored experimentally.

As noted previously, there are many methods for measuring the pitch length of helical liquid crystals, the most common method being the Grandjean-Cano technique.[5] The shortcomings for this method are that it requires a relatively large amount of material and it does not work particularly well when the pitch length is shorter than 100 μm or longer than 1mm.[61] However, using the approach of Raynes,[4,5,61] pitch lengths from about 100 μm to 2000 μm can be measured, and a much smaller quantity of the dopant is required. For instance, when measuring a high helical twisting power dopant it only requires 10^{-3} mg of the dopant, whereas several mg are required for testing a lower helical twisting power dopant. In addition, in order to fill a TN cell, approximate 5-10 mg of the nematic host is required, whereas at least 200 mg of the dopant is needed using the Grandjean-Cano technique. The difference in the required amount of substance for the measurement of the pitch stems from two factors. Firstly, the reverse twist disclination line method is extremely sensitive as even a small bowing of this disclination lines can easily be detected. Conversely, with a Cano wedge cell, as the pitch of the helix becomes longer, the distance between dechiralization lines increases and hence for very long pitch lengths the physical dimensions of the Cano wedge cell prohibit measurement of the pitch. Secondly, a small amount of material is required in order to fill a TN cell in comparison with that required to fill

a typical Cano wedge cell and, hence, the reverse twist disclination line method requires less of a given mixture and therefore less of the chiral dopant is required.

In terms of molecular structure, there is often no obvious relationship between an enantiomer itself and the helical twisting power. However, a detailed examination of chiral nematics that have only one chiral centre, as exemplified by the typical homologous series shown in Figure 1.23, reveals that the molecular structure is an important factor in determining the handedness of the helical structure of the phase.[1,71] Generally, as the atom count (n) by which the chiral centre is removed from the core it changes parity from odd (o) to even (e), and as a consequence the handedness of the helix also alternates from left to right or *vice versa*. Similarly, if the absolute spatial configuration of the stereogenic centre is inverted, *i.e.* from (R) to (S), the handedness of the helix also inverts. Therefore, the twist sense of the helix is dependent on both the absolute spatial configuration (R) or (S), and the position of the chiral centre within the structure of the compound relative to the rigid central core.

Gray and McDonnell[71] stated that the relationship between molecular structure and the handedness of the helical structure of the chiral nematic phase often conforms to the following rules: Sol Sed, Rod Rel, where (S) or (R) is the absolute spatial configuration of the chiral centre, e or o is the odd or even parity for the atom count which the chiral centre is removed from the core, and d or l describes the handedness of the helical structure. Figure 1.23 shows, with the aid of a space-filling molecular model, the effect of chain parity on the spatial positioning of the chiral centre. It was observed that as the aliphatic chain is extended between the chiral unit and the core, the substituent at the stereogenic centre moves back and forth with changing parity in this series. This strong dependence of the helical twist sense upon the structure of the mesogen strongly suggests that the helical twist sense is related in some way to the packing of the molecules in the chiral

nematic phase. Furthermore, it indicates that chiral information is transferred and amplified from the level of a single molecule to the macroscopic helical structure *i.e.* through many thousands of molecules. The Gray and McDonnell rules work very well for simple compounds that only have a single chiral centre and exhibit the chiral nematic phase. However, for more complex molecules and more highly ordered phase types, this empirical structure relationship does not necessarily work.
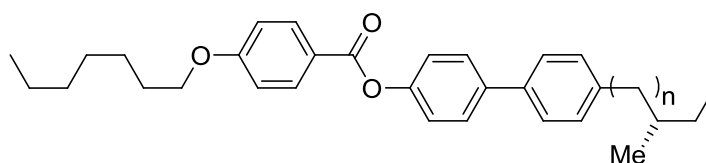
Figure 1.23: Chemical structure of a chiral liquid crystal where the parity is varied as a function of the methylene unit parity n.

Generally, it is found that the pitch of the helix decreases when the chiral centre is brought closer to the rigid core of the molecular framework. Table 1.2 illustrates this effect in the series of (*S*)-4-alkyl-4'-cyanobiphenyls.[71] As the chiral centre is moved towards the aromatic core of the material, its rotational freedom decreases, and its effect upon neighbouring molecules increases, which results in a shortening of the helical pitch length. Therefore, for relatively simple materials that have only one chiral centre, the pitch of the helix can often be predicted from the molecular structure of the compound under investigation.

n	Parity	Pitch Length (m)	Twist Sense
1	e	0.15	d
2	o	0.30	l
3	e	0.40	d

Table 1.2: Pitch length and twist sense depends on different chain number (n) and parity.

Although the equation for the helical twisting power expresses the chirality in terms of the enantiomeric excess, in reality, the nematic phase is far more sensitive to the presence of chiral materials than *ee* calculations show. This means any chiral materials, even those perhaps considered racemates from an *ee* point of view, could produce a measurable effect in an achiral nematic host. Thus, by definition a chiral dopant does not necessarily require a stereogenic centre. The chiral configuration can also correlate with the nematic host. According to the definition of chirality, dopants can be grouped into the following two classes.

1.8.3   Dopants Containing a Single Stereogenic Centre

Dopants with higher or lower helical twisting power are often useful for commercial and research purposes, so that people can design the dopant according to their requirements. Mesogenic functionalization is one of the most efficient ways for improving the helical twisting power value, while at the same time increasing the solubility in a nematic host. This method targets the incorporation of a stereogenic centre into an achiral material to give a material that is likely to exhibit a liquid crystal phase. For instance, the replacement of the hydroxyl group next to the chiral centre in (*R*)-2-octanol with a pro-mesogenic fragment, as shown in Figure 1.24, improved the HTP value from 0.8 μm^{-1} to 19.4 μm^{-1}, as measured in the host material MBBA.[72]
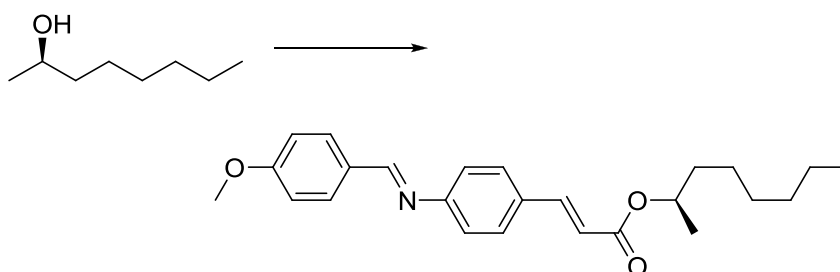
Figure 1.24: (*R*)-2-octanol (HTP = 0.8 μm^{-1}) is functionalized by a liquid crystal group (HTP = 19.4 μm^{-1}).[72]

The same principle can also be applied for chiral amines, see Figure 1.25.[73] When a mesogenic group is attached to (R)-1-phenylethanamine, the HTP value was found to increase from near 0 μm^{-1} to 43.2μm^{-1} when measured in the host 4-pentyl-4'-cyanobiphenyl, CB15.
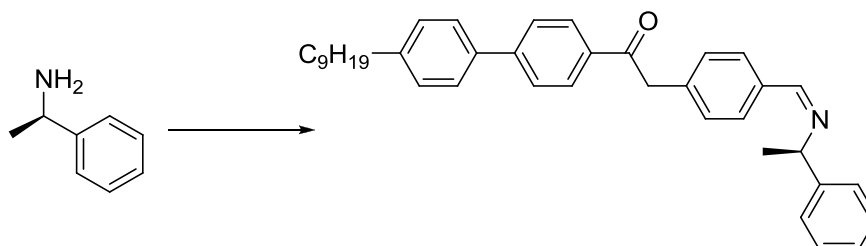
Figure 1.25: Rotational trapping of the stereogenic centre give a high HTP value.

Mesogenic functionalization of chiral materials is often the easiest approach for attaining target HTP values. Based on this principle, using a metallomesogen for the core to give axial chirality has become one of the most successful methods for preparing dopants with very large HTP values. For example, the ruthenium diketonate complex, shown in Figure 1.26, has a bipyridyl mesogenic group, the HTP value in the host MBBA achieves a very large value of 180 μm^{-1}.[74] Furthermore, a related trigonal bipyrimidal copper (II) complex using ligand A (see figure 1.27 for the structure of the ligand), gives similarly high HTP values (98 μm^{-1}) which were attributed to the propeller-like shape of the complex[75]
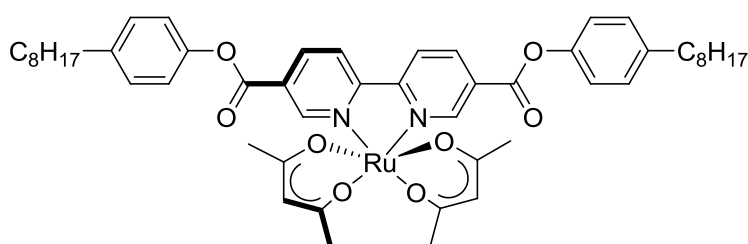
Figure 1.26: Chemical structure of ruthenium complex with a reported helical twisting power of 180 μm^{-1}
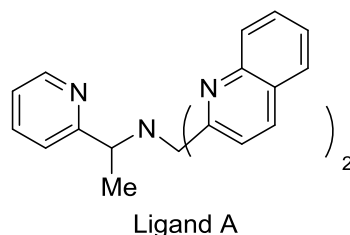
Ligand A

Figure 1.27: Chemical structure of Ligand A used to form a trigonal bipyrimidal copper complex.with high HTP of 98 μm^{-1}

1.8.4   Dopants Containing Axial Chirality

When there are no stereogenic centres present in a dopant, chirality can still arise from structural configuration (dissymmetry) and this form of chirality can also influence the nematic host. In fact, the HTP values for dopants with chiral dissymmetries have, to date, achieved higher values than for any other materials. The largest measured HTP was found for a dopant based on TADDOL ($\alpha,\alpha,\alpha',\alpha',$-tetraaryl-3-dioxolan-4,5-dimethanol).[76] As shown in Figure 1.28, the material has C_2 symmetry and therefore is chiral and will introduce a helical twist in nematic host.

TADDOL
Ar = 2-naphthalene
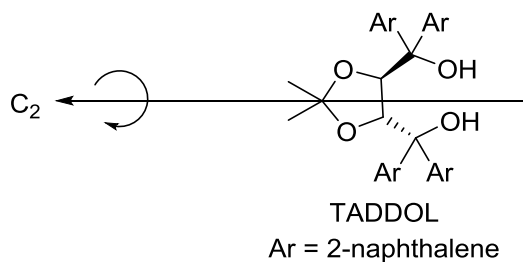
Figure 1.28: Chemical structure of TADDOL with a reported HTP of 405 μm^{-1}

The HTP value measured for TADDOLs (Figure 1.29) in 5CB is 405 μm^{-1}, which is remarkably large.[76] Even when different substitutes such as phenyl, 1-naphthyl, 2-naphthyl and 4-biphenyl are used to replace 9-phenanthryl groups, the HTP values are still above 100 μm^{-1}. It seems the influence of steric factors on the HTP value is not due to the material being 'mesogen' like. Hydrogen bonding is the main reason that makes TADDOL based compounds have such high HTP values.

There are two hydroxyl groups at the end of TADDOLs. The hydrogen bonding gives a seven-membered ring, which becomes firmer than an open ring. It therefore makes sense, when using metal complex as the stereogenic core, that the HTP value would be increased significantly.
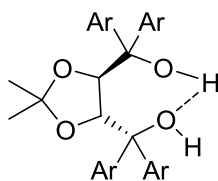
Figure 1.29: Hydrogen boding of TADDOLs and its conformational/configurational structure

Hydrogen bonding does not only affect such structures as TADDOL. Hydrogen bonding could also complex with an external molecule, as demonstrated by Eelkema and Feringa who used 3,3'disubstituted biphenols and amino alcohols complexed together by hydrogen bonding, see Figure 1.30.[77,78] They observed amplified helical twisting power compared to that of the uncomplexed materials.
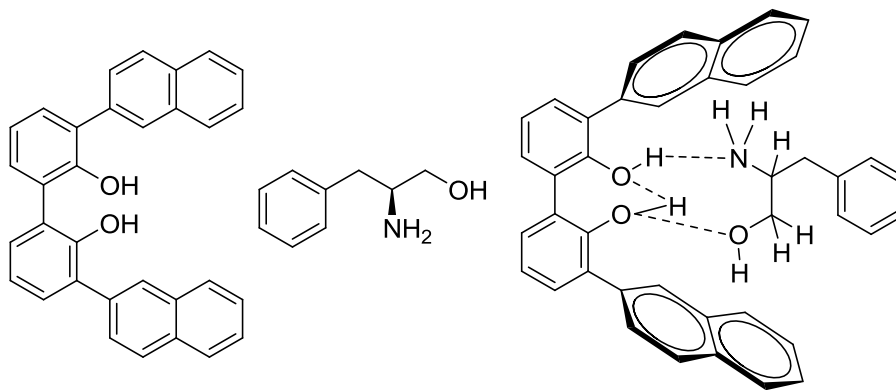
Figure 1.30: Amplification of the HTP via complexation with the dopant.[77]

When the hydroxyl groups in TADDOL are replaced with methoxy groups the HTP value drops from 100 to 55 μm^{-1}, thereby demonstrating that hydrogen bonding can serve to increase the HTP value.[76] When a siloxane bridge is used to replace the methoxy group, a closed ring is formed again, similar to the hydrogen

bonding case, see Figure 1.31. Obviously, the siloxane bridge in this material is more rigid than the hydrogen bonding in TADDOL (ca. 110 kJ mol^{-1} vs. 27 kJ mol^{-1}), but the HTP value falls dramatically from 100 to 23 μm^{-1}. The siloxane bridge therefore weakens the chiral induction power even more than methoxy substitution in derivatives of TADDOL.[76]
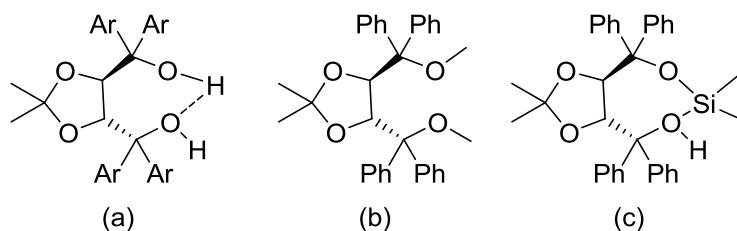
Figure 1.31: Chemical structure of chiral dopants (a), (b) and (c) with reported HTP values of 100, 55, and 23 μm^{-1}.[76]

The above case shows there is no immediately obvious explanation for the unpredictable results on substitution in TADDOL. The silicon oxygen 'bridge' bond (chemical bond) is far stronger than hydrogen bonding which should improve the HTP value in the ring system. The order of improving HTP should be bridge bond > hydrogen bond > open ring. Although this order does not apply in the TADDOL system, for the similar binaphthyl system, the order of bonding works as expected.[72]

The absolute conformation of 1,1'-binaphthyl based materials (see figure 1.32), either in cisoid or transoid conformation, can introduce a helix in a nematic liquid crystal. When using two methoxy substitutents in the 2,2′ positions of 1,1′-binaphthyl, compound **A**, therefore, the HTP value is relatively low at 1.5 μm^{-1} due to it still being a "quasi-open-ring" conformation where interannular twisting can occur.[79] When two hydroxyl groups were deployed in the 2,2′ positions of 1,1′-binaphthyl, compound **B**, the hydrogen bonding forms a weak seven-membered ring, resulting in an increase of the HTP value from 1.5 μm^{-1} to 32 μm^{-1}. Introducing a methylene unit connecting the two oxygen atoms increases

the HTP is increased further to 85 μm^{-1}, which is probably related to a decrease in the interannular twisting.[80] Moreover, when increasing the number of methylene units between the two oxygen atoms, the HTP values actually decreases slightly. For example, when there is a three-carbon linker present, compound **D**, the HTP value is 80 μm^{-1}, and a four-carbon linker, compound **E**, has a HTP value of 79 μm^{-1}. The reason for the decrease in HTP value with increased number of methylene units in the linking chain, is because as the number increases the ring becomes larger and more flexible, hence, the rigidity is decreased and the interannular twisting becomes easier. Despite the small decrease, the HTP values for materials with C-C linking units are still over two times the value for the hydrogen-bonded materials. See Figure 1.32 for the various comparisons.[79,80]
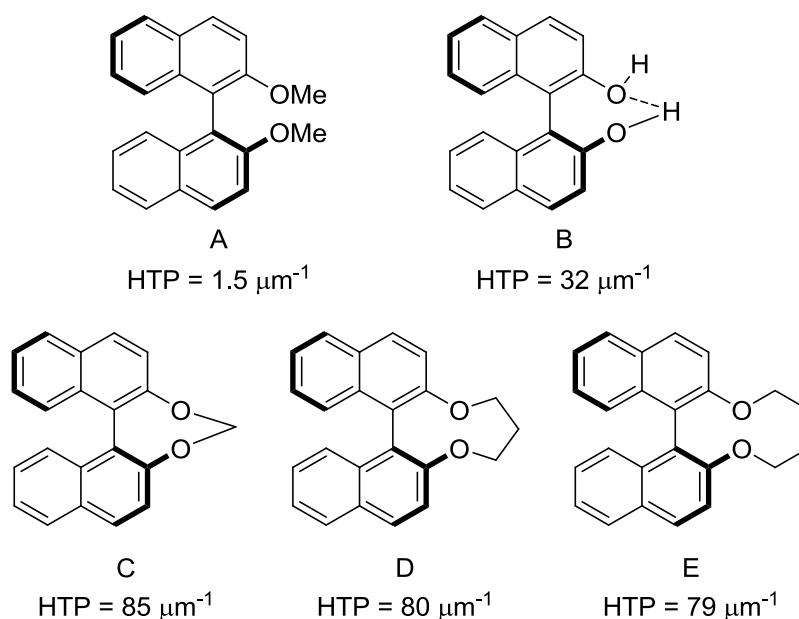
Figure 1.32: Chemical structures and HTP (μm^{-1}) values for some 2,2′-disubstituted 1,1′-binaphthyl systems.[79,80]

The structures covered so far range from simple chiral molecules to large metallomesogen complexes to two molecules bound through non-covalent interactions to enhance the helical twisting power. It is possible to obtain values of HTP ranging from nearly 0 μm^{-1} to over 400 μm^{-1}.[72,81] As chiral dopants induce helix formation into a nematic host, it is also possible to use a nematic host to

'sense' chirality, symmetry, conformation, and correlation (with other molecules) and so on, given the extreme sensitivity with which chirality influences the nematic host. However, although a large number of theoretical studies have been performed,[82-86] there is still no clear and comprehensive theory to explain how dopants influence the host, why chemical structure with slight difference could make magnitudes of difference in HTP value and why the same dopants behave very differently in different host systems.[87,88]

1.9 Sensing Chirality, Determining Enantiopurity and Assigning Spatial Configuration in Other Liquid Crystal Systems

1.9.1   Chiral Smectic C* and Ferroelectric Liquid Crystals

In the smectic C phase achiral, rod-like molecules are arranged in weakly organised layers, where the molecules are tilted on average at a temperature-dependent angle (θ) with respect to the layer planes.[89] Thus the phase has C_{2h} symmetry, as shown in Figure 1.33.[90]
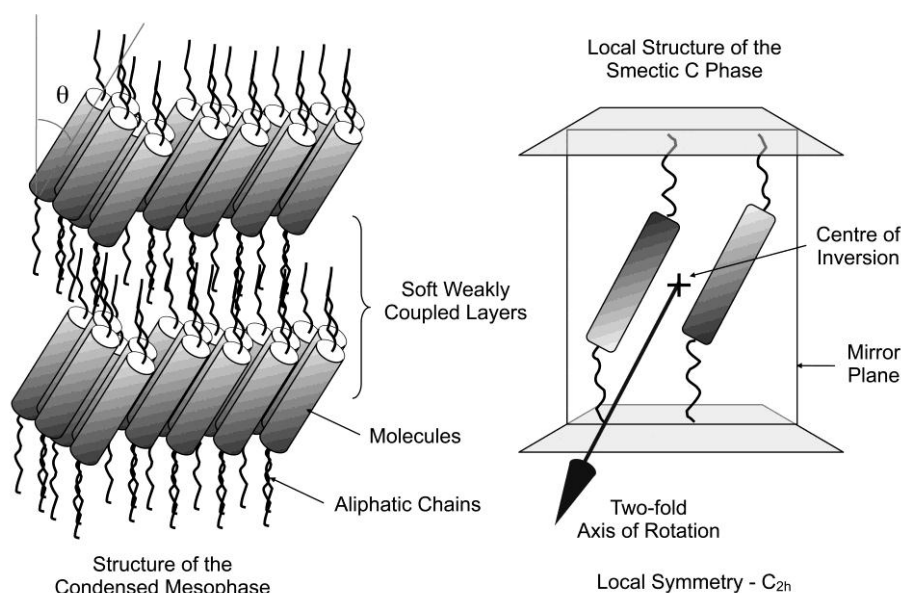
Figure 1.33: The structure of the achiral smectic C phase (left), where the local symmetry (right) is shown by a mirror plane perpendicular to the layers, a centre of inversion, and a two-fold axis of rotation perpendicular to the tilt, (drawing reproduced from reference 91 with the permission of the author.

When the smectic C phase is formed from the smectic A phase upon cooling, the temperature dependence of the tilt angle approximately takes the form:

$$(\theta)T = (\theta)_0(T_C - T)^{\alpha} \qquad (8)$$

where $(\theta)_T$ is the tilt angle at temperature T °C, $(\theta)_0$ is a constant, T_C is the smectic A to smectic C transition temperature, T is the temperature and α is an exponent

which is usually set equal to 0.5 however, typically the experimental value of the exponent is found to be less than 0.5.[92,93]

The molecules within the layers are locally hexagonally close-packed; but the ordering is only short range, extending over distances of approximately 15‒25 Å.[94] Over large distances the molecules are randomly packed, and in any one domain the molecules are tilted roughly in the same direction in, and between, the layers (see Figure 1.33 left). Thus, the tilt between successive layers extends over relatively long distances.

When chiral materials are introduced into the smectic C phase it becomes optically active in a way similar to that of the chiral nematic phase, *i.e.* the smectic C* phase has similar optical activity properties and also possesses a helical distribution of its molecules.[95] This helical structure is manifested in a rotation of the molecular tilt with respect to an axis that is perpendicular to the layer planes, as shown in Figure 1.34. Crucially, this rotation occurs in the same direction for a chiral material, which results in the formation of a helical molecular arrangement.[1] The helix can be either right-handed or left-handed depending on the chirality (absolute spatial configuration) of the constituent molecules. The pitch of the helix for most C* phases is commonly greater than one micrometer in length, showing that one pitch of the helix is composed of thousands of smectic layers. The angle by which the molecules are rotated from one layer to the next is therefore very small; typically on the scale of one-tenth to one-hundredth of a degree.
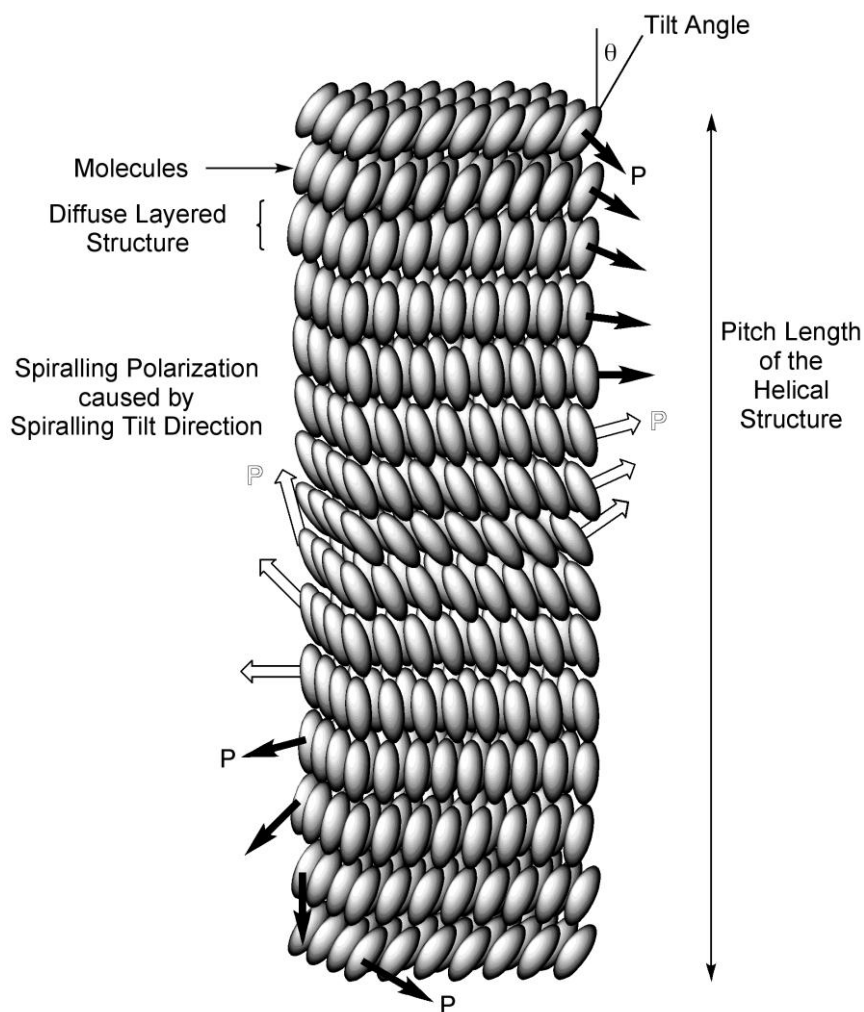
Figure 1.34: The helical macrostructre of the smectic C* phase, showing the direction of the spontaneous polarization (for details see later).

If the environmental symmetries for the achiral and chiral smectic C phases are compared.[96] For an achiral smectic C phase, as shown in Figure 1.33, the space or environmental symmetry elements are: a mirror plane perpendicular to the planes of the layers and containing the long axes of the molecules, a twofold axis of rotation normal to the mirror plane and parallel to the layers, and a centre of inversion. Thus, the symmetry is classed as C_{2h}, as shown in Figure 1.35. However, when this phase contains chiral molecules, the number of symmetry elements is reduced to a single twofold axis parallel to the layer planes and normal to the vertical planes that contain the long axes of the molecules; consequently the phase has a reduced symmetry of C_2. The result of the packing of the polar regions of the

molecules in these phases requires that a spontaneous polarization (Ps) act along the C_2 twofold axis normal to the tilt direction, as predicted by Meyer.[97] Based on this information alone, it would seem that the smectic C* phase should exhibit a bulk spontaneous polarization. Furthermore, as the smectic C* phase does not have a well-organized or rigid structure, it should be possible to reverse the direction of the spontaneous polarization by applying a field of known polarity, thereby rendering the smectic C* phase *ferroelectric*. However, as discussed previously, the smectic C* phase exhibits a helical structure and therefore the spontaneous polarization direction, which is tied to the tilt orientational ordering, is itself spiralling in a direction normal to the layers. Thus, when the helix makes one full $360\,^{\circ}$ turn, the polarization is averaged to zero. Therefore, the phase becomes non-polar in the bulk and is best described not as ferroelectric but instead as helielectric.[98]
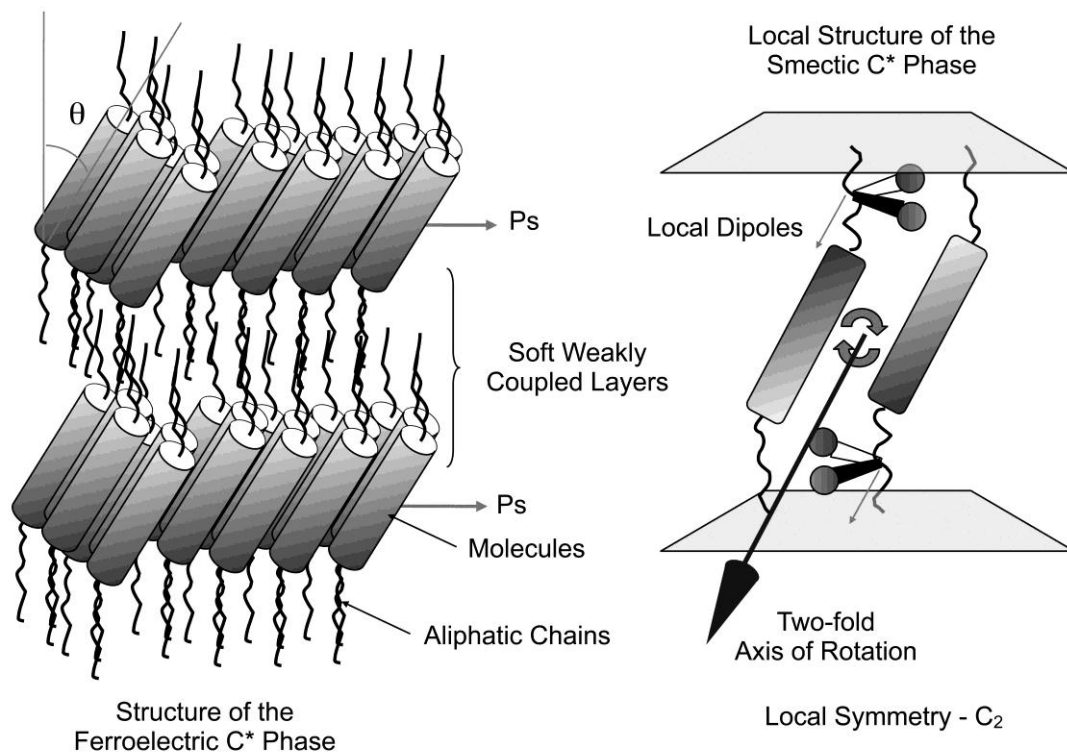
Figure 1.35: The structure of the chiral smectic C* phase (left), where the local symmetry (right) is shown by a two-fold axis of rotation perpendicular to the tilt, (drawing reproduced from reference 91 with permission of the author)

When sandwiched between ITO coated glass, for separations of the glass of sufficiently short distance, the helix becomes unwound.[99] With a suitable directionally rubbed alignment coating, the layers of the phase can be forced to be perpendicular to the substrates, this is called bookshelf geometry. Applying a DC electric field to the device, the spontaneous polarization will follow the direction of the field. For large enough fields the reorientation of the molecules is achieved and two stable states will be formed, as shown in Figure 1.36. Depending on the direction of the field, and the stereochemistry of the molecules, one orientation of the tilt director will be to the left of the rub direction of the alignment, the other will be to the right, as shown in the figure 1.36. Switching between the two state occurs *via* reversal of the electric field and through an angle of twice the tilt angle.[90,99] The polarization reversal, and hence the tilt angle, pass through a hysteresis loop in the process as shown. This is effectively a ferroelectric response,

and forms the basis for surface stabilized ferroelectric liquid crystal displays (SSFLCD).[99] The specific details of ferroelectric, and arguments related to their classification, are beyond the scope of this thesis and will not be discussed further. However, as noted above the switching process is dependent on the liquid crystal having broken symmetry and therefore chiral. Thus, the response to an electric field indicates that a materials is chiral, therefore it is a test for the presence of chirality. Secondly the direction of the switching is dependent on the absolute configuration of the stereogenic centre(s) of the smectic C materials, thus the switching can be used to determine spatial configuration (*R* or *S*).[42] Thirdly, the angle of the switching, which can be determined by experiment can also be influenced by the enantiopurity. These experimental results are dependent on the relationship between the direction of the spontaneous polarization relative to the orientation of the tilt and to the Sed/Rol relationships discussed earlier for chiral nematic materials. Figure 1.37 shows the link between tilt orientation and the direction of the spontaneous polarization. The orientation of the spontaneous polarization in a device of course depends on the direction of the applied field. Table 1.3 shows the relationship between the chiral nematic rules of Gray and McDonnell[71] to those of the spontaneous polarization for ferroelectric liquid crystals.[100,101]
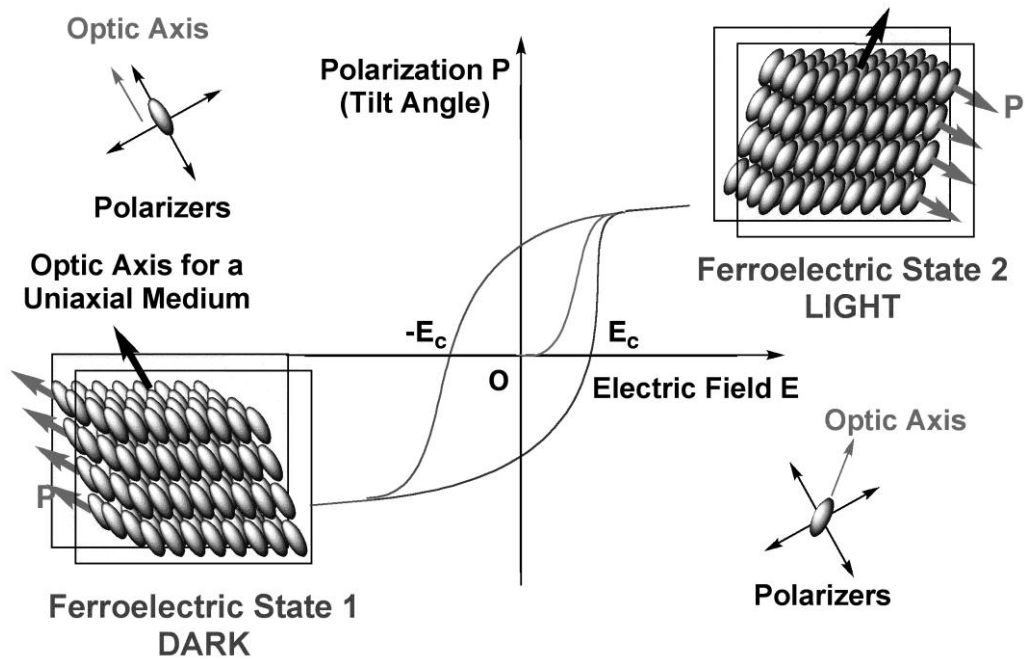
Figure 1.36: DC electric switching via a hysteresis loop for ferroelectric liquid crystals sandwiched between ITO coated glass. The two extreme switched states are shown with their spontaneous polarizations pointing into the glass substrates, left of figure pointing down, right of figure pointing up.
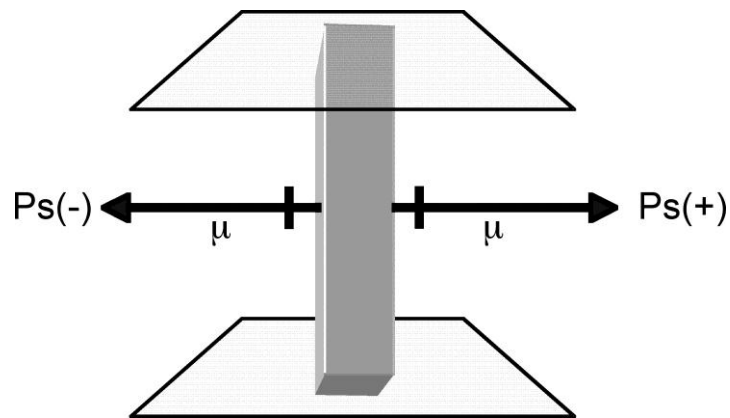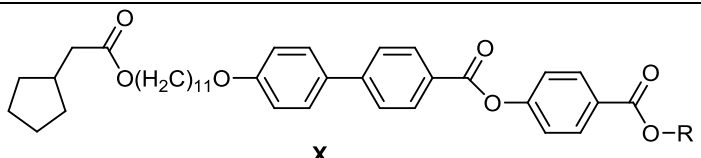
Figure 1.37: The relationship between the spontaneous polarization direction (C_2 axis in Figure 32) and molecular tilt. The molecule (grey block) in the figure is tilting away from the observer and the choice of polarization direction is either to the right Ps(+) or to the left Ps(−) in the plane of the page.

Inductive Effect	Spatial Config.	Spacer Parity	Rot^n of Plane Polarized Light	Helix Direction	Ps Direction
+I	S	e	d	LH	Ps(-)
+I	R	o	d	LH	Ps(-)
+I	R	e	l	RH	Ps(+)
+I	S	o	l	RH	Ps(+)
-I	S	e	l	RH	Ps(+)
-I	R	o	l	RH	Ps(+)
-I	R	e	d	LH	Ps(-)
-I	S	o	d	LH	Ps(-)

Table 1.3. The relationship between the inductive effect at the stereogenic centre, the absolute spatial configuration at the stereogenic centre, the parity of the methylene spacer (odd or even) linking the stereogenic centre to the molecular core, the rotation of plane polarized light through the bulk phase, the handedness of the helical suprastructure, and the direction of the spontaneous polarization.[100,101]
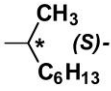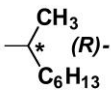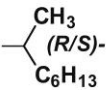
In terms of detection of chirality, determination of the spatial configuration, and the ability to determine enantiopurity the following study on ferroelectric liquid crystals is worthwhile describing. Compound X shown in Table 1.4 was synthesised from commercially available (*R*)-, (*S*)- and racemic 2-octanol (R represents 1-methylheptyl in the structure in Table 1.4). The phase transition temperatures, the magnitude of the spontaneous polarization, and the enantiopurities of the three materials are given in the table.[102,103] It is interesting to note that the phase transition temperatures and the phase (type) sequences are dependent on the enantiopurity. Now when the three materials were subjected to electrical field studies in planar aligned cells, surprisingly the racemate was found to respond, *i.e.* the racemate also possessed broken symmetry, and therefore was not truly racemic and behaved as a ferroelectric, as shown in Figure 1.38. The conclusion was that the racemate as sold commercially was not recemic at all, but had a slight imbalance in the relative proportions of the enantiomers.

X

R =

$\begin{array}{l} CH_3 \\ * \ (S)\text{-} \\ C_6H_{13} \end{array}$ K 39.2 (SmCA* 32.0) SmC* 79.6 TGBA 80.7 Iso Liq
Ps +, Ps 99 nCcm^{-2}, θ = 35.5° ee = 0.92

$\begin{array}{l} CH_3 \\ * \ (R)\text{-} \\ C_6H_{13} \end{array}$ K 37.0 SmC* 79.2 SmCα* 79.7 TGBA 81.9 Iso Liq
Ps -, Ps 92 nCcm^{-2}, θ = 36.5° ee = 0.88

$\begin{array}{l} CH_3 \\ (R/S)\text{-} \\ C_6H_{13} \end{array}$ K 35.7 SmC 81.0 SmA 87.5 Iso Liq
Ps +, θ = 22°

Table 1.4. Phase transitions, spontaneous polarization directions, and enantiopurities of (*R*)-, (*S*)- and racemic and 4-(1-methylheptyloxycarbonyl)phenyl 4'-[11-(2-cyclopentylacetoxy)undecyloxy]biphenyl-4-carboxylate (**X**).[102,103]

From the electroopic responses for the three materials (including the racemate), the spontaneous polarizations and the tilt angles of the smectic C* phases were measured as a function of temperature, as shown together in Figure 1.39. For the spontaneous polarization the value for the "so-called" racemate could not be determined because the enantiopurity was very low, whereas slight differences were observed for the two enantiomers. For the tilt angle measurements the two enantiomers exhibited very similar results, only because a threshold was reached where switching could not be obtained. The outcome from these results is that the differences in enantiopurities were detectable but not well-defined enough for actual determination. Thus for ferroelectric liquid crystals, chirality was easily detectable, the absolute spatial configuration could be determined, but the enantiopurity could not be measured.
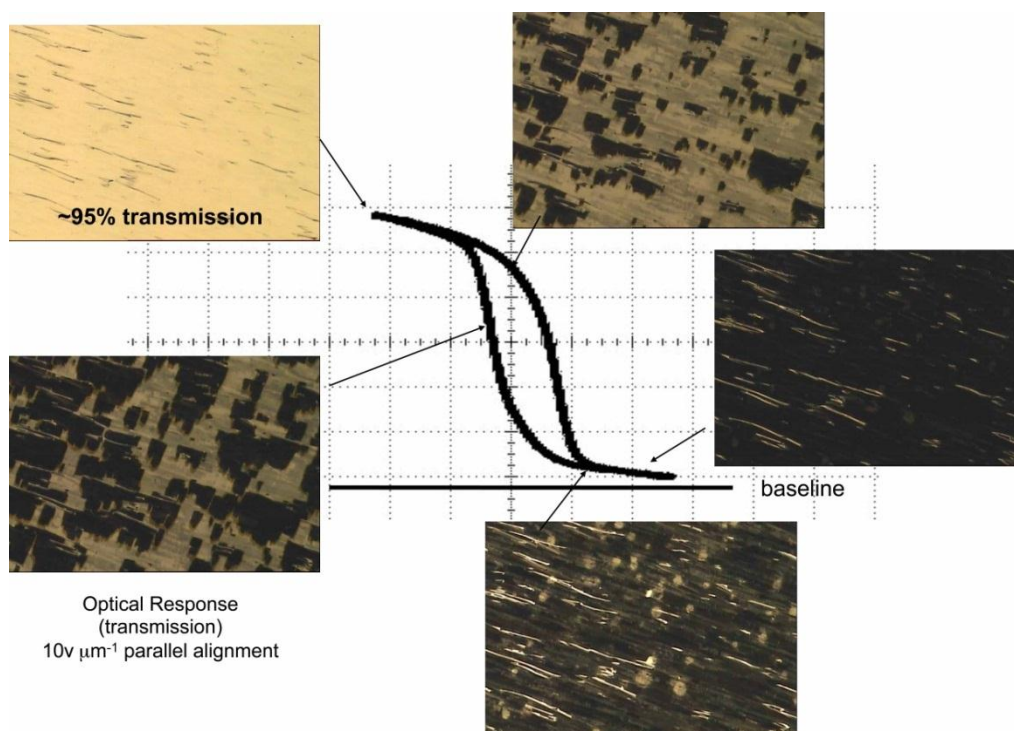
Figure 1.38: The optical response to a DC electrical field for racemic 4-(1-methylheptyloxycarbonyl)phenyl 4'-[11-(2cyclopentylacetoxy)undecyloxy]biphenyl-4-carboxylate, showing the hysteresis for the polarization (tilt angle). The response is ferroelectric and the materials is not racemic, i.e. chirality has been detected.[102]
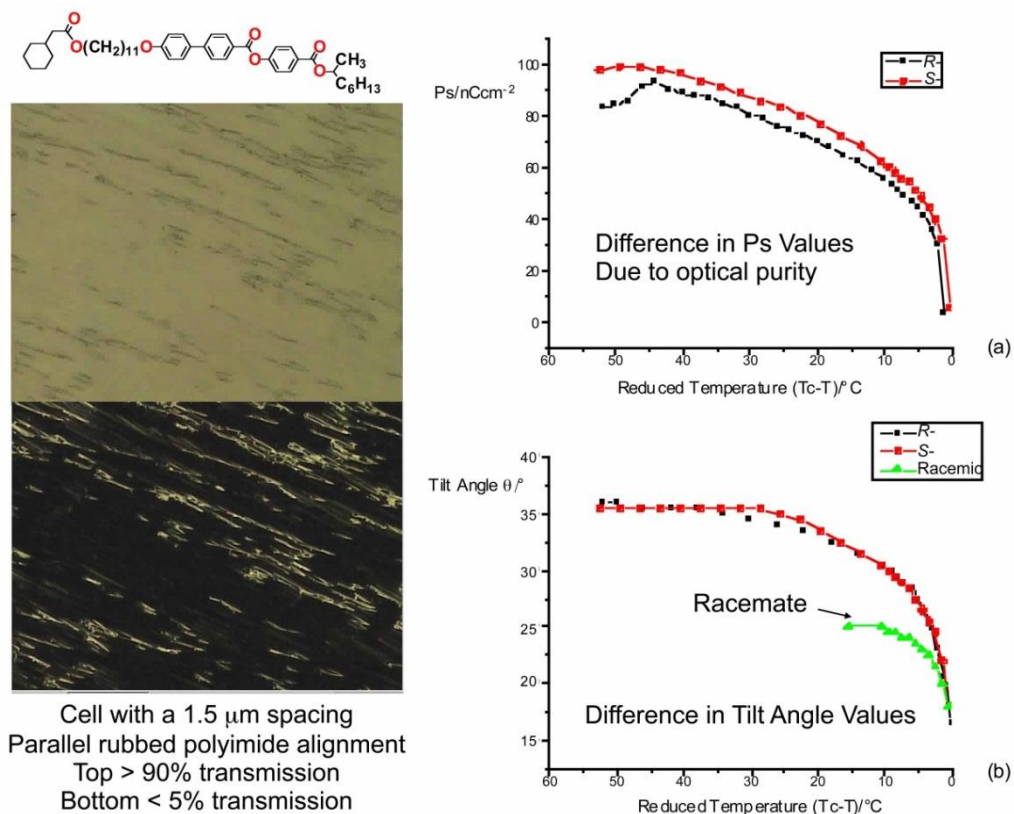
Figure 1.39: The measurement of the spontaneous polarization (nCcm^{-2}) and the tilt angle (°C) for (*R*)-, (*S*)- and racemic 4-(1-methylheptyloxycarbonyl)phenyl 4'-[11-(2cyclopentylacetoxy)undecyloxy]biphenyl-4-carboxylate. The data is not separated enough for determination of enantiopurity.[103]

1.9.2   Structures of the Achiral and Chiral Smectic A and A* Phases

For the smectic A phase, the rod-like molecules are arranged in weak layers so that their long axes are on average perpendicular to the layer planes, see Figure 1.40.[94] The molecules rapidly rotate about their long and short axes, and they are arranged so that there is no positional ordering in the planes or between the layers.[89] Therefore, there is only short range ordering extending over a few molecular centres at most (~15−25 Å). Perpendicular to the layers the molecules are essentially arranged in a one dimensional density wave, therefore, the layers must be considered as being diffuse. As a consequence, the concept of a lamellar mesophase is somewhat misleading because the layers are so diffuse that on a

macroscopic scale they are almost non-existent. In reality, the molecules are arranged within the layers in such a way that they are randomly tilted at slight angles with respect to the layer normal. This makes the layer spacing on average slightly shorter than the molecular length. Typically, the molecules are tilted anywhere up to about 14-15 ° from the layer normal. However, as the tilting is random across the bulk of the phase, the mesophase is also uniaxial, and has $D_{\infty h}$ symmetry.[104]

The structure of the smectic A* phase when it is composed of chiral molecules remains the same as that for the achiral phase. The molecules are arranged in diffuse disordered layers, and there is no long-range periodic order. However, because of the molecular chirality, the environmental symmetry is reduced to D_∞.[104] As a consequence, when an electric field is applied to a chiral smectic A* phase there will be a coupling of the electroclinic susceptibility to the field and the long axes of the molecules will tilt with respect to the layer planes, giving an apparent smectic C* structuring.[105] At a constant temperature, the tilt angle, for relatively low applied fields, varies linearly with the field, but at higher fields the relationship becomes non-linear. Overall this electrooptic phenomenon is called the electroclinic effect, and the region where there is a linear relationship is used in device applications. This effect was also used by Walba *et al* to determine enantiopurirties as follows.[106]
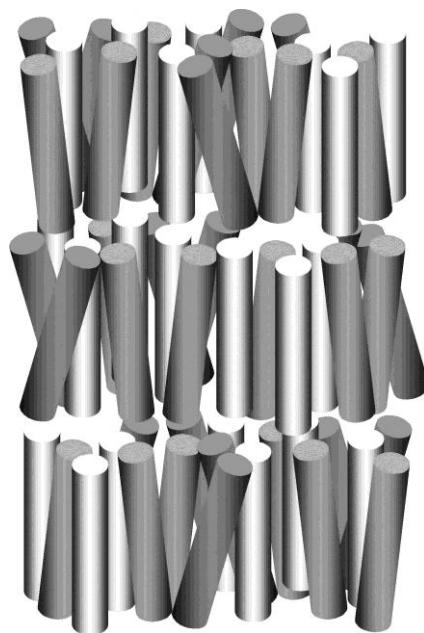
Figure 1.40: The structure of the smectic A phase showing the molecules as rods.

The compound in Figure 1.41, in its chiral form, was shown to exhibit an electroclinic effect, which was quite pronounced, and relatively temperature-independent close to the SmA*–SmC* transition. Therefore its racemic form was deemed a useful host, which could be doped with pharmaceuticals such as naproxen and pseudoephedrine (low Figure 1.41), and then the electroclinic response for the combined mixtures could be measured.[106]

SmC 24 SmA 33 Iso Liq (racemate)

(*S*)-Naproxen

(*S,S*)-Pseudoephedrine
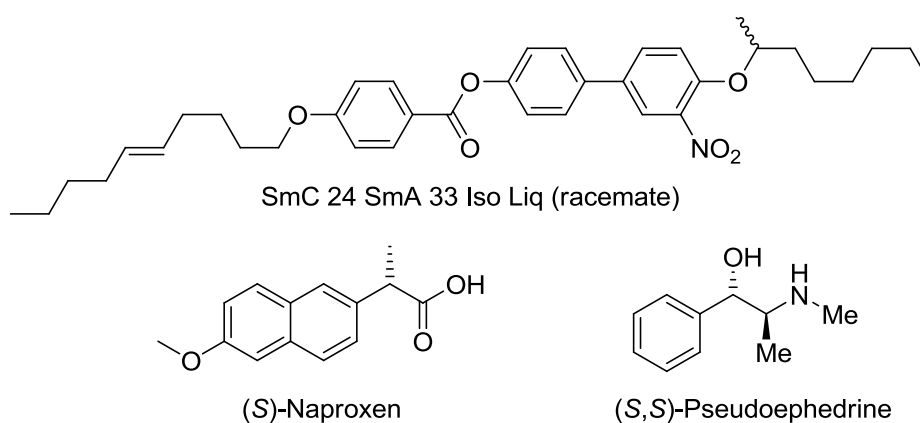
Figure 1.41: A high tilt "electroclinic" host achiral liquid crystal (top), test drugs used in the experimental studies to create chiral mixtures for which the electroclinic response (switching angle) could be measured.[106]

To give accurate measurements the electroclinic switching angle was required to be constant over a wide temperature range. So to demonstrate the method, three naproxen samples of varying *ee* values (0.25, 0.50, 0.75) were prepared by mixing with its own racemic mixture. Each of these materials as well as (*S*)-naproxen and the racemate were then doped at 1% by weight into the achiral host (top of Figure 1.41), via serial dilution.

Device cells, similar to those of SSFLCDs, were used and the chiral signal from the response from a square wave was recorded. As with ferroelectric devices, each cell was oriented with the rubbing direction (optic axis with no applied field) at 45 ° with respect to the polarizer, see Figure 1.42. In this geometry, the variation in intensity of transmitted light with small changes in orientation of the optic axis (+/- 0.1 °) was determined. This variation was claimed to be related to the enantiopurity. Thus this method was the same as with ferroelectric switching except that the tilt angle variation with field was more sensitive because of the coupling to the electroclinic effect, whereas for ferroelectric switching the tilt was saturated to give the maximum tilt angle, as shown in Figure 1.39.
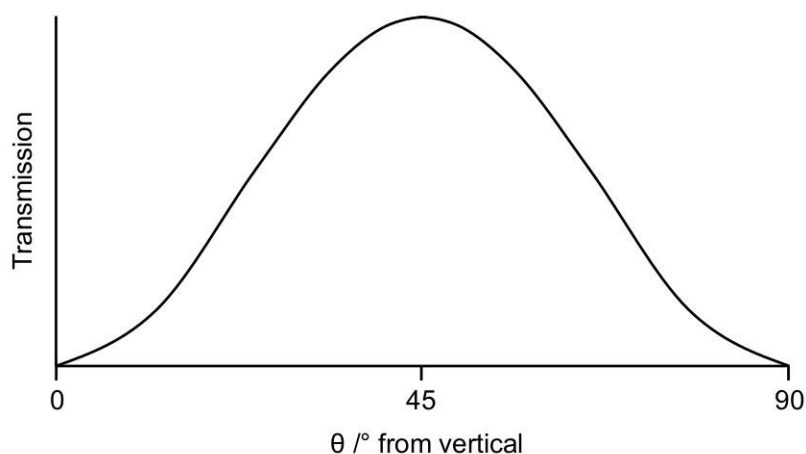
Figure 1.42: Plot of transmitted light intensity (I) versus optic axis orientation (θ), given as degrees from vertical (deg), when observed between crossed polarizer (POL) and analyzer (ANA) for a uniformly aligned SmA* LC cell (after Walba *et al.*)[106]

Thus, the switching angle was measured as a function of the maximum light intensity through the device (determined by a photomultiplier) as a function of constant field and temperature for the various mixtures of defined enantiopurity. The maximum range for the optic signal response (ΔI) was said to be related to the enantiopurity, *i.e.*, it was proposed that the electrooptic response and tilt were sensitive to enantiopurity.

It was found that chirally doped host shows a large chiral signal of $\Delta I \sim 1.4$ for naproxen (100% *ee*), or about eight times larger than the maximum signal obtained with naproxen in the conventional host. Importantly, as shown in Figure 1.43, the response is relatively temperature independent. These experiments showed that the ee value of an unknown sample of naproxen could be determined by using the method with an error of $+/-5\%$ *ee*. The amount of analyte in the probe beam in these experiments is approximately 15 picogram, and smaller samples sizes were envisioned.
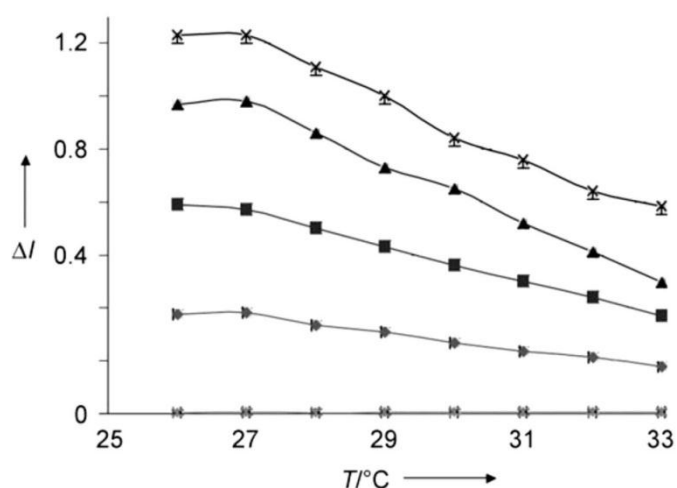
Figure 1.43: Chiral signal ΔI (given as the difference between two voltage readings on a photomultiplier) as a function of temperature for samples of naproxen of various ee values of naproxen in the host; from top to bottom: 100% ee (X), 75% ee (▲), 50% ee (■), 25% ee (◆), 0% (★) (baseline). [106]

Although the authors were confident in their projections, this method shares some of the problems experienced with other methods. There is an assumption that naproxen had an enantiopurity of 100%. It is unlikely that any one material would have such a level of enantiopurity. The value might be high for naproxen but not for other materials that would need a 100% *ee* value to standardise the results. Furthermore, as shown in the studies in chapter 4.8, derivatives prepared from racemic 2-octanol are invariably not racemic, and so there would be a contribution from the host. Thus in determination of *ee* to +/⁻ 5% and the uncertainty of the 100% value of the chiral dopant and the 0% value for the host, the overall uncertainty places this method lower than that of chiral GC/LC or NMR methods.

1.9.3   Contact Preparations In Determining Spatial Configuration

Another way of determining the spatial configuration of a chiral liquid crystal is to do a contact preparation with a material of known helical twist sense and also known spatial configuration. The material used may be a liquid crystal or a dopant in a liquid crystal host. The type of mesophase, which the studies performed in, may be nematic or smectic C*.[27]

The contact preparations are generated by putting a standard material with the substance for study on a microscope slide, and placing a coverslip over them. The materials are heated until in their liquid states, and the two liquids are allowed to meet by flowing together under capillary action to give a sharp contact region.

When viewing the contact region in the microscope two possibilities emerge. One where there is a clear boundary separating the two materials, and where the boundary texture starts to approximate that of an achiral phase. Alternatively the

boundary might show a continuous texture, with only the birefringence appreciably changing. Figure 1.44 shows a schematic of these two possibilities.
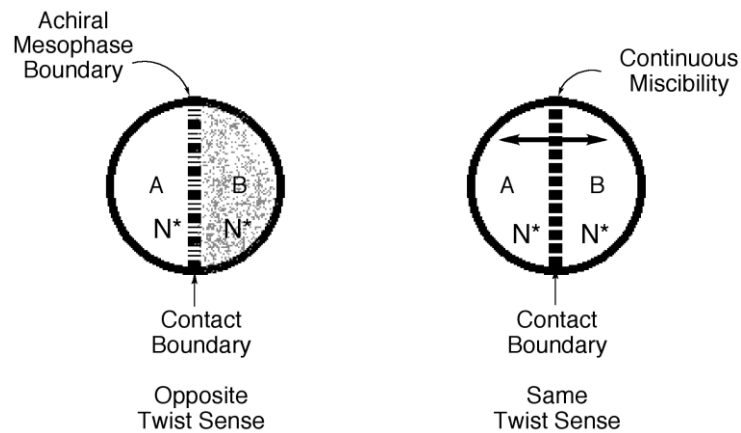
Figure 1.44: Two possible outcomes from a contact preparation between two materials that possess a helical macrostructure.

Figure 1.45 shows results that map onto Figure 1.44 for the chiral nematic phase. Figure 1.45 (left) shows the result from two nematogenic materials of opposite helical twist sense. The contact area running top right to bottom left has the texture of an achiral nematic phase, *i.e.* the helices are unwound, and therefore the regions either side of the nematic line must have opposite twists. Conversely, Figure 1.45 (right) shows continuity across the contact boundary, accompanied with a change in birefringence. For this result the two materials have the same twist sense.
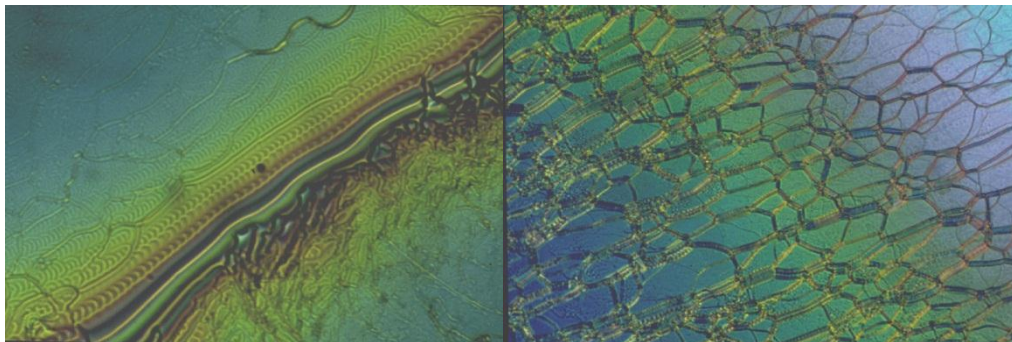
Figure 1.45: The contact regions between two chiral nematic materials, left the two materials have helicial structures of opposite twist sense, whereas, right, the two materials have the same helical twist sense (x100).

Knowing the spatial configuration of the standard material, and applying the Gray and McDonnell rules to both the standard and the target material, the absolute spatial configuration of the test compound may be determined.[71] However, this technique does not give any information on helical pitch length except that it is continually changing across the preparation. Information on enantiopurity is also not available from such experiments.

A similar picture can be drawn from the chiral smectic C* phase. In this case the texture is different, and instead of a *schlieren* a focal-conic texture is sought in the preparation. Focal-conics are decorated with pitch lines in the chiral variation of the phase.[94,107] For a standard–test material interface if the two have opposite twists the helices will unwind in the region of the boundary and the pitch lines will disappear, as shown for the two materials in Figure 1.46.
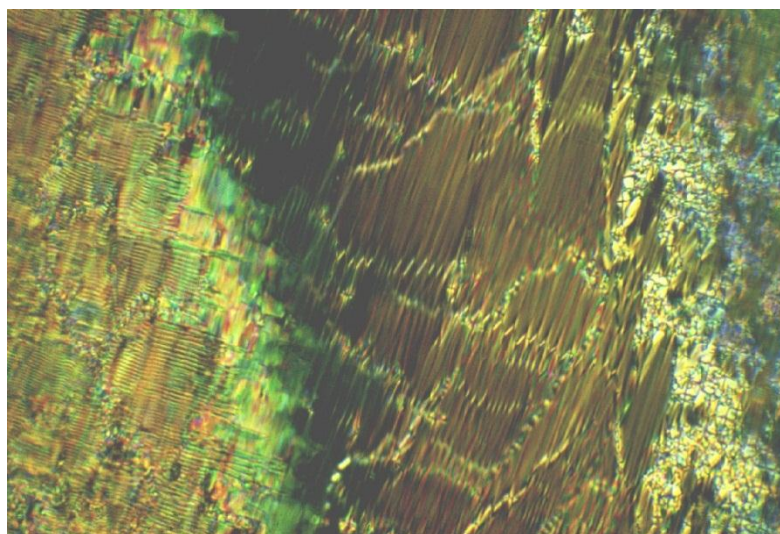
Figure 1.46: The contact region between two chiral smectic C* materials of opposite twist sense. Along the boundary between the two the helical structures compensate for each other, and the pitch disappears giving a normal smectic C phase (x100).

Applying the same principles for the Gray McDonnell rules,[71] developed for chiral nematic phases, to smectic C* phases (as described previously in Section 1.8.1),

the spatial configuration of the test material can be derived from the known configuration of the standard.

Contact preparations can also be made in display devices, in particular those based on ferroelectric liquid crystals such as the smectic C* phase, but others such as smectics I* and F* should not be precluded. Figure 1.47 shows a contact between two ferroelectric liquid crystals in a bookshelf-aligned cell. The two compounds have opposite spontaneous polarization directions, so when the DC field is inverted the light areas become dark and the dark areas become light, the angle between the two being twice the tilt angle. If the standard is dark to a positive upper plate then it will have a Ps(+) definition, and as a consequence the test material will be Ps(−). Applying the same rules as in chapter 4, the absolute configuration can be determined along with the helical twist sense. Again though, even the relative enantiopurity cannot be detemined.

Figure 1.47: The contact region between two chiral smectic C* materials of opposite spontaneous polarization direction. Along the boundary in the SSFLC cell, the two structures compensate for each other, and the phase becomes achiral and none ferroelectric (x100).

Overall this section shows that liquid crystal methods can be used to detect chirality, determine absolute spatial configuration, helical twist sense, and spontaneous polarization direction. However, the helical pitch length, the HTP, and the optical purity cannot be determined using the methods discussed in this section.

Chapter 2.   Aims

The aims of this project are to evaluate chirality in terms of the helical twisting power of chiral dopants in nematic hosts *via* 'the reverse-twist disclination line method'.[4,5,61]   Although it is a very important property of chiral materials, there is no well-developed principle to explain and predict the value of the Helical Twisting Power (HTP) of materials, either qualitatively or quantitatively. As discussed in the introduction, the HTP of a given material can be measured by the Cano-wedge method,[58] however this method typically requires large quantities of materials which are not always available.[108] Other methodologies have been tested for use as chirality detectors,[109-111] and as sensors for spatial configuration,[112] for example ferroelectric and electroclinic liquid crystals devices.[106] These devices detect chirality to a low limit, but cannot determine the enantiopurity. However, they also have high degrees of uncertainty, which make them of little use in quantitative applications, and they remain only of qualitative use.

In this work, the HTP of different kinds of chiral dopant, and other chiral materials will be investigated using the 'reverse twist disclination line method'. This will primarily involve studying mixtures of these chiral materials in a nematic host via the use of TN cells in order to investigate the disclination lines formed. Furthermore, different nematic hosts will also be employed so as to understand how the interaction between the various host/dopant combinations studied affect the measured HTP values. A more detailed overview of the aims of this work are given in the sections that follow.

2.1 Liquid Crystal Materials

2.1.1   Oxazoline-based Dopants

The first study will be to test 'the reverse twist disclination method' out on standard materials available in York. The experiments will be used to examine if there is any forthcoming relationships between the HTP values of the dopants tested.

The oxazoline-based dopants to be tested, shown in Figure 2.1, have been found to exhibit blue phases and TGB phases when mixed with an achiral nematic host.[113,114] The HTP values of three different chiral oxazoline-based materials will be investigated. The difference in molecular structure will be used to speculate as to how structural factors might influence the measured HTP values of the oxazoline-based dopants.
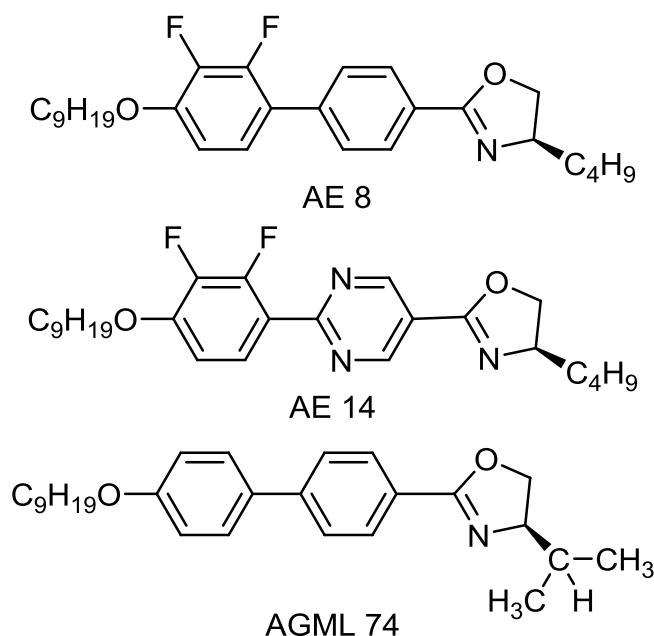
Figure 2.1: The structure of chiral oxazoline-based material AE8, AE14 and AGNL74.

2.1.2 High HTP value dopants

There are a number of high HTP value dopants that have been synthesised and reported.[72] The majority of the high HTP value dopants in the literature are not liquid crystalline, and many are metal complexes or TADDOL-based materials and hence their solubilities in nematic hosts are generally poor. R1011 and S1011 are a pair of high HTP dopants that are commercially available from Merck (Figure 2.2).[115] Each enantiomer will be used in the preparation of mixtures and will be subjected to the 'reverse-twist disclination line method' of analysis and the measured HTP values compared with literature values. With aid of molecular modelling, their gross conformations will be analysed and compared with those of other high HTP dopants in order to explore the factors that can enhance HTP.
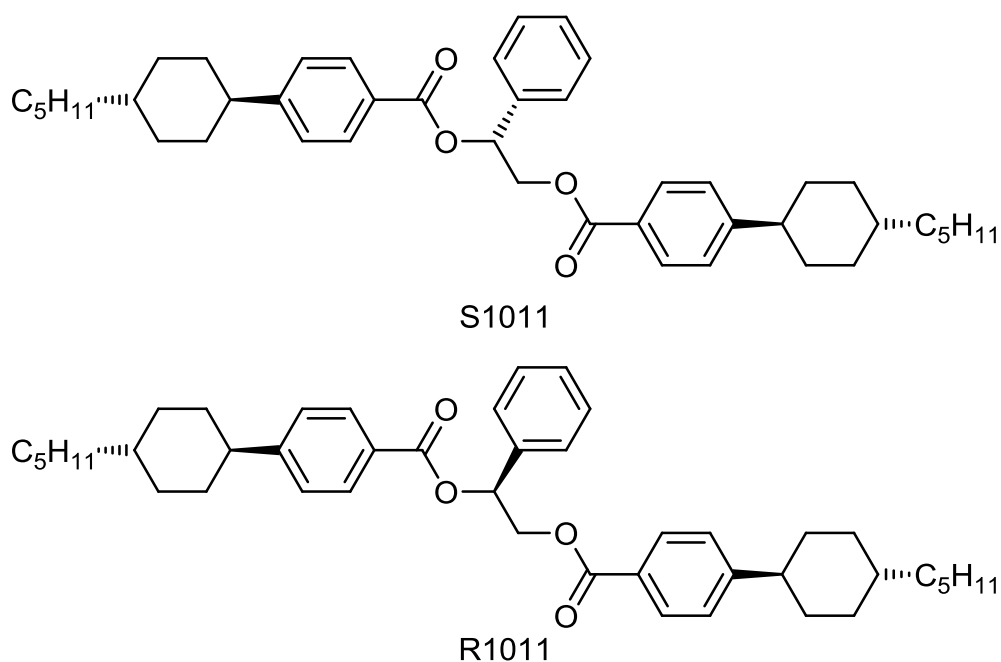
Figure 2.2: The structure of enantiomers R1011 and S1011.

2.1.3 Difluorobiphenylcyclohexane-based chiral dopants

trans-4-cyclohexyl(2,3-difluorobiphenyl) (CDFBP) based host materials and chiral dopants, see Figure 2.3, are very valuable commercial materials for

ferroelectric liquid crystal displays, with the mesogenic core unit conferring both low birefringence and moderate negative value of dielectric anisotropy.[116-119] Four structurally similar cyclohexyl(2,3-difluorobiphenyl)-based chiral dopants will be evaluated; the role of functional groups at the setereogenic centres in influencing the HTP values will be discussed.
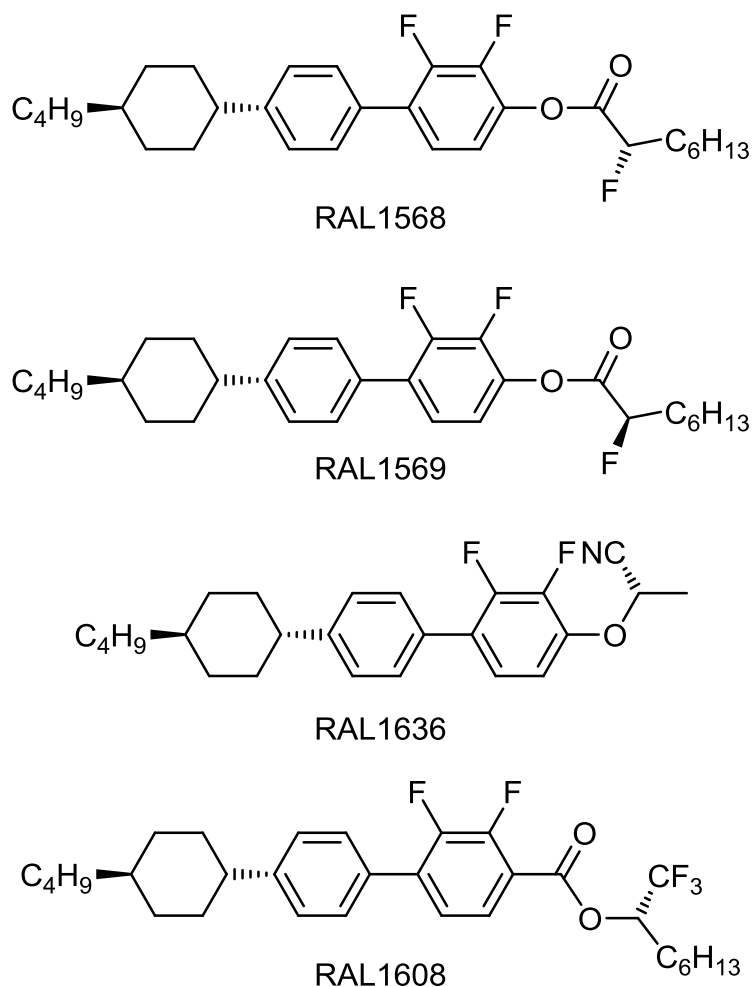
Figure 2.3: The structure of the diflourobiphenylcyclohexane-based chiral dopants

2.2 Non-Liquid Crystalline Materials and Materials with Complex Structures

2.2.1 Pharmaceuticals

Due to the high sensitivity of the TN reverse-twist disclination method it can also be used to sense the chirality of non-liquid crystal materials, provided they exhibit sufficient solubility in a nematic host. This has potential in quality control of pharmaceuticals where one enantiomer is desired and one is not. As such the most notorious drug safety issue of the last century,[120] the two enantiomers of thalidomide, see Figure 2.4, will be evaluated, and their HTP values measured. By doing so, it is predicted that differences in optical purity can be discerned, raising the possibility of determining enantiopurity.

(*R*)–Thalidomide   (*S*)–Thalidomide
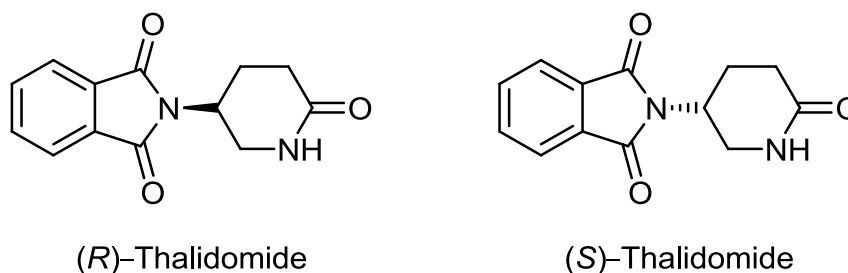
Figure 2.4. The enantiomers of Thalidomide.

2.2.2 Sugars and Sugar Based Supermolecular Liquid Crystals.

D-glucopyranoside as a mesogenic functionalized supermolecular liquid crystal, **A4** (see Figure 2.5), will also be investigated by the 'reverse-twist disclination line method'.[121] The fusion of mesogenic groups onto D-glucopyranoside has previously been shown to give a large increase in HTP values. However, the sensitivity of the 'reverse twist disclination line method' will allow this claim to be subjected to further scrutiny.

A4
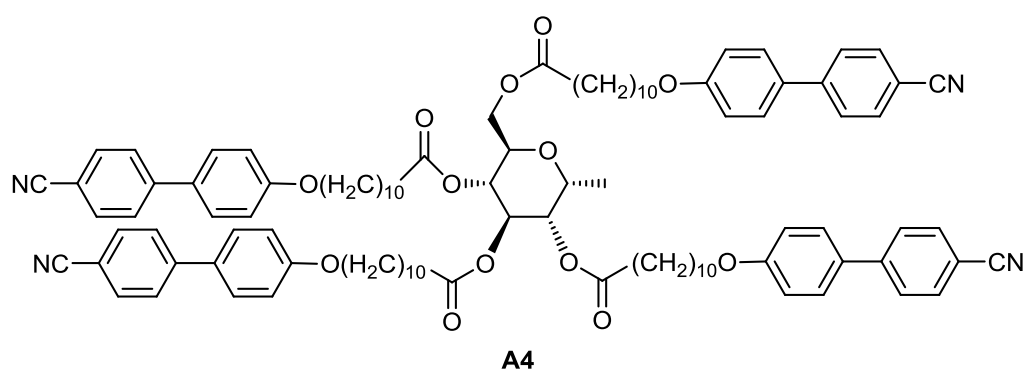
Figure 2.5. The structure of the super molecular liquid crystal **A4**.[121]

2.2.3 Investigation of Synthetic Pathways using the 'the reverse-twist disclination line method'

It had been suggested that ferroelectric behaviour had been observed in an apparently racemic material.[102,103] Materials of similar structure will be synthesised and the presence of chirality evaluated. The target molecules will be prepared *via* Mitsunobu[122] and Steglich[123] esterification reactions separately, and under different conditions and reagents, because it is at these steps that variation in enantiopurity was expected to have occurred. The target molecules will also be synthesised from racemic 2-octanol and chiral 2-octanol (Figure 2.6). The HTP values of all the target materials will be evaluated *via* 'the reverse-twist

disclination line method' in order to determine whether symmetry breaking on the macroscopic scale can occur during the Mitsunobu or Steglich reactions.
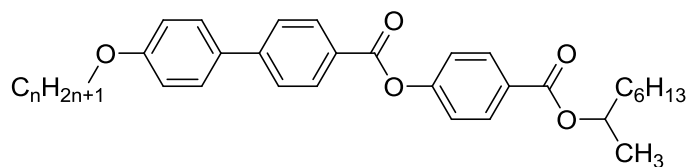
Figure 2.6: The structure of target molecule to be synthesized, n=10, 11.

Chapter 3. Experimental

3.1 Synthetic Work

3.1.1   Starting Materials, Reagents and Solvents

Unless otherwise noted, all of the starting materials and reagents were obtained from Fluorochem, Sigma-Aldrich, Apollo Scientific or AlfaAesar and used without purification. All solvents were obtained from Fisher, with the exception of anhydrous THF, which was purchased from Sigma-Aldrich, and used without purification.

The coupling agent *N*-(3-Dimethylaminopropyl)-*N*′-ethylcarbodiimide hydrochloride (EDAC) was purchased from CarboSynth and used without purification.

3.1.2   Thin Layer Chromatography and Column Chromatography

Where possible, the progress of chemical reactions was assessed by thin layer chromatography using a suitable solvent system. Silica coated aluminum plates (Kieselgel 60 F-254) were purchased from Merck and were visualized under UV light (254 nm or 365 nm) or by oxidation with aqueous potassium permanganate solution. In all cases, separations achieved *via* column chromatography were carried out using silica gel (Fluka, 70-230 mesh, 63 μm – 200 μm particle size). When required, increased flow rates were achieved *via* the use of flash techniques.

3.1.3   Nuclear Magnetic Resonance (NMR) Spectroscopy

Proton and carbon NMR spectra were recorded on a JEOL ECX or a Bruker spectrometer operating at a frequency of 400 MHz (^{1}H) or 100.5 MHz (^{13}C). The

residual protic solvent was used as an internal standard in all cases and chemical shifts are quoted in ppm (δ). Abbreviations used to denote the multiplicity of the peaks observed are defined below.

s – singlet	dd – doublet of doublets
d – doublet	ddd – doublet of doublet of doublets
t – triplet	dt – doublet of triplets
q – quartet	tt – triplet of triplets
quint – quintet	ttt – triple, triple triplet
sex – sext	m – multiplet
sept – septet	

3.1.4   Mass Spectrometry (MS)

Mass spectra were recorded on a Waters GCT premier MS-Agilent 7890A GC spectrometer (EI) or on a BrukermicrOTOF MS-Agilent series 1200LC spectrometer (ESI).

3.1.5   Infrared Spectroscopy (FT-IR)

Infrared spectroscopy was performed using a Shimadzu IR prestige-21 which was equipped with a Specac diamond ATR IR insert.

3.1.6   High-Performance Liquid Chromatography (HPLC)

High performance liquid chromatography was performed using a Shimadzu Prominence modular system, using a LC-20A liquid chromatograph, a SIL-20A autosampler, a CTO-20A column oven, a SPO-20A dual wavelength UV-Vis

detector, a CBM-20A communications bus and an Alltech C18 column (5 μm pore size, 10 x 250 mm). The detector was set at two appropriate wavelengths, which were determined from data collected from solution based UV-Vis spectroscopy experiments for each material.

3.1.7   Polarised Optical Microscopy (POM)

Thermal polarized optical microscopy (x100 magnification) was performed using a Zeiss Axioskop 40 Pol microscope and a Metter FP82HT furnace, which was controlled by a Mettler FP90 control unit. An Infinity X-21 digital camera was used to capture photomicrographs. All the photos were taken under Infinity X Capture software.

3.1.8   Differential Scanning Calorimetry (DSC)

Differential Scanning Thermograms were recorded using a Mettler DSC822^e unit operating with the Star^e software. In each case a scan rate of 10 °C min^{-1} was used. The results obtained were normalized in relation to an indium standard (onset = 156.55 $\pm$ 0.2 °C, ΔH = 28.45 $\pm$ 0.40 J g^{-1}).

3.2 Synthetic Discussion

Due to the nature of the investigations described in Chapter 7 a number of different synthetic methodologies were used to prepare different batches of compounds **11** and **12**. In general, these methods can be distinguished based upon two factors: (i) the coupling reaction used in order to introduce the 1-methylheptyl unit into the molecular architecture; and (ii) the protecting group used to protect the phenolic intermediate. These methods will be discussed in more details later in this Section.

Regardless of the method used to prepare different batches of compounds **11** and **12**, the synthetic procedure required the preparation of the biphenyl-based intermediates **2** and **4** (see Scheme 3.1). First, *O*-alkylation of 4'-hydroxybiphenyl-4-carbonitrile with 1-bromoundecane or 1-bromodecane introduced the long aliphatic chain to give biphenyl compounds **1** and **3** respectively in >90 % yield. Then, hydrolysis of the nitrile group with sulphuric acid afforded the desired carboxylic acids **2** and **4** in good (>80 %) yield after crystallization from ethanol/THF/diethyl ether (10:1:1).
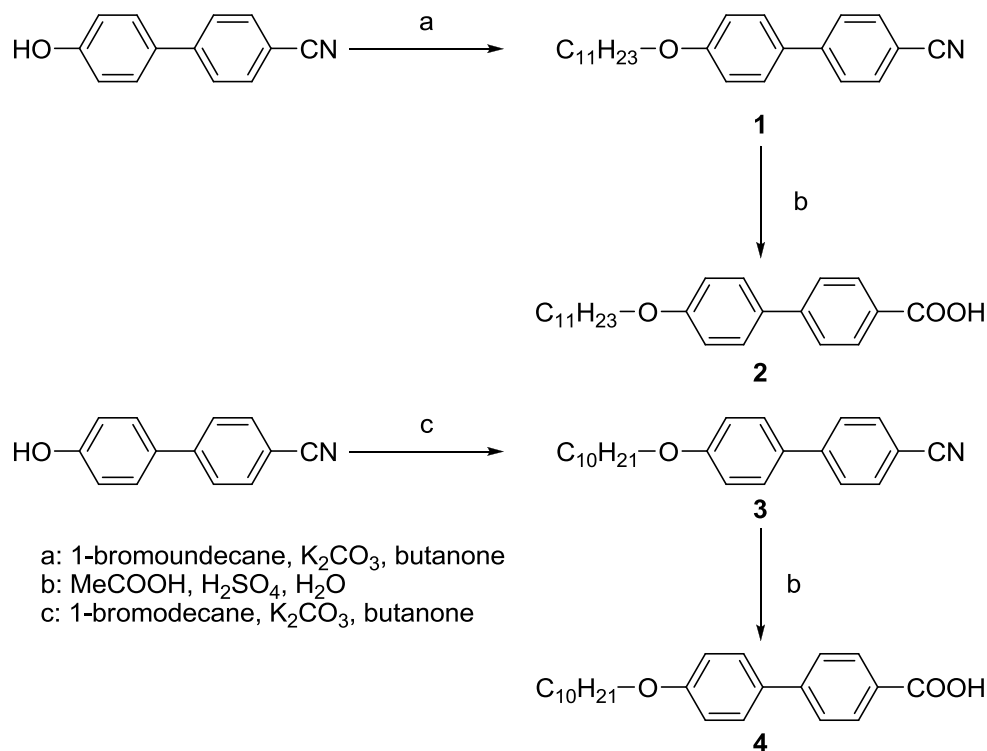
Scheme 3.1: Preparations of carboxylic acids **2** and **4**.

Next, compounds **2** and **4** were used in the preparation of compounds **11** and **12**. As mentioned previously a number of different synthetic methodologies were used to prepare these two compounds. These different routes, and the different batches of compounds **11** and **12** prepared, are detailed in the sections that follow.

3.2.1   The Preparation of Compounds 11a and 11b

The first two batches of compound **11** that were synthesized were prepared by two different methods. However, the first step in the preparation of both **11a** and **11b** involved the reduction of commercially available 2-octanone with sodium borohydride (Scheme 2). This reaction, conducted using methanol as the solvent, afforded the product, 2-octanol, as a colourless oil in quantitative yield. This batch of 2-octanol (**5**) is referred to as Oct-2 in Chapter 7. The red arrows in Scheme 2 show the methodology used in order to prepare compound **11a**. Firstly, 4-hydroxybenzoic acid was protected with methyl chloroformate to give

carboxylic acid **6** in 93 % yield after crystallization from ethanol. Then, alcohol **5** (Oct-1 which was prepared by Dr Stephen Cowling *via* the reduction of 2-octanone with sodium borohydride) was reacted with **6** under Mitsunobu reaction conditions, using DIAD as the coupling agent, to afford ester **7**. In this step it was important that the reagents were added slowly at 0 ℃ and that the reaction was allowed to warm to room temperature as a slightly different procedure was employed to investigate the impact of reaction conditions on the properties of different batches of compound **11**. Pleasingly, subsequent deprotection of the methyl ester group using ammonia gave the desired phenol **8a** in quantitative yield, ready to be coupled with carboxylic acid **2** (Scheme 3.2). Finally, the coupling reaction between phenol **8a** and carboxylic acid **2**, using EDAC**,** a catalytic amount of DMAP, and DCM as the solvent furnished compound **11a**.

The first step in the preparation of compound **11b** involved the reaction of 4-hydroxybenzoic acid with benzylbromide using aqueous potassium hydroxide and ethanol as the solvent system. This procedure afforded the carboxylic acid **9** in excellent (95 %) yield after crystallization from ethanol. The resulting benzyl protected acid was then reacted with compound **5** (Oct-1) in a Steglich esterification using EDAC as the coupling agent and a catalytic amount of DMAP, to provide the ester **10**. Deprotection of the benzyl group by treatment with 10 % palladium-on-carbon furnished the desired phenol **8b**. Finally, the Steglich esterification of **8b** with the carboxylic acid **2** gave **11b**.
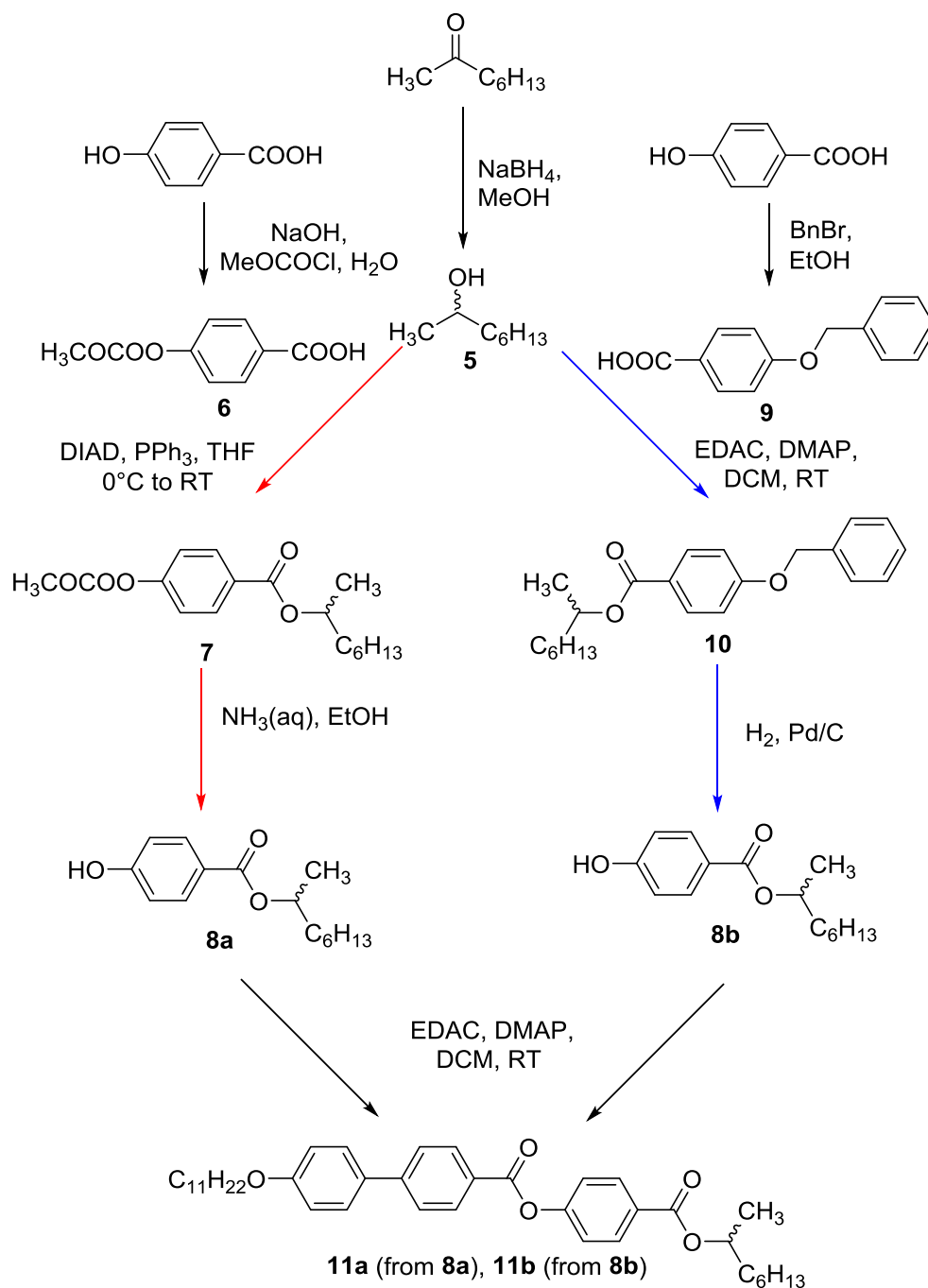
Scheme 3.2: Preparation of compounds **11a** and **11b**.

3.2.2 The Preparation of Compounds 11c and 11d

In order to further investigate the process of preparing compound **11**, and to examine the reproducibility of the properties of compound **11** with respect to the synthetic procedure used in its preparation, another four batches of compound **11**

were synthesised using the methodology presented in Scheme 3.3. These batches of compound **11** differ in the methodology used to prepare the protected esters **7c-f**. The source of 2-octanol, the conditions used for the coupling reaction used to prepare **7c-f**, and the yields associated with these reactions are shown in Table 3.1. Once **7c-f** were obtained, deprotection of the carbamate protecting group using aqueous ammonia in ethanol afforded the corresponding acids (**8c-f**) in quantitative yield. These acids were then coupled with compound **2** to give compounds **11c-f** in good yield (between 75% to 92%).
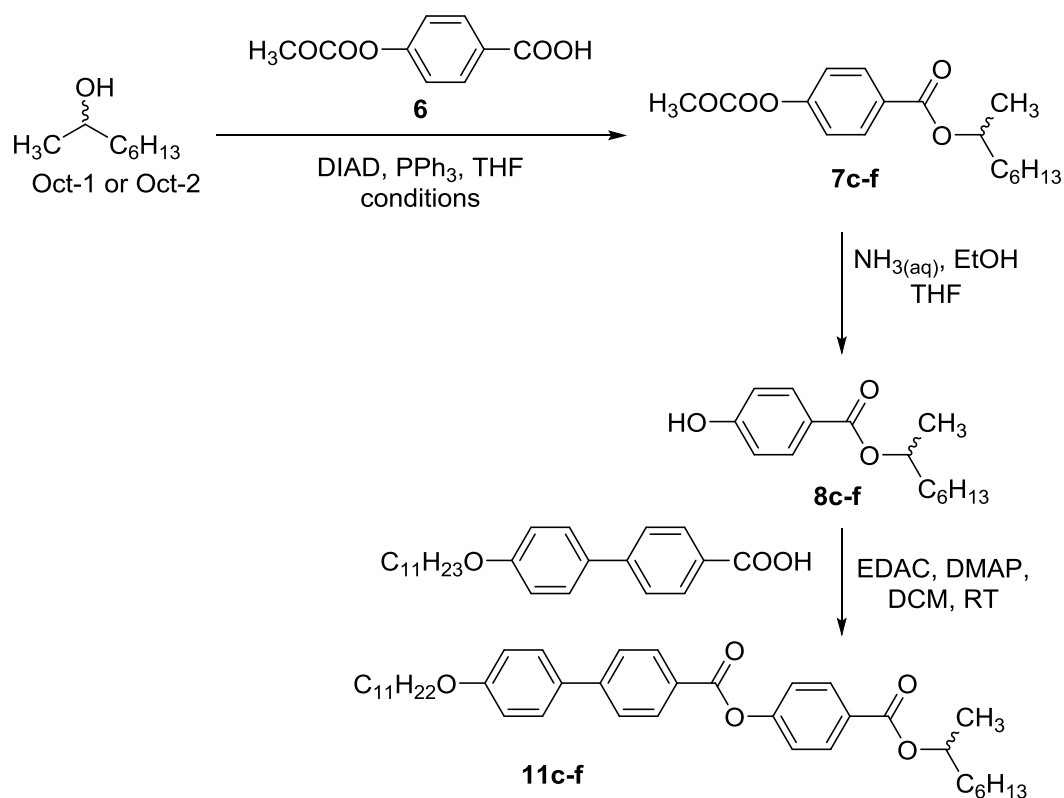
Scheme 3.3: Preparation of compound **11c –f**.

Compound	Alcohol Used	Mitsunobu Conditions	Yield (%)
7c	Oct-1	DIAD added dropwise at 0 ℃ and reaction allowed to warm to room temperature	48
7d	Oct-2	DIAD added dropwise at 0 ℃ and reaction allowed to warm to room temperature	46
7e	Oct-1	DIAD added dropwise at 25 ℃	55
7f	Oct-2	DIAD added dropwise at 25 ℃	57

Table 3.1: Details of the Mitsunobu reactions used in the synthesis of compounds **7c-7f**.

3.2.3 The Preparation of Compound 12

In order to further investigate the impact of the Mitsunobu reaction on the potential enantiomeric excess of liquid-crystalline products, different batches of compound **12** were prepared using different coupling reagents. Again, both Oct-1 and Oct-2 were used, and the reactions were carried out using the benzyl-protected phenol **9**, the synthesis of which is detailed in Scheme 3.2. The synthetic pathways to ester **12** are shown in Scheme 3.4 Generally, the key Mitsunobu reaction of alcohol **5** with carboxylic acid **9** afforded the desired esters (**10a-f**) in good to excellent yields (75-90 %).The chemical structures of the coupling agents used in are shown at the bottom of Scheme 3.4 and full details of the yields of the coupling reactions are given in Table 3.2. Deprotection of **10a-f** using hydrogen and 10 % palladium-on-carbon afforded the carboxylic acids **8a-f** in quantitative yields. Compounds **8a-f** were then coupled with compound **4** using EDAC and a catalytic quantity of DMAP in DCM, affording compounds **12a-f** in high (> 75 %) yields.
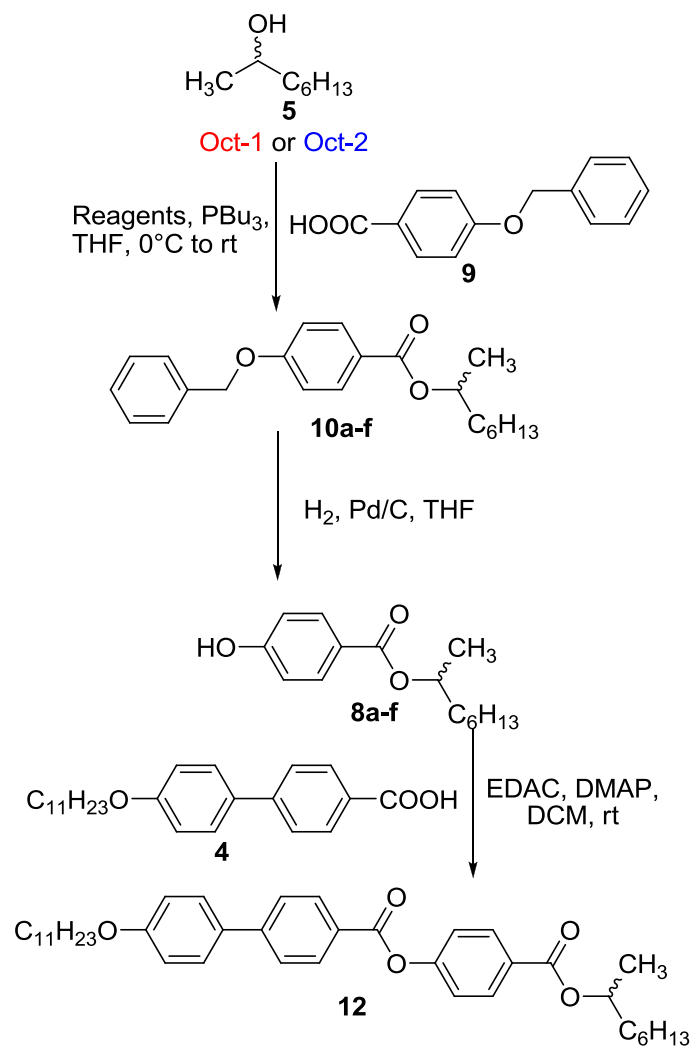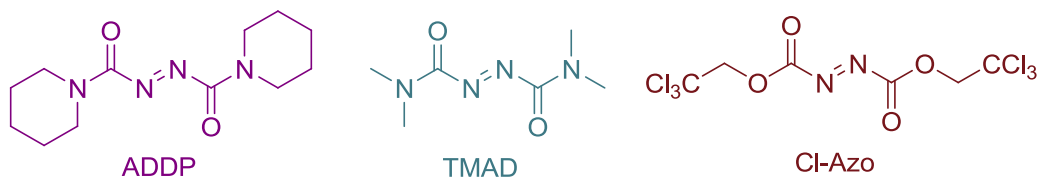
Scheme 3.4: The synthetic methodology used to prepare different batches of compound **12.**

Compound	Coupling Agent Used	Alcohol Used	Yield (%)
10a	ADDP	Oct-1	49
10b	ADDP	Oct-2	52
10c	TMAD	Oct-1	41
10d	TMAD	Oct-2	31
10e	Cl-Azo	Oct-1	81
10f	Cl-Azo	Oct-2	62

Table 3.2: Details of the Mitsunobu reactions used in the synthesis of compounds **10a-10f**.

3.3 TN Cells and Preparation of Mixtures

All of the TN cells used in this thesis were supplied by AWAT through the Military University of Technology in Warsaw, Poland. The cells were stated as being 14.4 μm thick but were checked, and used as supplied. The general structure of a TN cell is shown in Figure 3.1. A TN cell is constructed from two pieces of glass, which are held together by optical glue. The inner surface of both pieces of glass are coated by a polymer, which is treated so as to give homogeneous alignment of a nematic liquid crystal. The alignment direction of the top piece of glass is rotated 90 degrees relative to the lower piece, giving a twist in the director field of a nematic liquid crystal. To ensure a uniform thickness a number of spacers are placed between the two glass plates. Fortunately for this work, these spacers often help to act as archoring points for the disclination lines in the nematic phase when the cell is filled. The small holes either side of the cell are to allow filling with a target material and the escape of air from the cell during filling.
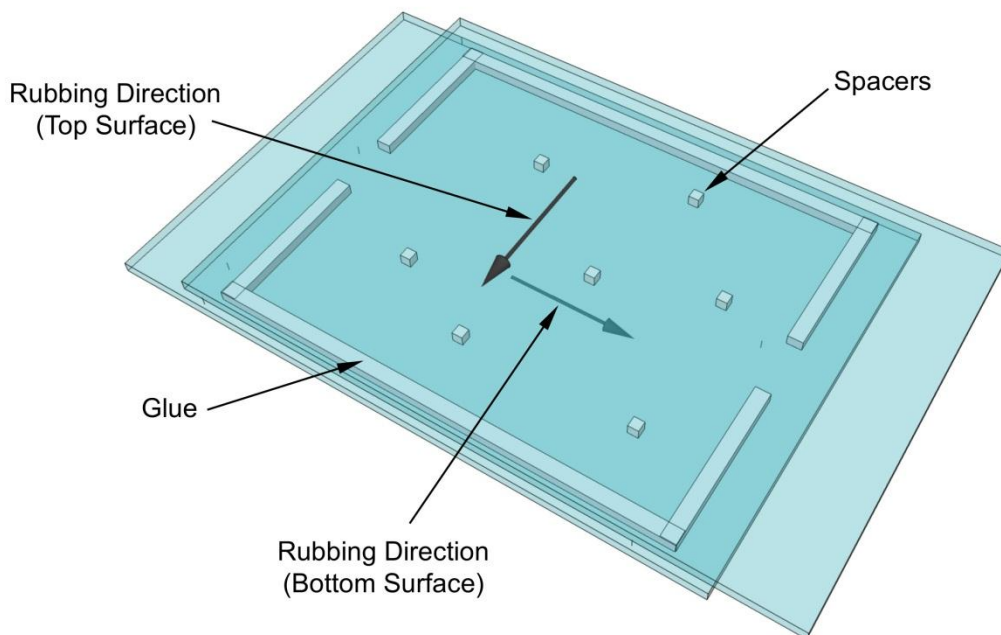
Figure 3.1: Cartoon depiction of the general structure of a TN cell.

Of the mixtures to be prepared, the majority are only required in very low concentration. For instance, if 5 mg total weight of a mixture is required at dopant concentration of 0.012 %, then only 0.0006 mg, or 600 ng of dopant are required. It is impossible weight in such small amounts without specialist equipment for weighing and dispensing small quantities of material. Thus, the best solution for preparing mixtures was that mixtures be prepared on larger scale between 50 mg to 200 mg, depending on the minimum concentration required for a given experiment. By weighing out small quantities of the dopants and accurately diluting them to give a stock solution, it was possible to prepare low concentration mixtures with high accuracy.

Specifically, by weighing out around 1 mg of a given dopant into a small vial, then dissolving into 1 ml of DCM it was possible to use a microsyringe (1 μl) to transfer the dopant into E7 host with high accuracy. The host/dopant solution mixture was dissolved into 2 ml of DCM to ensure that the dopant and E7 host were all dissolved in one homogenous phase. The vial was placed into an ultrasonic water

bath for 30 seconds to agitate the solution and ensure good mixing. The vial was then left at 60 ℃ overnight to remove all DCM from the mixture. TN cells were filled *via* capillary forces. By using a pipette to transfer one or two droplet at the edge of TN cell, which had been preheated to about 60 ℃, a droplet of the mixture would become an isotropic liquid. The lower viscosity of an isotropic liquid vs a nematic phase aids the filling of the cell. After each TN cell was filled, it was moved on a glass plate, allowed to cool and left overnight to make sure all the disclination lines had become stable.

3.4 Method to Measure the Radius of Curvature

Once the mixtures were successfully filled into TN cells and suitable disclination lines were obtained through slowly cooling the sample into the nematic phase from the isotropic liquid, the radius of curvature of several (5-10) disclination lines were measured and an average value determined. Typically, the disclination lines were pinned between two spacers within the cell, as shown in Figure 3.2. In order to determine the radius of curvature, photomicrographs depicting the relevant disclination lines were printed and a straight line terminating at two points of the disclination line was drawn. It should be noted at this point that this line is effectively a chord of the circle extrapolated from the curved disclination line (see the red line in Figure 3.2). From this chord line the lengths a and b shown in Figure 3.2 can be determined and it can be stated that distance from the central point of the circle to the chord is given by r-b, where r is the radius of the extrapolated circle *i.e.* the radius of curvature. Furthermore, as shown in Figure 3.2, the radius of curvature can be defined as the hypotenuse of a triangle with sides a and r-b respectively, as shown in Figure 3.2.
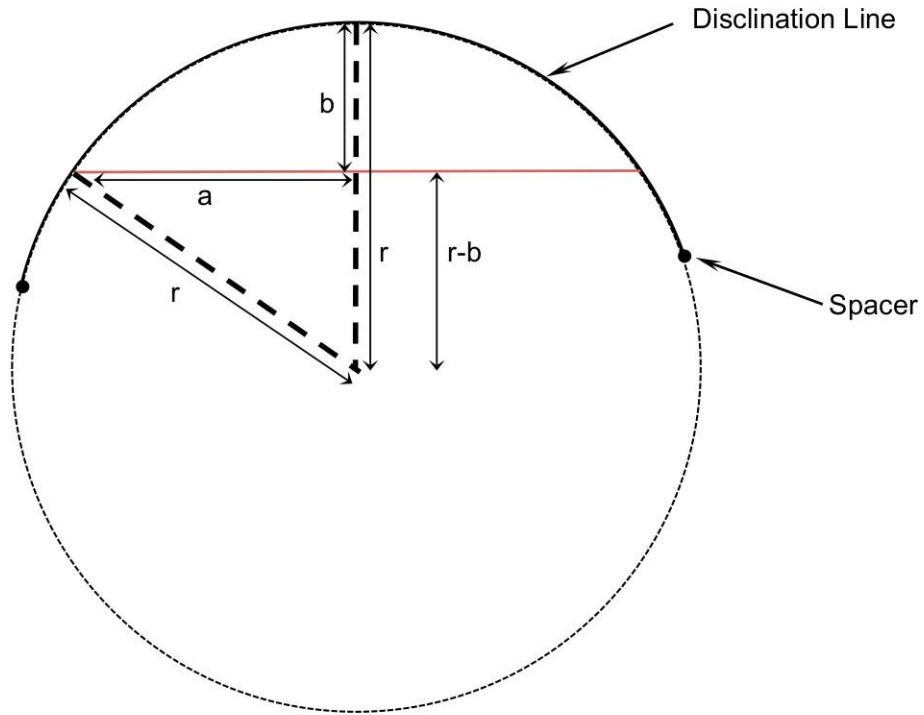
Figure 3.2: Schematic representation of the parameters used in the determination of the radius of curvature.

Therefore, from Pythagorean theory the following relationship can be determined:

$$r^2 = a^2 + (r - b)^2 \qquad (9)$$

and it can therefore be deduced that:

$$2rb = a^2 + b^2 \qquad (10)$$

and hence:

$$r = \frac{a^2 + b^2}{2b} \qquad (11)$$

Therefore, from the measurements of the lengths a and b made from print-outs of photomicrographs showing disclination lines for a given mixture or material, the radius of curvature r could be determined using equation 11, regardless of the position of the chord line that was selected.

Chapter 4. Results and Discussions

4.1 Standardization of detecting helical twisting power of chiral dopants *via* 'the reverse-twist disclination line method'

As previously noted the "reverse twisted disclination line method" was invented by Raynes,[5] who also used this method to investigate CB15, allowing its helical twisting power (HTP) to be measured. Therefore, CB15 has become a standard compound for investigations of other materials utilizing the "reverse twisted disclination line method" to determine HTP. .

The helical twisting power value of CB15 has been measured *via* the Grandjean-Cano wedge and photo-aligned axially symmetric liquid crystal films, both of which are standard techniques for determination of HTP values.[124] Therefore, at the start of the research that underpins this thesis, it was deemed worthwhile using the "reverse twisted disclination line method" for evaluating CB15 again before testing other dopants. In this way the reproducibility was confirmed, thereby establishing a standard procedure when using the "reverse twisted disclination line method".
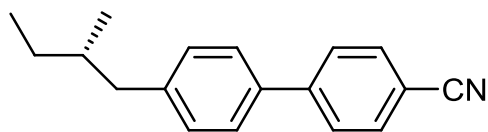
Figure 4.1: The chemical structure of the chiral dopant (*S*)-4-(2-methylbutyl)-4'-cyanobiphenyl (CB15).

In the previously published work by Raynes the concentration range of CB15 in E7 was between 0.0013% to 0.012 %.[5] In this work mixtures of CB15 in E7 were prepared with concentrations ranging from 0.002527% to 0.01212%, close to

those values originally used. Photomicrographs showing the disclination lines formed by mixtures of CB15 and E7 at various concentrations are shown in Figure 4.2.

(a)   (b)   (c)

(d)   (e)   (f)

(g)   (h)   (i)

(j)   (k)   (l)
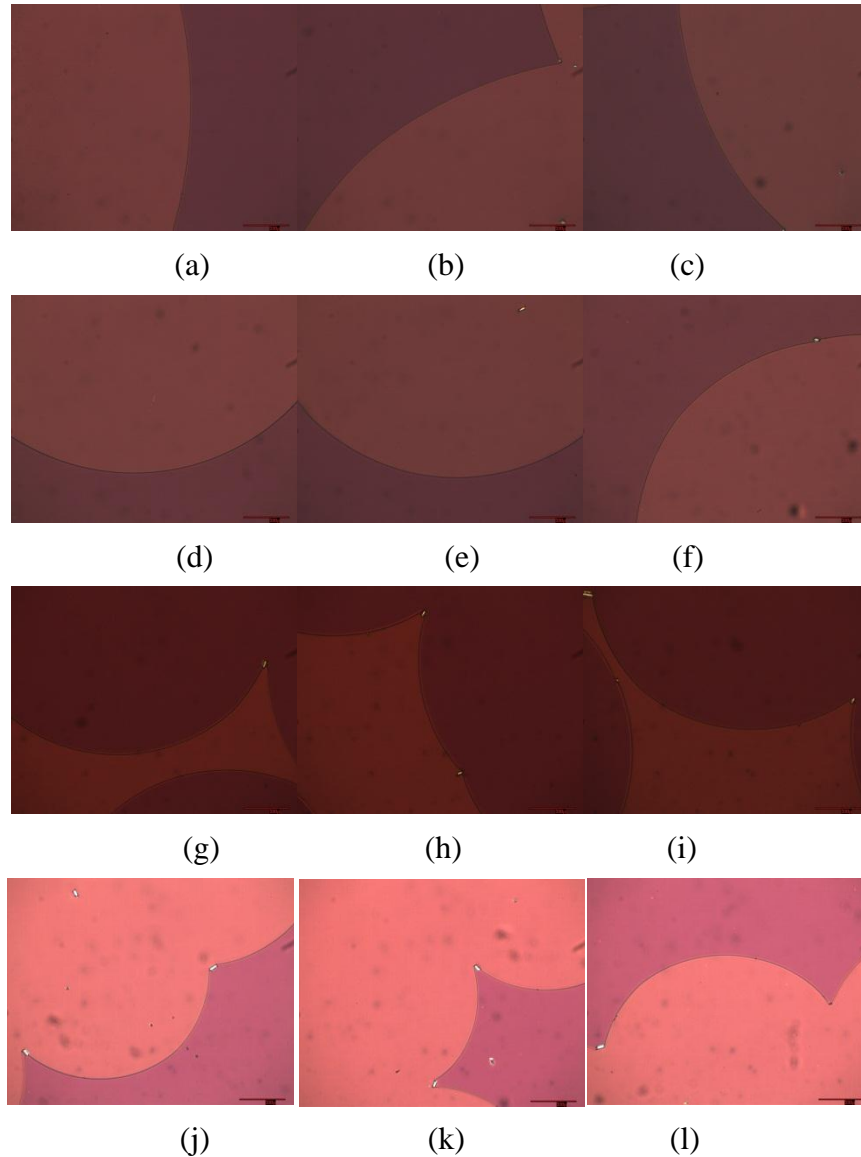
Figure 4.2: Photomicrographs (x50) showing the reverse-twist disclination lines formed in 14.4 µm thickness TN cells at concentrations of CB15 in E7 for (a)-(c) 0.002527 wt%; (d)-(f) 0.005342 wt%; (g)-(i) 0.007406 wt% and (j)-(l) 0.01212 wt%.

The disclination lines became more curved when the concentration was increased as shown in Figure 4.2 Plates ((j)-(l)) appear lighter than the others due to the backlight of microscope being adjusted, it should be noted that this does not influence the measurements.

The radii of curvature of disclination lines in each concentration were calculated as shown Table 4.1

Concentration (wt%)	Radii of curvature (µm)	Reciprocal of Radii (1/µm)
0.002527	1663	0.000601
0.005342	951	0.001052
0.007406	715	0.001398
0.01212	456	0.002193

Table 4.1: The concentrations, radii of curvatures (µm) and reciprocal of the radii (1/µm) of CB15 in E7.

In order to calculate the helical twisting power of CB15, a plot of the reciprocal radius of curvature as function of concentration in E7 for CB15 was created, the result being given in Figure 4.3. From the gradient of the linear relationship, the HTP of CB15 in E7 was determined to be $8.34 \mu m^{-1}$.
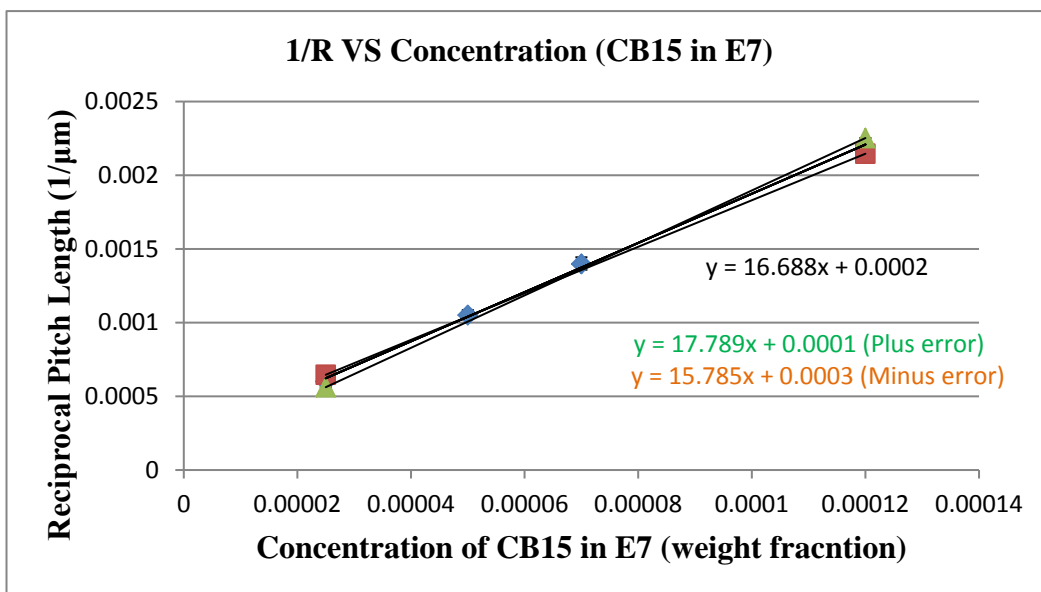
Figure 4.3: A plot of 1/R versus concentration for CB15 in E7.

In Figure 4.3, all of the experimental results fit very well to the best linear fit to the data, the R ^{2}of the slope was determined to be 0.9998, *i.e* nearly a perfect fit. The HTP value was determined to be 8.34 µm^{-1}. The green number is the plus error, and orange number is the minus error. Thus the results with error is 8.34±1.00µm^{-1}, which compares well with the literature value, measured using the same method, of 9.3 µm^{-1}.[5] Interestingly, the HTP of CB15 was reported as 7.17 µm^{-1} as measured using the axially symmetrical LC film, whereas another literature report gave as approximately 8 µm^{-1}.[124,125] Furthermore, the value was reported to be 8.8 µm^{-1} when measured using the Grandjean-Cano wedge method.[5]

Thus, the result of 8.34 µm^{-1} appears to be in reasonable agreement with other published works, and therefore the experimental technique of using the "reverse twisted disclination line method" to determine HTP can be trusted to give accurate results. Additionally, the methodology of preparing mixture and measuring the radii of curvature, which described in experimental section, is appropriate and accurate, as demonstrated by the high R^2 value. In terms of sensitivity curved disclinations lines can be seen, and the radii of curvature measured, at levels of

0.001 wt%, i.e 1 in 100,000 (1 gm in 100 kilos). Thus for the chiral dopant CB15, 2.5 g in 100 kg of E7 will give a pitch length of 3.2 mm, which can be measured.

4.2 Studies of Oxazoline-based Chiral Dopants in the E7 Nematic Host

Oxazoline-based chiral dopants have been shown to be capable of inducing blue phases and TGB phases when doped into achiral liquid-crystalline host mixtures.[126] Given the recent interest in blue phase liquid crystal displays, these materials, and the mechanism by which they promote the formation of blue phases, are of particular interest. Thus, in order to gain an insight into the chiral induction properties of oxazoline-based dopants, the chiral dopant AE8 (see Figure 4.4) was doped into E7 in order to determine its helical twisting power *via* 'the reverse-twist disclination line method'.[5] Photomicrographs showing the disclination lines formed by mixtures of AE8 and E7 at various concentrations are shown in Figure 4.5.
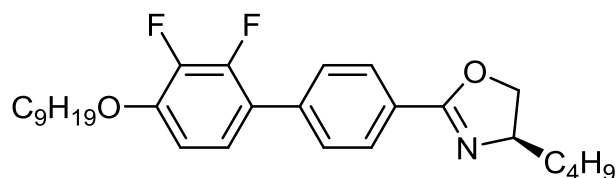
Figure 4.4: The structure of the chiral oxazoline-based material AE8.
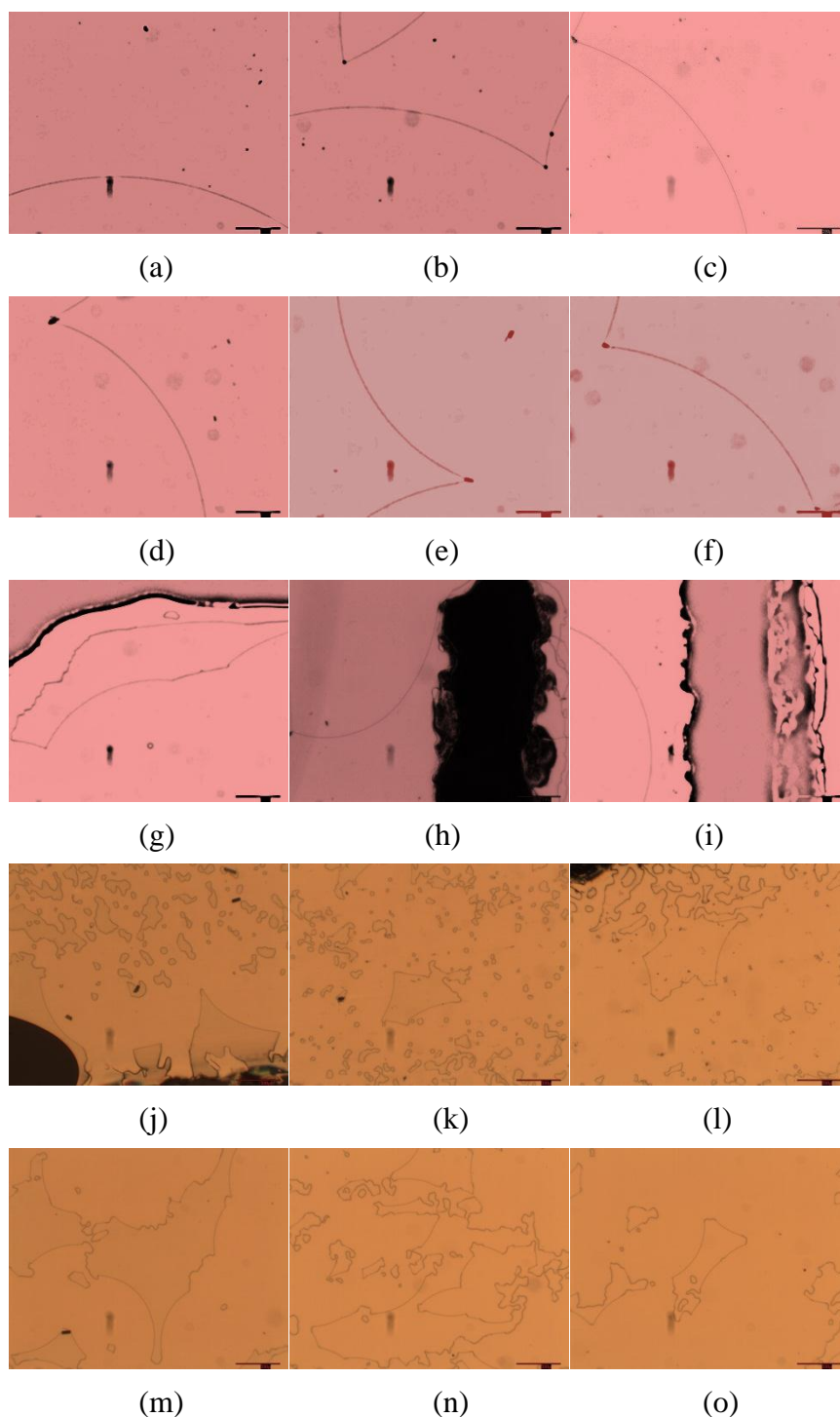
Figure 4.5: Photomicrographs (x50) showing the reverse-twist disclination lines of the mixtures of AE8 in E7 formed in 14.4 μm thickness TN cells at a concentration of (a)-(c) 0.008536 wt%;(d)-(f) 0.01088 wt%; (g)-(i) 0.02168 wt% of AE8; (j)-(l) 0.03311 wt% of AE8; and (m)-(o) 0.04335 wt%.

It can be seen from the photomicrographs presented in Figure 4.5, the radii of curvature of the disclination lines formed by mixtures of AE8 in E7 decreases with

increasing concentration of the chiral dopant. In addition, it is clear from Figure 4.5 (m-o) that when the radii of curvature becomes approximately equal to 200 μm, the measurement is reaching the limitation of the method because the disclination lines begin to form closed disclination loops rather than curves. The calculated radii of curvature at the concentrations investigated are presented in Table 4.2 and are shown graphically in Figure 4.6. It can be seen from Figure 4.6, there is a linear relationship of the reciprocal pitch length as a function of concentration. The slope of the trend line fitted to this linear relationship is 8.9383 and therefore the HTP is 4.47 μm^{-1}.[5]

Concentration (wt%)	Radii of curvature (μm)	Reciprocal of Radii (1/μm)
0.008536	1126	0.000812
0.01088	1231.2	0.000888
0.02168	510.6	0.00196
0.03311	335.4	0.00298
0.04335	260	0.00385

Table 4.2: The concentrations, radii of curvatures and reciprocal of radii of AE8 in E7.
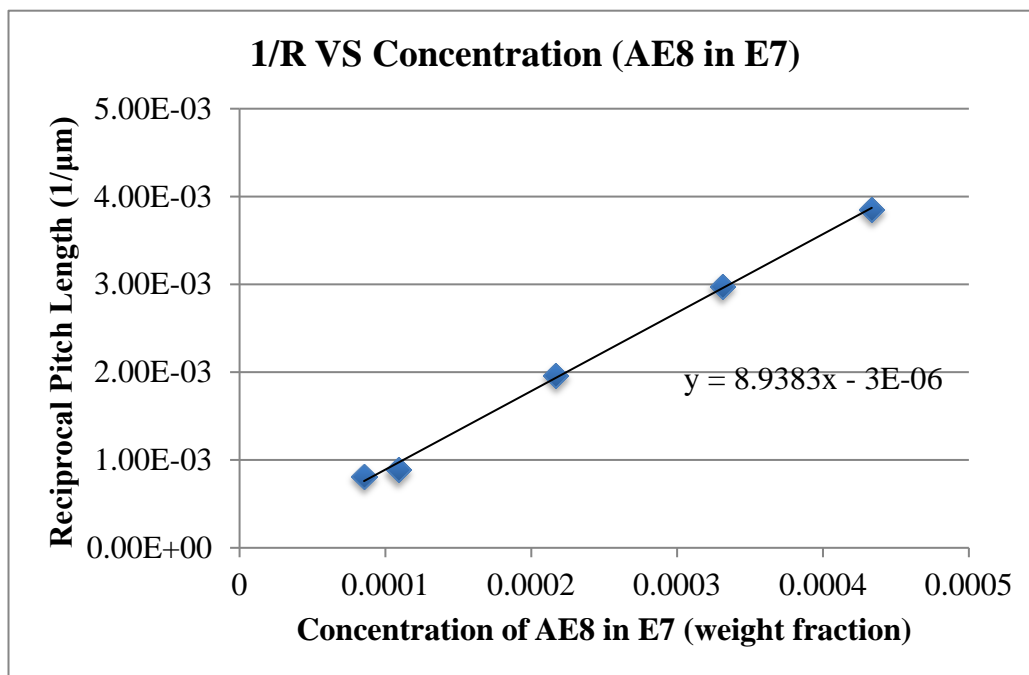
Figure 4.6: The slope of 1/R VS concentration for AE8 in E7.

In order to further investigate the chiral induction properties of chiral oxazoline-based materials, mixtures of AE14 and AGML74 (see Figure 4.7) in E7 were prepared and analysed using the methodology described for AE8 above. It can be seen from Figure 4.7, AE14 has a similar chemical structure to that of AE8, with the difference being that one of the phenyl rings has been replaced by a pyrimidine ring. Conversely, AGML74 contains an isopropyl functionality at the stereogenic centre and a biphenyl ring system. Photomicrographs showing the resulting reverse-twist disclination lines for these mixtures are shown in Figure 4.8 and Figure 4.9 respectively, and plots showing the variation in the reciprocal pitch length as a function of concentration are shown in Figures 4.10 and 4.11 respectively.
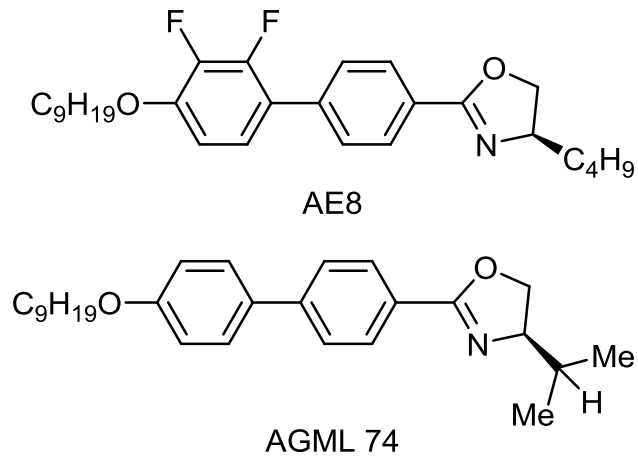
Figure 4.7: The chemical structure of AE14 and AGML74

(a)   (b)   (c)

(d)   (e)   (f)

(g)   (h)   (i)
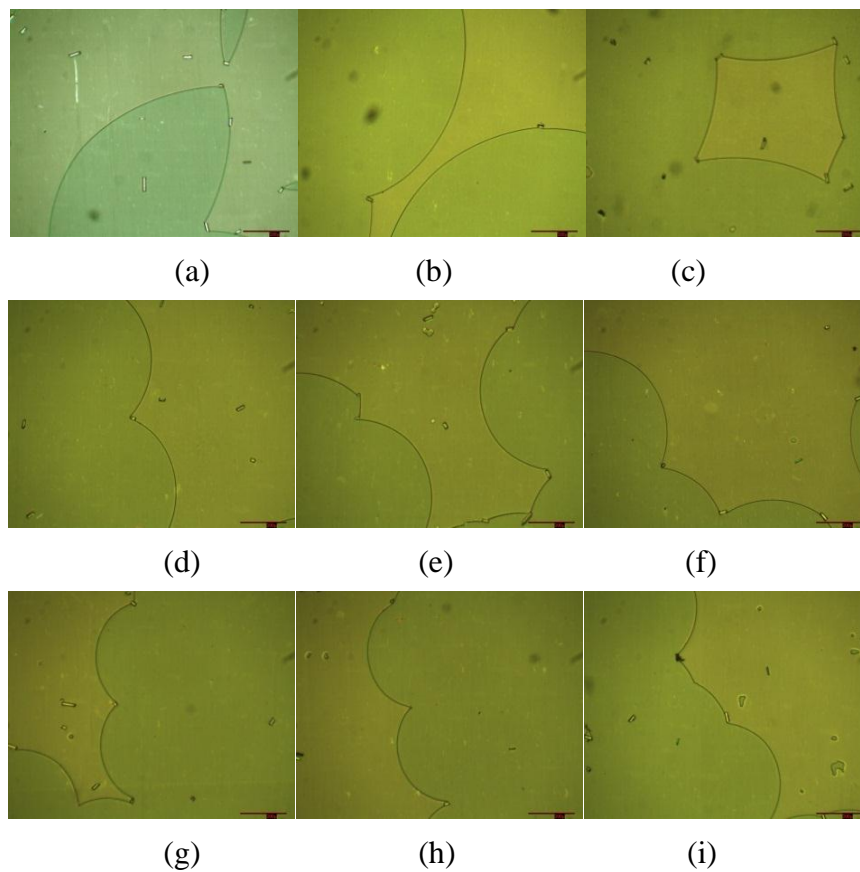
Figure 4.8: Photomicrographs (x50) showing the reverse-twist disclination lines of the mixtures of AE14 in E7 formed in 14.4 μm thickness TN cells at a concentration of (a)-(c) 0.03765wt% ;(d)-(f) 0.06835wt%; (g)-(i) 0.09252wt%.
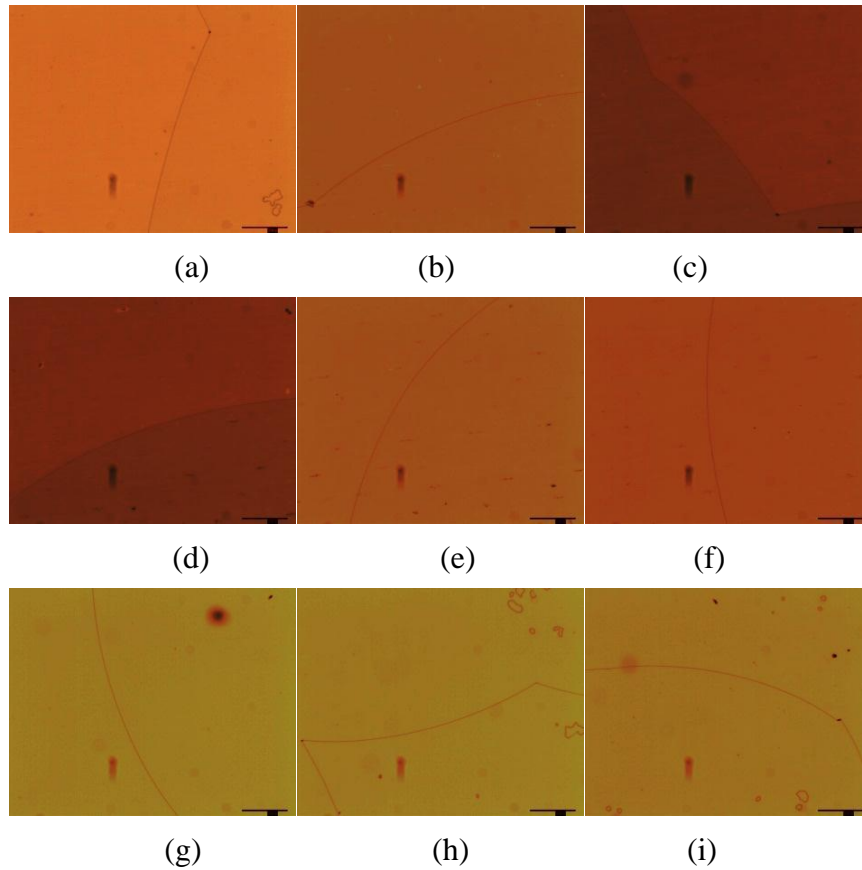
Figure 4.9: Photomicrographs (x50) showing the reverse-twist disclination lines of the mixtures of AGML74 in E7 formed in 14.4 μm thickness TN cells at a concentration of (a)-(c) 0.05217wt% ;(d)-(f) 0.06366wt%; (g)-(i) 0.08445wt%.
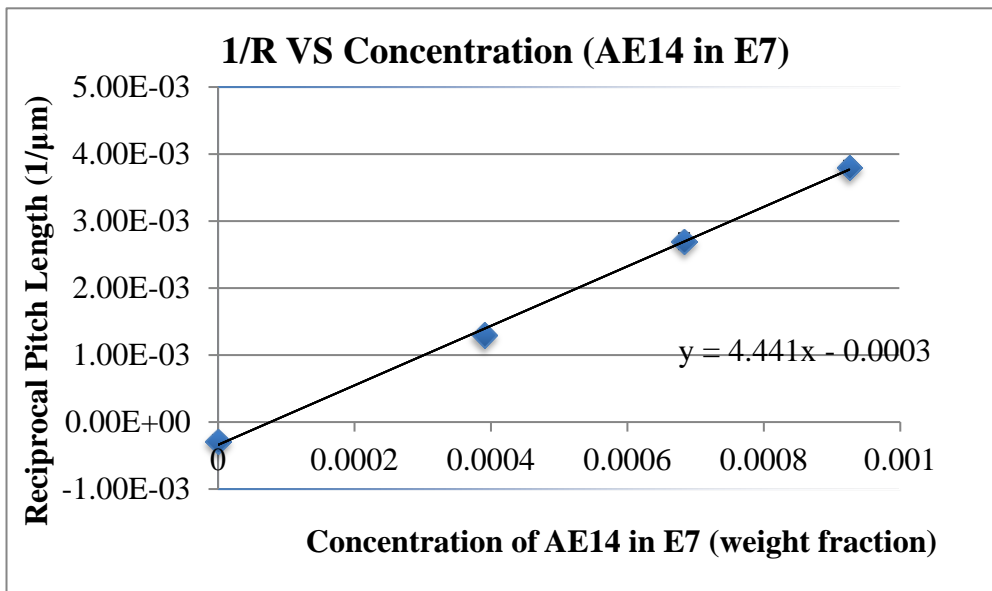
Figure 4.10: The slopes of 1/R VS Concentration AE14 in E7.
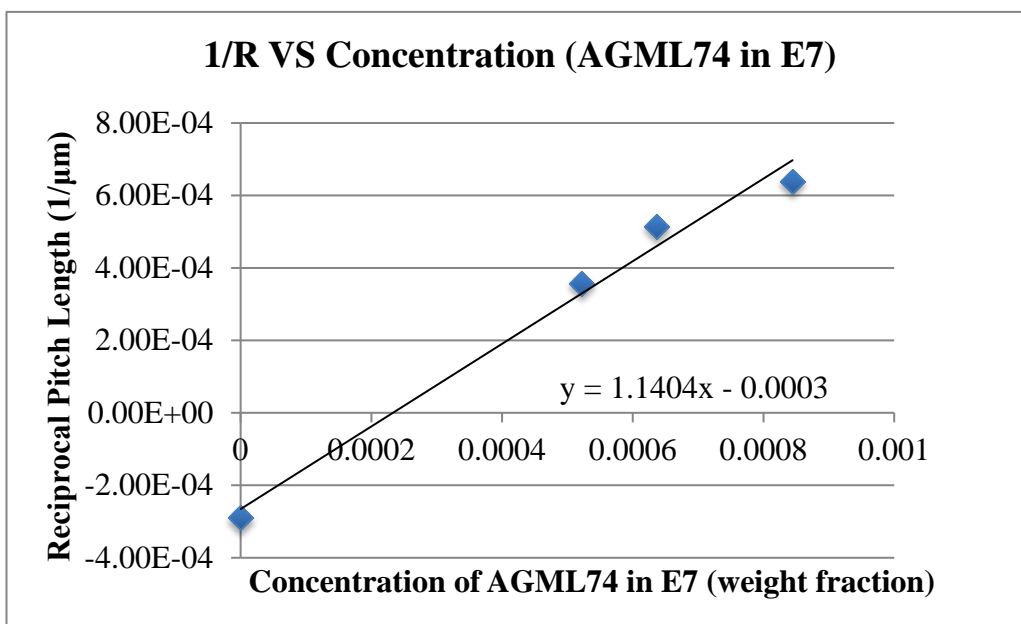
Figure 4.11: The slopes of 1/R VS Concentration AGML74 in E7.

It can be seen from the photomicrographs presented in Figure 4.8 and Figure 4.9, the radii of curvature of the disclination lines formed by mixtures of AE14 and AGML74 in E7 decreases with increasing concentration of the chiral dopants. As expected, the plots of the reciprocal pitch length as a function of concentration for both AE14 and AGML74 in E7 show a linear relationship, as shown in Figures 4.10 and 4.11 respectively. The zero data point for undoped E7 is negative in both cases, which will be discussed later. The calculated HTPs for the two dopants, alongside the HTP of AE8 for comparison, are shown in Table 4.3.

Materials in E7	HTP (μm^{-1})
AE8	4.47
AE14	2.22
AGML74	0.57

AE8
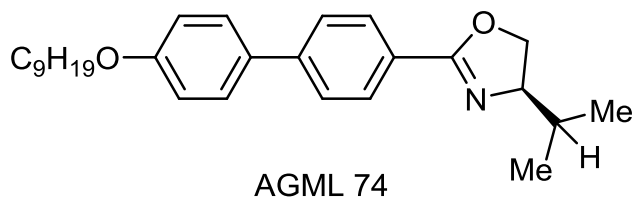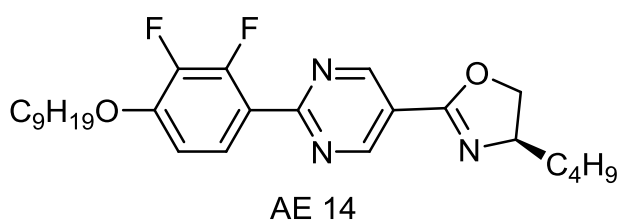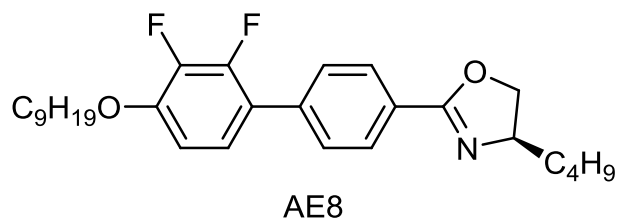
AE 14

AGML 74

Table 4.3: The helical twisting power of AE8, AE14 and AGML74 in E7.

It can be seen from Table 4.3, that the helical twisting powers (HTPs) of the three chiral dopants are very different. AE8 has the largest HTP value, which is 4.47μm^{-1}, the HTP of AE14 is in the middle, and AGML74 has the smallest value. Thus, it is clear from these results that AE8 is better able to transfer molecular chirality to the nematic host E7 than either AE14 or AGML74. Although trends regarding the variation of HTP as a function of molecular structure have been investigated for some systems, it is often difficult to identify the specific relationships between molecular structure and HTP.[127,128] However, it is interesting to consider the factors that may be responsible for the variation in HTP in AE8, AE14 and AMGL74. It is known that the HTP should increase if the chiral dopant material is more compatible with the liquid crystal host. The molecular

lengths, determined using Gaussian 09, of AE8, AE14 and AGML74 are very similar (24.63 Å, 25.56 Å and 23.45 Å respectively), thereby suggesting that this is probably not the main factor influencing the HTP.[129] A comparison of the minimized energy conformations of the three dopants (Figure 4.12) reveals that AE8 favours a twisted conformation of the biphenyl unit due to steric repulsion between the substituents on the two phenyl rings. Conversely, the presence of the hetrocyclic ring in the AE14 system, allows the phenyl ring and the pyrimidine ring to be coplanar. It is therefore tempting to suggest that the AE8 has a higher HTP because it favours a twisted conformation. However, the minimum energy conformation of AGML74 is also twisted, but this material has the lowest HTP of the three dopants studied, thereby suggesting that although molecular conformation is likely to play role, the relationship between HTP and molecular structure in these materials is not this simple.

Another factor that may play a role in the difference in HTP values between the three materials is their polarity. As can be seen from Figure 4.12, which shows the charge density of the minimized energy conformers of AE8, AE14 and AGML74, that AE14 possesses more polar functionalities than AE8, which, in turn, is more polar than AGML74. Hence, there is no clear relationship between the overall polarity of the molecular architectures and the values of the HTPs in this series.

There are no clear trends in this series and it therefore seems that the relationship between molecular structure and HTP is complex, and may depend upon the relative balance between many competing factors, such as polarity, shape, conformational stability, electrostatic interactions etc. For example, there are two fluorine atoms in a phenyl ring in AE8 and AE14, which could affect the HTP values. Fluorine is the most electronegative element and thus is a strong electron withdrawing group, which induces more electrostatic potential in AE8 and AE14 than for the corresponding AGML74. In addition, the lateral fluorine atoms would

make rod like molecules have stronger lateral interactions, which might be expected to leads to a more ordered packing of the molecules for AE8 and AE14 than AGML74.[130] However, in E7 the three dopants will interact with the host, breaking up the pairwise interactions between the cyanobiphenyl and cyanoterphenyl based systems, thereby reducing the dipole-dipole interactions. The lateral-fluoro substituted materials will probably repel the host and thereby stabilize the formation of the nematic phase, whereas the non-fluorinated material would enable easier formation of an ordered structure. Thus, this analysis tends to conclude that AGML74 would have the lowest value of the HTP, which is the result observed.
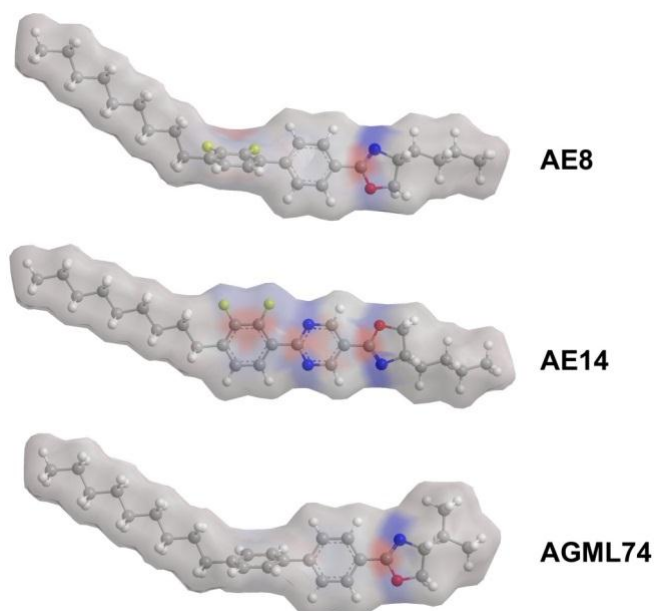
Figure 4.12: Minimized energy conformations and charge density surfaces of AE8, AE14 and AGML74. Geometry optimisation and charge density calculations performed using the MMFF94 force field as implemented in Chem3D.

Although AGML74 has the smallest HTP value there is also a very interesting observation that has been made on a material based on its structure. When the *iso*-propyl unit is replaced with a *tert*-butyl group attached to the stereogenic centre, see Figure 4.13, in a mixture with an achiral host it was found to exhibit a blue phase and TGB$_A$ phase as shown by Goodby and co-workers.[131] This result

suggests that for compounds to exhibit blue phase high HTP values may not be a prerequisite.[132] Alternatively it may be because the tertiary butyl group has a fixed non-flexible arrangement lateral to the oxazoline ring, and it is the projection of this group off the molecular long axis that causes the local molecular packing to form a twisted arrangement.
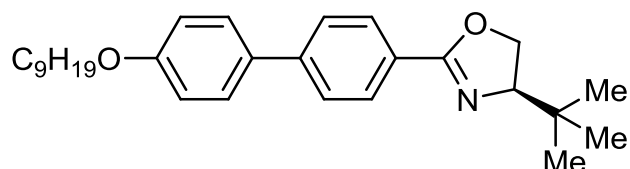
Figure 4.13: The structure of the compound which exhibit TGB$_A$ and blue phase.

4.3 Detection of Optically Active Drugs (Thalidomide) in the E7 Nematic Host

4.3.1   Chirality and Medicine

Enantiomers of a chiral drug have identical physical and chemical properties in an achiral environment. In a chiral environment, however, one enantiomer may display different chemical and pharmacological behaviour compared with the other enantiomer. More than half of the drugs on the market are chiral compounds and about 50% of these are racemates rather than single enantiomers.[133] Because living systems are chiral themselves, each enantiomer of a chiral drug molecule can potentially behave very differently *in vivo*. There is an increase in the desire for enantiomeric purity in synthesized drugs because often the distomer, the enantiomer that does not produce the desired biological effect, can in fact not only be of no use but can also have side effects. For example, penicillamine exists as (*S*)-penicillamine and (*R*)-penicillamine (see Figure 4.14). It is the (*S*)-isomer that is active toward the treatment of Wilson's disease, a defect in the body's ability to

97

metabolize copper, since it can bind with copper strongly. In contrast, the (R)-isomer can cause blindness and is toxic.[134]

(S)-Penicillamine   (R)-Penicillamine
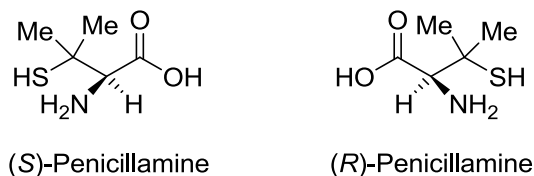
Figure 4.14: Chemical structures of the two enantiomers of penicillamine.

Thalidomide, see Figure 4.15, was responsible for one of the most notorious drug-safety issues of the 20th century. Thalidomide was synthesized first by the drug company called CIBA in 1954.[135] At the time, thalidomide was very useful as a sedative/tranquiliser and especially for treating pregnant women experiencing morning sickness, which made it popular and it was used worldwide under 37 different trade names.[136,137,138] However, since there is a stereogenic centre present in thalidomide, each enantiomer has very different function and effect when *in vivo*. Unfortunately, thalidomide created an irreversible problem for the newborn baby whose mother took thalidomide during their gestation. Thalidomide was proved to lead to congenital defects in bones and organs of infants.[137] Due to these adverse and irreversible effects, thalidomide was banned in Europe and Canada in the 1960s.[139] After 30 years, in 1998 thalidomide came back to the market as a drug for the treatment of erythema nodosum leprosum lesions.[138] Scientists discovered that the (S)-(-)-thalidomide potently inhibits release of tumour necrosis factor (TNF) α from periphera mononuclear blood cells. The (R)-(+) thalidomide could react with the forebrain's sleep receptors, which would cause sedative properties.[140]

(*R*)–Thalidomide   (*S*)–Thalidomide
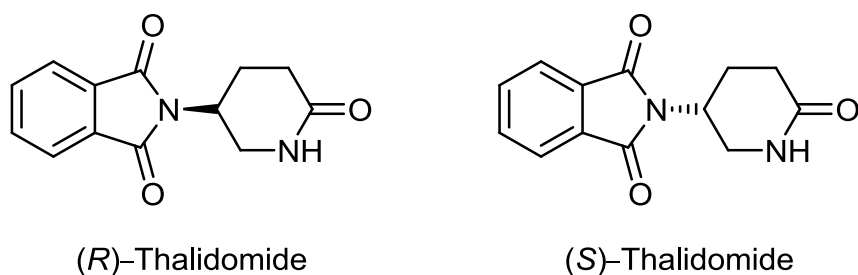
Figure 4.15: The chemical structures of the two enantiomers of Thalidomide.

Despite the disaster caused by thalidomide, researchers found thalidomide still has potential value for use in the treatment of cancers such as myeloma and also for various inflammatory diseases.[141,142] Thus, it is very important for quality control purposes to be able to detect the enantiomeric excess for thalidomide and other drugs. Furthermore, it is interesting to determine the helical twisting power of chiral drugs *via* 'the TN reverse-twist disclination method'.

4.3.2 Studies of (*R*)-(+)-Thalidomide in E7 Nematic Host

In order to compare with the oxazoline-based chiral dopants' results, mixtures of thalidomide in E7 were prepared and analysed using the same methodology and TN cells as described previously. Although thalidomide is soluble in dichloromethane, the solubility in E7 was unknown. Thus, a small amount of thalidomide was dissolved in E7.

The disclination lines obtained were examined by polarized light microscopy (x50), and the photomicrographs are shown in Figure 4.16. It can be clearly observed that the disclination lines are curved, which means that (*R*)-(+)-thalidomide is soluble in E7 at a concentration of only 0.002374 wt%, which is comparable with the disclination line of AE8 in E7, at a concentration of 0.008536 wt%. The radii of the curvature are very similar; they are 1196 μm for

(R)-(+)-thalidomide, and 1231 μm for AE8, respectively. Therefore, this suggests that (R)-(+)-thalidomide might have a greater HTP than AE8 in E7.

| (a) | (b) | (c) |
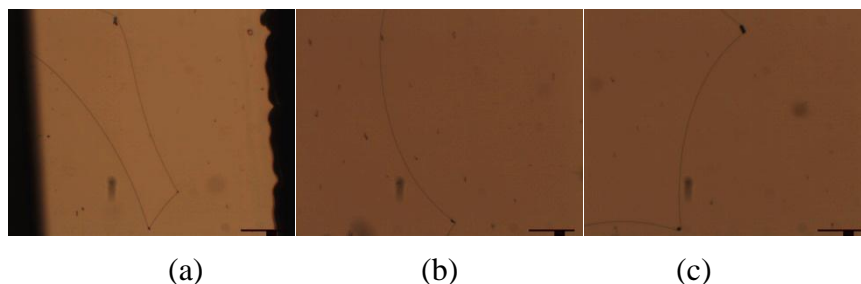
Figure 4.16: (R)-(+)-Thalidomide in E7 mixture at a concentration of (a)-(c) 0.002374 wt%.

In order to obtain the helical twisting power value of (R)-(+)-thalidomide, the concentration of (R)-(+)-thalidomide in E7 was increased. In Figure 4.17, pictures (a)-(c) show that the disclination lines do not curve very much, however, with increasing the concentration, the disclination lines becoming increasingly bent. When comparing the pictures (d)-(f) with (a)-(c), the disclination lines become more curved and more lines form in the cell. Consequently, the radii of curvature for different concentrations were measured. These are shown in Table 4.4.
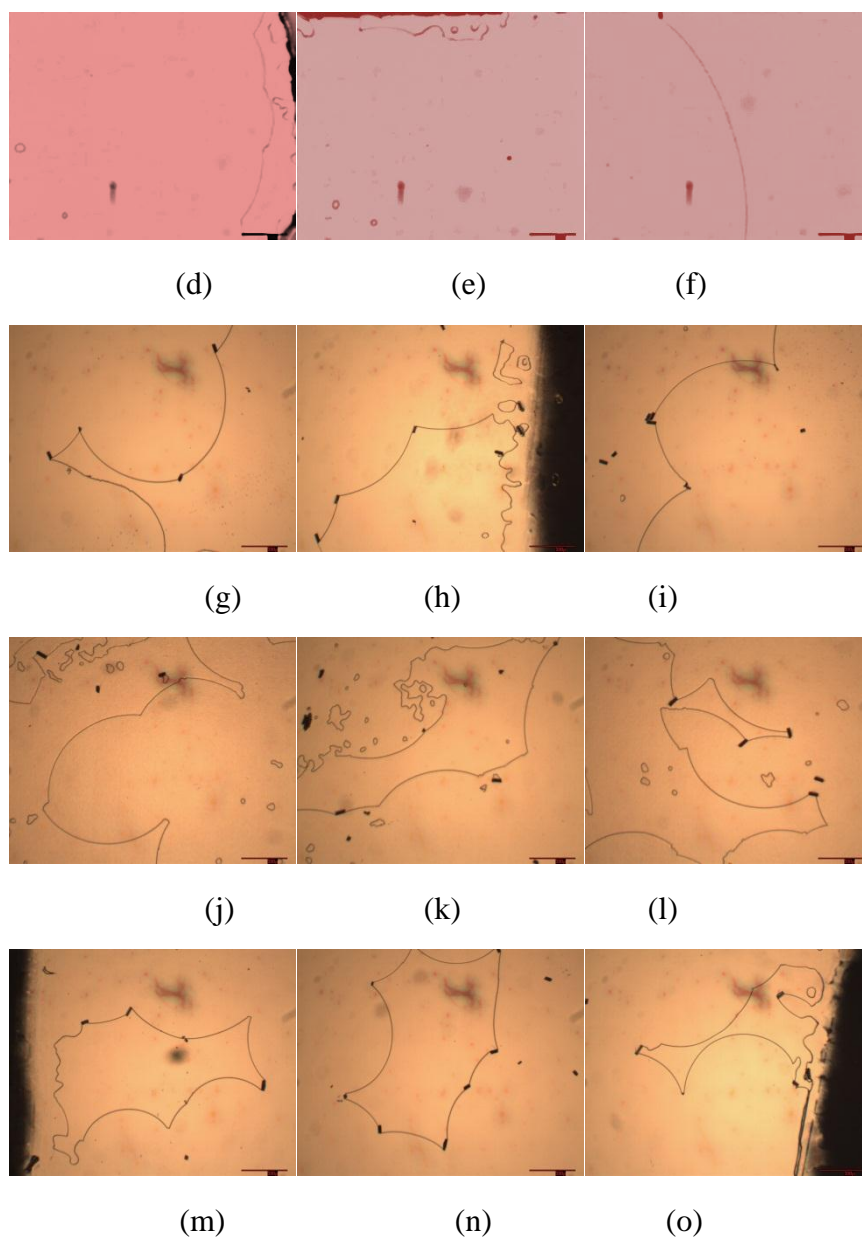
Figure 4.17: Photomicrographs (x50) showing the reverse-twist disclination lines of the mixtures of (*R*)-(+)-thalidomide in E7 formed in 14.4 μm thickness TN cells at concentrations of (a)-(c) 0.002374 wt%; (d)-(f) 0.003304 wt%; (g)-(i) 0.004426 wt% (j)-(l) 0.006262 wt% and (m)-(o) 0.009219 wt%.

Concentration (wt%)	Radii of curvature (µm)	Reciprocal of Radii (1/µm)
0.002374	1197	0.000836
0.003303	488	0.00205
0.004425	429	0.00233
0.006261	353	0.00283
0.009218	223	0.00448

Table 4.4: The concentrations, radii of curvatures (µm) and reciprocal of the radii (1/µm) of (*R*)-(+)-thalidomide in E7.

A plot of the reciprocal radius of curvature as a function of concentration in E7 for (*R*)-(+)-thalidomide in E7 is given in Figure 4.18. From the gradient of the slope, the HTP of (*R*)-(+)-thalidomide in E7 was determined to be 22.95 µm^{-1}.
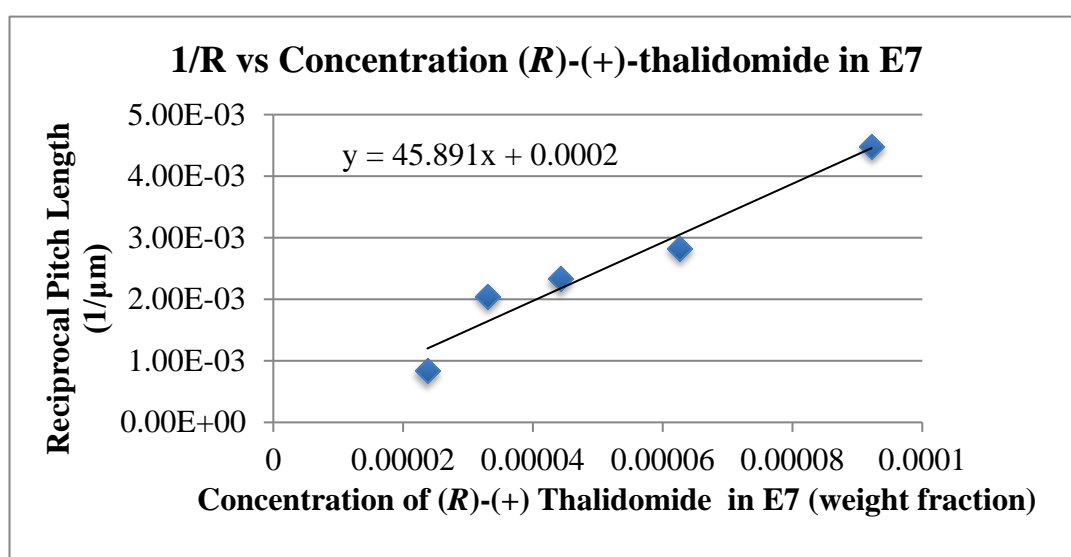
Figure 4.18: The slopes of 1/R VS Concentration (*R*)-(+)-thalidomide in E7.

In Figure 4.18, the slope is not perfectly linear as it was with AE8 in E7. In particular, the first and second data points deviated from the linear fit. Several factors could be possible for this observation. Firstly, the solubility of (*R*)-(+)-thalidomide in E7 is unknown, however the results show that (*R*)-(+)-thalidomide forms disclination lines at all concentrations tested, implying

102

that solubility is not an issue. However, because of the extreme sensitivity of nematic host to the chiral dopant indicates that (R)-(+)-thalidomide does not necessarily dissolve completely in E7. For instance, while E7 is white and cloudy at the room temperature by itself, and (R)-(+)-thalidomide is a light yellow crystal by itself, when the two materials were mixed together no precipitation was observed. However, considering the amount of (R)-(+)-thalidomide used to prepare the mixture, which was only several μg, even if there were small quantities of precipitate it would be very difficult to detect by the human eye. Secondly, the error that results from local thickness variation within the TN cells could also account for this observation. The error from the TN cell arises due to pre-twist, which the angle of rubbing direction of the two pieces of glasses is not exactly 90 °, and there is strong evidence to confirm that the TN cells are not set at exactly 90 °. Pure E7 was filled into the cells as showed in Figure 4.19. As there is no chiral dopant in E7 a straight disclination line should be observed, however the observation of curved disclination lines suggested that the angle between the rubbing directions in the TN cell is not exactly 90 °. Then there is a question about the experimental error and how much this might influence the results.

(a)   (b)
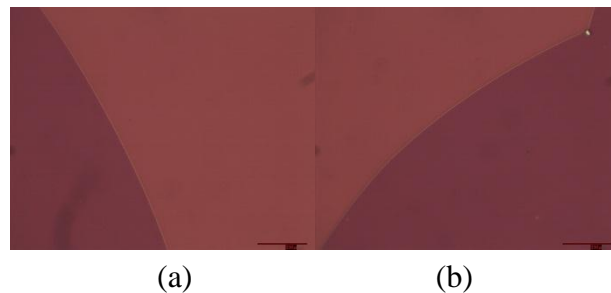
Figure 4.19: Curved disclination lines observed in neat E7 in standard TN cell.

In an attempt to explore the pre-twist of the TN cell, the disclination lines of pure E7 were measured. The average value of the radii of curvature approximately 3000 μm^{-1}. According to the equation reported by E. P. Raynes, the pre-twist was calculated to be less than 0.864 [5]

In the manufacture of TN cells a large parent cell is created and divided into roughly five to twelve smaller cells. It is these smaller cells that are used in this work. This means that any error that results from variation in the parent cell is only constant for every five to 12 TN cells used in these experiments. Although the error from each cell may vary, the pre-twist angle was always lower than 1 °.

Thus, all of the above factors above may influence the results. The correlation between E7 and (R)-(+)-thalidomide should also be discussed. In general, the HTP of (R)-(+)-thalidomide was found to be higher than all the oxazoline based dopants examined, see Chapter 4.2. The largest measured HTP for an oxazoline dopant was $4.47 \mu m^{-1}$ (AE8 in E7), compared with $22.95 \ \mu m^{-1}$ for (R)-(+)-thalidomide. The reasons for this difference between thalidomide and the oxazoline based dopant will be discussed later. The helical twisting power of (S)-(−)-thalidomide, the opposite enantiomer of (R)-(+)-thalidomide, was also measured. It is worthwhile testing the helical twisting power of (S)-(−)-thalidomide in order to find out if the pair of enantiomers have the same helical twisting power, which would be expected to be the same if the ee% is the same.

4.3.3 Studies of (S)-(−)-thalidomide in the E7 Nematic Host

The same method used for the preparation and the detection of the helical twisting power for (R)-(+)-thalidomide was used for the studies of (S)-(−)-thalidomide in the nematic host E7. Five samples of different concentrations of (S)-(−)-thalidomide in E7 were filled into TN cells, with photomicrographs showing the curved disclination lines formed by these mixtures in TN cells are shown in Figure 4.20.
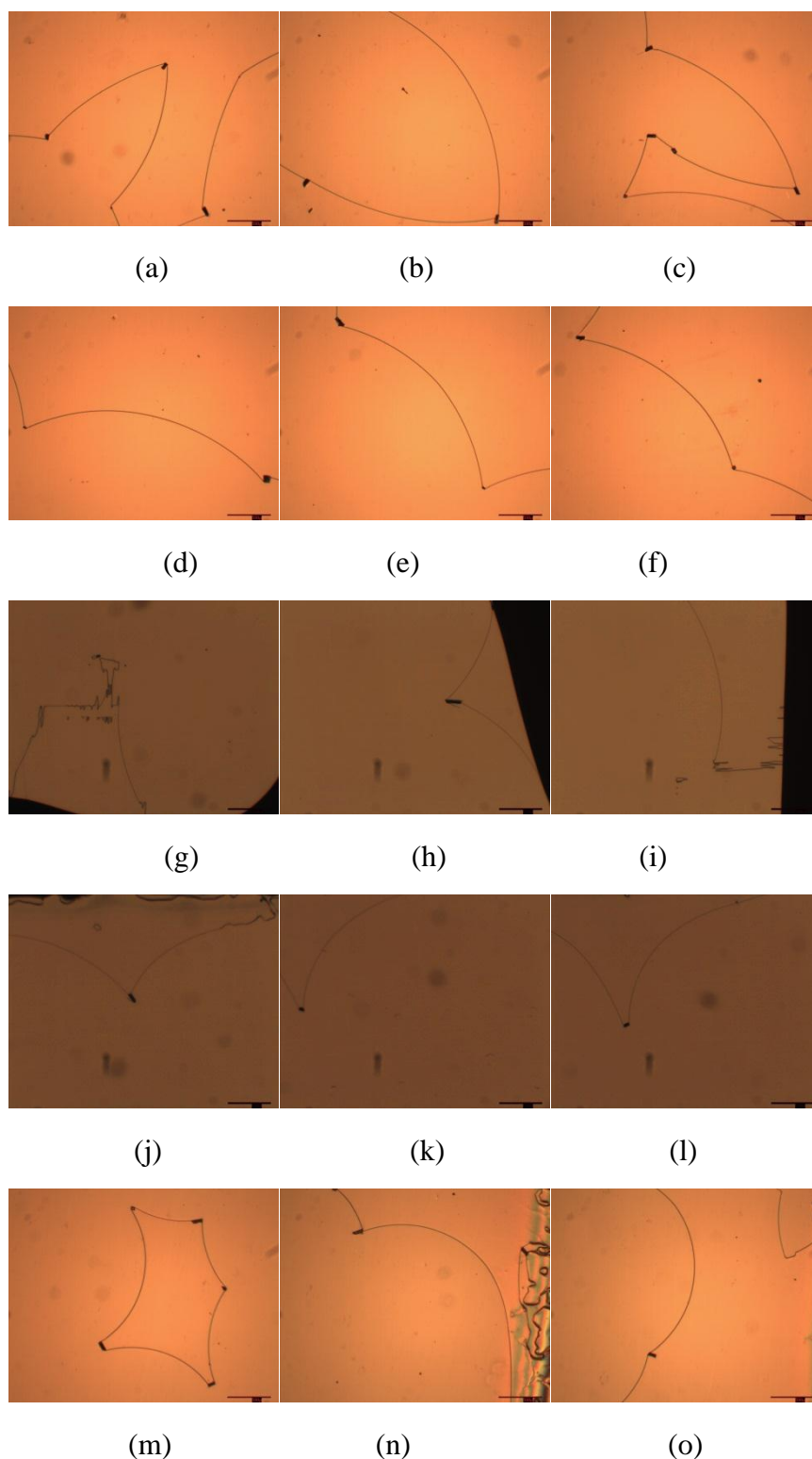
Figure 4.20: Photomicrographs (x50) showing the reverse-twist disclination lines of the mixtures of (*S*)-(⁻)-thalidomide in E7 formed in 14.4 μm thickness TN cells at a concentration of (a)-(c) 0.0007777 wt%; (d)-(f) 0.0009862 wt%; (g)-(i) 0.001797 wt%; (j)-(l) 0.002689 wt%, and (m)-(o) 0.003366 wt%.

From group (a) (b) (c) to group (m) (n) (o) the disclination lines become more tightly curved with increasing concentration. All the disclination lines curves are smooth, however, for group (g) (h) (i), the disclination lines do not form because they tend to build up close to the edge of the cell, and so no disclination lines can be found in the centre of the cell at all. Especially in picture (g), there is only one curved disclination line pictured however, there are some straight and zig-zag shaped disclination lines present. Considering this phenomenon also occurred in the other series of dopant studies, in this case it was not treated as a coincidence. The reason for this behaviour will be discussed later at the end of the section.

Concentration (wt%)	Radii of curvature (µm)	Reciprocal of Radii (1/µm)
0.0007777	1034	0.000968
0.0009862	896	0.00112
0.001797	776	0.00129
0.002689	639	0.00156
0.003366	465	0.00215

Table 4.5: The concentrations, radii of curvatures (µm) and reciprocal of radii (1/µm) of (*S*)-(-)-thalidomide in E7.

All the radii of the disclination lines of (*S*)-($^-$)-thalidomide were measured, and the data are shown in Table 4.5. A plot of the reciprocal radius of curvature as a function of concentration in E7 for (*S*)-($^-$)-thalidomide in E7 is given in Figure 4.21. The 3rd data point is taken from pictures (g)-(i) in Figure 4.20, and as stated previously these tended to show zig-zag shaped defect lines. Given that this data point does not deviate from the linear fit it can be concluded that these zig-zag defects do not strongly influence the final result.
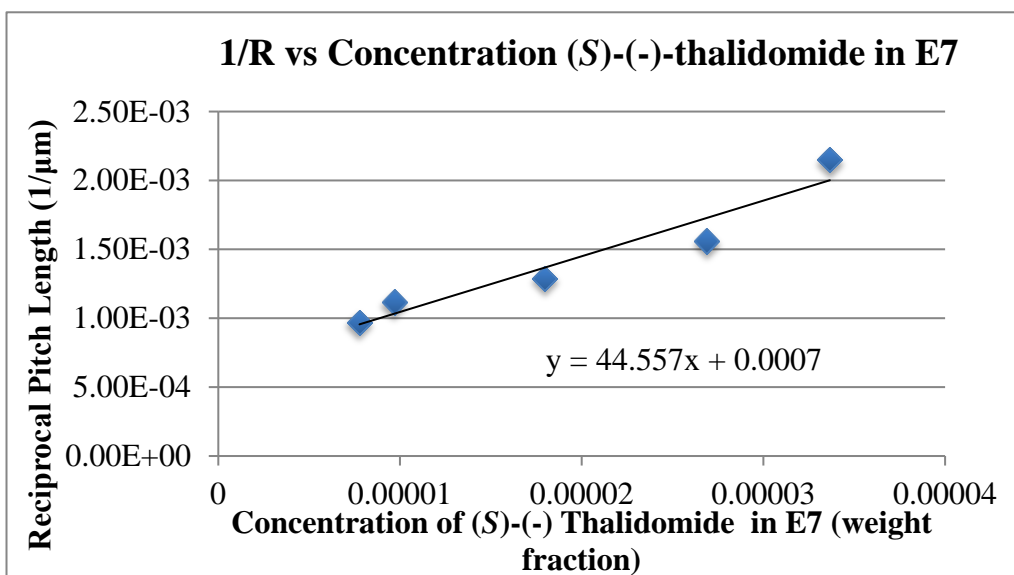
Figure 4.21: Graph of 1/R VS concentration for (*S*)-(-)-thalidomide in E7.

According to the slope, the helical twisting power of (*S*)-(−)-thalidomide is 22.28 μm^{-1}, slightly smaller than the HTP value of (*R*)-(+)-Thalidomide which was measured to be 22.95 μm^{-1}. The origin of this deviation is hard to accurately define. Firstly, they were measured in different TN cells, which are from different batches, thus, the pre-twist of the cell may have an effect. Secondly, although both enantiomeric materials were commercial products supplied by Sigma-Adrich with enantiomeric excesses above 98%, it still does not mean both enantiomers have identical optical purities. For instance, 98.1% and 99.9% will be all labelled as $\geq$ 98% pure by Sigma-Aldrich. Small variations would still influence the results.

Despite the slightly differences of the helical twisting power values, the result for (*S*)-(−)-thalidomide suggests that 'the reverse-twist disclination line method' is a suitable way to detect the helical twisting power of thalidomide. It can determine the enantiomeric excess of thalidomide, whether it is racemic (straight disclination lines) or chiral (curved disclination line). This is potentially applicable to quality control in pharmaceutical production. This method for detecting drugs was reported first by Goodby *et. al* in 2009 where (−)-menthol and Ibuprofen were examined.[7] They found that the helical twisting power of (−)-menthol was

measured to be 1 μm^{-1} in E63 host. A sample of Ibuprofen, which was labelled as racemic, was determined to be chiral. Secondly, thalidomide gives HTP values greater than 20 μm^{-1} for both enantiomers, larger than those of some liquid crystal chiral dopants.

In order to investigate the high helical twisting power of thalidomide, the minimum energy conformations of both enantiomers were obtained at the B3LYP/6-311G* level of theory, followed by calculation of dipole and polarisability tensors at the same level of theory. Calculations were performed using the Gaussian 09 suite of software running on the YARCC cluster at the University of York.[129] The optimised geometry of (*R*)-(+)-thalidomide is given in Figure 4.20 (top). The isoindoline-1,3-dione and piperidine-2,6-dione subunits are perpendicular to each other, making a 'propeller-like' structure. Although the two phenyl rings are also perpendicular to each other in all the oxazoline series of compounds, see Figure 4.20 (lower), the whole view of AE8 for example is zigzag shaped rather than propeller shaped like thalidomide. The shape of the molecules is postulated to be the main reason for (*R*)-(+)-thalidomide having a much higher helical twisting power than the oxazoline based dopants.
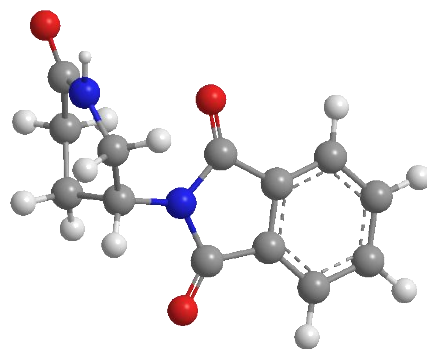
(*R*)-(+)-thalidomide
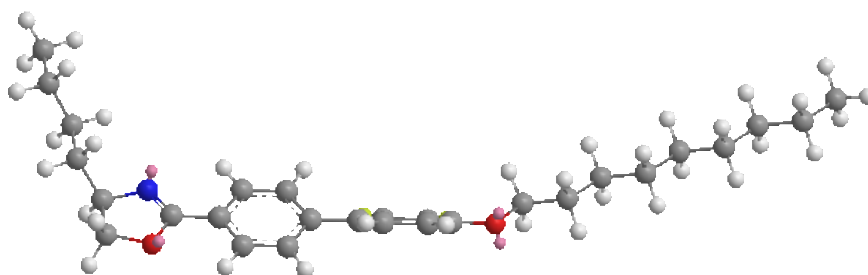
AE8

Figure 4.22: Minimum energy conformations of (*R*)-(+)-thalidomide and AE8 as obtained at the B3LYP/6-311G* level of theory.

In the literature, dopants with propeller shaped molecular structures are generally found to have large values of helical twisting power.[143] For instance, 4,6,7,11,13,14-hexahydro-4,11-diazadibenzo-octalene-5,12-dione does not even have a stereogenic centre, and it can only form the pitch because of its dissymmetric configuration due to restricted interannular rotation about the Ph-Ph bond. The helical twisting power of 4,6,7,11,13,14-hexahydro-4,11-diazadibenzo-octalene-5,12-dione was found to be 58 μm^{-1} in E7.[144]
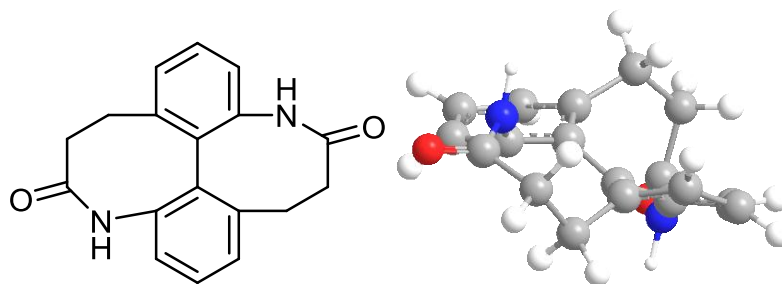
Figure 4.23: Chemical structure and configuration of the atropisomeric axially chiral 4,6,7,11,13,14-hexahydro-4,11-diazadibenzo-octalene-5,12-dione.

The topology of propeller shaped dopants can also be extended to metal ligand based dopants, as mentioned in the introduction to this thesis. Some metal complexes have been found to exhibit large values of the helical twisting power.[143] Although the mechanism of how metal complexes interact with nematic hosts is currently unknown, the shape of the molecules presented is a very important reason for this property-structure correlation. As shown in Figure 4.24, the space filling 3D structure of the ruthenium complex discussed in the Introduction clearly exhibits a propeller-like shape of the core while the two terminal chains are like paddles, with the ruthenium atom at the centre core.[145]
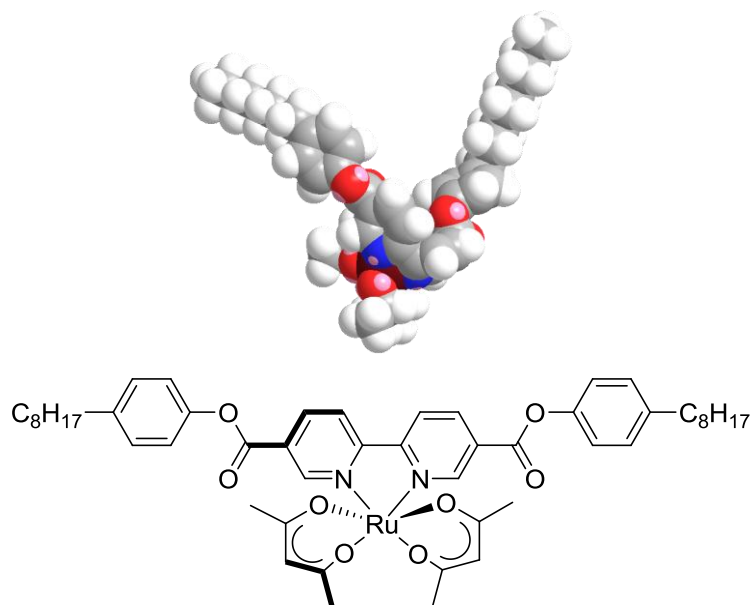
Figure 4.24: 3D conformation and chemical structure of ruthenium complex that has a reported HTP of 180 μm^{-1}.(obtained at the B3LYp/6-311G*level of theory)

When looking back at the structure of (R)-(+)-thalidomide, in comparison with the ruthenium complex, they both have roughly propeller shaped molecular structures. However, the helical twisting power values for the two molecules are hugely different, with the ruthenium complex being around 9 times larger than (R)-(+)-thalidomide. The reason could be caused by the bigger 'paddle' (long carbon chain) of the metal complex. Using this as a design principle, if (R)-(+)-thalidomide was functionalized with two long carbon chains, the helical twisting power may be significantly increased.

According to the results presented thus, the molecular shape persistence affects the helical twisting power value. However, helical twisting power is not an intrinsic property of the dopant, but depends heavily on the host used and this will now also be discussed. In an attempt to explore the correlation between E7 and the dopant, the polarisability and dipole were calculated using the same theory in Gaussian 09 software, see Table 4.6.[129]

Material	Mean Polarisability($\mathring{A}^3$)	Anisotropic Polarisability($\mathring{A}^3$)	Dipole (Debye)
8OCB	42.77	39.33	7.45
7CB	39.33	34.58	6.51
5CT	49.27	52.70	6.80
5CB	35.39	32.49	6.47
E7	38.67	35.73	6.67

Table 4.6: Polarisability and dipole of E7, taken to be a weighted average of its constituent components, as determined at the B3LYP/6-311G* level of theory.

As E7 is a multiple component nematic host, each individual component was measured first, and then percentage weighted average of each of the components was used to obtain the average dipole and polarisability values. Then, the dopants were also measured, since AE8 has the highest helical twisting power value of all

of the oxazoline based dopants it was used to make comparisons with (R)-(+)-thalidomide in the section below, see Table 4.7.

Material	Mean Polarisability(Å^3)	Anisotropic Polarisability(Å^3)	Dipole (Debye)
AE8	52.79	37.56	2.09
(R)-(+)-thalidomide	22.94	10.67	5.36

Table 4.7: Calculated Polarisabilities and dipole moment of AE8 and (R)-(+) thalidomide.

As shown in Tables 4.6 and 4.7 AE8 has larger values of the mean and anisotropic polarisability than thalidomide. They are very close to E7, which probably as they are of similar shape and composition. However, the dipole of AE8 is only 2.09 D, which is lower than 5.3589 D of (R)-(+)-thalidomide. From the data above, it suggests that the dopant that has a higher dipole can achieve higher helical twisting power, perhaps due to stronger dipole-dipole interactions. However this is a simplistic way of viewing a complex interaction, as stronger dipole moments do not necessarily translate to stronger interactions between the host and dopant.[146] Interestingly, when checking back over the other two oxazoline based dopants, AE14 actually has a higher dipole than AE8 with a value of 3.62 D. However, AE14 only has a HTP of 2.22 μm^{-1}, which is half the value of AE8. Thus far, it is very difficult to define how the mean polarisability, the anisotropy of polarisability and the dipole moment dominate the helical twisting power. All of these factors might actually compete with one another to give a suitable HTP.

The length of AE8 is 26.0 Å, whereas the weighted average length of the components of E7 is about 18 Å (8OCB: 21.6 Å, 5CB: 16.6 Å; 5CT: 20.9 Å and 7CB: 19.1 Å). However, (R)-(+)-thalidomide is only 9.9 Å. Furthermore, if only the aromatic ring system was measured, the distance between the diflurorophenyl to 4,5-dihydrooxazole is 10.8 Å and the distance for the terphenyl is 11.5 Å. Thus,

the core sizes of the dopants are close to the core size of host. Furthermore, the helical twisting power will vary with other hosts. For example, the helical twisting power of (4R,5R)-2,2-dimethyl-4,5-diphenyl-1,3-dioxolane is 17.8 μm^{-1} in E7 and 5.4 μm^{-1} in MBBA, respectively, *i.e.* it is higher for the better matched host with respect to the length of the aromatic cores, as shown in Figure 4.25.

(4R,5R)-2,2-dimethyl-4,5-diphenyl-1,3-dioxolane

biphenyl core component in E7   MBBA core
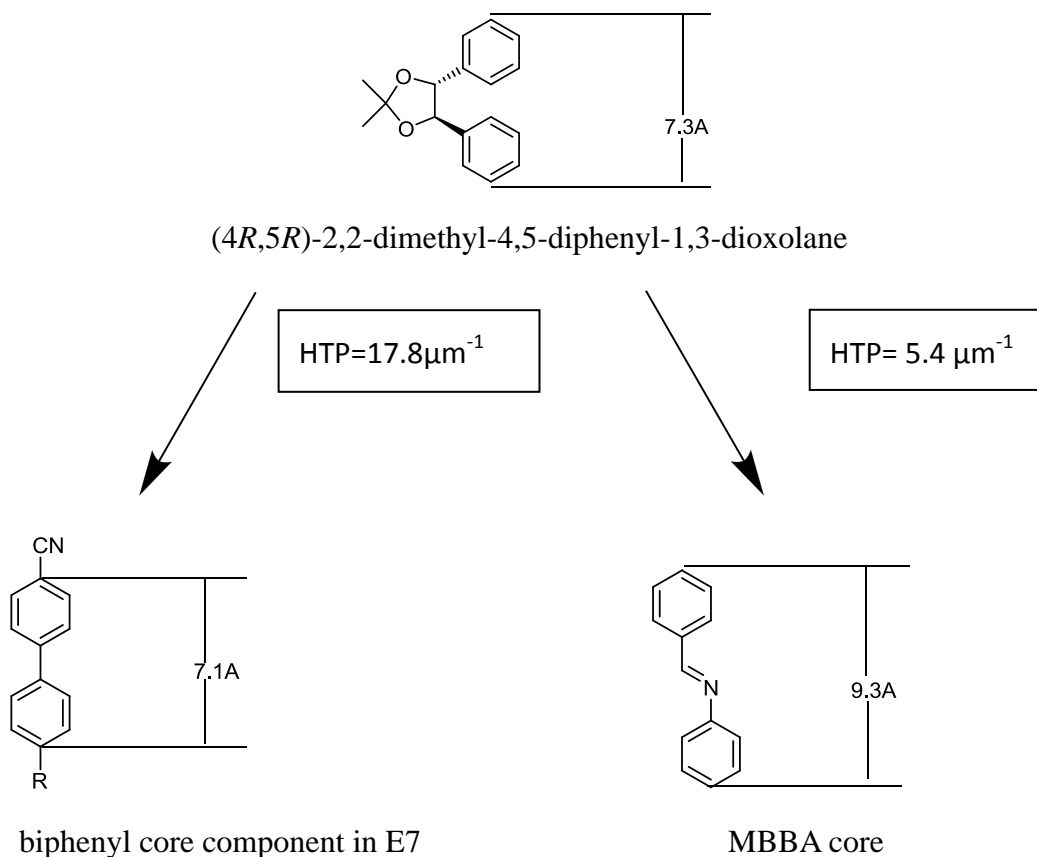
Figure 4.25: The comparative core sizes of the chiral dopant (4R,5R)-2,2-dimethyl-4,5-diphenyl-1,3-dioxolane and those of biphenyl and MBBA and the effect on helical twisting power.[143]

In summary, both the helical twisting power of enantiomers of thalidomide were measured in a TN cell using the reverse twist disclination method. Surprisingly, their values are significantly higher than oxazoline based liquid crystal dopants. The main reason could be that the configuration of thalidomide is more rigid and thus a greater stereochemical effect is observed than for rod-shaped dopants.

Furthermore, the dipole, and induced dipolar interactions, could be other potential factors that need to be considered.

4.4 Studies of R1011 and S1011 chiral dopant in the E7 and PCH7 nematic Hosts.

High helical twisting power dopants can induce short pitch length helices, which is one of the most valuable properties for display applications of chiral nematic liquid crystals.[147] Numerous high helical twisting power dopants have been prepared, such as TADDOL, chromium complexes and ruthenium complexes, as discussed in the Introduction, see Figure 4.26.[76,145,148] Although useful materials as dopants, their solubilities and viscosities in nematic hosts are not high and low enough respectively for them to be useful in display applications. Thus chiral liquid crystalline dopants have been developed which are likely to be soluble in nematic hosts and to have similar viscosities to the host.

HTP = 102 μm^{-1} in MBBA   HTP = 146 μm^{-1} in MBBA
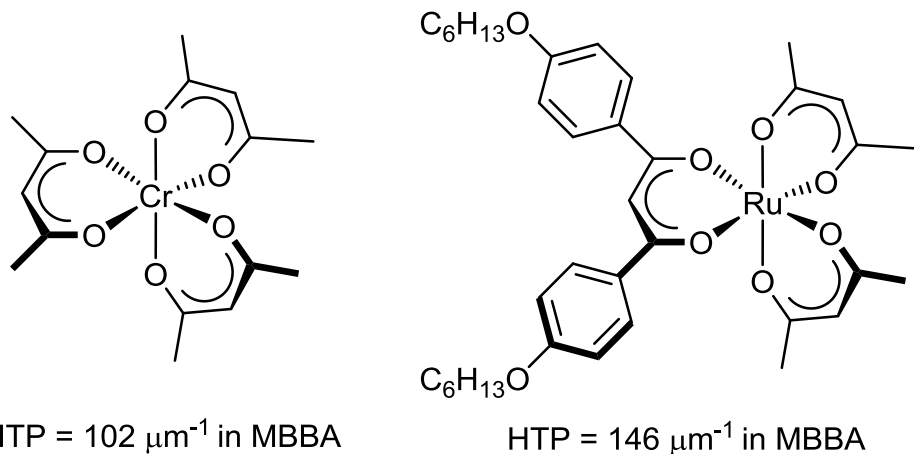
Figure 4.26: The chemical structures of high HTP chromium and ruthenium complexes.[145,148]

Heppke and co-workers synthesised S1011, which has a relatively high helical twisting power, 38 μm^{-1} in E7, and a relative high solubility of 4% in E7, making this material potentially useful for commercial applications. R and S1011 are best

described as a dimer in which there are two PCH5 mesogenic units adjoined *via* an alkyl spacer bearing a stereogenic centre, see Figure 4.27.

Figure 4.27: The chemical structures of S1011 and R1011.[149]

The helical twisting power of S1011 was determined, as described in this chapter, *via* 'the reverse-twist disclination line method'. Also, in an attempt to discover how the chemical structure of the host influences the HTP value, it was measured in both E7 and PCH7 (see Figure 4.28 for the structure of PCH7) as hosts systems. Furthermore, the opposite enantiomer of S1011, R1011, was also tested in order to evaluate relative optical purities. In theory these should give identical results for the same values of *ee*, with any deviation due to experimental error.
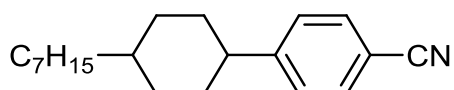
Figure 4.28: Chemical structure of the nematic host PCH7.

In order to keep the experimental framework constant, R1011 and S1011 in E7 were analysed using the same methodology described in previous sections of this Chapter. Considering that R1011 and S1011 are both known to have high values of the helical twisting power and that "TN-cell" method has a very high sensitivity, very low concentrations of the dopants were used.

Similarly, because R1011 is known to have a high helical twisting power it is possible that stable curved disclinations in the cell would not be achieved, and instead the defects would annihilate leaving a uniformly aligned specimen, thereby again highlighting the need to use low concentrations of this material. Therefore, relatively low concentration (<0.0006 wt%) mixtures of the dopant in E7 were made up first to investigate the stability of the disclinations in relation to concentration. The disclination lines formed at this concentration were barely curved as shown in Figure 4.29 (a) to (c). This indicated that slightly more dopant was required for further studies, the photomicrographs for which are shown in Figure 4.30 (d to o).

(a)   (b)   (c)
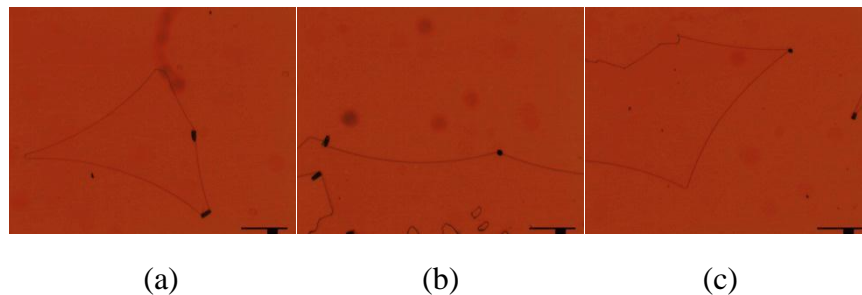
Figure 4.29: Photomicrographs (x50) showing the reverse-twist disclination lines of the mixtures of R1011 in E7 formed in TN cells thickness of 14.4 μm at a concentration of 0.0005888 wt% (a)-(c).
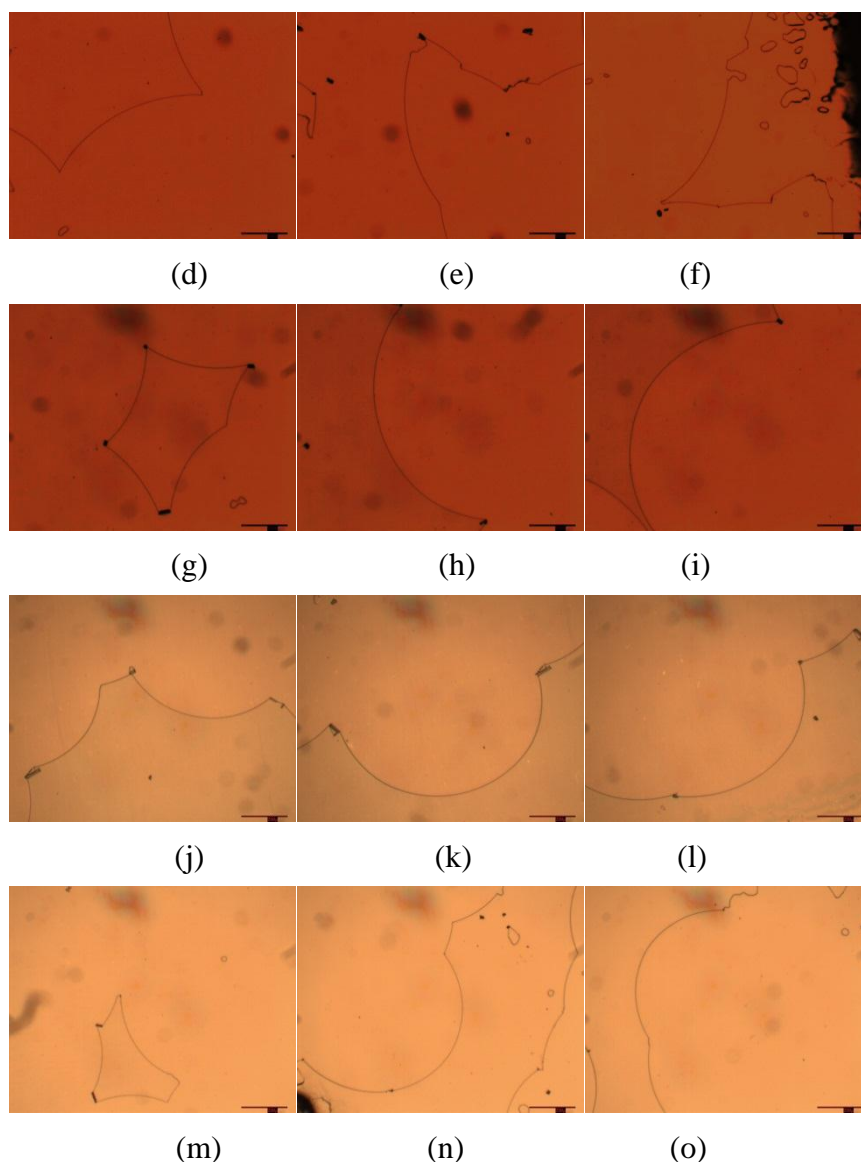
Figure 4.30: Photomicrographs (x50) showing the reverse-twist disclination lines of the mixtures of R1011 in E7 formed in TN cells of 14.4 μm thickness at concentrations of (d)-(f) 0.001177 wt%; (g)-(i) 0.001753 wt% (j)-(l) 0.002345 wt% and (m)-(o) 0.002964 wt%.

With the increasing concentration of R1011 in the mixtures the disclination lines become more curved as expected. However, at the concentration of 0.001177 wt% shown in pictures of (d)-(f) in Figure 4.30, the disclination lines were not well formed in the TN cells, and as shown in picture (f) a few small disclination loops can be seen. A similar problem also occurred in the experiments on thalidomide as a dopant. It was suspected that this occurred as a result of the low soluability of thalidomide in E7. However, as this effect was also observed in the case of R1011,

117

given the high solubility of R1101 in E7 (circa 4 wt%), the argument that solubility is causing this effect can be refuted.

In order to determine the helical twisting power of R1011 in E7, the radii of curvature for different concentrations were calculated, as shown in Table 4.8.

Concentration (wt%)	Radii of curvature (μm)	Reciprocal of Radii (1/μm)
0.0005888	1100	0.000908
0.001177	727	0.00138
0.001753	577	0.00173
0.002345	468	0.00214
0.002964	360	0.00278

Table 4.8: The concentrations, radii of curvatures, and reciprocal of radii of R1011 in E7.

A plot of the reciprocal radius of curvature as a function of concentration in E7 for R1011 in E7 is given in Figure 4.31. From the gradient of the slope of the linear fit to the data, the HTP of R1011 in E7 was determined to be 38.09 μm^{-1}.
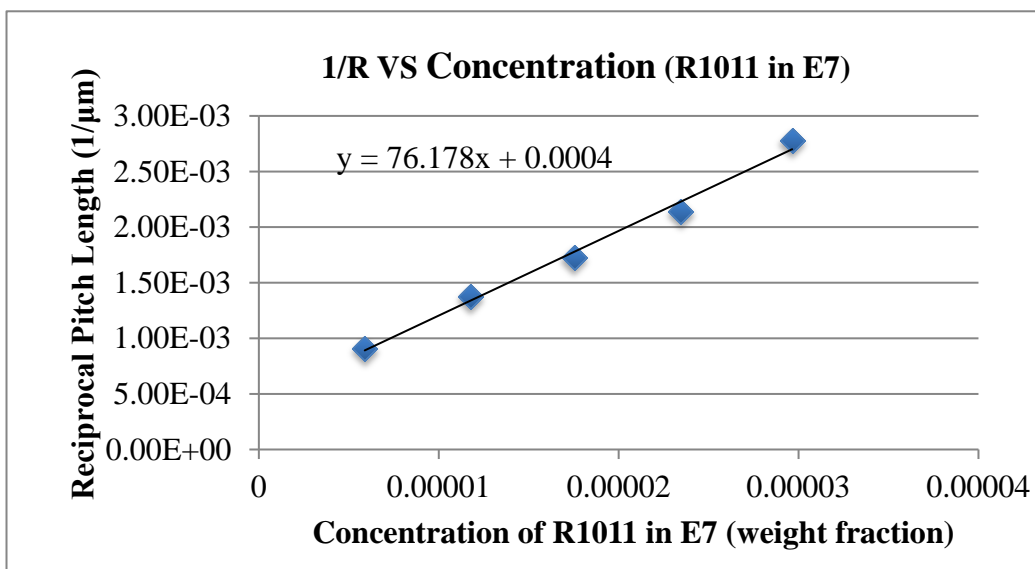
Figure 4.31: The slope of 1/R versus concentration of R1011 in E7.

Although the helical twisting power of R1011 in E7 has not previously been measured, its enantiomer, S1011, has been reported to be 38 μm^{-1} in E7.[150] Considering the helical twisting power of enantiomers of the same *ee* (pure or derived by separation of enantiomers from a racemate) should be the same and with the excellent agreement of the linear fit to the data ($R^2 = 0.991$) for R1011, it can be reasoned that the phenomena observed in picture in Figure 4.30 (f) did not influence the final result. Thus, the helical twisting power value determined for R1011 is in excellent agreement with previous values and confirms the accuracy of the reverse twist disclination method for measuring HTP.

As shown previously with studies on thalidomide, the helical twisting powers determined for the enantiomers were not necessarily exactly identical due to the enantiopurities. Thus, even though the HTP for S1011 had been measured previously, it was still deemed worthwhile determining the helical twisting power *via* 'the reverse-twist disclination line method'. Thus, in order to compare the result with R1011, mixtures of S1011 in E7 were prepared and analysed using the same procedure.

Surprisingly, at lower concentrations of S1101 at 0.0005%, there were no disclination lines formed in the TN cells. Therefore, concentrations of 0.001713 % and above for S1011 in E7 were employed in the following studies, as shown in Figure 4.32.

(a)   (b)   (c)

(d)   (e)   (f)

(g)   (h)   (i)

(j)
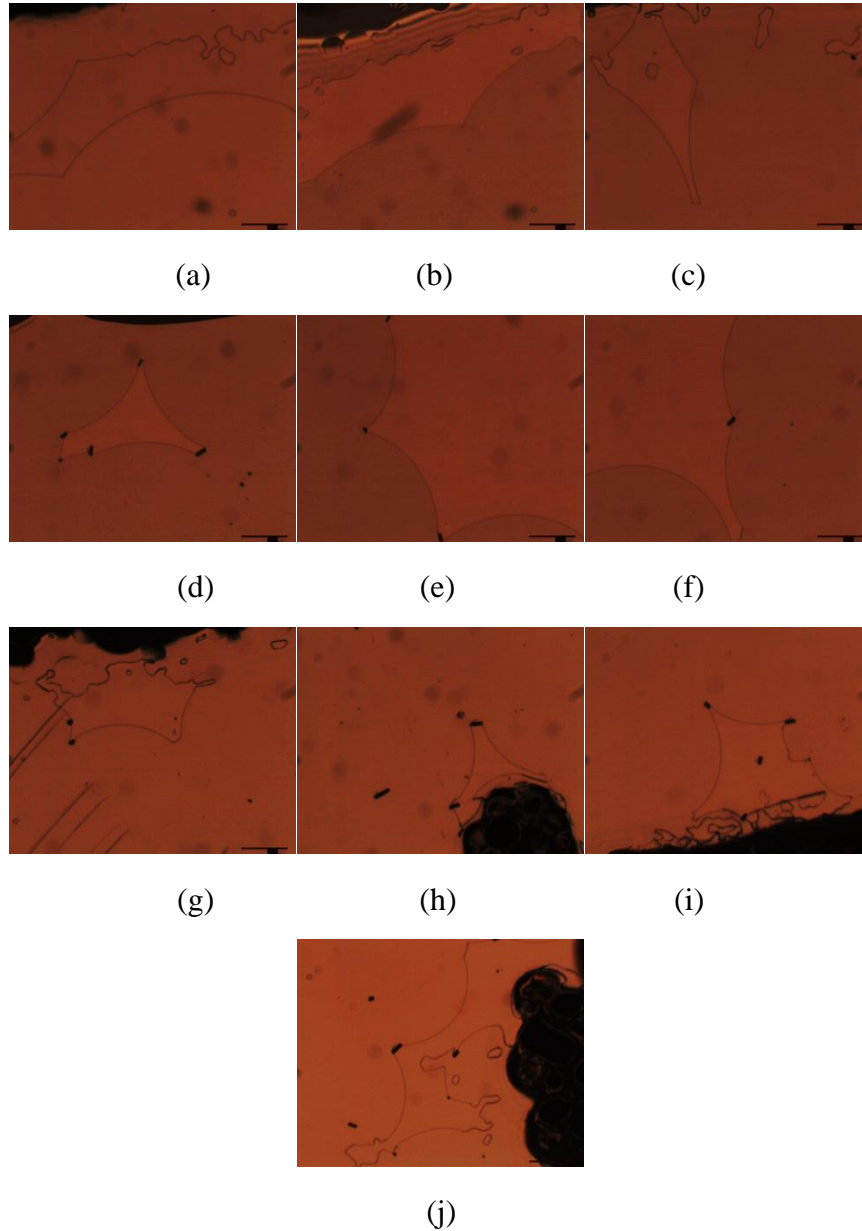
Figure 4.32: Photomicrographs (x50) showing the reverse-twist disclination lines of the mixtures of S1011in E7 formed in TN cells of 14.4 μm thickness at a concentration of (a)-(c) 0.001713 wt% ;(d)-(f) 0.002870 wt%; (g)-(i) 0.003428 wt% and (j) 0.004127 wt%.

Although fewer disclination lines form at the concentration of 0.001177 wt% of R1011 in E7, in general a satisfactory number of disclination lines were formed for

measurements to be made. For concentrations ranging from 0.003428 wt% to (j) 0.004127 wt% of S1011 in E7, it can be seen from pictures (g)-(j), fewer and fewer disclination lines were formed. In picture (g), the straight lines could actually be scratches on the surface of the cell, which can be ignored for the purposes of the measurements. The black areas in the pictures are the edges of the cell. The reason why disclination lines prefer to forming close to the edge of cell at certain concentrations is unknown. In the picture (j), irregular disclination lines are exhibited between two smooth curved disclination lines. The reason for this behaviour might be due to defects in the cell, or movement of the cell when taking pictures under the lens of microscope.

However, S1011 did not perform quite the same as R1011 in TN cells, and only four different concentration groups could be measured, as shown in Table 4.9.

Concentration (wt%)	Radii of curvature (μm)	Reciprocal of Radii (1/μm)
0.001713	843	0.00119
0.002870	462	0.00216
0.003428	355	0.00282
0.004127	312	0.00321

Table 4.9: The concentrations (wt%), radii of curvatures (μm), and reciprocal (1/μm) of radii of S1011 in E7.

Despite having only four data points, these were still enough to generate the helical twisting power of S1011 in E7. From the gradient of the slope of the line for best fit to the data, the HTP of S1011 in E7 was determined to be 44.93 μm^{-1}, as shown in Figure 4.33. This value is different from the reported literature value of 38μm^{-1} in E7. The R ^{2}value of the linear fit is close to unity (0.9938) indicating that even with only four data points the HTP could be obtained with a high level of confidence. This suggests that the difference between the literature and

experimental values is not caused by the error of preparation of the mixture and the defect lines from the TN cell. If there were any errors or defects in the preparation and the TN cell, the data points would not show linear behaviour, thereby giving a lower R^2 value, however this was not the case.
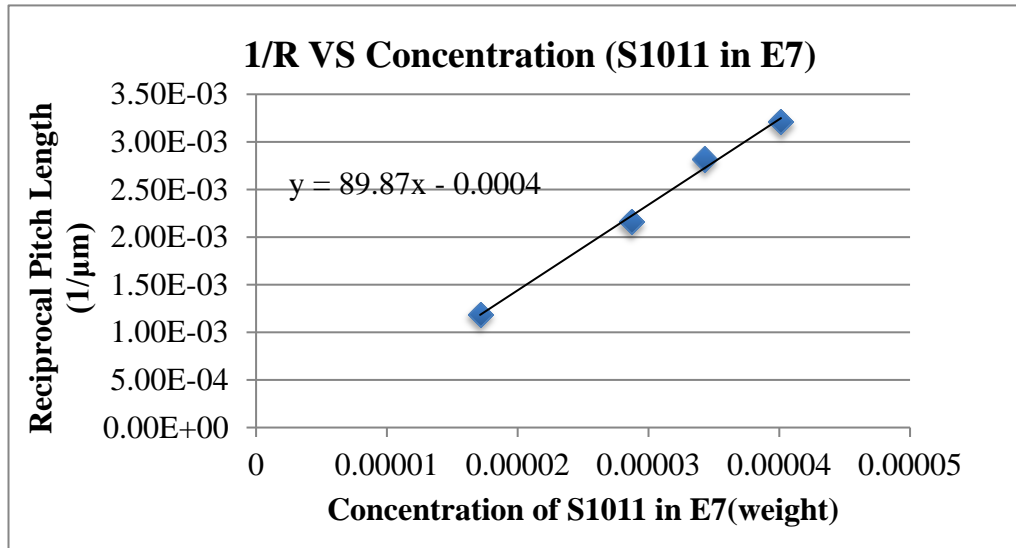
Figure 4.33: The slopes of 1/R VS concentration S1011 in E7.

In order to discover why S1011 behaves so differently in E7 compared to R1011, and how the chemical similarity of the dopant and host affect HTP values, mixtures of R1101 and S1101 in the host PCH7 were prepared. Thus, photomicrographs of the disclination lines formed by mixtures of R1011 and S1011 in the PCH7 at various concentrations are shown in Figure 4.34 and 4.35 respectively.
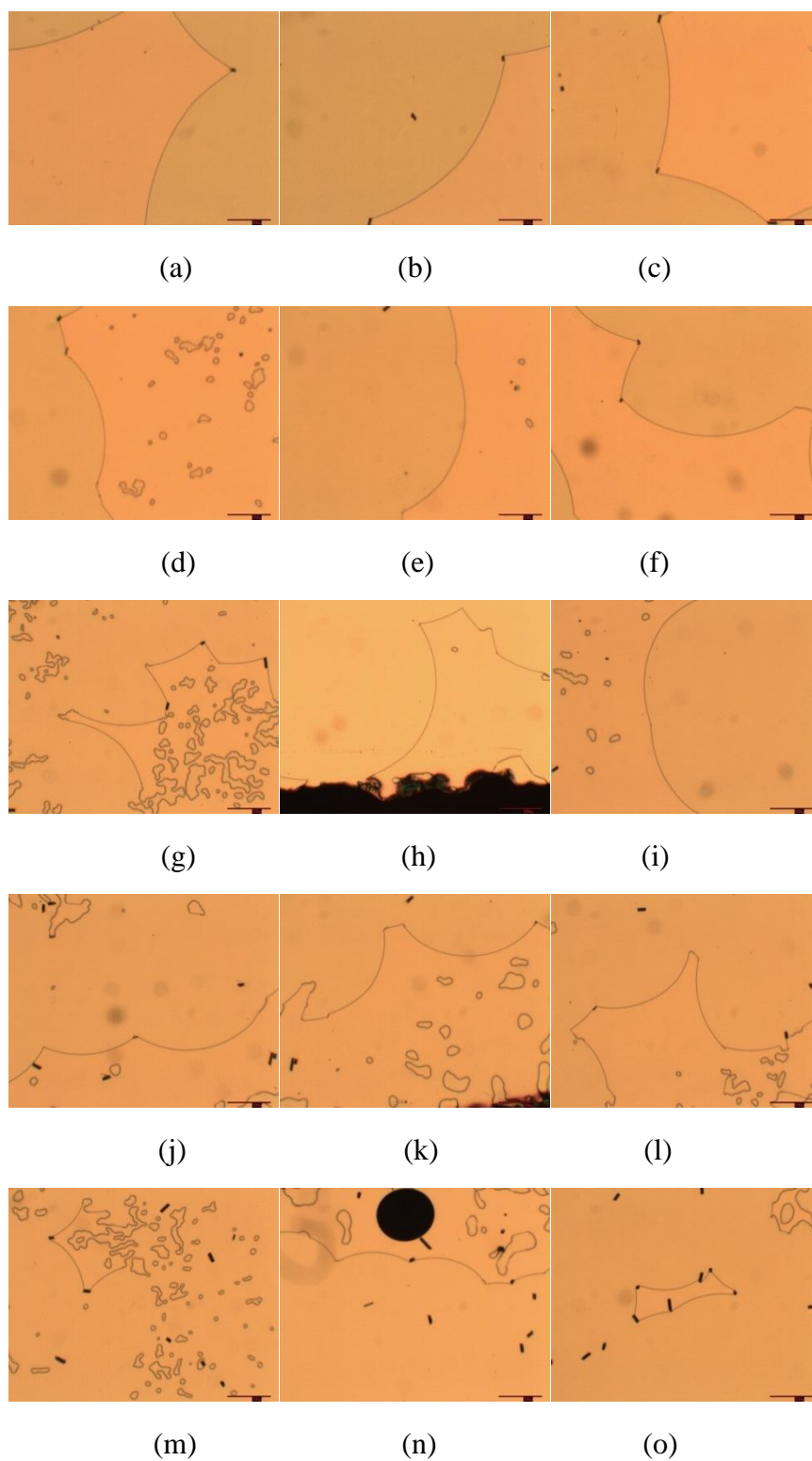
Figure 4.34: Photomicrographs (x50) showing the reverse-twist disclination lines of the mixtures of R1011 in PCH7 formed in TN cells of 14.4 µm thickness at a concentration of (a)-(c) 0.001186 wt% ;(d)-(f) 0.001769 wt%; (g)-(i) 0.002367 wt% (j) - (l) 0.002943 wt% and (m) – (o) 0.003544 wt%.
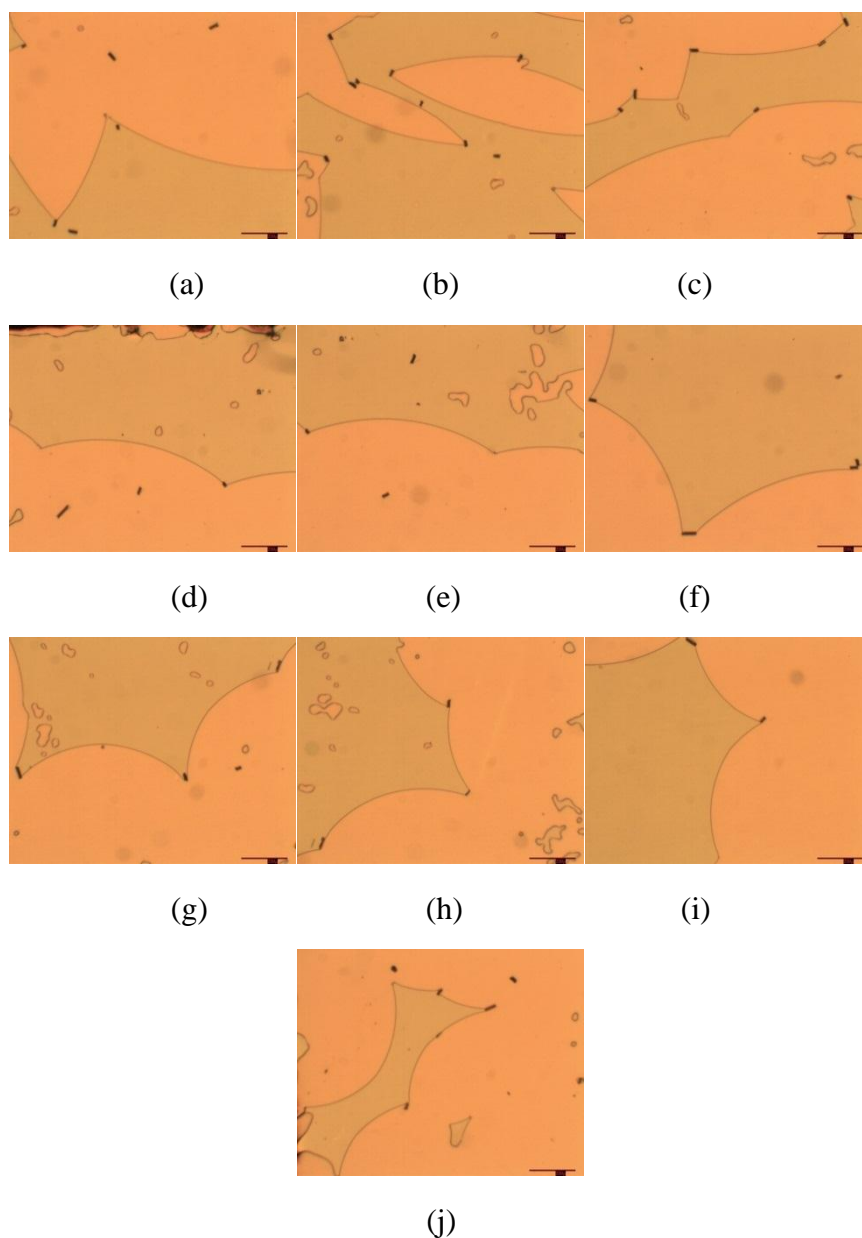
Figure 4.35: Photomicrographs (x50) showing the reverse-twist disclination lines of the mixtures of S1011 in PCH7 formed in TN cells of 14.4 μm thickness at a concentration of (a)-(c) 0.001143 wt% ;(d)-(f) 0.001711 wt%; (g)-(i) 0.02293 wt% (j) 0.002862 wt%

The solubility of R1011 and S1011 in PCH7 has not been reported previously. During preparation of the mixtures of R1011 and S1011 in PCH7, there are no specific differences made or observed with respect to E7 as the host, apart from the process of filling the mixtures into the cell. The mixtures of R1011 and S1011 in PCH7 took less time to fill than the mixtures of R1011 and S1011 E7 due to the

lower viscosity of the system. However, as shown in Figure 4.34 and Figure 4.35, there are more disclination lines in the PCH7 based mixtures than for the analogous E7 systems. The small irregular disclination lines couldn't be eliminated, see picture (g) and (m) in Figure 4.34, and lots of small disclination loops were found. However, these defects did not affect the curved disclination lines that were being used in the analytical procedures, because they are existed inside the domains rather than interrupting the existing disclination lines themselves. Furthermore, apart from pictures (h) and (k) in Figure 4.34, which were taken near to the edge of the cell, all the disclination lines were formed in the centre of TN cells. In addition, there are more spacers shown in the pictures in Figures 4.34 and 4.35 than in Figure 4.30 and 4.32. This accounts for the increased number of disclination lines observed in these preparations in comparsion to those made with E7 as the host as the spacers used in the constructions of TN cells are often the point around which the disclination lines nucleate. This idea is further reinforced by the fact that cells containing few spacers were found to be incapable of giving stable disclination lines, even for pure E7. Thus, it can be concluded the number of spacers in the cell, not just and the different hosts, R1011 and S1011 form more or less disclination lines in centrain preparations..

In order to obtain helical twisting power of R1011 and S1011 in PCH7, the radii of the disclination lines in Figure 4.34 and 4.35 were measured. All of the data was used analytically to generate the linear fits to the data, as shown in Figures 4.36 and 4.37. Through the determination of the gradient to the slope, the helical twisting power of R1011 and S1011 in PCH were determined to be 42.99 μm^{-1} and 52.54 μm^{-1} respectively.
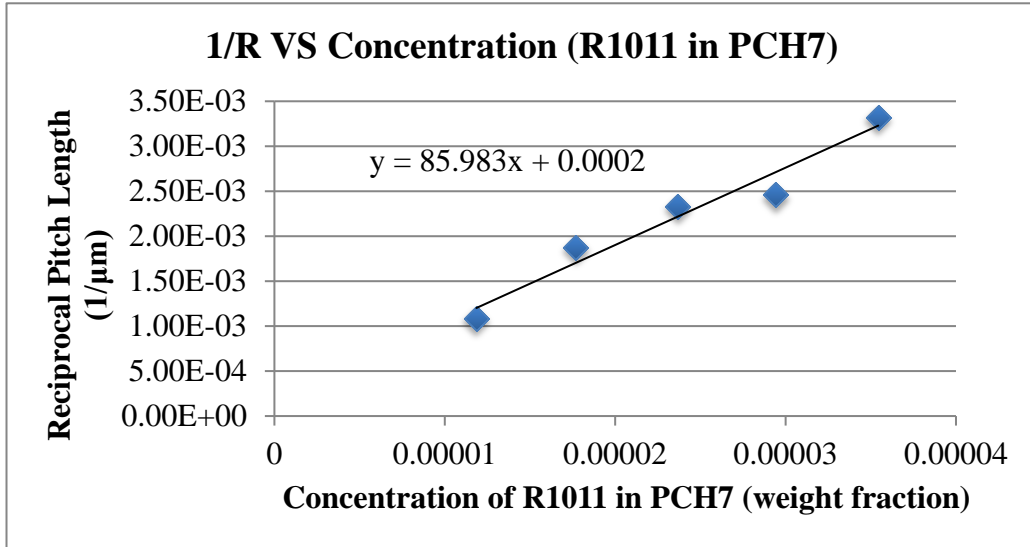
Figure 4.36: The slopes of 1/R VS Concentration R1011 in PCH7.
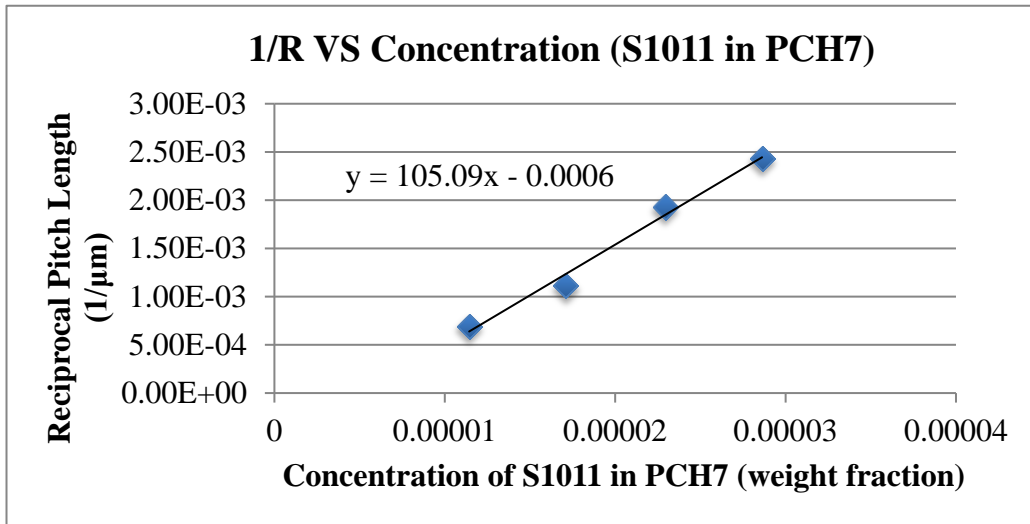
Figure 4.37: The slopes of 1/R VS Concentration S1011 in PCH7.

As expected, the sense of chirality (as inferred from measured HTP values) of R1011 and S1011 were larger when dissolved in PCH7 than in E7. The scale of amplification of R1011 and S1011 in PCH7 were very similar with the values for both dopants increasing between 10% to 20%, see Table 4.10. The reason why these changes (12% and 17%) occur may be related to the pre-twist from the TN cell, which, as discussed previously, can possibly contribute up to a 5% error in the measured value. However, if this effect is caused by the correlation between the dopant and the host the change of helical twisting power value would have increased or decreased by a larger amount, as it appears to have done in this case.

126

Therefore, it seems that the host does, in this case, have an important impact on the HTP of R1101 and S1101. Factors related to the host dependency of the HTP will be discussed in more detail in Section 4.7.

	HTP value in E7 (μm^{-1})	HTP value in PCH7 (μm^{-1})	Percentage Increase
R1011	38.09	42.99	12%
S1011	44.93	52.54	17%

Table 4.10: Comparisons of the helical twisting power of R1011 and S1011 in E7 and PCH7.

The reason of why R1011 and S1011 can achieve HTP values in excess of 35 μm^{-1} is worthy of discussion. In order to investigate this, the minimum energy conformations of R1011 were obtained at the B3LYP/6-311G* level of theory, see Figure 4.38, and calculation of the dipole and polarisability tensors at the same level of theory were conducted, see Table 4.11.
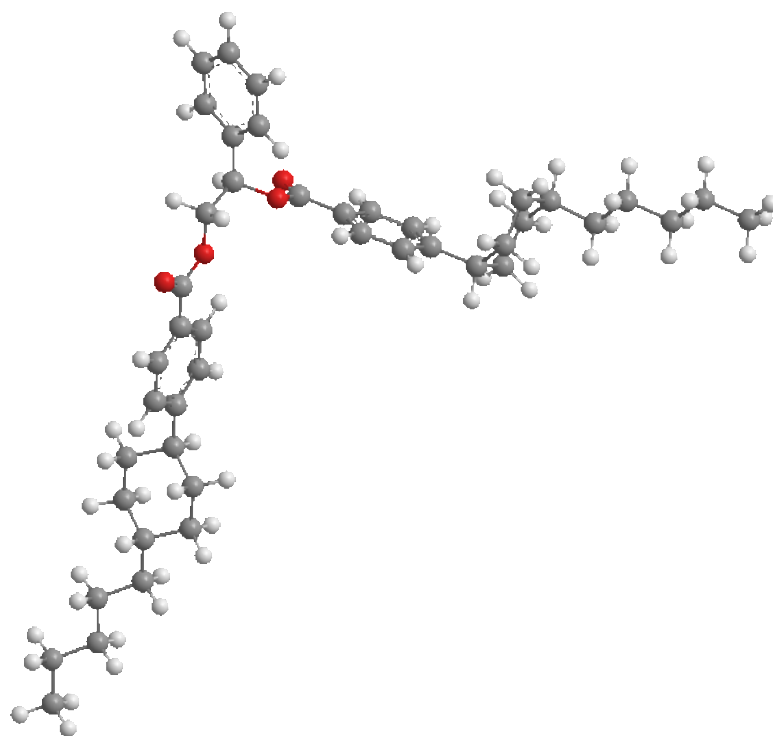
Figure 4.38: Minimum energy conformation of R1011 as obtained at the B3LYP/6-311G* level of theory.

Material	Mean Polarisability($\mathring{A}^3$)	Anisotropic Polarisability($\mathring{A}^3$)	Dipole (Debye)
R1011	75.48	13.29	2.59
(*R*)-(+) thalidomide	22.94	10.67	5.36

Table 4.11: Polarisability and dipole of R1011 and *R*(+) Thalidomide, as determined at the B3LYP/6-311G* level of theory.

Interestingly, the minimum energy conformation of R1011 exhibits a propeller shape. In the thalidomide section, Chapter 4.3, dopants with propeller shaped molecular structures were hypothesised to be important for inducing high helical twisting powers. As discussed in the thalidomide section, the isoindoline-1,3-dione and piperidine-2,6-dione have aromatic rings that are oriented perpendicular to each other, which appears to increase the ability to induce twist. Obviously, in the structure of R1011, the central laterally attached

ring is perpendicular to the two phenylcyclohexane units. Thus, the whole conformation of R1011 can be seen as a three paddle propeller. Because the shapes and sizes of the paddles are bigger than the paddles in thalidomide, this makes R1011 a larger propeller molecule, and thereby it also is larger in terms of helical twisting power. Additionally, the PCH5 moieties of R1011 are mesogenic functional groups that increase the solubility of R1011 in a host, again helping to improve the twisting power. These results suggest that because the mesogenic groups in the dopant are structurally similar to that of the host, the dopant has the potential to introduce more twist in the PCH7 host than it does for the E7 host. Hence the results again demonstrate that the HTP is host dependent, this effect is discussed in more detail in Section 4.7.

As can be seen from the polarisability and dipole calculations for R1011, (Table 4.11), the dipole of R1011 is actually smaller than for (*R*)-(+)-thalidomide because thalidomide possesses the highly polar isoindole dione moiety. However, both the mean and anisotropic polarisability of R1011 are larger than those of (*R*)-(+)-thalidomide due to the larger molecular size. Thus, for these systems, in contrast to the gross molecular shape, the dipole and polarisability seem to have no discernible impact on the measured HTP values, although they may influence solubility between dopant and host.

In summary, the helical twisting power of R1011 and S1011 has been measured, and the results obtained for S1011 deviates somewhat from those reported literature values. The reason for this is unknown, however it may be caused by the dopant itself as both the studies showed that S1011 had larger HTPs in E7 and PCH7 than R1011. This suggests the results are not coincidental, and indicate that the sample examined may have a different optical purity than the material from which previous values were obtained. However, the results for R1011 are in excellent agreement with literature values. Thus generally speaking, for high

helical twisting power dopants 'the reverse-twist disclination line method' is a suitable means for measuring HTP values.

Overall, these results suggest that R1011 is a consistent product, probably from the same batch, whereas S1011 is inconsistent from one batch to another, and/or its manufacturing process is not consistent. Moreover, the two enantiomers are probably not separated from a racemic mixture, or if they were one enantiomer preferentially was isolated. Lastly, it is clear from these studies that the method could be used to identify forgeries, contaminants, and chirality in commercial products.

4.5 Studies of diflourobiphenylcyclohexane-based chiral dopants in the E7 nematic host.

Materials based on the *trans*-4-cyclohexyl(2,3-difluorobiphenyl) (CDFBP) core are some of the most widely studied liquid crystals due to their intrinsically low birefringence and moderate negative values of dielectric anisotropy. These materials are often used as ferroelectric host mixtures, and there has been significant work on chiral dopants using this core system, given the attractive properties of ferroelectric liquid crystal displays.[151]

The CDFBP-based chiral dopants investigated in this chapter were synthesised by Dr R. A. Lewis (University of Hull, UK), and were used as received without further purification. For two materials both enantiomers were supplied. In the previous section, two pairs of enantiomers were examined (*R*)-(+)-thalidomide and (*S*)-(−)-thalidomide as well as the chiral dopants R1011 and S1011. It is interesting to note that the measured helical twisting power (HTPs) for both enantiomers of thalidomide were nearly identical, which were $22.28 \mu m^{-1}$ for

(S)-(−)-thalidomide and 22.94μm^{-1} for (R)-(+)-thalidomide. For the enantiomers of R1011 and S1011, however, their values were very different, *i.e.*, 38.09 μm^{-1} for R1011 and 44.93μm^{-1} for S1011 when measured in the nematic host E7. Considering thalidomide is a small molecule drug, whereas R1011 and S1011 possess 'mesogenic units', the correlations between them and the E7 nematic host are different. Extending this study it was deemed worthwhile examining if there was a correlation/trend in the results in order to see if there a general trend could be identified. Thus, one pair of CDFBP-based chiral dopant enantiomers were studied to find out whether or not different "so-called" pairs of enantiomers have the same helical twisting power. Furthermore, in the four CDFBP-based chiral dopants examined (Figure 4.39), the functional groups attached to the stereogenic centre included F, CN and CF$_3$. The polarities of these functional groups are very different form each other and polarity at the stereogenic centre and their effects on helical twisting power have not yet been evaluated in this work. Therefore the results from this chapter extend the use of 'the reverse-twist disclination line method' for determining HTP into another regime, whereby stronger intermolecular actions and surface polar interactions may be relevant.

RAL1568

RAL1569

RAL1636

RAL1608
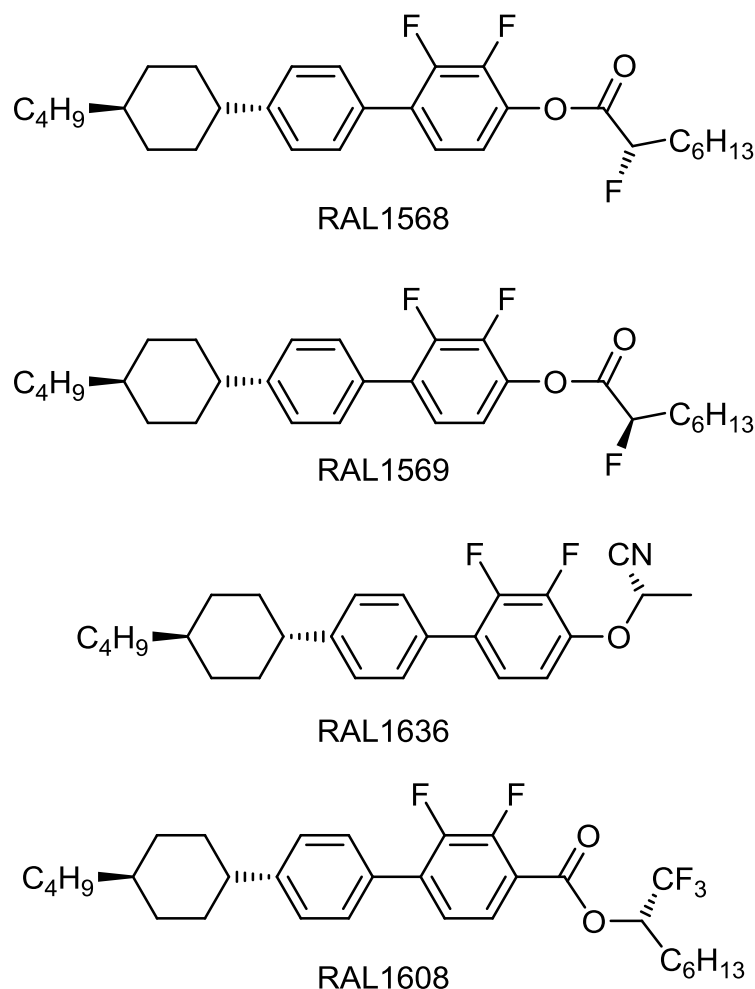
Figure 4.39: The chemical structures of the *trans*-4-cyclohexyl(2,3-difluorobiphenyl)-based chiral dopants studied.

The HTP of four CDFBP-based chiral dopants initially studied were measured *via* 'the reverse-twist disclination line method'. In order to make comparisons with previous results, all of the mixtures were prepared as described in previous chapters, with the data analysed using the same methodology.

RAL1568, with a fluorine atom attached to the stereogenic centre, was examined first. Considering the small size of the groups appended to the stereogenic centre, RAL1568 was expected not to have very high helical twisting power value. Therefore, relatively high concentrations of RAL1568 in E7, compared to the concentrations used for R1011 (lowest concentration for R1011 was 0.0005888

wt%), were prepared. Photomicrographs showing the disclination lines formed by mixtures of RAL1568 in E7 at various concentrations are shown in Figure 4.40.

(a) (b) (c)

(d) (e) (f)

(g) (h) (i)

(j) (k) (l)

(m) (n) (o)
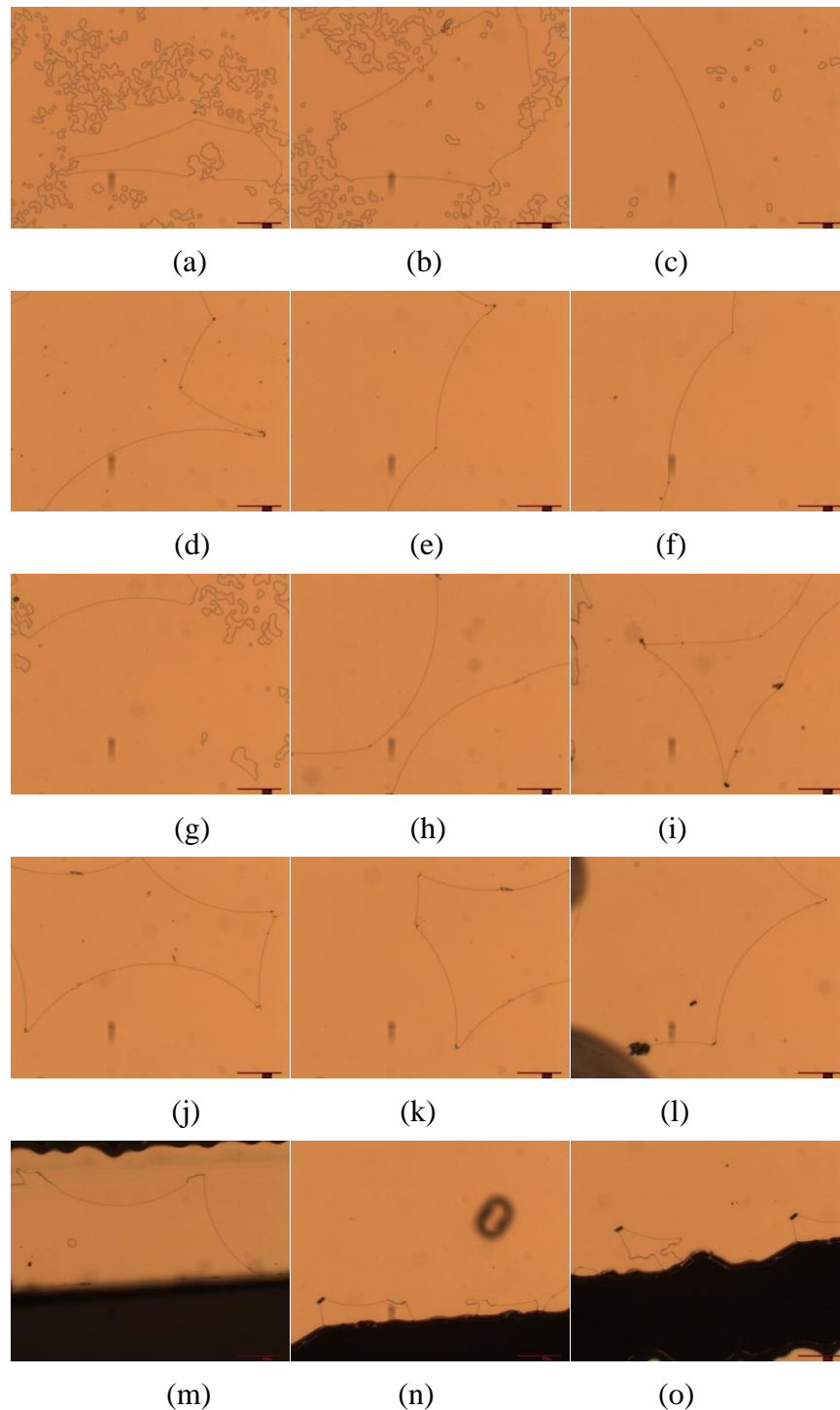
Figure 4.40: Photomicrographs (x50) showing the reverse-twist disclination lines of the mixtures of RAL1568 in E7 formed in 14.4 μm thickness TN cells of 14.4 μm thickness at concentrations of (a)-(c) 0.02033 wt%; (d)-(f) 0.02800 wt%; (g)-(i) 0.03231 wt%; (j) - (l) 0.03825 wt%; and (m) – (o) 0.04379 wt%.

Anomalously, for the lowest concentration (0.02033 wt%), Figure 4.40 (a)-(c), disclination lines did not form as expected. It can be seen clearly that there are lots of small irregular shaped spots in the cell. The reasons for this are unknown, but it was demonstrated by miscibility that at this concentration the dopant was completely soluble in the host. As the concentration of the dopant in the mixture was increased, there were more curved disclination lines formed, which can be seen in Figure 4.40 (g) to (i). All of these photomicrographs were taken at a magnification of x50 for mixtures with concentrations higher than 0.02033 wt%. In the highest concentration (0.04379 wt%) disclination lines became quite scarce, thereby indicating that at this concentration, the radii of curvature of the disclination lines was very small, and in the TN cell only one domain tends to form at these concentrations, rather than two domains separated by a disclination line. Furthermore, as the disclination lines tend to form between two spacers, when the distance of two spacers is larger than the radii of curvature of the disclination lines, the lines form from one spacer to the edge of the cell (see picture (o)). Thus, in a similar way the irregular shaped spots in pictures (a)-(c) might also be caused by defects within the TN cell.

In order to obtain values of the helical twisting power of RAL1568 in E7, the radii of curvature for the different concentrations were calculated, as shown in Table 4.12.

Concentration (wt%)	Radii of curvature (μm)	Reciprocal of Radii (1/μm)
0.02033	1594	0.000627
0.02800	877	0.00114
0.03231	733	0.00136
0.03825	661	0.00151
0.04379	444	0.00225

Table 4.12: The concentrations, mean radii of curvatures (μm), and mean reciprocal of radii (1/μm) of RAL1568 in E7.

A plot of the reciprocal radius of curvature as a function of concentration in E7 for RAL1568 in E7 is given in Figure 4.41. From the gradient in the slope, he HTP of RAL1568 in E7 was determined to be 3.17 μm^{-1}.
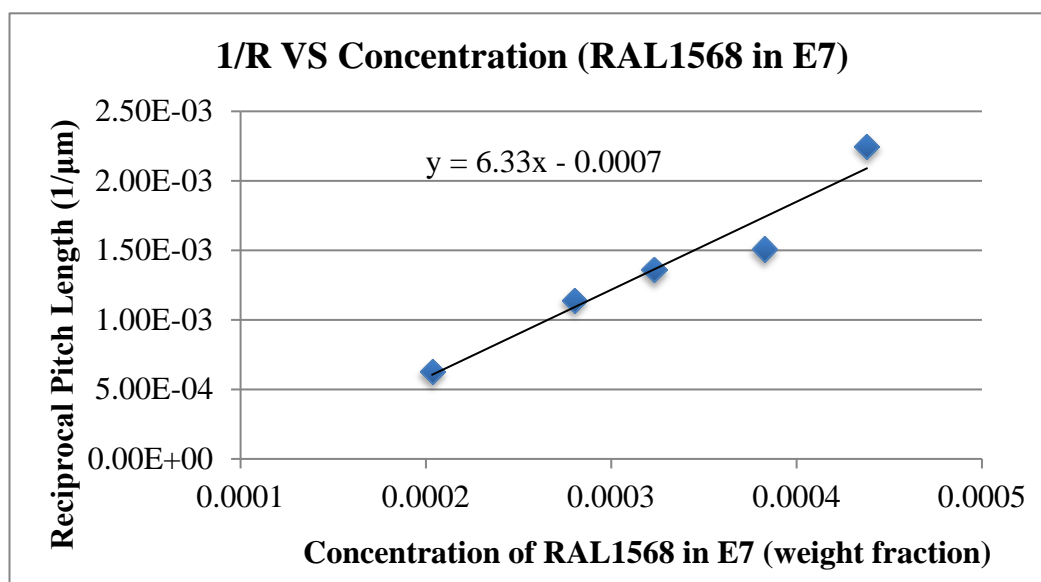
Figure 4.41: The slopes of 1/R vs. concentration of RAL1568 in E7.

It can be seen from Figure 4.41, the slope of the linear fit to the data is linear apart from the fourth data point, which is off set a little. Thus the fitting R^2 value was 0.9422, which is not as good a correlation as achieved in other studies, because the fourth data point deviates some way off the slope. However, the irregular shaped spots observed in TN cells at the concentration of 0.02033 wt% did not appear to influence the final result (the first data point in Figure 4.41) as it seems not to deviate from the slope. Thus, although the reason for these irregular shaped spot defects in the TN cell is not clear, and this phenomenon did not appear very often, the data was, fortunately, not affected thereby giving support to the robust nature of the method.

The resulting value of the helical twisting power of RAL1568 is 3.17 μm^{-1} was found to be relative low compared with R/S1011 and thalidomide, and even lower than AE8, which is only 4.47 μm^{-1}. So in order to ensure that this result was not due to the impurity of the material it was deemed worthwhile examining the other enantiomer, RAL1569. If the result of RAL1569 is close to or identical with RAL1568, then the helical twisting power of this dopant can be confirmed, as each enantiomer should have the same helical twisting power, assuming they have the same optical purity. If the values of HTP are not the same then it is still interesting to speculate on the differences between them.

Photomicrographs showing the disclination lines formed by mixtures of RAL1569 in E7 at various concentrations are shown in Figure 4.42.


(a) (b) (c)

(d) (e) (f)

(g) (h) (i)

(j) (k) (l)
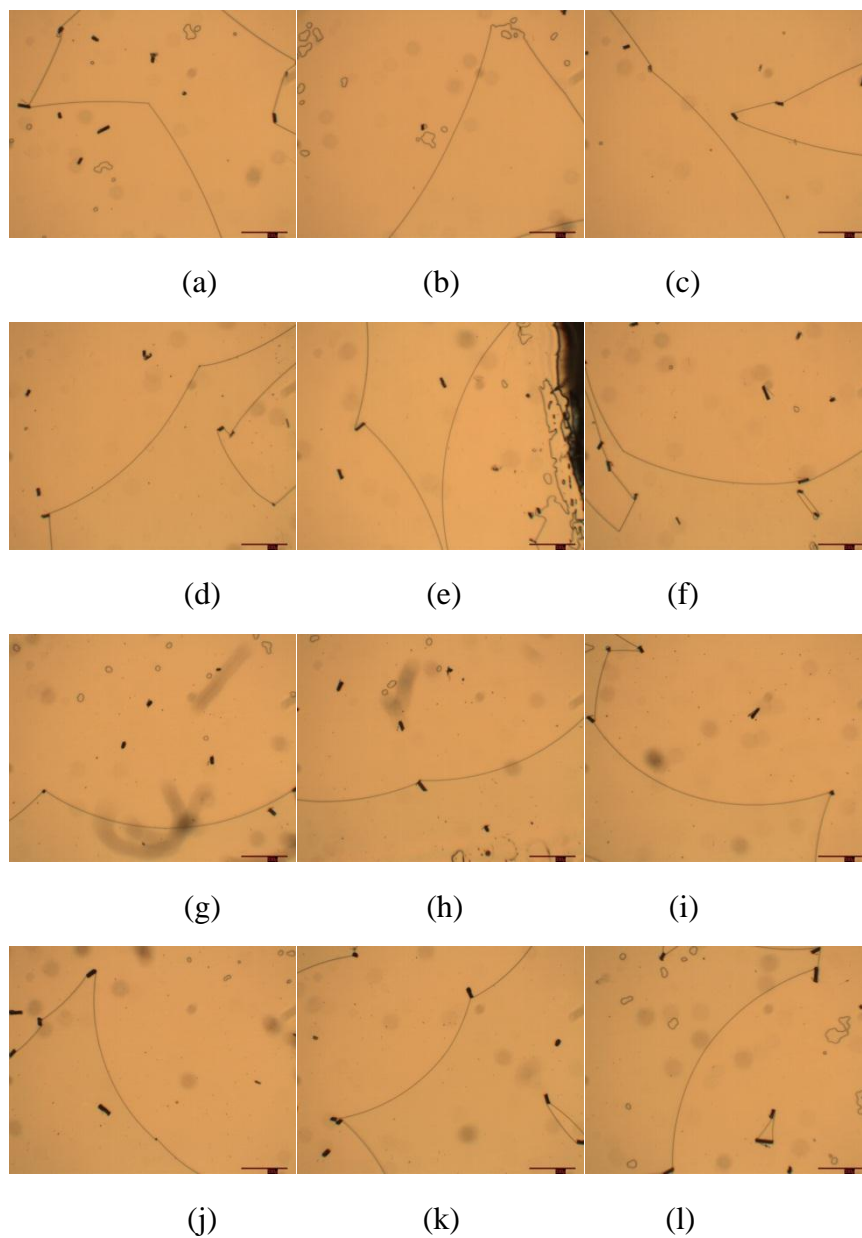
Figure 4.42: Photomicrographs (x50) showing the reverse-twist disclination lines of the mixtures of RAL1569 in E7 formed in 14.4 µm thickness TN cells of 14.4 µm thickness at concentrations of (a)-(c) 0.002270 wt%;(d)-(f) 0.006831 wt%; (g)-(i) 0.009114 wt%; and (j)-(l) 0.01339 wt%.

The irregular shaped spots were still seen in some preparations such as in photomicrographs (a), (b) and (l). In comparison to Figure 4.40 pictures (a) to (c), however, have fewer of these unusual spots. Interestingly, from all the pictures in Figure 4.42, more spacers were found in the TN cells than the cells used in Figure 4.40. Therefore, the number of spacers in the TN cell seemingly is one of the most important reasons governing the formation of curved disclination lines.

In order to obtain the helical twisting power of RAL1569 in E7, the radii of curvature in different concentrations were calculated and are presented in Table 4.13.

Concentration (wt%)	Radii of curvature (μm)	Reciprocal of Radii (1/μm)
0.002270	2062	0.000485
0.006831	1230	0.000812
0.009114	896	0.00112
0.01339	831	0.00120

Table 4.13: The concentrations, mean radii of curvatures (μm), and mean reciprocal of radii (1/μm) of RAL1569 in E7.

A plot of the average reciprocal of the radius of curvature as a function of concentration in E7 for RAL1569 in E7 is given in Figure 4.43. From the gradient of the linear fit to the data, the HTP of RAL1569 in E7 was determined to be 3.38 μm^{-1}.
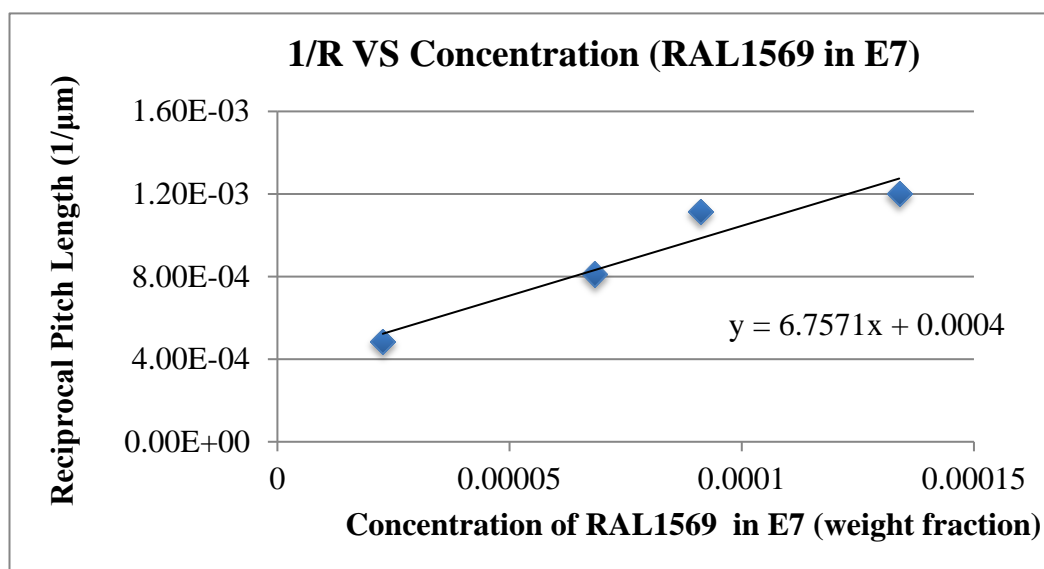
Figure 4.43: The slopes of 1/R vs. concentration for RAL1569 in E7

The helical twisting power values of the enantiomers RAL1568 and RAL1569 were very close, at 3.17μm^{-1} and 3.38μm^{-1} respectively. The slight difference is only 6%, which can be accounted for by differences in optical purity, errors derived from the TN cell measurements or different pre-twist values of the cells used. The reasons why RAL1568 and RAL1569 do not give as high HTP values as R/S1011 will be discussed towards the end of this chapter.

The next dopant to be studied was RAL1636, shown in Figure 4.39. In comparison to RAL1568 and RAL1569, which possess a fluoro substituent attached to the stereogenic centre, for RAL1636 a much more polar cyano is located at this site. Additionally the terminal chain length was reduced in length from C6 to C1, thereby complicating a direct comparison between the two sets of materials. Moreover the nitrile units are known, in some systems, to strongly interact.

The same methodology was again used for preparing and analysing the mixtures of RAL1636 in E7. Photomicrographs showing the disclination lines formed by mixtures of RAL1636 in E7 at various concentrations are shown together in Figure 4.44.
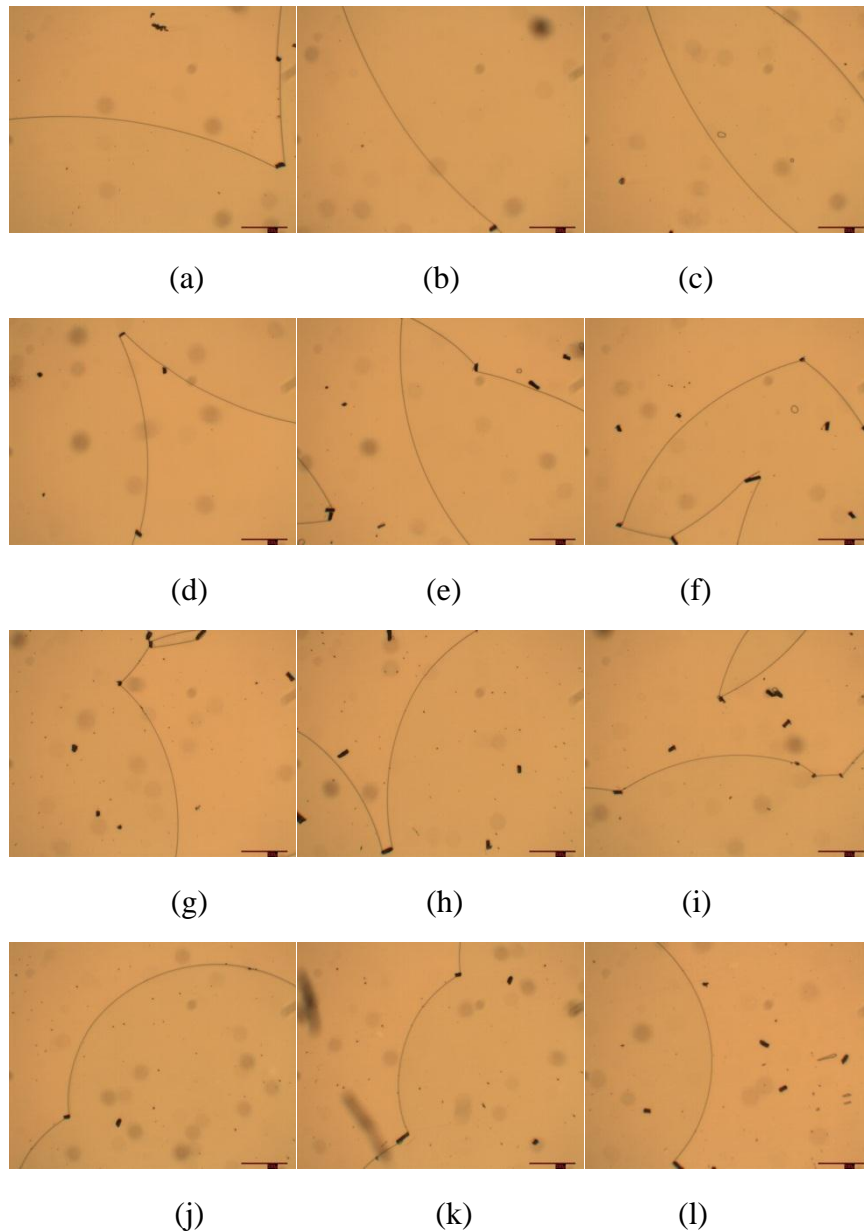
Figure 4.44: Photomicrographs (x50) showing the reverse-twist disclination lines of the mixtures of RAL1636 in E7 formed in TN cells of 14.4 μm thickness at a concentration of (a)-(c) 0.006996 wt%;(d)-(f) 0.01038 wt%;(g)-(i) 0.01393 wt%; and (j)-(l) 0.01730 wt%.

The behaviour of RAL1636 is as expected from all the previous studies of dopants, giving curved disclination lines at all concentrations. It is clear that as the concentration increased, the radii of curvature decreases gradually. In order to obtain the helical twisting power of RAL1636 in E7, the radii of curvature in different concentration were calculated and are presented in Table 4.14.

Concentration (wt%)	Radii of curvature (μm)	Reciprocal of Radii (1/μm)
0.006996	2047	0.000489
0.01038	1244	0.000804
0.01393	878	0.00114
0.01730	608	0.00174

Table 4.14: The concentrations, mean radii of curvatures (μm), and mean reciprocal of radii (1/μm) of RAL1636 in E7.

A plot of the mean/average reciprocal radii of curvature as a function of concentration in E7 for RAL1636 in E7 is given in Figure 4.45. From the gradient of the slope of the line for best fit to the data, the helical twisting power of RAL1636 in E7 was determined to be 5.92 μm^{-1}.

1/R vs Concentration (RAL1636 in E7)

$y = 11.847x - 0.0004$
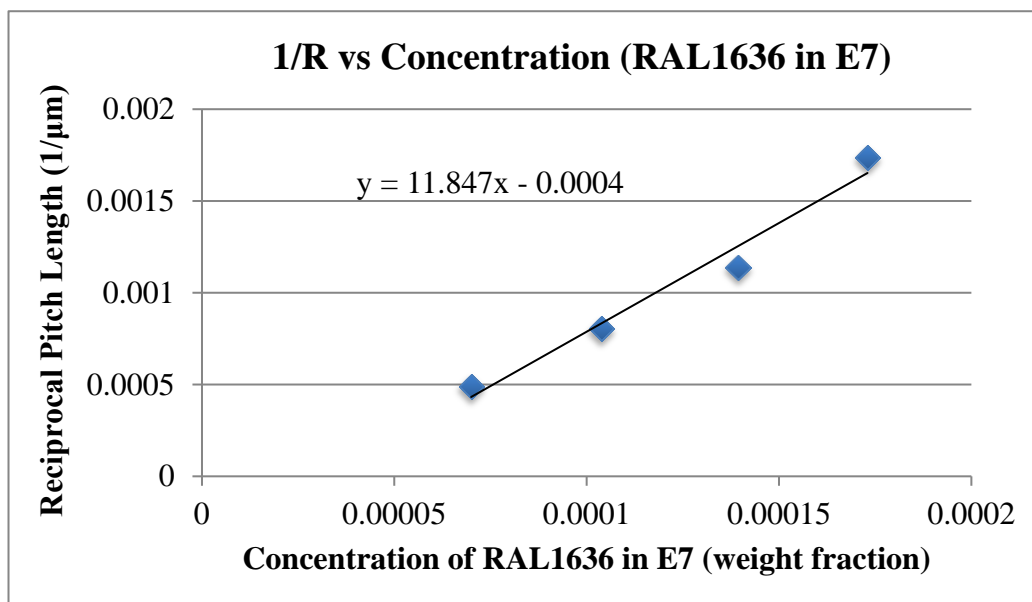
Figure 4.45: The slopes of 1/R vs. Concentration RAL1636 in E7.

Although all the data collected is not a perfectly linear line (R^2 value of 0.9713), apart from the third data point the other three points are very close to a linear fit. The helical twisting power value of RAL1636 (5.92 μm^{-1}) is larger than the value for RAL1568 (3.17μm^{-1}) and RAL1569 (3.38μm^{-1}). Although it is difficult to say for centrain at this point, the reason for this difference could be that the cyano group is more polar than F in RAL1568 and RAL1569 or that RAL1636 somehow interacts better with the host. Alternatively, this difference could be due to steric factors, or a combination of steric and electronic influences.

The last dopant of this group to be studied was RAL1608. The chemical structure of RAL1608 is very similar to that of RAL1568 (RAL1569), with the only difference being that the fluorine atom is replaced by CF_3, as shown in Figure 4.39.

In an attempt to discover how the polarity of the groups adjoined to the stereogenic centre influence helical twisting power, RAL1608 was also examined by the reverse twist disclination method. Photomicrographs of the disclination lines formed by mixtures of RAL1608 in the E7 at various concentrations are shown in Figure 4.46.
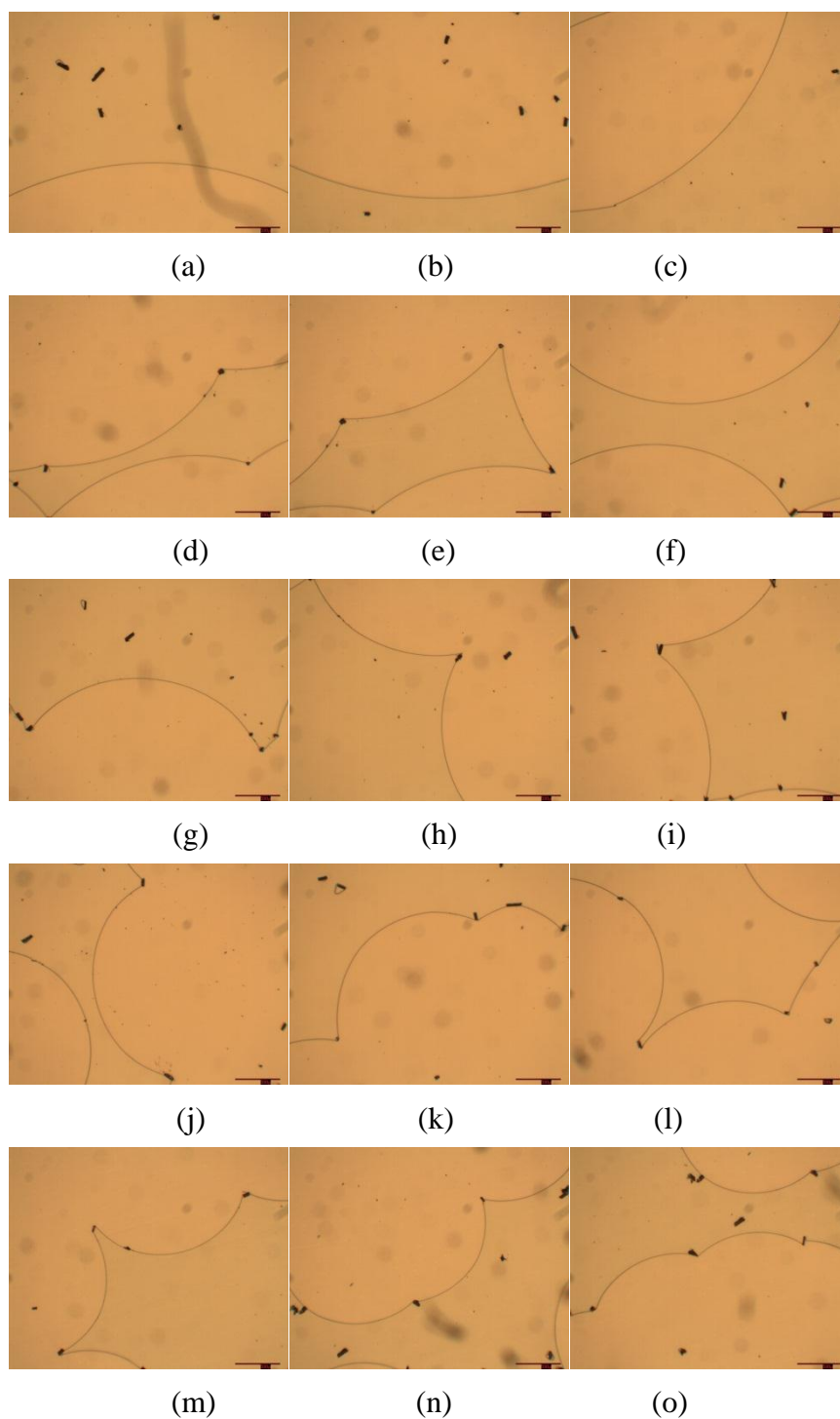
Figure 4.46: Photomicrographs (x50) showing the reverse-twist disclination lines of the mixtures of RAL1608 in E7 confined in 14.4 μm thickness TN cells at a concentration of (a)-(c) 0.003050 wt%; (d)-(f) 0.006191 wt%;(g)-(i) 0.009316 wt% (j)-(l) 0.01232 wt%; and (m)–(o) 0.01540 wt%.

In order to obtain the helical twisting power of RAL1608 in E7, the radii of curvature in different concentration was calculated, and the results are given in Table 4.15.

Concentration (wt%)	Radii of curvature (μm)	Reciprocal of Radii (1/μm)
0.003050	1466	0.000682
0.006191	875	0.00114
0.009316	631	0.00158
0.01232	469	0.00213
0.01540	377	0.00265

Table 4.15: The concentrations, mean radii of curvatures (μm), and mean reciprocal of radii (1/μm) of RAL1636 in E7.

A plot of the reciprocal radius of curvature as a function of concentration in E7 for RAL1608 in E7 is given in Figure 4.47.
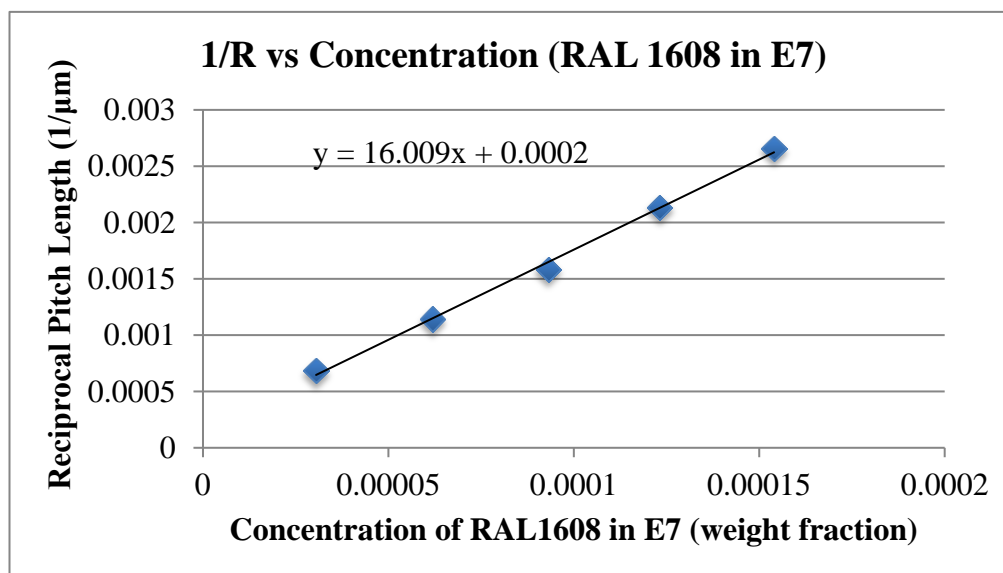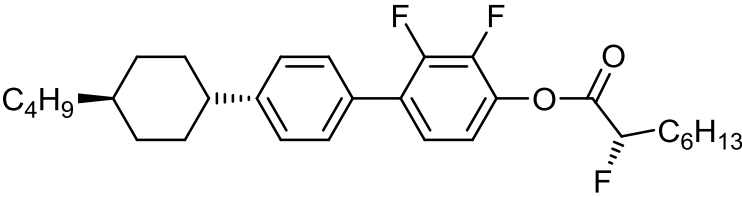
Figure 4.47: The slopes of 1/R VS Concentration RAL1608 in E7.

In this case, the combined results obtained from the various concentrations were consistent, and with the data being in excellent agreement with a linear fit (R^2=
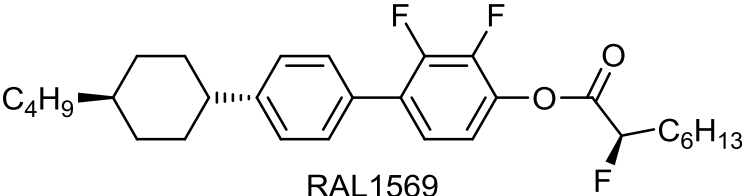
0.99733). In addition, the helical twisting power of RAL1608 was determined to be 8.00 μm^{-1}, which is the highest value for the RAL dopants tested in the host E7, as shown in Table 4.16.

Dopant	HTP (E7, μm^{-1})
RAL1568	3.17
RAL1569	3.38
RAL1636	5.92
RAL1608	8.00
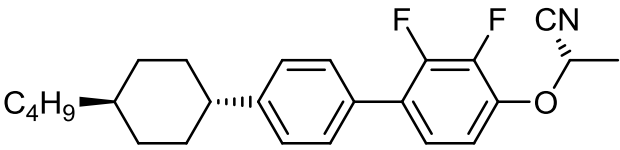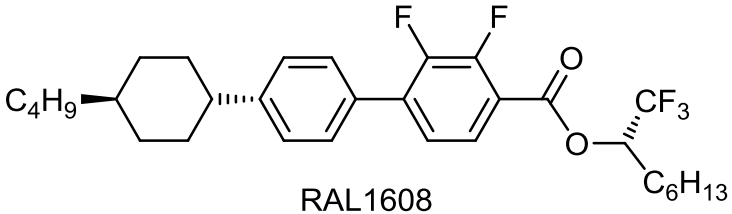
RAL1568

RAL1569

RAL1636

RAL1608

Table 4.16: The helical twisting power value of the RAL series dopants in E7.

First, it is worth comparing RAL1608, which has the highest HTP values of the series, and RAL1568/RAL1569, which have the lowest. Considering their chemical structures are very similar, and the only difference as mentioned before is the lateral substituents CF_3 and F at the stereogenic centre. There are two basic physical property differences between CF_3 and F which are size and polarity.
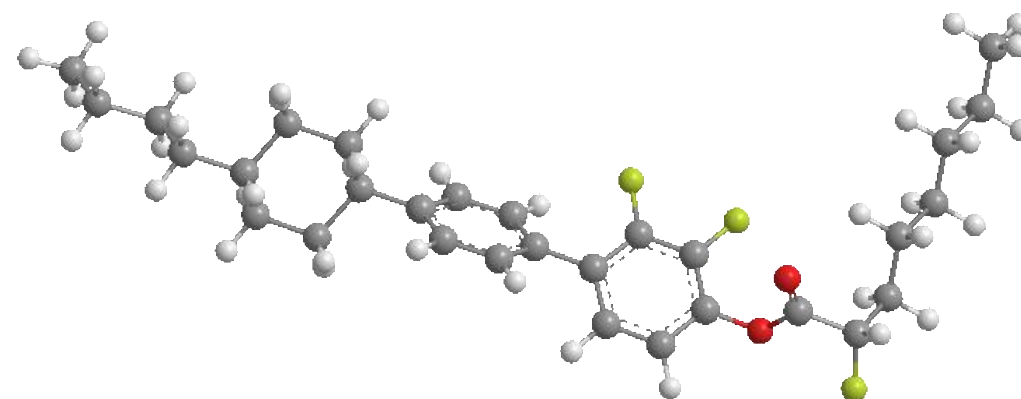
RAL1568
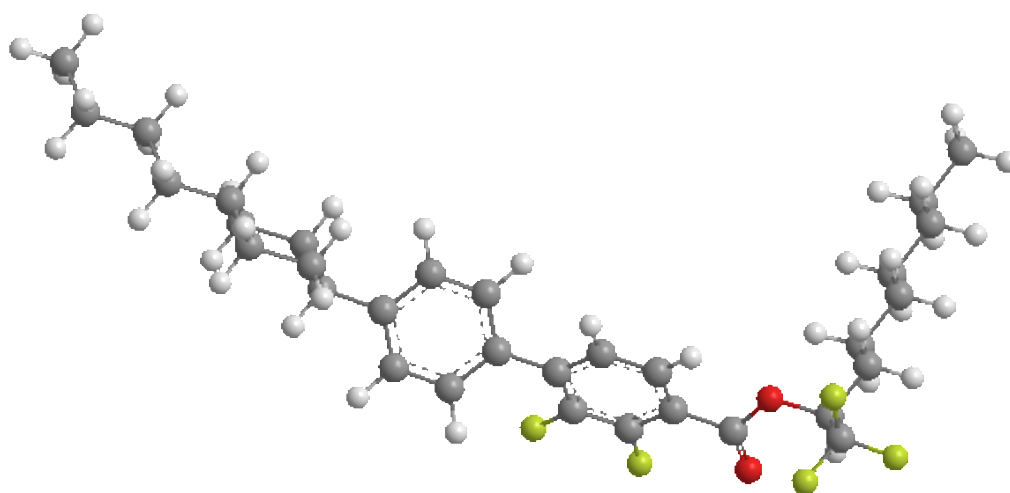
RAL1608

Figure 4.48: Minimum energy conformations of RAL1568 (top) and RAL1608 (bottom) as obtained at the B3LYP/6-311G* level of theory.

The minimum energy conformations of RAL1568 and RAL1608 were obtained at the B3LYP/6-311G* level of theory, followed by calculation of the dipole and polarisability tensors at the same level of theory using the Gaussian 09 suite of software. From Figure 4.48 both their conformations are V-shaped, and so the

147

"propeller" helical twisting power enhancement is not relevant in this situation as proposed for thalidomide. The stereogenic centre for both RAL compounds is a carbon atom, and not the metal complex dopant described in introduction, where the core is bigger in size and connected with several large branching units. Conversely, the difference in size between the CF_3 and F units is not enormous as shown in Figure 4.48. Therefore, the size difference is likely not the main reason for the difference in helical twisting power, although it should be noted that the trifluoromethyl-substituent at the setereogenic centre has less rotational freedom about the molecular long axis than the fluoro-substituent.

In an attempt to explore polarity differences between these materials, the polarisability and dipole of RAL1568 and RAL1608 were calculated using the B3LYP/6-311G level theory in Gaussian 09 software, and the results are listed in Table 4.17.

Dopant	Mean Polarisability($\mathring{A}^3$)	Anisotropic Polarisability($\mathring{A}^3$)	Dipole (Debye)
RAL1568	52.65	29.60	1.86
RAL1608	57.46	37.30	4.68

Table 4.17: Polarisability and dipole of RAL1568 and RAL1608 as determined at the B3LYP/6-311G* level of theory.

Obviously, in comparison to the fluorine atom, the relatively larger polarity of CF_3 dominates as RAL1608 has a much larger dipole moment than RAL1568. At the same time, the mean polarisability and anisotropic polarisability, *i.e* the ability of the electron distribution to change in a polar medium or electric field, of RAL1608 are also greater than RAL1568. The most interesting point is that the dipole of RAL1608 is 2.52 times that of RAL1568 and the helical twisting power of RAL1608 is also 2.52 times that of RAL1568. Since there are no further similar comparative studies done so far, it cannot be certain whether the values are simply

148

coincidental. It is therefore very difficult to confirm that the enhancement of the dipole with respect to dopants of similar chemical structure will cause the same scale of enhancement to the value of the helical twisting power. However it can be concluded that a strong polar substituent in the stereogenic centre can amplify the helical twisting power relative to dopants of similar structure.

It is also worth comparing RAL 1568 and RAL1636. Although the structures of RAL1568 and RAL1636 are not as similar as those of RAL1568 and RAL1608, it is still worthwhile studying their conformations. The minimum energy conformations of RAL1568 (Figure 4.48) and RAL1636 (Figure 4.49) were obtained at the B3LYP/6-311G* level of theory, followed by calculations of their dipole and polarisability tensors at the same level of theory.
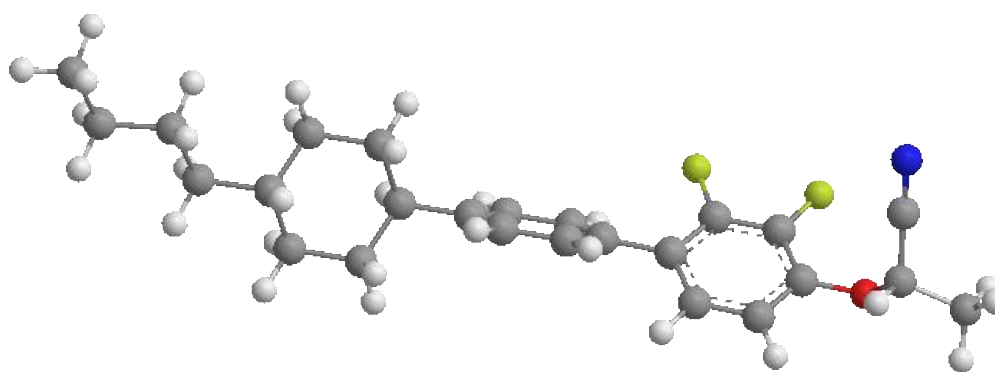
RAL1636

Figure 4.49: Minimum energy conformation of RAL1636 as obtained at the B3LYP/6-311G* level of theory.

Interestingly, compared with the minimum energy conformation of RAL1568, the minimum energy conformation of RAL1636 is very different because even in the gas phase it is rod-shaped due to the lack of long aliphatic chains. This is another piece of evidence that suggested that the "propeller-shaped effect" does not exist for the RAL series of dopants. As the "rod-shaped" RAL1636 has a larger helical twisting power than the V-shaped RAL1568, the "propeller" shape effect does not seem to apply in these compounds. Considering the CN substituent is more polar

149

than the F substitute, so that the RAL1636 has a larger dipole, RAL1636 still does not have large differential in comparison with RAL1568. This may be because the stereogenic centre in RAL1568 is connected with the diflouro biphenyl by an ester group, whereas for RAL1636 the stereogenic center is connected *via* an ether group. Furthermore, there is a C_6 aliphatic carbon chain bonded to the stereogenic centre in RAL1568, whereas RAL1636 for there is cyano and methyl substituent connecting with the stereogenic centre. This means for RAL1636 the end group carrying the stereogenic centre has freedom to rotate, and therefore the dipolar coupling between molecules is relatively weak. Nevertheless, it is still worthwhile discovering if the polarisability or dipole differences are the main reasons behind the differences in helical twisting power.

The polarisability and dipole of RAL1568 and RAL1636 were calculated using the same theory in Gaussian 09 software, the results for which are shown in Table 4.18.

Dopant	Mean Polarisability(Å^3)	Anisotropic Polarisability(Å^3)	Dipole (Debye)
RAL1568	52.65	29.60	1.86
RAL1636	44.03	33.04	5.13

Table 4.18: Polarisability and dipole of RAL1568 and RAL1636 as determined at the B3LYP/6-311G* level of theory.

Although the CN substituent is more polar than F substituent, when combining the difference between C_6 and methyl end chains, which affect molecular rotation as well as the molecular size and shape, the actual HTPs are not radically different. However, in total, the dipole and polarisability of RAL1636 is bigger than that for RAL1568, which might explain the difference in HTP. All the data in Table 4.18 shows that a bigger dipole can, in these cases, produce higher helical twisting powers.

Finally, it is very interesting to compare RAL1636 and RAL1608. Although the dipole of RAL1636 is even bigger than RAL1608, due to the CF_3 substituent contributing to the polarity, the mean polarisability of RAL1608 is bigger than RAL1036. In this case, it suggests that when the net dipole moments of two materials are very similar, the more polar functional substituent at the stereogenic centre can induce a higher helical twisting power.
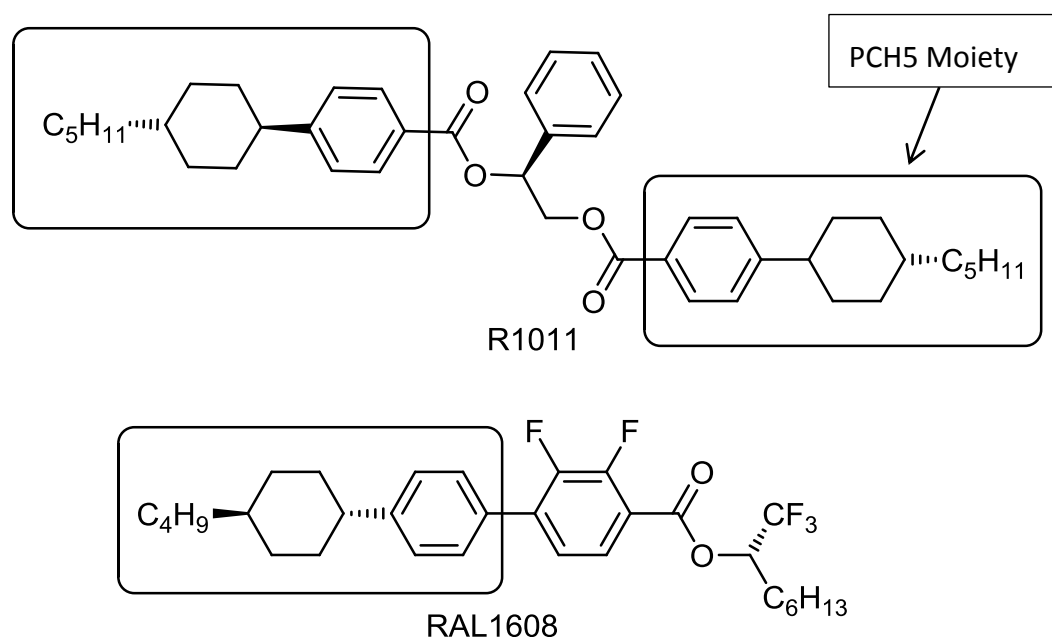
Figure 4.50: The chemical structures of the chiral dopants R1011 and RAL1608, with the structurally similar components highlighted for comparison.

Interestingly, in comparison with R1011, RAL1608 also has a similar moiety, which consists of a phenyl ring, *trans*-cyclohexene unit and aliphatic chain. The difference in length of the C_5 and C_4 chains can be ignored in this situation. However, the helical twisting power of R1011 is 4.7 times bigger than RAL1608, even though RAL1608 has highest helical twisting power value of all of the CDFBP-based chiral dopants. Although the mechanism that causes the large difference is still unknown, the "propeller" effect could be enhancing the helical twisting power value of R1011. Moreover, R1011 is also a dimer, and recently Proni and co-workers reported a dimer that has a significantly large helical

twisting power value of 242.3µm^{-1} in E7 (Figure 4.51).[152] The dimer is based on BINOL, and has a much higher HTP than is usual for non-dimeric BINOL-based dopants.[72] Thus, dimerization may be considered another effect for increasing the helical twisting power value.
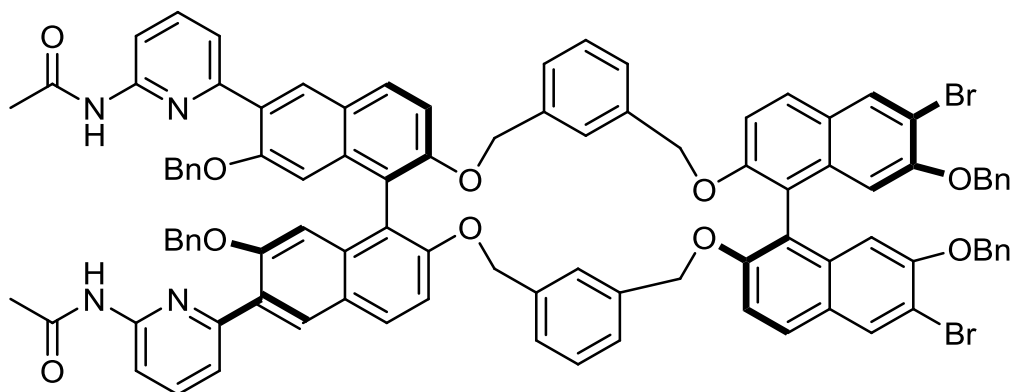
Figure 4.51: The structure of BINOL dimer.

In summary, four CDFBP-based chiral dopant were examined *via* the reverse twist disclination method. RAL1608 has a larger helical twisting power (8.00 µm^{-1}), than the other RAL and oxazoline-base dopants studied yet it still far smaller than both of high helical twisting power dopants R/S1011 and thalidomide. From these measurements, and in conjunction with molecular modelling, it can be reasoned that more polar substituents at the stereogenic centre, based on similar molecular structures, enhance the helical twisting power.

4.5.1   Investigation of an Unknown Material

The next pair of dopants to be studied was RAL1601 and RAL1636, where RAL1601 was supposedly the enantiomer of RAL1636, shown in Figure 4.39. The same methodology was used for preparing and analysing the mixtures of RAL1601 in E7 for comparative studies with RAL1636. Photomicrographs

showing the disclination lines formed by mixtures of RAL1601 in E7 at various concentrations are shown in Figure 4.52.
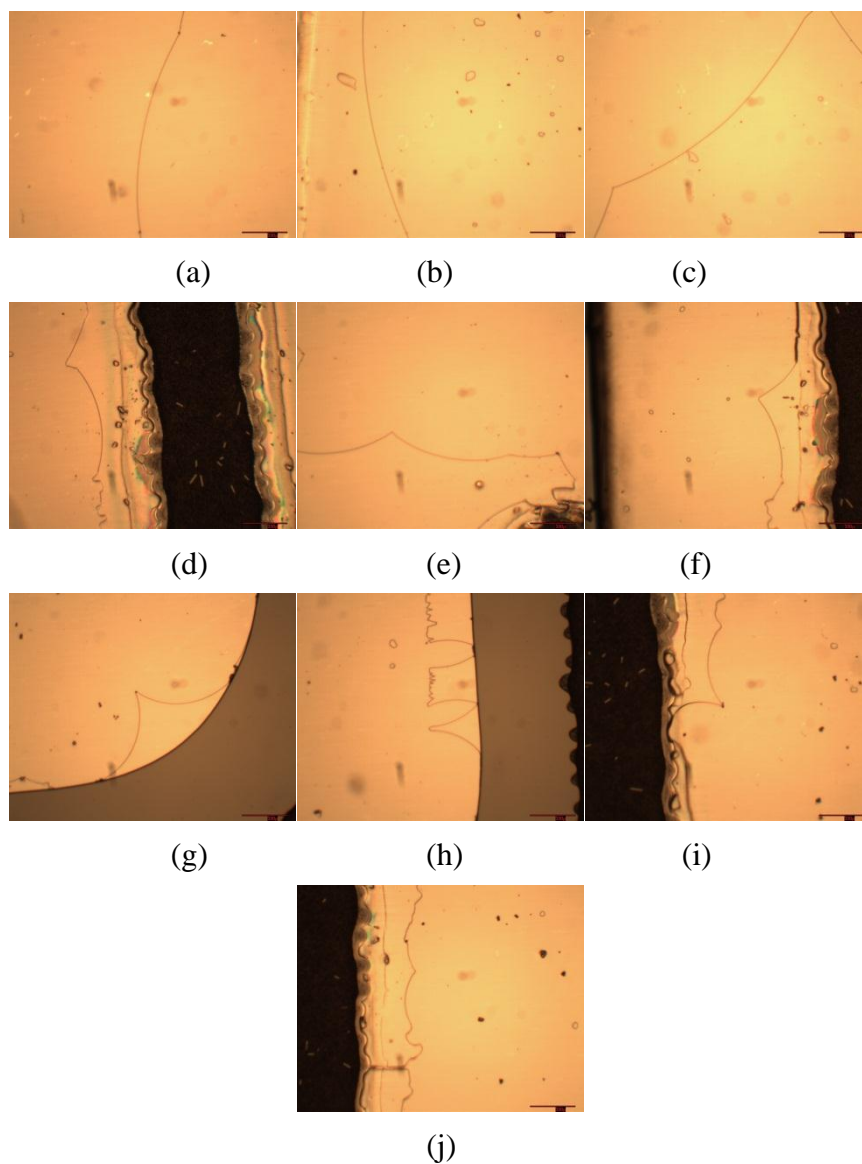
Figure 4.52: Photomicrographs (x50) showing the reverse-twist disclination lines of the mixtures of RAL1601 in E7 formed in TN cells of 14.4 μm thickness at a concentration of (a)-(c) 0.04582 wt%; (d)-(f) 0.09067 wt%; (g)-(i) 0.1404 wt%; and (j) 0.2336 wt%.

Surprisingly, although RAL1601 and RAL1636 were expected to be enantiomers they did not behave the same way in E7, assuming that similar data should be obtained for RAL1601 as for the other enantiomeric dopant tested previously. From the studies of RAL1601, it can be seen from Figure 4.50 that the disclination

lines did not form to the same extent as in the other mixtures. What is more, from the pictures (a)-(c), the curvature of the disclination lines is not very large, possibly as the concentration was not high enough at only 0.04582 wt%. However, even when the concentration was increased to 0.09067 wt%, the disclination lines were still not particularly curved (see the Figure 4.52 (d)-(f)), with the disclination lines appearing less in the centre of the TN cell and only observed close to the edge of the cell. When the concentration of RAL1601 in E7 was 0.1404 wt% the radii of disclination lines became very small. The results proved that the concentration jump from 0.09067 wt% to 0.1404 wt% probably is too much, so that the radii of curvature of the disclination lines are either too big or too small. Therefore, four more mixture of RAL1601 in E7 were prepared with concentrations of 0.005489 wt%, 0.008247 wt%, 0.01100 wt% and 0.01385 wt%. All of the mixtures were prepared so as to be between 0.04582 wt% to 0.1404 wt%. The aim of this was to obtain more results, thereby allowing a more accurate calculation of HTP values. Unfortunately, all these results were even more unusual and raised more questions than answers. Only straight lines were found in the cell, demonstrating that there was no chiral induction in the mixture at all (see in Figure 4.53).


(a)   (b)

(c)   (d)
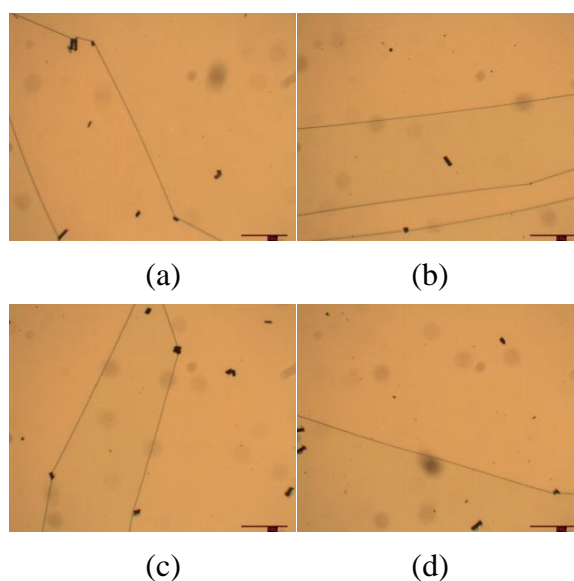
Figure 4.53: Photomicrographs (x50) showing the reverse-twist disclination lines of the mixtures of RAL1601 in E7 formed in TN cells of 14.4 μm thickness at a

concentration of (a) 0.005489 wt%;(b) 0.008247 wt%;(c) 0.01100 wt% and (d) 0.001385 wt%.

The results shown in Figure 4.52 suggested that more concentrated mixtures needed to be prepared. Thus, 0.2336 wt% of RAL1601 in E7 was prepared and yet even at this concentration there was only one curved disclination lines found in the whole TN cell, see Figure 4.52 picture (j). Thus, the helical twisting power of RAL1601 appeared not to be constant. Therefore, data from Figure 4.52 was used to determine the HTP. The gradient shown in Figure 4.52 gives a HTP value of 1.06 μm^{-1}.
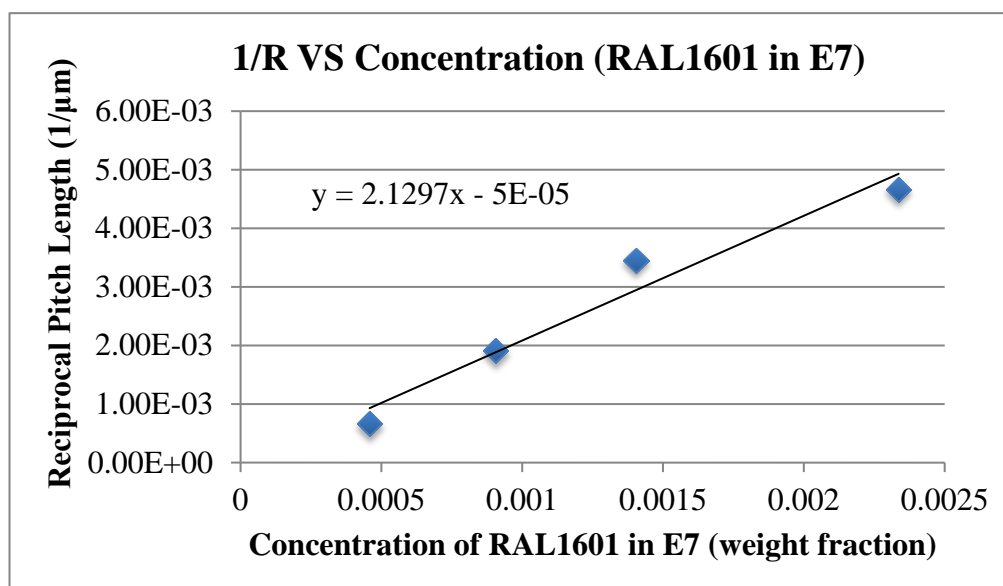
Figure 4.54: The slopes of 1/R vs. Concentration RAL1601 in E7.

However, if the data from Figure 4.53 were used, the helical twisting power value of RAL1601 would be 0 μm^{-1}. Due to the unexplained and unexpected result for RAL1601 and RAL1636, it was thought that RAL1601 might not be correctly labelled and was not the enantiomer of RAL1636. Therefore, the chemical structures of the two materials were investigated by NMR. The NMR spectrums of the two are depicted in Figure 4.55, and conclusively show that RAL1601 and RAL1636 are not enantiomers at all but rather are quite different compounds. In

155

the comparison of proton NMR spectrums of RAL1601 and RAL1636, it showed RAL1636 and RAL1601 have very similar branching groups, but they do not have the same chemical structures.
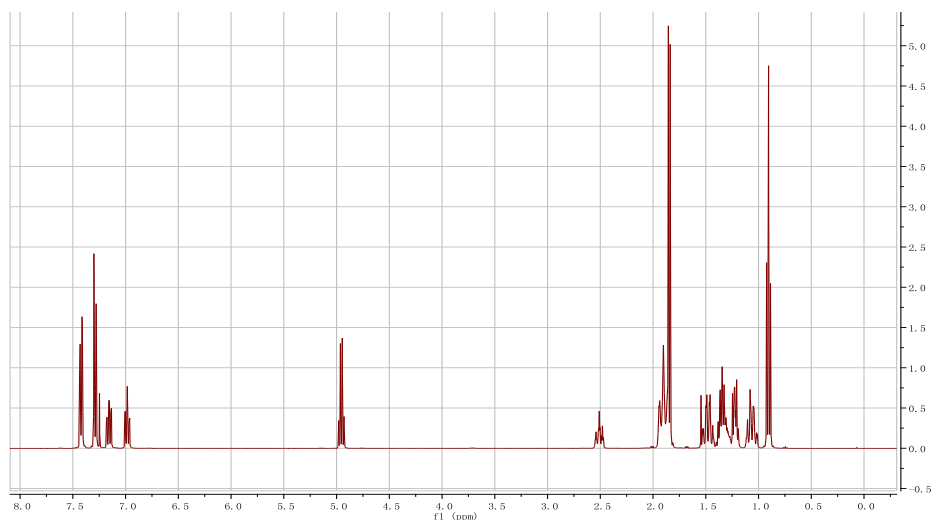
Proton NMR spectrum of RAL1636.
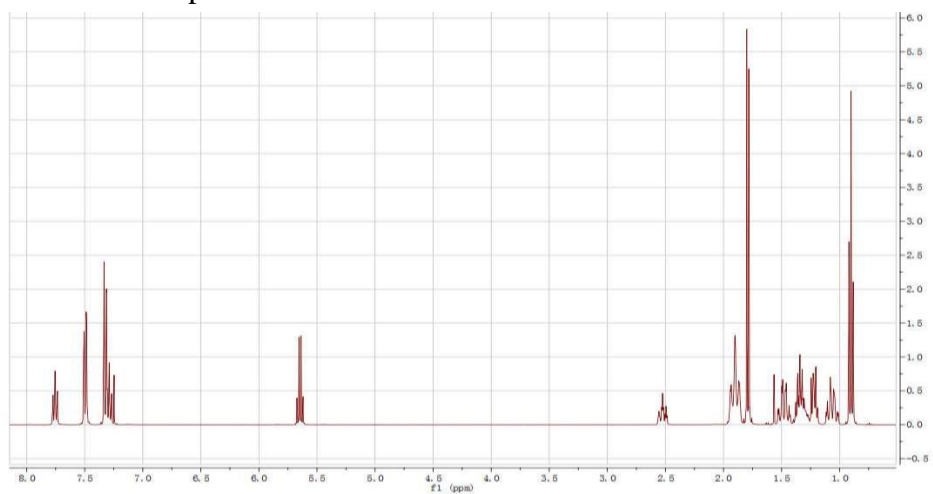
Proton NMR spectrum of RAL1601.
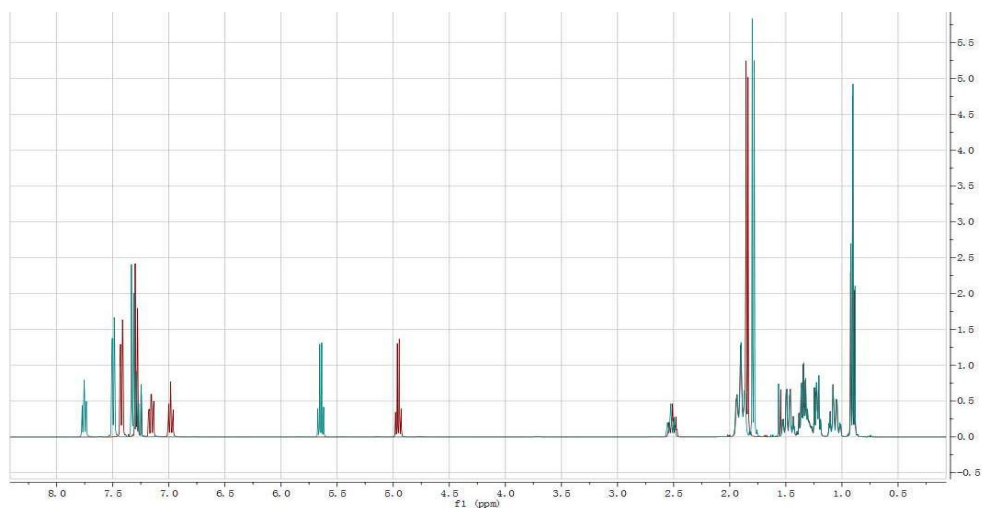
The overlaid proton NMR spectra of RAL1601 and RAL1636. (Green is RAL1636 red is RAl1601) **Figure 4.55:** Proton NMR spectra of RAL1601 (top) RAL1636 (centre) and overlaid spectra of RAL1601 and RAL1636 (bottom).

The following conclusions can be drawn from this latter study:

1. The 'reverse-twist disclination line method' shows that RAL1601 and RAL1636 are different compounds and not enantiomers.

2. RAL1636 is a chiral compound.

3. RAL1601 may be chiral, but its enantiopurity would be low, and it could even be a racemate. More likely it is not chiral at all.

4. NMR confirms the two materials are different substances.

5. The 'reverse-twist disclination line method' can be used to detect chirality, and to use chirality as a disciminating technique between materials of different type, or batches of enantiomers of differing optical purities.

6. The level of sensitivity of the 'reverse-twist disclination line method' means that the technique can be used in security or analytical devices.

4.6 Studies of a Chiral Supermoelcular Sugar Dopants in E7.

Since the discovery of liquid crystals, a large number of chemically different materials that exhibit LC phases have been synthesised. Supermolecular liquid crystals are one of the most interesting groups of materials as they consist of mesogenic functional groups, like liquid crystal polymer, but yet in a low molecular weight system.[6] Supermolecular materials composed of methyl α-D-glucopyranoside as a chiral core unit with cyanobiphenyl mesogenic groups were prepared by Goodby and co-workers.[121] These supermolecular materials exhibited nematic and smectic A phases. In this chapter, the helical twisting power of methyl α-D-glucopyranoside and a methyl α-D-glucopyranoside based supermolecular liquid crystal were determined *via* 'the reverse-twist disclination line method'. It was anticipated that these studies would allow determination of how the helical twisting power value changes when the material is functionalised with mesogenic groups, *i.e* how chirality from a central molecular scaffold is transmitted to the periphery of the molecular architecture.

Methyl α-D-glucopyranoside is a monosaccharide belonging to the glucose family of sugars. At first glance from its molecular structure it might be expected to give a low value of the HTP, despite having five stereogenic centres. This is because although there are four hydroxy groups and a methyl group connected with the chiral scaffold none of these groups have strong interactions with the E7 host. Furthermore, the configuration of the molecule is nearly flat, so that the "stereo effect" (propeller effect) may not "appear" when it is dissolved in E7.
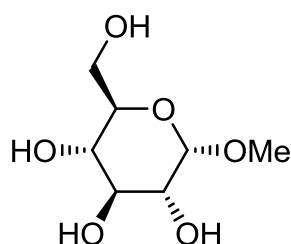
Figure 4.56: Structure of methyl α-D-glucopyranoside

As the methyl α-D-glucopyranoside was expected to have a low helical twisting power, a relatively high concentration of methyl α-D-glucopyranoside in a mixture with E7 was prepared, so as to allow measurements to be made. Although the solubility of methyl α-D-glucopyranoside in E7 had not previously been reported, considering its structure, it was not expected to be more soluble than R1011 in E7, the solubility limit of which is 4 wt%. In consideration of all of these factors, a 0.03592 wt% of methyl α-D-glucopyranoside in E7 was prepared, and the 'reverse-twist disclination' method was used to determine the HTP, as shown in Figure 4.57.

(a)	(b)	(c)
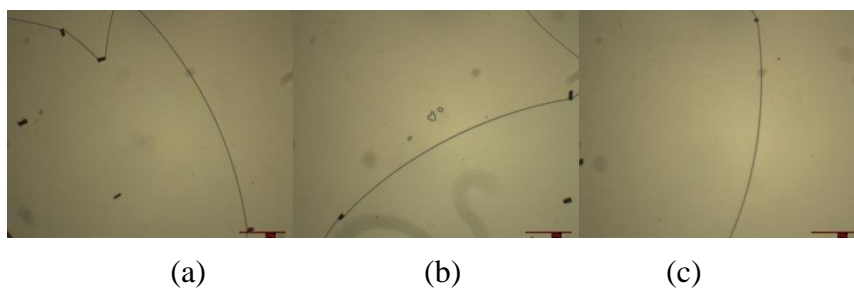
Figure 4.57: Photomicrographs (x50) showing the reverse-twist disclination lines for mixtures of methyl α-D-glucopyranoside in E7 formed in TN cells of 14.4 μm thickness at a concentrations 0.03592 wt%.

Interestingly, although the maximum solubility of methyl α-D-glucopyranoside in E7 is unknown, the curved disclination lines in Figure 4.55 confirm that methyl α-D-glucopyranoside in E7 induces chirality into the host. In addition, the disclination lines formed as shown in Figure 4.57 were very smooth, which suggests that methyl α-D-glucopyranoside interacts well with E7.

As the disclination lines were not particularly curved more concentrated mixtures were prepared. During the process of preparing the mixtures in 0.05609 wt%; 0.07155 wt% and 0.09894 wt% concentrations there was no precipitate observed, which confirmed that methyl α-D-glucopyranoside is soluble in with E7 at all of the concentrations studied.
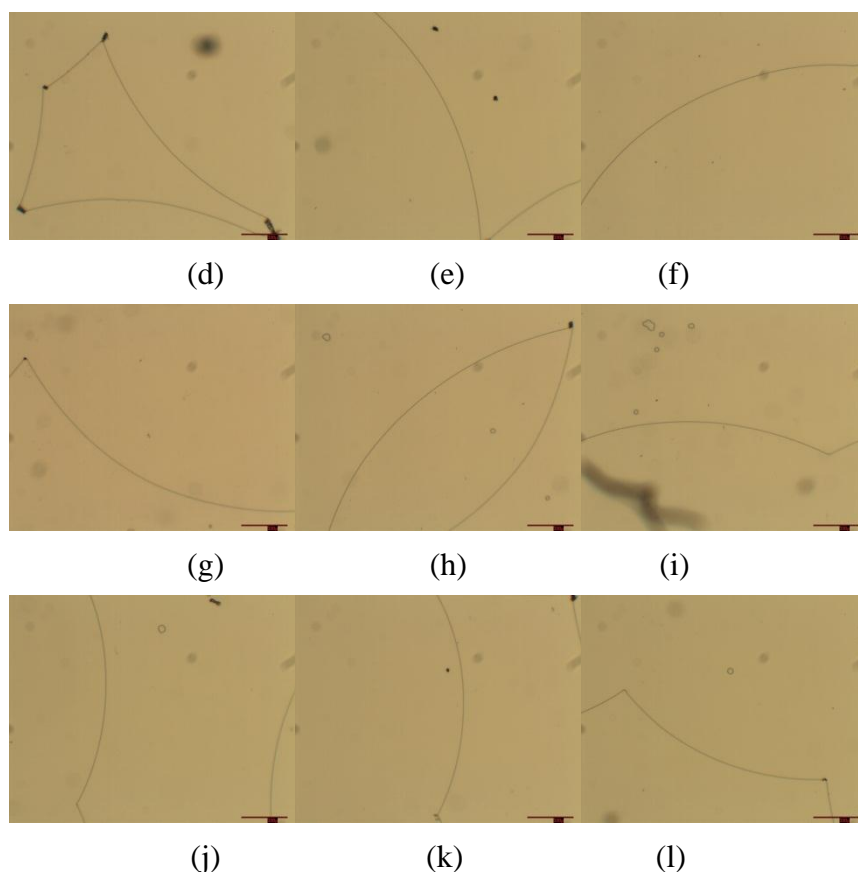
Figure 4.58: Photomicrographs (x50) showing the reverse-twist disclination lines of the mixtures of methyl α-D-glucopyranoside in E7 formed in 14.4 μm thickness TN cells at a concentration of (d)-(f) 0.05609 wt%; (g)-(i) 0.07155 wt%; and (j)-(l) 0.09894 wt%.

The disclination lines, shown in Figure 4.58, did not become much more curved as the concentration was increased. Thus, methyl α-D-glucopyranoside appeared not to have a very high helical twisting power value, as was hypothesised earlier. In order to determine the exact value of the helical twisting power of methyl α-D-glucopyranoside in E7, the radii of curvature for different concentrations were calculated, as shown in Table 4.19.

Concentration (wt%)	Radii of curvature (µm)	Reciprocal of Radii (1/µm)
0.03592	1881	0.0005316
0.05609	1321	0.0007568
0.07155	1304	0.0007666
0.09894	1061	0.0009427

Table 4.19: The concentrations (wt%), radii of curvatures (µm), and reciprocal (1/µm) of radii of methyl α-D-glucopyranoside in E7.

Using the data above in Table 4.19, a slope of 1/R vs concentration was made as shown in Figure 4.59.
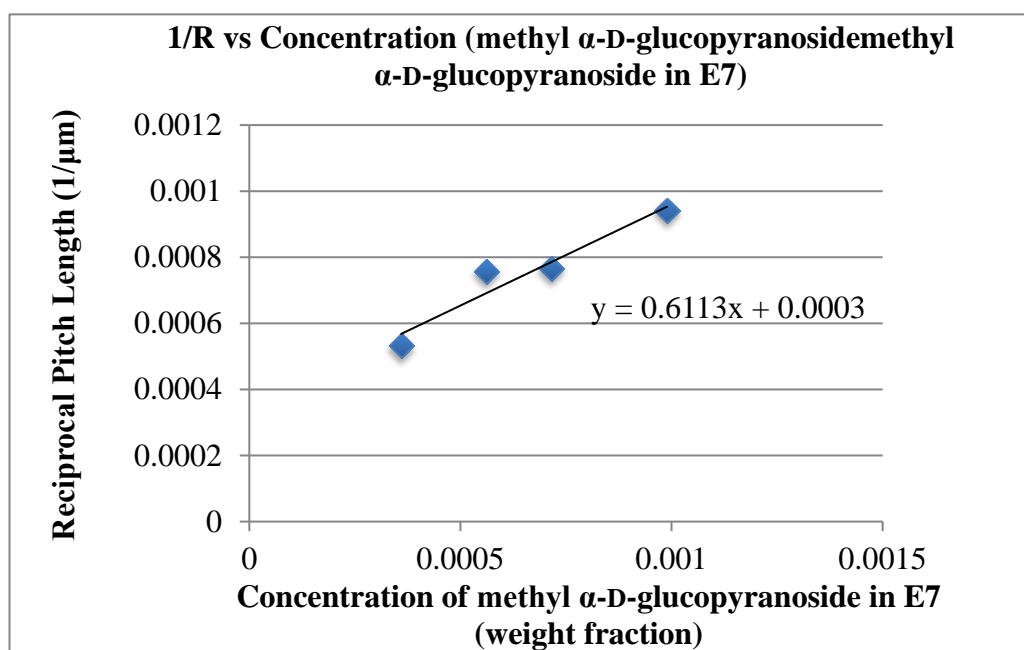
Figure 4.59: The slope of 1/R VS concentration for methyl α-D-glucopyranoside in E7.

Despite the fact that the concentration of methyl α-D-glucopyranoside in the mixture was increased, the radii of curvatures of the disclination lines did not increase significantly. However, the helical twisting power of methyl α-D-glucopyranoside could be calculated, the result being 0.31 µm^{-1}. This value is the lowest value that has been measured to date *via* this method. Although the

162

result is very close to 0 μm^{-1}, the four data points fit very well to the gradient of the slope. The data for the concentration of 0.05609 wt% seems to deviate from the slope a little, which generated a relative lower R^2 value of 0.9283. However, these results clearly confirm that methyl α-D-glucopyranoside induces chirality into the E7, even though its correlation with E7 is very weak.

Although methyl-D-glucopyranoside is chiral, its molecular structure is somewhat near spherical, and the four hydroxy groups and methyl group would not be expected to interact with E7 host particularly strongly. Because of these features, the chirality of the sugar is not being transmitted to the bulk phase of E7. This may be reason why its helical twisting power value is very low. In order to explore this further, methyl α-D-glucopyranoside with four cyanobiphenyl mesogenic groups appended to each free hydroxyl group was studied (Figure 4.60). This supermolecular material, code named **A4**, was synthesised by Belaissaoui *et al*, and is based on methyl α-D-glucopyranoside.[121] It has four mesogenic functional groups, and once dissolved in E7, it was expected to induce chirality in E7 host more effectively than the parent sugar due to the greater structural similarity between the host and the dopant.
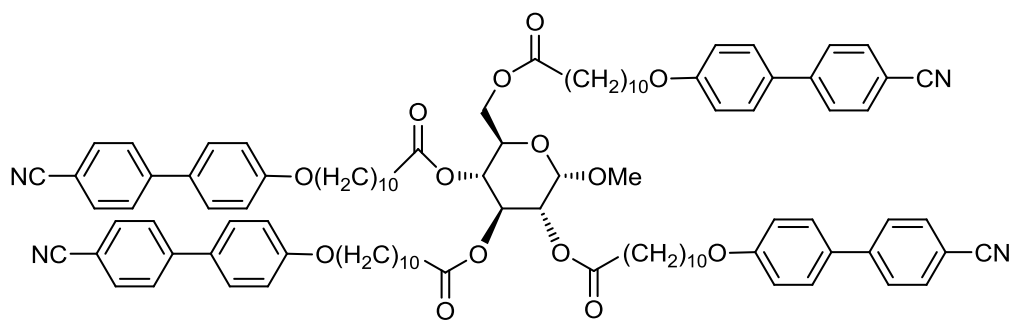
Figure 4.60: The structure of the chiral dopant **A4** as reported by Belaissaoui *et al*.

As predicted, A4 has higher solubility in E7 than the parent methyl α-D-glucopyranoside, but in the concentration of 0.02857%, there was not a satisfactory number of disclination lines formed in the cell for measurements to be made. There were only two disclination lines found in the cell; however the reason for this is unknown. As the disclination lines are curved (see Figure 4.61) it can be stated that **A4** has definitely induced the chirality into the E7 host and it appears to have a greater helical twisting power value than methyl α-D-glucopyranoside.

(a)   (b)

Figure 4.61: Photomicrographs (x50) showing the reverse-twist disclination lines of the mixtures of A4 in E7 formed in 14.4 μm thickness TN cells at a concentration of (a),(b) 0.02856%

In order to obtain more data, additional mixtures were prepared. Interestingly, when the concentration was increased to 0.03538 wt%, more disclination lines were formed than at the concentration of 0.02856%. When the concentration reached to 0.04696 wt%, less disclination lines were formed. However, at the highest concentration of 0.05149 wt%, a satisfactory number of disclination lines were formed again. This interesting phenomenon could be caused by the number

of spacers in the individual TN cell, suggesting that the number of disclination lines is not related to the concentration of each mixture, but to the cell fabrication. It can be seen from the photomicrographs for each concentration that more disclination lines were formed when the cell contained more spacers. This observation is consistent with the observations made for other mixtures presented in this chapter.
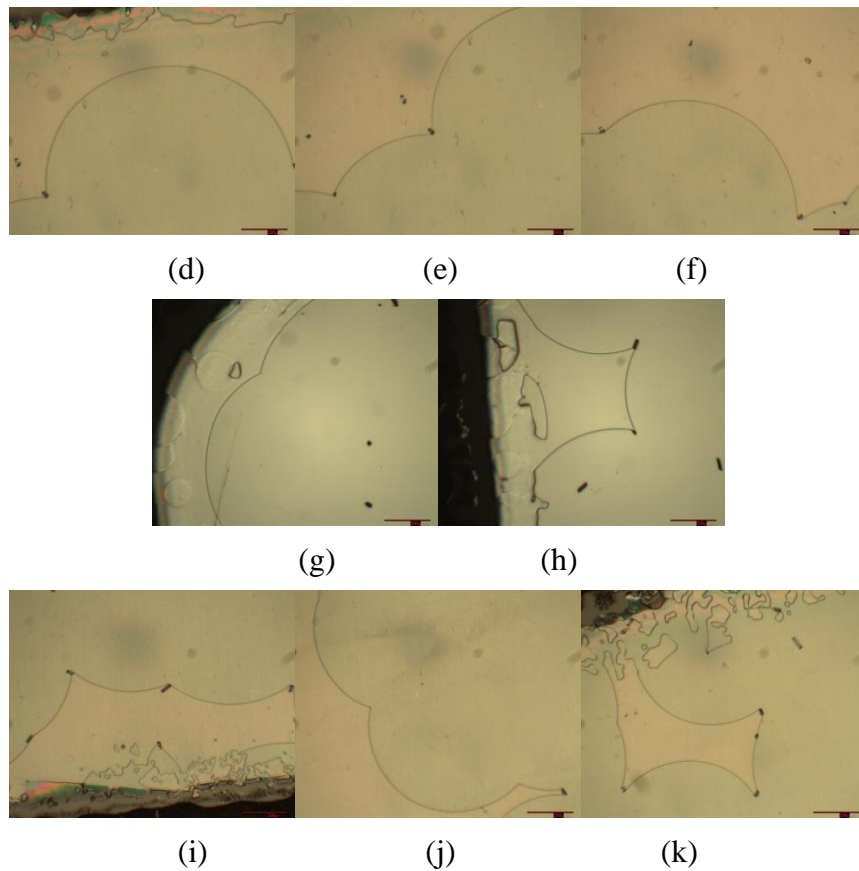
Figure 4.62: Photomicrographs (x50) showing the reverse-twist disclination lines of the mixtures of **A4** in E7 formed in 14.4 μm thickness TN cells at a concentration (d)-(f) 0.03538 wt%;(g)-(h) 0.04696 wt% and (i)-(k) 0.05149 wt%.

In order to determine the helical twisting power of **A4** in E7, the radii of curvature for different concentrations were calculated, as compiled in Table 4.20.

Concentration (wt%)	Radii of curvature (μm)	Reciprocal of Radii (1/μm)
0.02856	599	0.001669
0.03538	514	0.001944
0.04696	434	0.002255
0.05149	393	0.002547

Table 4.20: The concentrations (wt%), radii of curvatures (μm), and reciprocal (1/μm) of A4 in E7.

Using the data from Table 4.20, the slope of 1/R versus concentration for A4 in E7 was generated, as shown in Figure 4.63. The helical twisting power of AE4 was found to be 1.79 μm^{-1}. It can be seen in Figure 4.6.8 that the data was well fitted to a linear trend line (R ^{2}= 0.97816).
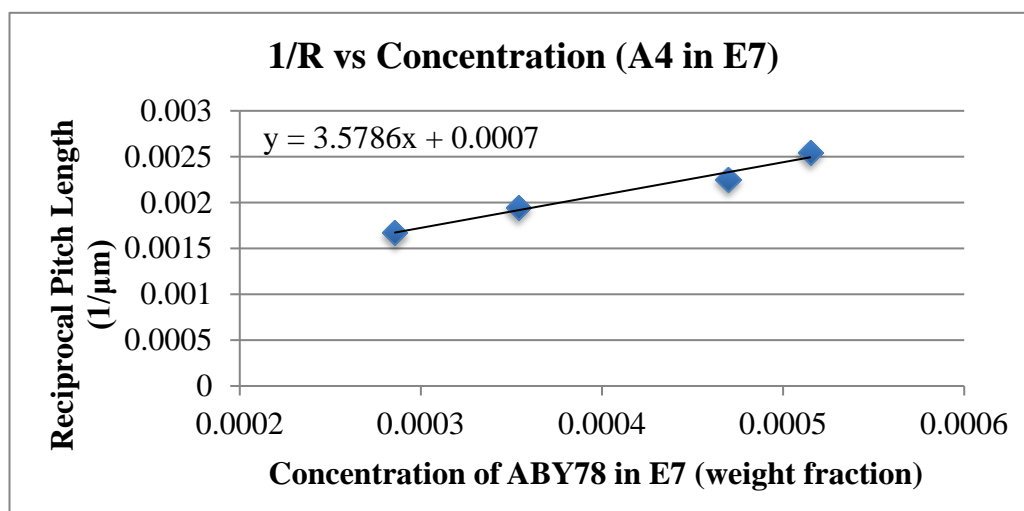
Figure 4.63: The slope of 1/R VS concentration for AE4 in E7.

In order to further investigate why methyl α-D-glucopyranoside and A4 have such low helical twisting powers in comparison to the previously studied dopants, the minimum energy conformations of methyl α-D-glucopyranoside and A4 were obtained at the B3LYP/6-311G* level of theory in Gaussian 09.

It can be seen from Figure 4.64, that the minimum energy conformation of methyl α-D-glucopyranoside is very different compared with the previous results. The equitorial arrangement of the hydroxyl groups means that they are positioned in a circular way around the edge of the ring. This has the effect of producing an almost symmetrical structure, which reduces the degree of chirality, and so there is no strong stereo conformation effect as for thalidomide, which has a "propeller" shape, enhancing the helical twisting power.

methyl α-D-glucopyranoside

A4
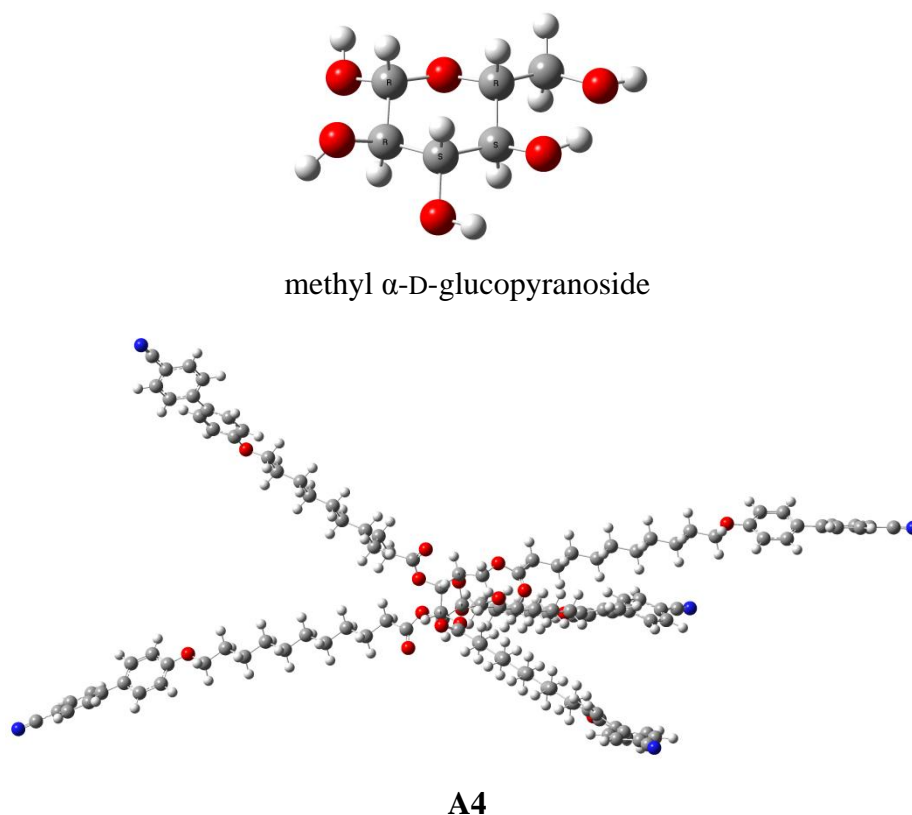
Figure 4.64: Minimum energy conformations of methyl α-D-glucopyranoside (top) and A4 (bottom) as obtained at the B3LYP/6-311G* level of theory.

However, in **A4** the overall conformation is, broadly speaking, a "propeller" shape, but with the four arms it has more of symmetrical shape. Despite the fact that the "propeller" shape in previous studies always produced a higher helical twisting power value (as discussed for thalidomide and R/S1101), for **A4**, it only increased the helical twisting power from 0.42 μm^{-1} to 1.79 μm^{-1}. It therefore seems that, as

the aliphatic chains between the biphenyl and ester groups in **A4** are very flexible, due in part to their length, they are not rigid enough to support the "propeller" shape of **A4** when in solution in E7.

Although the helical twisting power value of **A4** is just 1.79 μm^{-1}, which is lower than all the dopants that had been measured before, apart from AGML74 which is 0.42 μm^{-1}, it is worthwhile considering that the helical twisting power of methyl α-D-glucopyranoside is only 0.31 μm^{-1}. Thus, the helical twisting power of methyl α-D-glucopyranoside has already been amplified 5.7 times by the cyanobiphenyl mesogenic groups. It seems that the presence of mesogenic functionalization is very efficient way of increasing helical twisting power. This is in good agreement with previously presented results. For example, Kuball reported that when (*R*)-(1*R*)-1-phenylethylamine was linked to a bicyclohexene based mesogenic functional group, the helical twisting power increased from less than 1μm^{-1} to 28.6 μm^{-1} in ZLI 1695.[153,154]
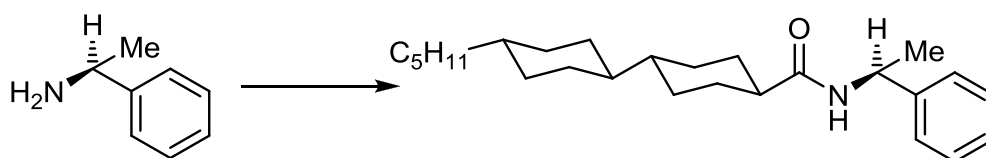
Scheme 4.1: (*R*)-(1*R*)-1-phenylethylamine linking to bicyclohexene.

Overall, the helical twisting power of methyl α-D-glucopyranoside and its mesogenic functionalized material **A4** were measured. The conformation and functional groups of methyl α-D-glucopyranoside could not effectively induce chirality into E7, and a low HTP of 0.31 μm^{-1} resulted. With the incorporation of mesogenic functional groups (cyanobiphenyl units), **A4** achieved a HTP of 1.79 μm^{-1}, but because of length and flexibility of the aliphatic chains, the amplification effect associated with the mesogenic groups and the "propeller" shape was limited. However, if a material with shorter aliphatic spacer chains were to be prepared this

may give higher values of the HTP due to the fact the mesogenic units are no longer rotationally decoupled from the core.

4.7 Studies on the Host Dependency of the Helical Twisting Power

The helical twisting powers of all of the chiral dopants studied so far have been measured in the nematic host E7. However, there are an enormous number of different nematic hosts that have been synthesised and formulated. Different hosts will typically exhibit different properties such as viscosity, dielectric anisotropy and the temperature range of the phase(s). Although some hosts are single components, many (such as E7) contain multiple components. Therefore, it is worthwhile examining if the measured value of helical twisting power varies when different nematic hosts are used.

Based on previous results, CB15 was selected as the first chiral dopant to be investigated. All in all, three different nematic hosts were employed for the experiments to determine whether the helical twisting power exhibits significant host dependency. The first nematic host studied was BL036, which is a commercial nematic host obtained from Merck Ltd. BL036 is also known to be a 7 component mixture based on E7.[63]
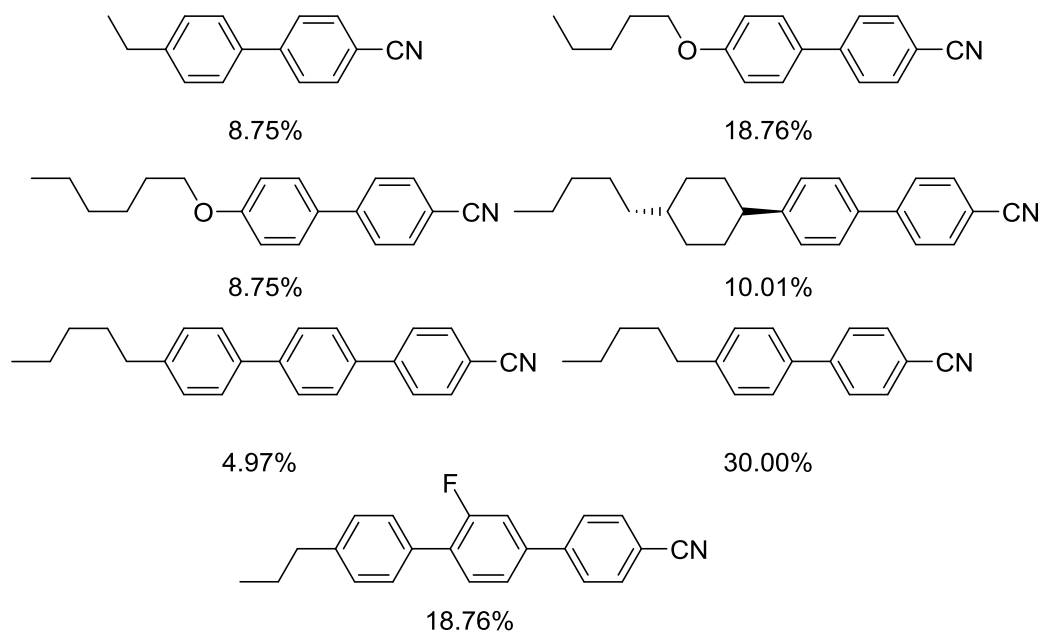
Figure 4.65: The molecular structures of the components of BL036 and its composition.[155]

In order to measure the values for the HTPs of mixtures of CB15 in BL036, specimens were prepared under the same conditions and concentration ranges as those used in the studies of CB15 mixed with E7. Photomicrographs showing the disclination lines formed by the mixtures of CB15 and BL036 at various concentrations are shown in Figure 4.66.

In comparison to CB15 in E7, the curvature of the disclination lines formed by CB15 in BL036 did not vary as significantly between the concentrations from 0.002464 wt% to (g)-(i) 0.007383 wt%. However, in the concentration of 0.01231 wt%, the number of disclination lines formed was notably fewer than for CB15 in E7 at the comparable concentration of 0.01212 wt%. At such high concentrations the disclination lines were only found close to the edges of TN cell, as shown in slides (l) and (m) of the figure.

The radii of curvature of disclination lines for each concentration were calculated and the results are presented in Table 4.21.

Concentration (wt%)	Radii of curvature (μm)	Reciprocal of Radii (1/μm)
0.002464	1861	0.000537
0.004898	1237	0.000809
0.007383	686	0.00146
0.009770	539	0.00185
0.01231	458	0.00218

Table 4.21: The concentrations, radii of curvatures (μm) and reciprocal of the radii (1/μm) for mixtures of CB15 in BL036.
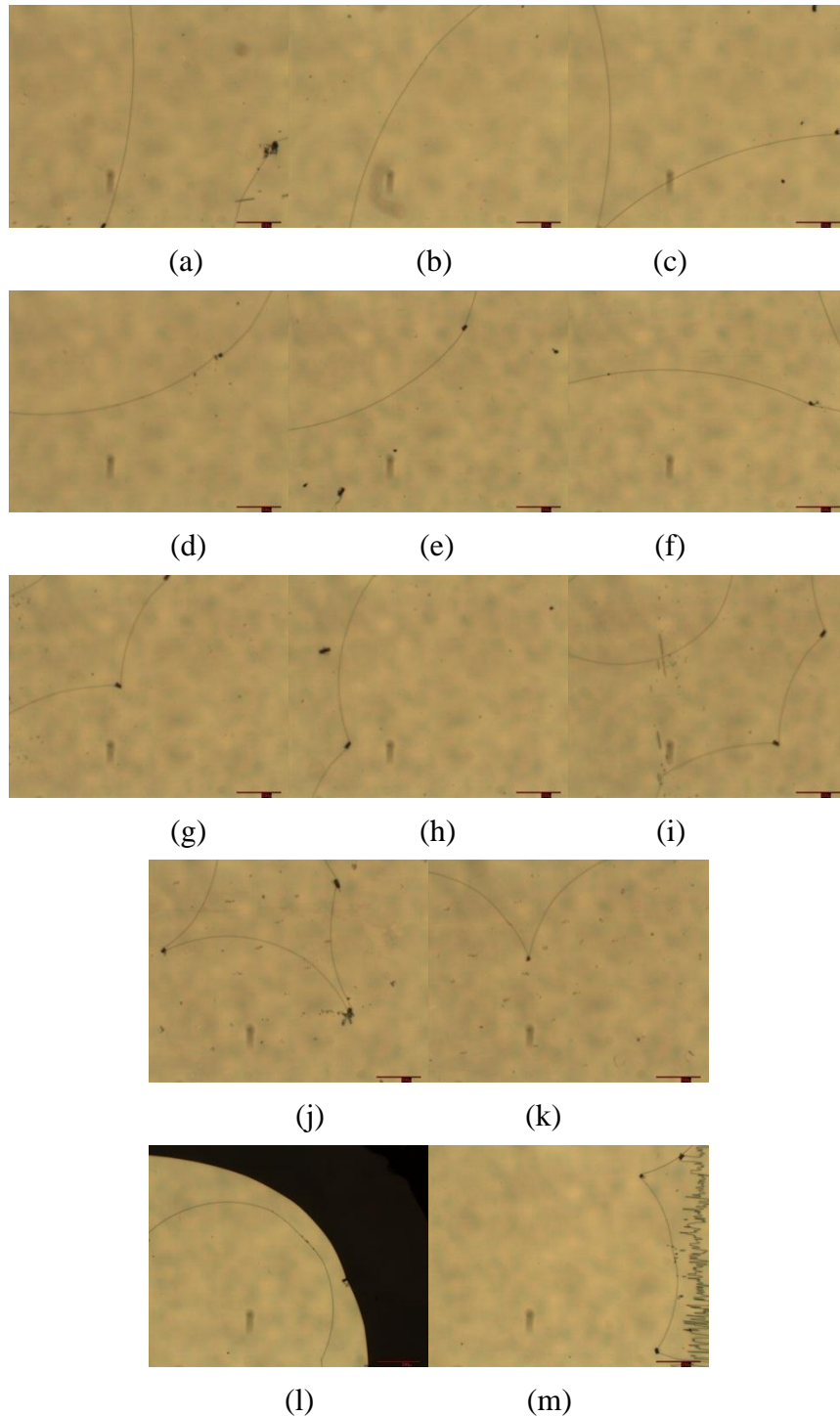
Figure 4.66: Photomicrographs (x50) showing the reverse-twist disclination lines of the mixtures of CB15 in BL036 formed in 14.4 μm thickness TN cells at concentrations of (a)-(c) 0.002464 wt%; (d)-(f) 0.004898 wt%; (g)-(i) 0.007383 wt% ;(j)-(k) 0.009770 wt%, and (l)-(m) 0.01231 wt%

In order to calculate the helical twisting power of CB15, a plot of the reciprocal radius of curvature as function of concentration in BL036 for CB15 was made, and

is presented in Figure 4.67. From the gradient of the slope of the best fit to the data, the HTP of CB15 in BL036 was determined to be 8.87 μm^{-1}.
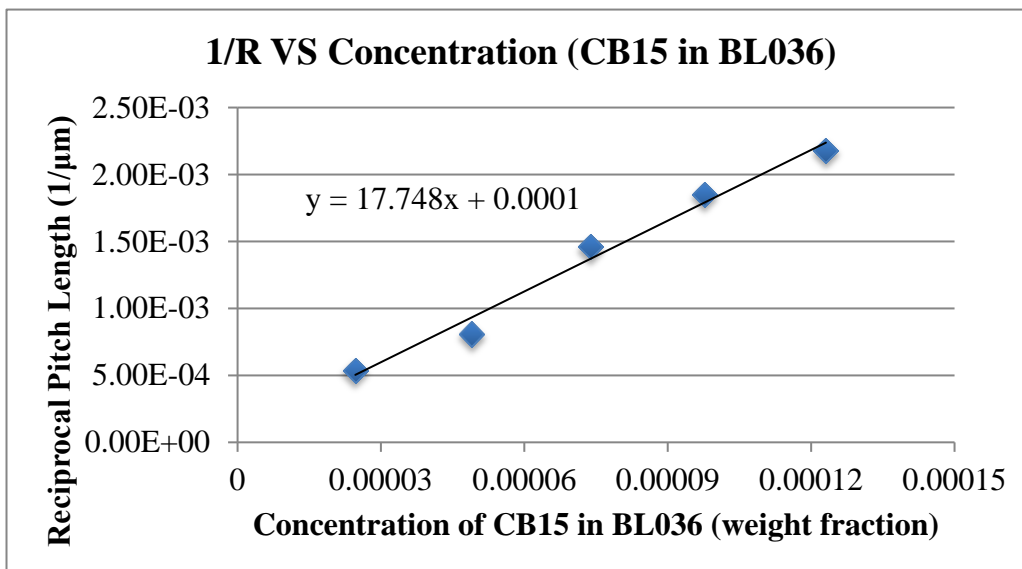
Figure 4.67: A plot of 1/R VS versus concentration for CB15 in BL036.

The HTP value of CB15 in BL036 is slightly greater than that in E7, which was determined to be 8.34 μm^{-1}. Due to the difference in HTP values for CB15 in BL036 and E7 being only 6%, it cannot be certain that the HTP value in BL036 was amplified by the host, or if the 6% increase was caused by some other factors such as errors or variations with respect to the TN cells used. In order to verify that dopants could exhibit greater HTP values in BL036 than in E7 more investigations were required. These investigations will be discussed later in this section.

PCH7, the second host employed in this chapter, is a single component nematic host. In comparison to E7, which is a mixture of three cyanobiphenyl and one cyanoterphenyl liquid crystals as shown in introduction chapter, the structure of 4-(4'-hetylcyclohexane benzonitrile) is a cyclohexene 4-cyanophenyl based liquid crystal. The interaction between the host and dopant were predicted to be quite different in PCH7 in comparison to E7 given the significant differences in chemical structure. The HTP value for CB15 was determined in PCH7 over

concentrations of the same range as determined in E7, i.e., between 0.002467 wt% to 0.01228 wt%, even though the measurements in E7 were somewhat erratic.
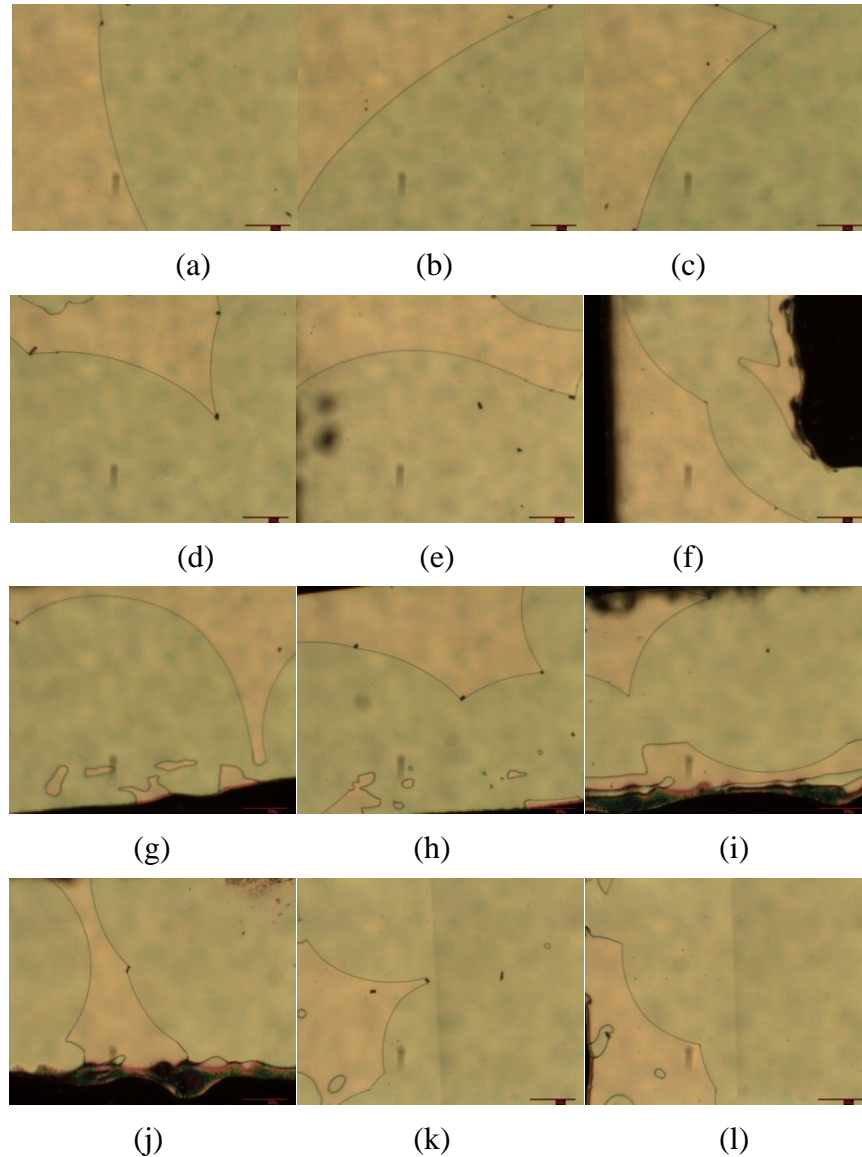
Figure 4.68: Photomicrographs (x50) showing the reverse-twist disclination lines of the mixtures of CB15 in PCH7 formed in 14.4 μm thickness TN cells at concentrations of (a)-(c) 0.002467 wt%; (d)-(f) 0.004903 wt%; (g)-(h) 0.007325 wt%; (i)-(j) 0.009708 wt%, and (k)-(l) 0.01228 wt%.

Initially the solubility of CB15 in PCH7 was unknown, however there was no precipitation observed during examination or preparation of the mixtures. However, the number of disclination lines formed in the mixtures was not satisfactory, apart from the 0.002467 wt% concentration, *i.e.*, at the lowest

concentration examined. In addition, and as shown in pictures (g) and (m), there were irregular shaped spots found in the cells. This was also found in a previous test for thalidomide in E7, therefore, appearance of the spots was not expected to influence the result. The radii of curvature of disclination lines for each concentration were calculated and are presented in Table 4.22.

Concentration (wt%)	Radii of curvature (μm)	Reciprocal of Radii (1/μm)
0.002467	1684	0.000593
0.004903	758	0.00132
0.007325	574	0.00174
0.009708	506	0.00198
0.01228	431	0.00232

Table 4.22: The concentrations, radii of curvatures (μm) and reciprocal of the radii (1/μm) of CB15 in PHC7.

Using the data above, a plot of the reciprocal radius of curvature as function of concentration in PCH7 for CB15 was created. From the gradient of the linear relationship, the HTP of CB15 in BL036 was determined to be 8.41 μm^{-1}
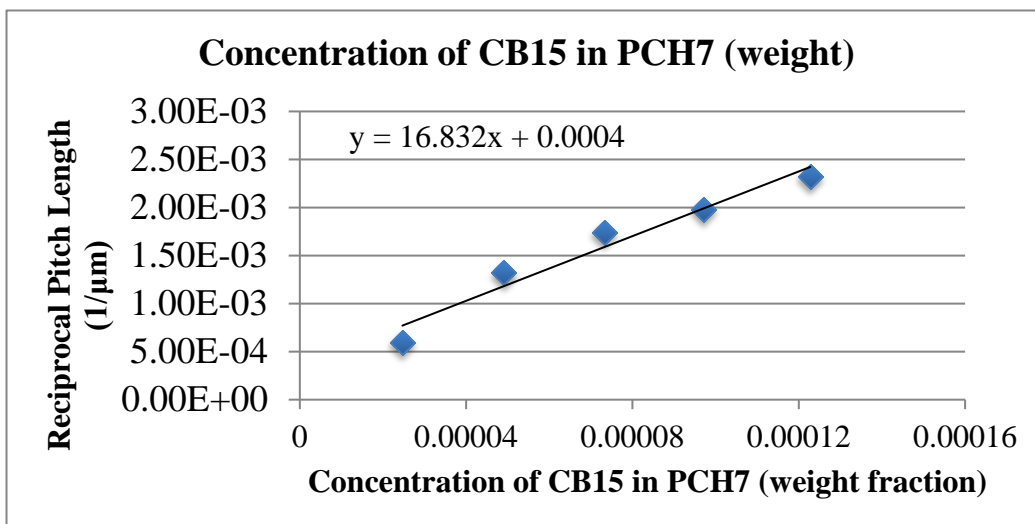
Figure 4.69: A plot of 1/R VS versus concentration for CB15 in PCH7.

The measured HTP value for CB15 in PCH7 is very similar to CB15 in E7, but is still smaller than the value measured in BL036. Given that CB15 has a 4-cyanobiphenyl core whereas, PCH7 possesses a 4-cyanophenylcyclohexane core, the interactions between the dopant and host were expected to be quite different, thus giving a different HTP value, in comparison to that of CB15 and in E7. However, the values of the HTP of CB15 were quite similar for both host materials (8.41 μm^{-1} for PCH7 and 8.34μm^{-1}), and the differences are within the anticipated margin of error.

The last nematic host studied was ZLI559, which is also a nematic host from Merck Ltd. As it is a commercial host, very little detail is known about its composition. So as to make comparison with previous studies the concentration range of CB15 in ZLI559 was also kept the same as in previous measurements.
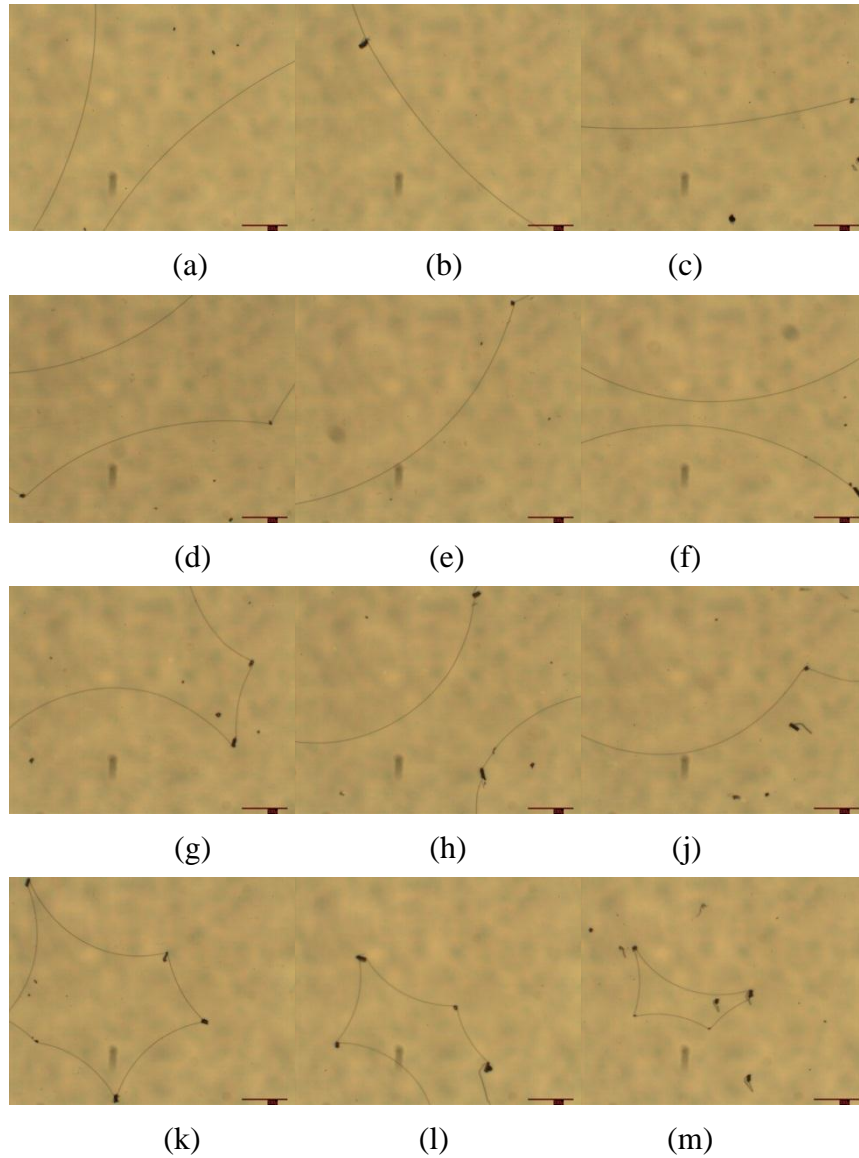
Figure 4.70: Photomicrographs (x50) showing the reverse-twist disclination lines of the mixtures of CB15 in ZLI559 formed in 14.4 μm thickness TN cells for concentration of (a)-(c) 0.002446 wt%; (d)-(f) 0.004927 wt%; (g)-(i) 0.007408 wt%; (k) 0.009873 wt%, and (l)-(m) 0.01233 wt%.

Unlike BL036 and PCH7 disclination lines formed very easily and in satisfactory numbers for each concentration when using ZLI559 as the host. From the

photomicrographs in Figure 4.70, picture (m) shows that even when the radii of curvature is very small, there is still a large enough number of disclination lines in the cell to allow for good measurements of the radii of curvature. The radii of curvature of disclination lines for each concentration were measured, and are presented together in Table 4.23.

Concentration (wt%)	Radii of curvature (μm)	Reciprocal of Radii (1/μm)
0.002446	2400	0.000417
0.004927	1232	0.000812
0.007408	706	0.00142
0.009873	481	0.00208
0.01233	423	0.00236

Table 4.23: The concentrations, radii of curvatures (μm) and reciprocal of the radii (1/μm) for CB15 in Z559.

For the lowest concentration prepared (0.002446 wt%), the radii of curvature was 2400 μm, which was the largest radii measured for these experiments, and in comparative studies with both BL036 and PCH7. However, when the concentration was increased, the radii of curvature were actually smaller than those measured for BL036 and PCH7. Thus, CB15 gave the highest measured HTP value when using ZLI559 as the host. A slope of the reciprocal radius of curvature as function of concentration in ZLI559 for CB15 was thus created. From the gradient of the linear fit to the data, the HTP of CB15 in ZLI559 was determined to be 10.4 μm^{-1}
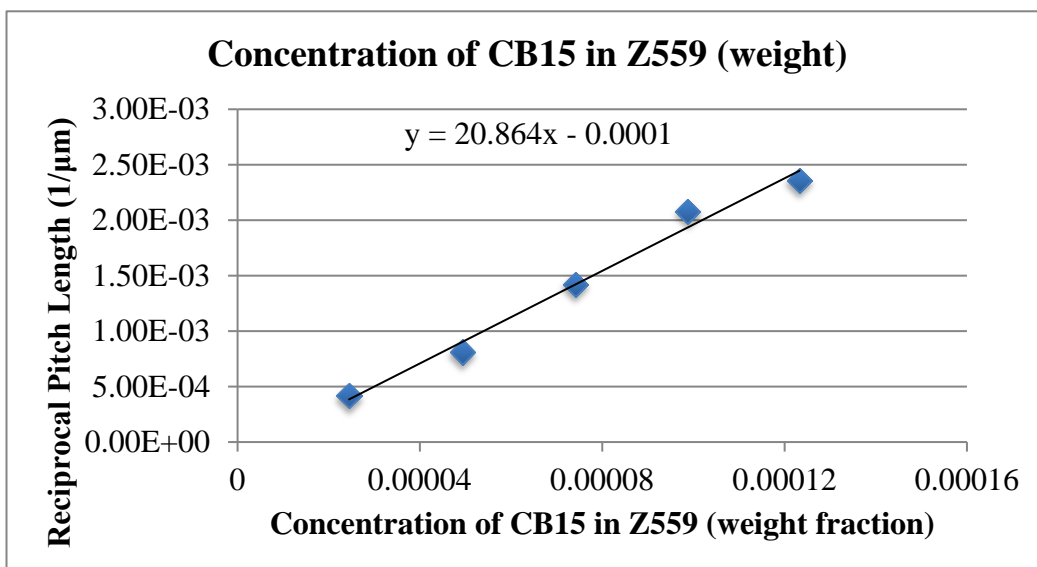
Figure 4.71: A plot of 1/R VS versus concentration for CB15 in Z559.

In summary, the HTP value of CB15 was measured in four different nematic hosts, and a host dependency was apparent. Clearly, the HTP value of a dopant is not the same across the hosts tested irrespective of the error associated with the studies, *i.e.* it is not an intrinsic property of the dopant, but rather exists as a property between a given host/dopant pair. CB15 achieved the highest HTP value using ZLI559 as a host, suggesting that CB15 interacts better with ZL1559 than the other hosts studied. However, this does not mean that ZL1559 can always offer the highest HTP value for every dopant, not even in the other three hosts used in this study. Rather, it is specific for a given host/dopant pair. For example, BL036 is based on E7, although there are only three additional components in BL036, it still apparently gives a 6% higher HTP value for CB15, see Table 4.24.

Nematic Host	E7	BL036	PCH7	ZL1559
HTP of CB15 (μm^{-1})	8.34	8.87	8.41	10.4

Table 4.24: The HTP value of CB15 in the various hosts studied.

Following on from the results on CB15, all of the dopants studied previously were tested with hosts BL036, PCH7 and ZL1559 *via* the same methodology. For the sake of brevity, all the photomicrographs of disclination lines and mixture concentration data are presented in the chapter 6 experimental annex.

The HTP of oxazoline-based dopants were determined in BL036, PCH7 and ZL1559, and the associated measurements of the HTP are presented in Table 4.25.

Nematic Host	E7	BL036	PCH7	ZL1559
HTP of AE8 (μm^{-1})	4.47	4.77	2.88	4.36
HTP of AGML74 (μm^{-1})	0.42	1.60	0.36	0.10
HTP of AE14 (μm^{-1})	2.22	5.27	0.75	2.36

AE8

AGML 74

AE 14
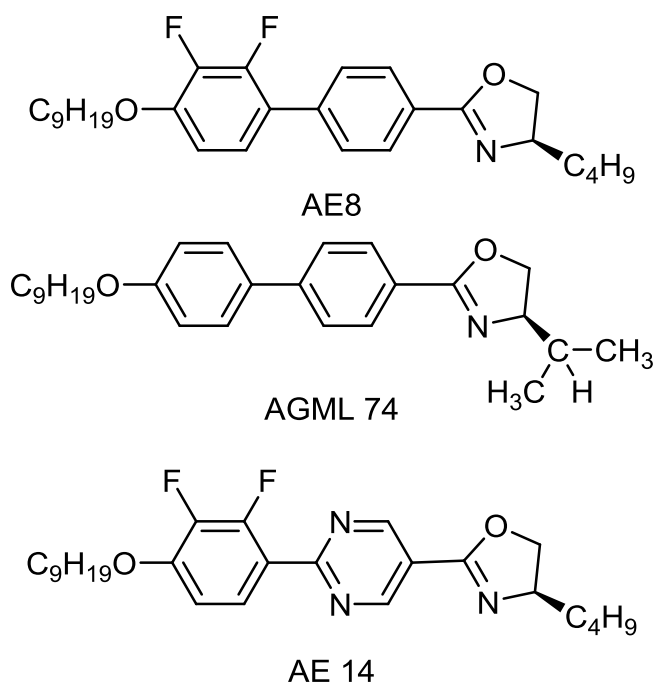
Table 4.25: The HTP of oxazoline based dopants in E7, BL036, PCH7 and ZL1559 respectively.

The host BL036 gave consistently higher HTP values of the dopants than E7 irrespective of the oxazoline dopant used. Interestingly, the HTP of AE8 in BL036 was not amplified whereas for AGML74 and AE14 there was a significant

increase over the value measured for E7. Although the PCH7 host did not change HTP of CB15 very much, the HTP values for oxazoline based dopants mixed with PCH7 were consistently lower than for both E7 and BL036. Although ZLI559 gave a large increase in the HTP of CB15 relative to the other hosts studied, there was virtually no increase for the oxazoline dopants compared to E7 for AE8 and AE14, but there was a large decrease for AGML74. For all oxazoline dopants ZL1559 gave smaller HTP values than BL036.
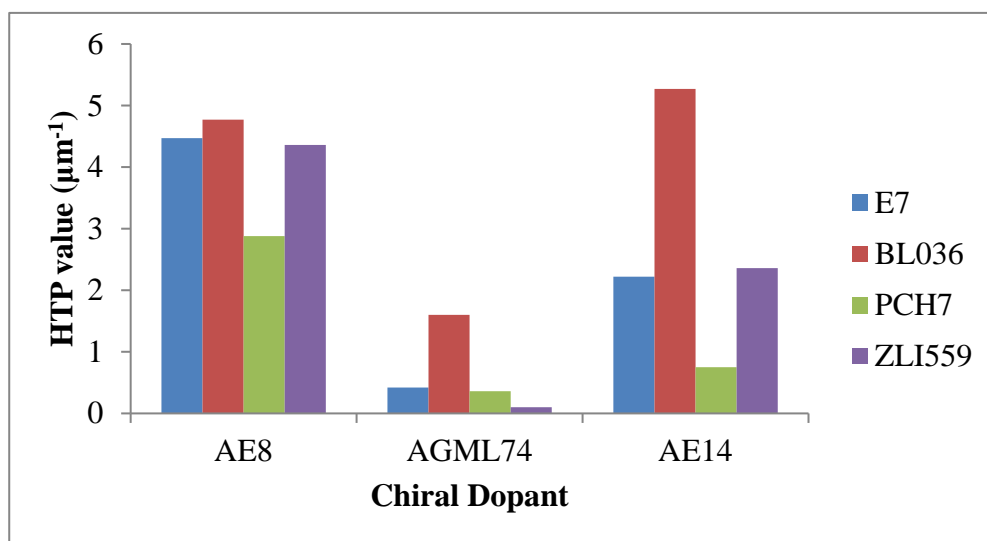
Figure 4.72: The HTP trends for oxazoline based dopants in E7, BL036, PCH7 and ZL1559 hosts respectively.

As the HTP of oxazoline-based dopants varies depending on the host; it seemed worthwhile discovering how commercial high HTP dopants would behave in different hosts. As mentioned in chapter 4.4, the HTP values of R1011 and S1011 were determined, using the "reverse-twist disclination line method", in PCH7 and E7, with the HTP having higher values in PCH7 than E7. It was concluded that because R1011 and S1011 have similar mesogenic units as PCH7 (4-alkylcycohexyl phenyl group), this might be one of the reasons why higher HTP values were measured in PCH7 than E7. Furthermore, the twist elastic coefficient (K_{22}) of the host would be expected to affect the HTP value, with higher values of K_{22} giving lower HTP values.[156] The twist elastic coefficient of E7 and PCH are

181

6.5 pN and 2.5 pN respectively, thereby supporting the experimental observation that R1101 and S1101 exhibit higher HTP values in PCH7 than in E7.[157]

Interestingly, when 1/R was plotted against concentration for R1011 and S1011 in BL036, the slopes were not absolutely linear. In the literature it is reported that the slope of the HTP would not necessarily always be linear when the concentration of dopant is increased.[158] Thus, it may be for the concentrations studied the relationship has ceased to be linear for S1101/R1101 in BL036. Therefore, higher concentrations were investigated thereby providing more data points, as shown in Figure 4.73.
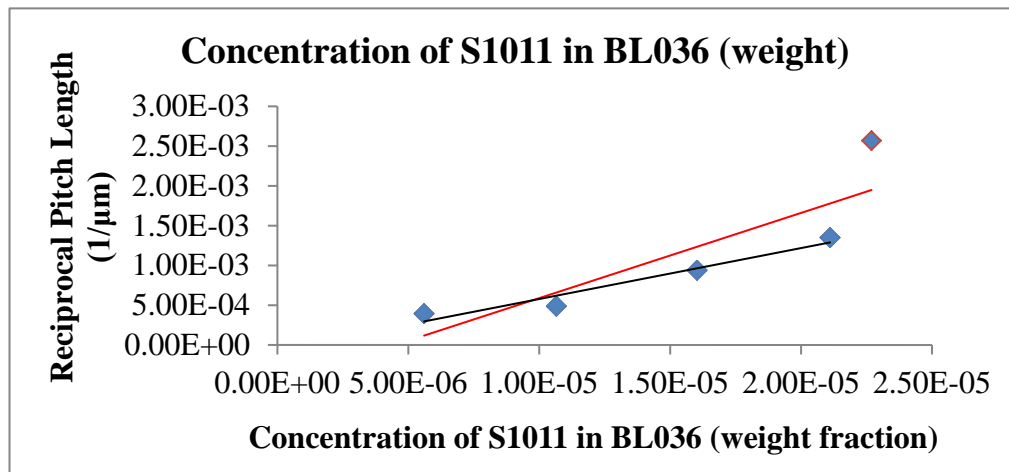
Figure 4.73: Plots of 1/R as a function of concentration, with a linear fit of the data for S1011 in BL036; The red line is a linear fit for all data points while the black line is a linear fit for only the first four data points.

As shown in Figure 4.73 the 5th data point deviates significantly from linearity. A linear fit for all data points gave an R^2 value of 0.7546, yet when this was excluded the R^2 value increased markedly to 0.9465. Given the large difference in the gradient of each slope the HTP of S1011 could be 32.04 μm^{-1} or 53.59 μm^{-1} depending on which slope is used to obtain the HTP value. It is still difficult to be certain which value of the HTP of S1011 is 32.04 μm^{-1} or 53.59 $\mu m^{-1}$is correct. Similarly, the HTP of R1011 was also determined in BL036, see Figure 4.74.
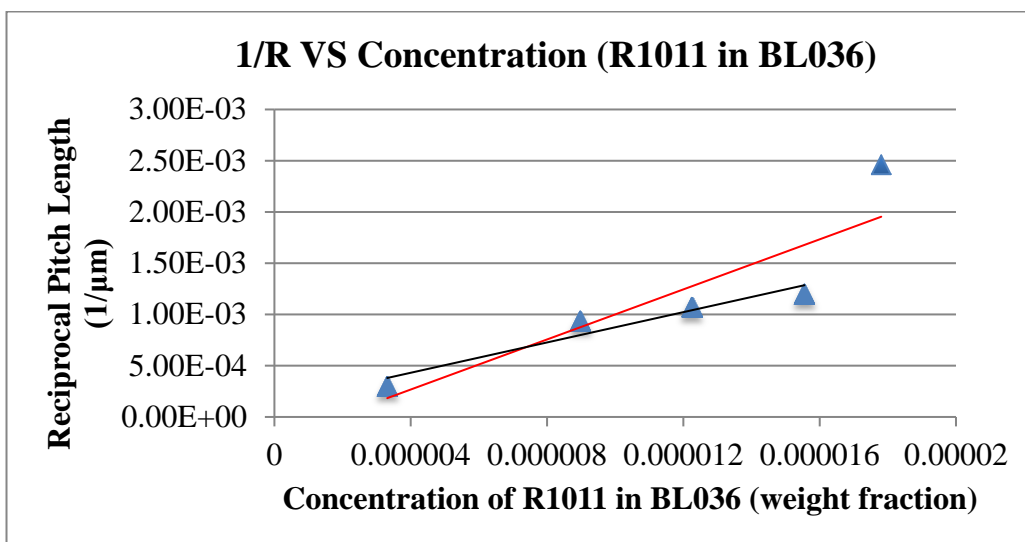
Figure 4.74: Plots of 1/R as a function of concentration, with a linear fit of the data for R1011 in BL036; The red line is a linear fit for all data points while the black line is a linear fit for only the first four data points.

The same situation was also observed in the case of R1011, the data point for the most concentrated dopant in the mixture is further removed from the slope. A linear fit for all data points gave an R^2 value of 0.7811, however excluding the 5th data point an R^2 value of 0.9294 was attained. The results from each linear slope give HTP values of 61.01 μm^{-1} and 36.97 μm^{-1} for the 5-data point and 4-data point fits respectively. The HTP values for the dopants, as determined in E7, were 33.09 μm^{-1} = 44.93 μm^{-1} for R and S 1101 respectively. Given that BL036 is a host based on E7 it is possible that these materials might have higher HTP values in BL036 than in E7, as demonstrated by oxazoline-based dopants. Thus, according to all the factors, it is better to say that the HTP of R1011 and S1011 in BL036 are 36.97μm^{-1} and 32.04μm^{-1} respectively. The rationale for this assignment is that for low concentrations, the dopant molecules are less likely to associate with one another, but as the concentration of the dopant is increased in the mixture with the host, interactions between the dopant molecules become more significant, thereby leading to non-linear effects with respect to the radius of curvature as a function of concentration..

183

This phenomenon observed for of R1011 and S1011 in BL036, did not materialise when determining the HTP values of R1011 and S1011 in the hosts ZLI559 and PCH7. The HTP of R1011 and S1011 in all different hosts are presented in Table 4.26.

Nematic Host	E7	BL036	PCH7	ZLI559
HTP of R1011 (μm^{-1})	38.09	36.97	42.99	42.38
HTP of S1011 (μm^{-1})	44.94	32.04	52.54	30.76
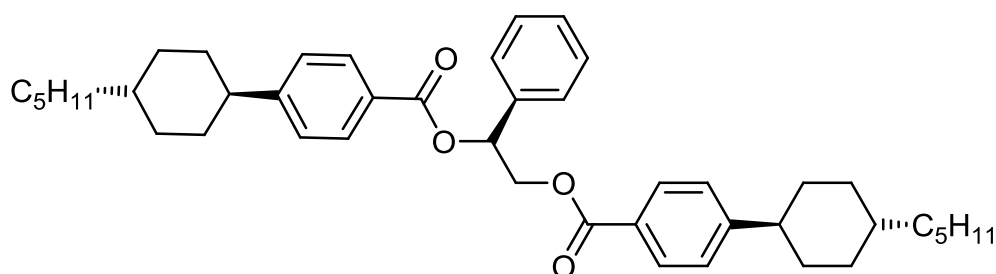
R1011
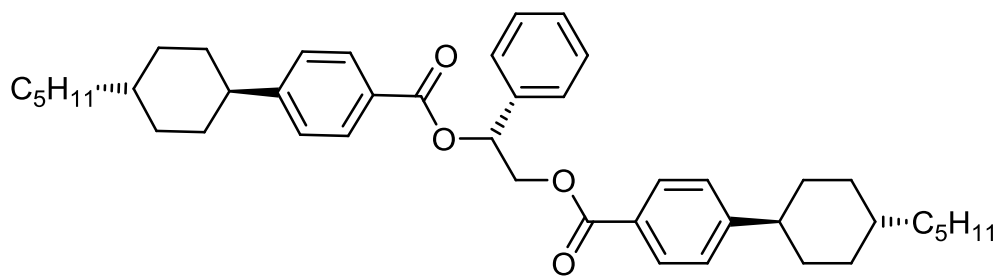
S1011

Table 4.26: The HTP values for R1011 and S1011 in the hosts E7, BL036, PCH7 and ZLI559 respectively.

The HTP values for R1011 in the different host are somewhat consistent, however, S1011 gives higher HTP values in E7 and PCH7 than for BL036 and ZLI559. Due to the similarity in the chemical structures of dopants R1011 and S1011 and the host PCH7, the enhancement conferred by this host relative with the other three hosts studied is not surprising. This result suggests that when the chemical structure of the dopant is similar with the host, it may induce chirality more

strongly, thereby leading to higher HTP values. What is interesting, however, is that the trends for the values of the HTPs of the various hosts are not the same for the R1011 and S1011 dopants. This may be due to the fact that the dopants have differing enantiopurities. At higher concentrations of the dopants, the degree of the interactions of the enantiomers (*R* to *S* and *R* to *R* and *S* to *S*) may differ, thereby leading to differing values of the HTPs.

The HTP of both enantiomers of thalidomide were also measured using the four different hosts encountered thus far. The results for the two enantiomers are shown below in Table 4.27.

Nematic Host	E7	BL036	PCH7	ZLI559
HTP of (+)-Thalidomide (μm^{-1})	22.38	21.42	30.08	23.52
HTP of (−)-Thalidomide (μm^{-1})	22.95	23.61	30.17	20.23
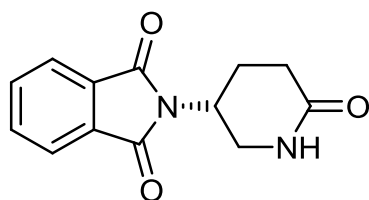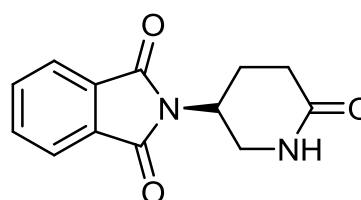
(+)–Thalidomide   (−)–Thalidomide

Table 4.27: The HTP values for both enantiomers of thalidomide in hosts E7, BL036, PCH7 and Z559 respectively.

Despite thalidomide being very different from R1011 and S1011 in chemical structure, the enantiomers achieved their highest HTP values in PCH7, possibly as a consequence of PCH7 having a lower K_{22} than E7. In reference to the HTP in E7, the values measured in BL036 were not increased, whereas the HTP of thalidomide in ZLI559 is very similar to that measured in E7 and BL036. It is also interesting that the trends for the HTPs were similar for the two enantiomers,

possibly as a result of the fact that the two isomers of thalidomide have similar enantiopurities.

Cyclohexyl-(2,3-diflurobiphenyl)-based dopants were the last family of materials to be examined in different hosts. The results obtained, in a similar way to the studies above, are shown in Table 4.28.

Nematic Host	E7	BL036	PCH7	ZLI559
HTP of RAL1568 (μm^{-1})	3.13	5.01	2.30	4.88
HTP of RAL1569 (μm^{-1})	3.38	5.90	3.90	3.43
HTP of RAL1636 (μm^{-1})	5.92	5.92	5.84	5.09
HTP of RAL1608 (μm^{-1})	8.00	8.88	7.91	11.06
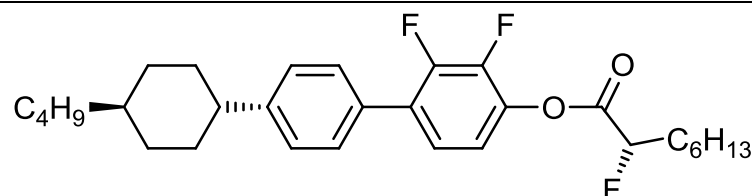
RAL1568
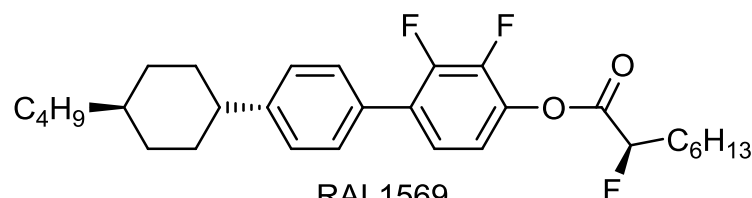
RAL1569
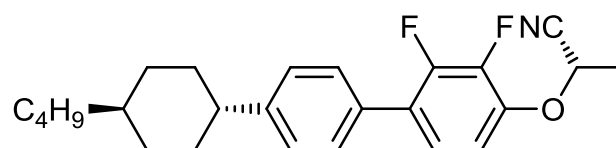
RAL1636
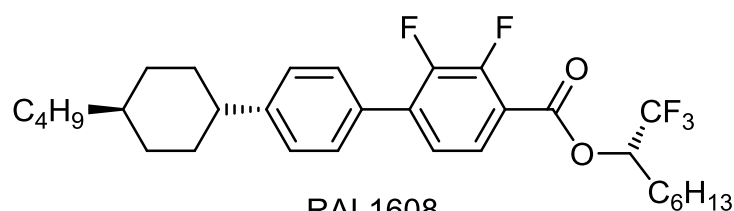
RAL1608

Table 4.28: The measured HTP values of diflourobiphenylcyclohexane-based dopants in hosts E7, BL036, PCH7 and ZLI559 respectively.

In comparison with other cyclohexyl-(2,3-diflurobiphenyl)-based dopants, RAL1608 always achieved the highest HTP with respect to all of all the dopant used. Similarly, RAL1636 always appeared in the second place. The relative ordering of the HTP values of the cyclohexyl-(2,3-diflurobiphenyl)-based dopants did not change when the host was changed, nor similarly did it for the

oxazoline-based dopants. The HTP of cyclohexyl-(2,3-diflurobiphenyl)-based dopants in BL036 is larger than in E7, echoing the trend seen with the oxazoline based dopants. However, the HTP of R1011, S1011 and thalidomide in BL036 is quite similar as in E7. This suggests that when the chemical structure of the dopant is closer to the rod-like liquid crystal structures often used in hosts, larger HTP values are obtained in BL036 than in E7. Conversely, when the dopant is less rod-like the enhancement of the HTP seen for BL036 relative to E7 is absent.
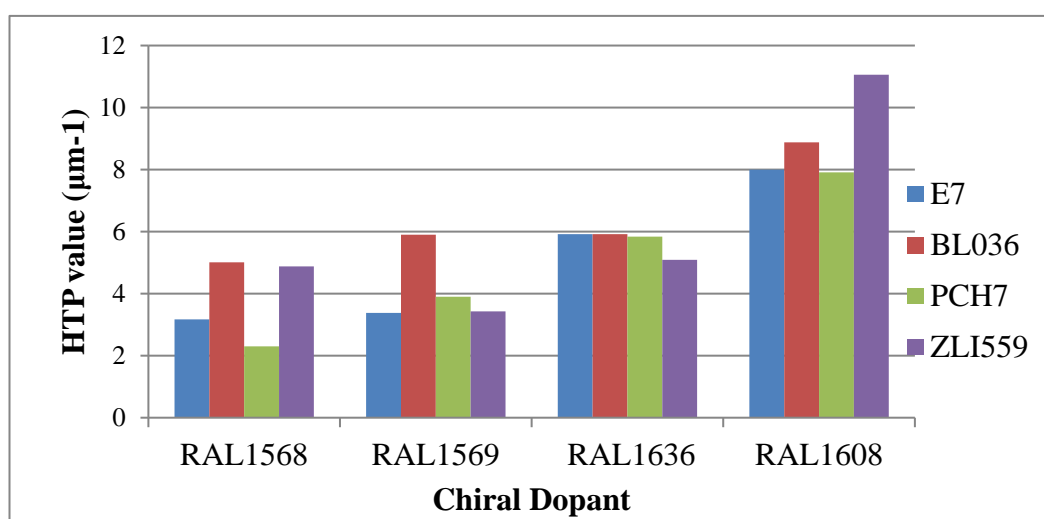
Figure 4.75:   Plot of helical twisting power for the four RAL dopants in four different nematic hosts (E7, BL036, PCH7, ZLI559)

The HTP values of R1011 and S1011 and thalidomide achieved their highest value in PCH7, presumably because PCH7 has a relatively lower K_{22} than the other hosts studied. However, cyclohexyl-(2,3-diflurobiphenyl)-based dopants and oxazoline-based dopants possessed lower values when measured in PCH7 in comparison with other hosts.

Therefore, from all of these results, it suggests that the idea that higher values of K_{22} for the hosts reduces the HTP value   may only apply for materials that tend to give high HTP values, such as R1011 and S1011 or thalidomide.[156] However it could be because R1011, S1011 and thalidomide, through the "propeller-shape

effect", can interact better with PCH7 than with other hosts, but this has to be tempered by the fact that PCH7 is the only one component nematic host of all of the hosts that were examined. Lastly, it should be noted for mixtures possessing high concentrations of a dopant that dopant-dopant interactions may drastically affect the comparative results for the HTP. This is exemplified in comparisons of materials of differing enantiopurities of the dopant which will affect the R-S interactions relative to the R-R and S-S interactions.

4.8 Detection of Chirality in Products from Racemic Starting Materials

Recently, Cowling *et al.*reported that two racemic materials (compounds **I** and **II** in Figure 4.76), which are similar in structure to the well-studied antiferroelectric liquid crystal MHPOBC (also shown in Figure 4.76).[159] [160] The two compounds were reported to exhibit ferroelectric switching in the smectic C phase. This result is extremely unusual as the smectic C phase which was formed by achiral molecules, or by a racemic mixture, has local C_{2h} symmetry, which is too high to allow for ferroelectric behaviour. Ferroelectric behaviour can only be observed when this symmetry is reduced to C_2 *via* the inclusion of a chiral material, or by having an excess of one enantiomer in a mixture. However, as exemplified in Section 1.8.1, although switching characteristic of a ferroelectric material was observed for these two materials (**I** and **II**), *i.e.* switching that proceeds *via* a hysteresis loop, the values of the spontaneous polarization for these materials were too small to determine experimentally, thereby suggesting that the enantiomeric excesses for the materials are small. Nonetheless, these results are interesting as they suggest that the supposedly racemic materials compound **I** and **II**, could be optically active, even though no chiral materials are used in their preparation. It should also be noted at this point that these materials, and intermediates used in

their synthesis, have been prepared independently by several different individuals and in each case the final product showed ferroelectric switching. It therefore seems unlikely that the observed ferroelectric response occurs as a result of a chiral impurity formed during the synthetic process or by contamination of reagents or starting materials. Instead, it appears that at some point during the synthesis of the two compounds, de-racimization occurs.
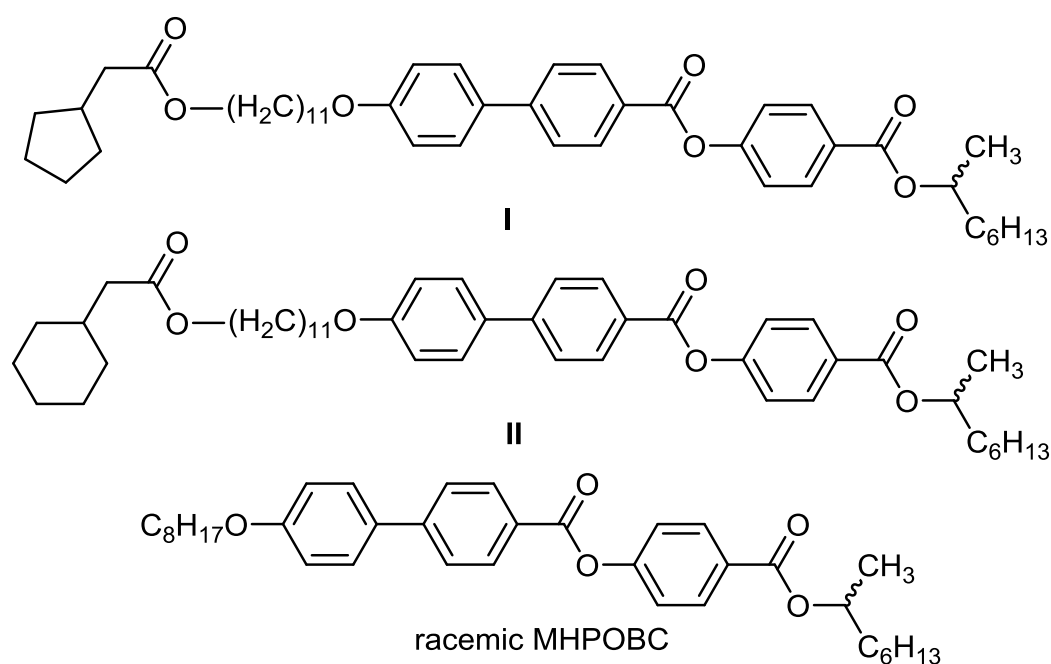
Figure 4.76: The chemical structures of **I** and **II**.[159,160,161]

The synthetic routes used to prepare compounds **I** and **II** (shown in Scheme 4.2) are identical until the final step, which involves an esterification to install the terminal cyclohexyl or cyclopentyl unit. The reagents and conditions for this final transformation are identical although cyclopentylacetic acid or cyclohexylacetic acid are used to prepare **I** and **II** respectively.
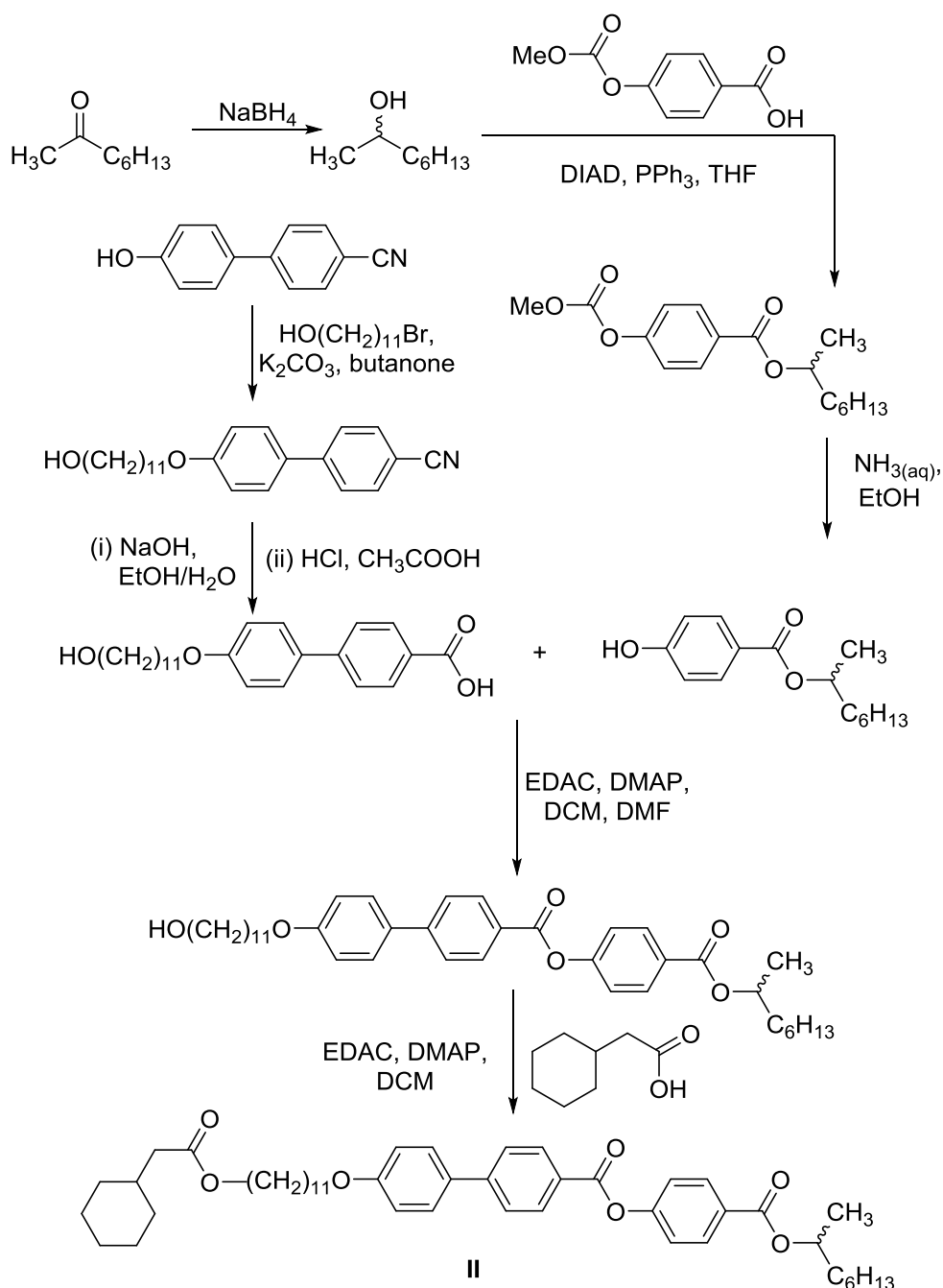
Scheme 4.2: The synthetic pathway used by Cowling et.al to prepare the final 1-methylheptyl-terminated material (Compound **II**).

There are two reactions used in the synthesis of compounds **1** and **2**, which could directly influence the substitution pattern at the prochiral centre. The first is the reaction used to form the stereogenic centre, *i.e.* the reduction of 2-octanone with sodium borohydride to give 2-octanol. The second is the esterification of the protected phenol with 2-octanol, which involves the reaction of the hydroxyl

group at the pro-sterogenic centre. Interestingly, if this esterification step is performed using the Mitsunobu reaction, as it was in the literature reports of Cowling *et al.*, then the the final product (**I** or **II**) is chiral and displays ferroelectric switching. Conversely, if this transformation is performed using a Steglich esterification, the resulting final compound is racemic. It therefore appears that there is some form of chiral induction that occurs in the Mitsunobu esterification step.

The fact that the Mitsunobu reaction yields a chiral product whereas the Steglich esterification does not can be partially rationalized *via* consideration of the mechanisms of the two reactions. For example, the mechanism of the Mitsunobu reaction, see Scheme 4.3, firstly involves the reaction of triphenylphosphine with the coupling agent to form an intermediate betaine, which then deprotonates the carboxylic acid. Nucleophilic attack of the alcohol (2-octanol in Scheme 4.3) results in the formation of the complex intermediate X, which disassociates to form the reactive species Y as shown.
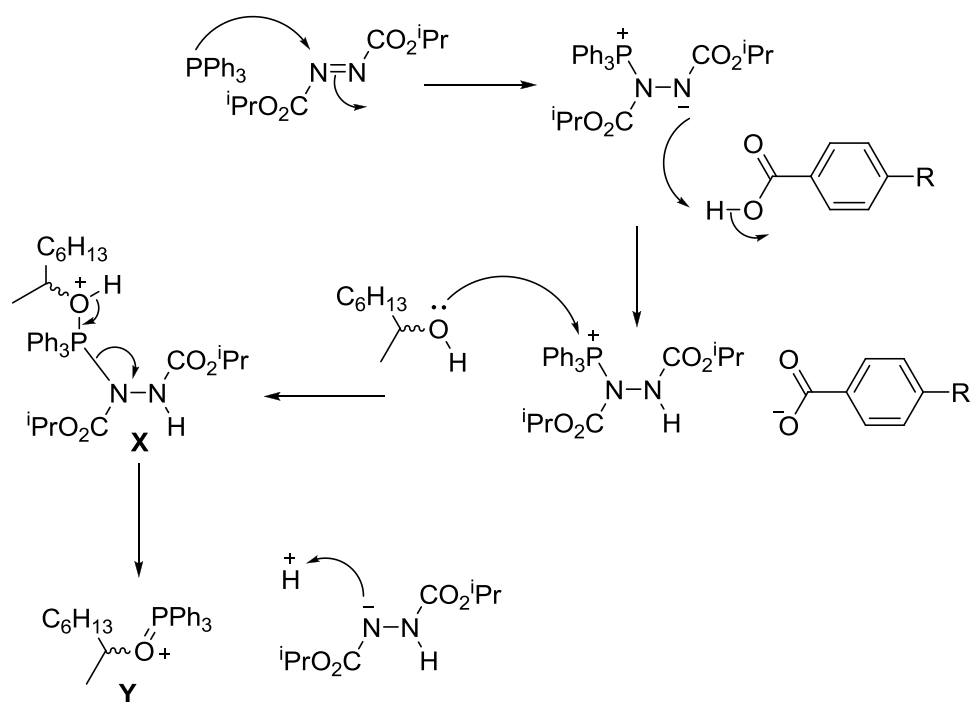
Scheme 4.3: The mechanism of the Mitsunobu reaction.[162]

Nucleophilic attack of this intermediate by the deprotonated carboxylic acid results in the loss of triphenylphosphine oxide and the formation of the desired ester product. However, as can be seen from the Scheme 4.4, when a chiral secondary alcohol is used, there is an inversion of the configuration at the chiral centre in the final step due to the backside attack of the nucleophillic species, as shown in the bottom of Scheme 4.4.

Reaction Proceeds with Inversion of Stereochemistry
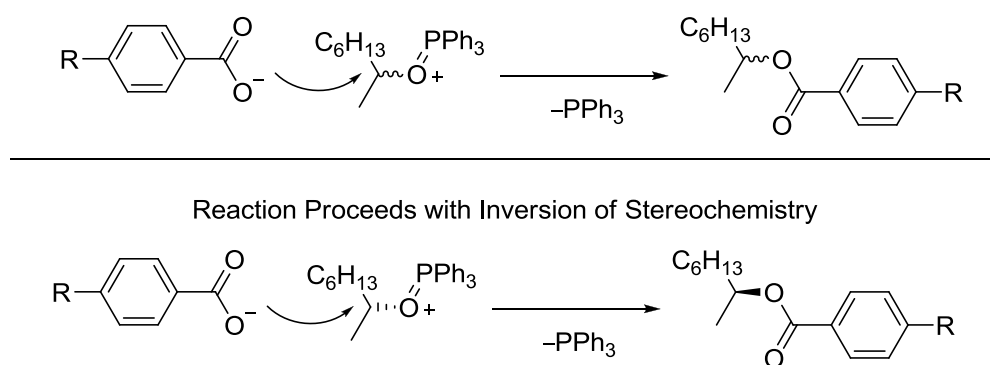
Scheme 4.4: The final step of the mechanism of the Mitsunobu reaction.

In contrast, the mechanism of the Steglich esterification is significantly different. The first step of the reaction involves the reaction of the carboxylic acid with the carbodiimide coupling reagent to form an active *O*-acylisourea as shown in Scheme 4.5.
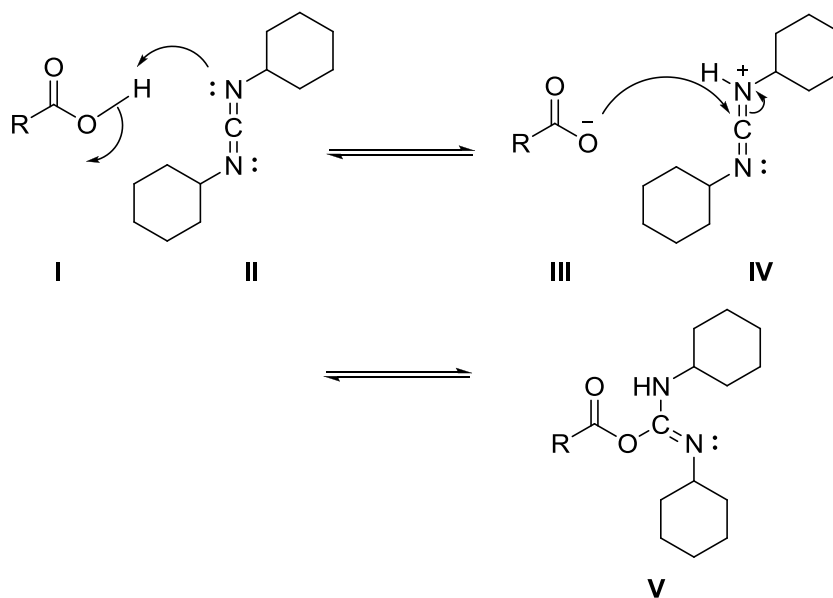
Scheme 4.5: The first step of the mechanism of the Steglich esterification reaction.

The next step of the mechanism involves acyl transfer from the *O*-acylisourea to DMAP, which is followed by nucleophilic attack of the alcohol to give the desired ester (Scheme 4.6). Crucially, in this mechanism, the alcohol simply acts as a nucleophile, and therefore no inversion of the configuration at the chiral centre is possible.
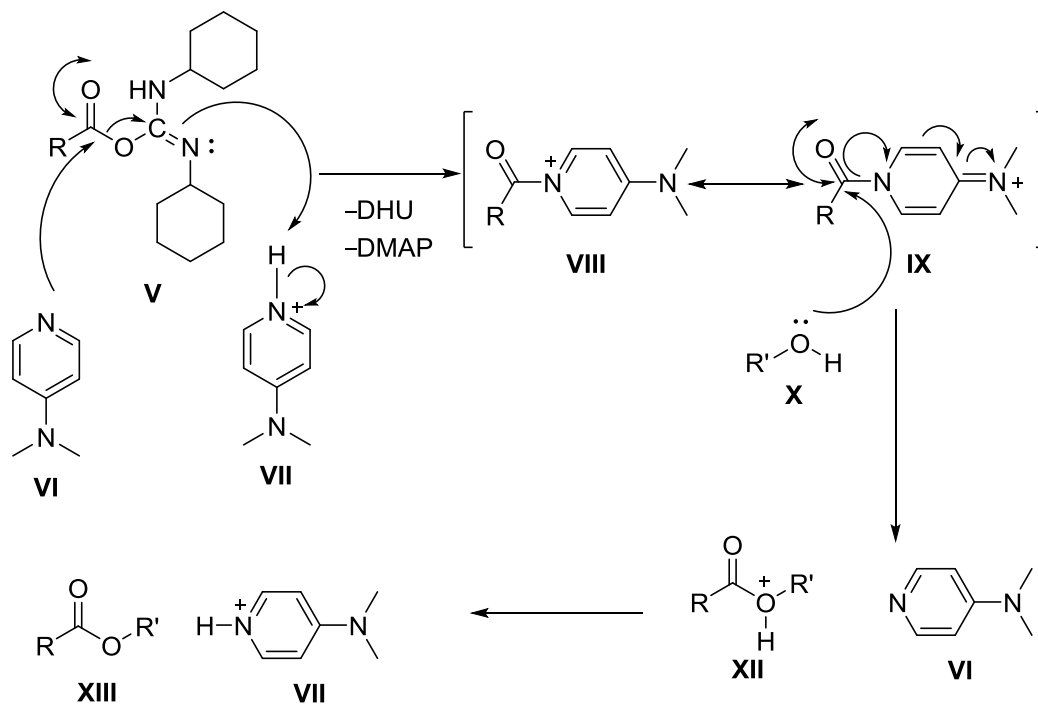
Scheme 4.6:. The final steps in the mechanism of the Steglich esterification.

From a comparison of the mechanisms of the two types of esterification reaction it is clear that the Mitsunobu reaction can lead to a direct change at the chiral centre, whereas in the Steglich esterification the chiral centre remains unchanged. It is therefore impossible for the Steglich esterification to give a non-racemic product if the alcohol used in the esterification is racemic. On the other hand, it is possible for the Mitsunobu reaction to give a chiral product if there is an imbalance in the inversion of the configuration at the chiral centre in the final mechanistic step, *i.e.* in principle (*R*) could be formed in preference to (*S*), or *vice versa*, even if the starting alcohol is racemic. A summary of the differences between the Mitsunobu and Steglich esterifications is given in Figure 4.77.

Figure 4.77: A comparison of the Steglich and Mitsunobu reactions. Figure reproduced with permission.[44]

As shown in the previous Chapters of this thesis, the reverse twist disclination line method is an extremely sensitive method for detecting chirality and for measuring the HTP. It was therefore anticipated that this method could be used confirm the results obtained by Cowling *et al.* and to determine whether or not the Mitsunobu reaction leads to the de-racimization of a racemic mixture of 2-octanol. In order to investigate this, compounds **11** and **12** were prepared *via* a number of different synthetic methods. These materials are structurally similar to those reported by Cowling *et al.* with the exception that they possess a linear alkyl chain rather than an alkyl chain terminated by a cyclohexyl or cyclopentyl end group. The thermal behaviour of these two materials, as determined by polarized optical microscopy and differential scanning calorimetry, is shown in Table 4.29. Details of the preparation of these two materials, along with their analysis, is given in the experimental section.

Transition Temperatures/ ℃

No.	n	Cr		SmI		SmC$_A$		SmC		SmA		Iso.
12	10	●	70.4	(●	41.0)	●	109.7	●	123.7	●	134.9	●
11	11	●	52.1	–	–	●	94.8	●	123.3	●	136.1	●

Table 4.29: The thermal behaviour of compounds **11** and **12** (℃).

On cooling both compound **11** and compound **12** from the isotropic liquid, the smectic A phase separated from the isotropic liquid in the form of batonnets, which coalesced to form a fan-like texture containing characteristic focal-conic defects (Figure 4.78). Other areas of the sample appeared to be optically extinct, thereby confirming the assignment of this phase as a smectic A phase. Further cooling of both of the materials resulted in a transition to the smectic C phase, which was accompanied by the breaking of the fans and the appearance of a *schlieren* texture showing exclusively 4-brush defects (Figure 4.78, c and d). For both compounds **11** and **12**, a transition from the smectic C phase to another mesophase, which also exhibited a *schlieren* texture, was observed. In preparations made between untreated glass substrates, it was difficult to determine the exact nature of the defects associated with the *schlieren* texture of this lower temperature phase as the texture was not well defined (Figure 4.79). However, in uncovered droplets both 2- and 4-brush defects were clearly observed (see Figure 4.79b) thereby confirming that this phase is an anticlinic smectic C phase.
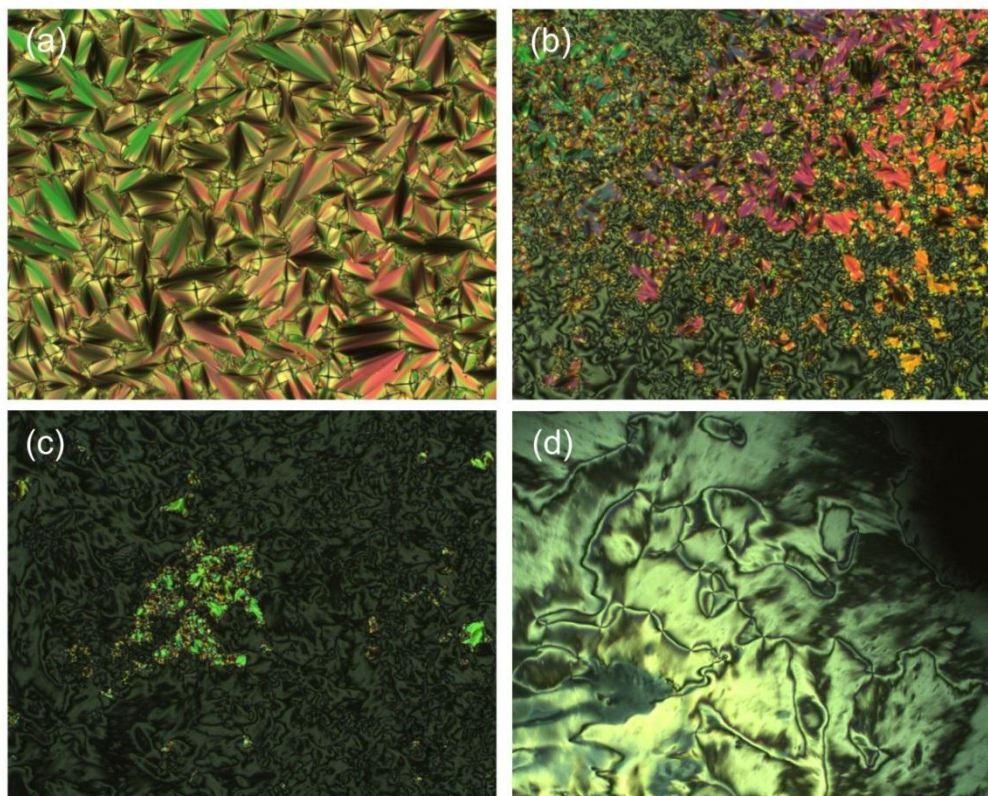
Figure 4.78: Photomicrographs (x100) showing (a) the texture of the smectic A phase of compound **11** at 130 ℃; (b) the texture of the smectic C phase of compound **12** at 115 ℃; (c) the texture of the smectic C phase of compound **12** at 120 ℃; and (d) texture of the smectic C phase of compound **11** in an uncovered droplet at 115 ℃.

2-Brush Defects
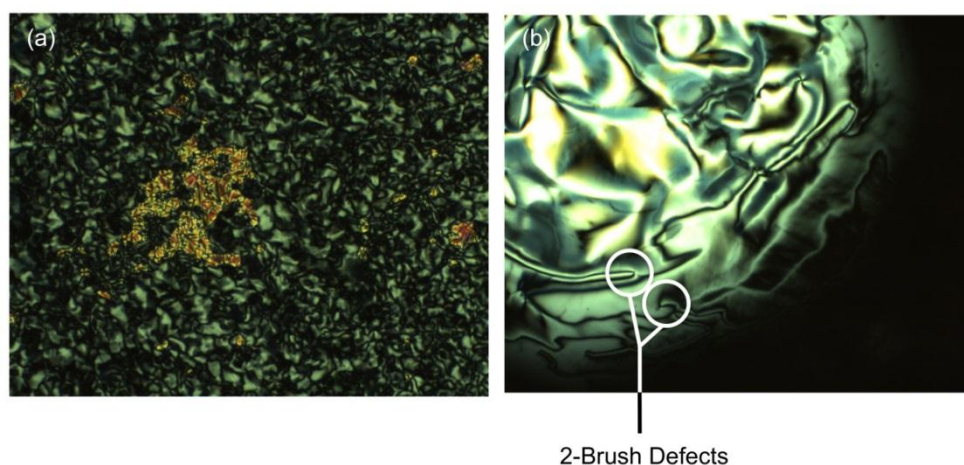
Figure 4.79: Photomicrographs (x100) showing (a) the texture of the SmC$_A$ phase of compound **12** at 100 ℃; (b) the smectic C$_A$ phase of compound **12** in an uncovered droplet at 100 ℃.

Overall, compounds **11** and **12** show very similar thermal behaviour. The clearing points of the two materials are very similar, as are the SmA-SmC transition temperatures. There is, however, a slight decrease in the thermal stability of the smectic C_A phase caused by adding one methylene unit to the terminal chain of compound **11** to give compound **12**. Furthermore, compound **12** exhibits a smectic I phase which is absent in the longer chain homologue (**11**). Given that both compound **11** and compound **12** have very similar structures to the well-known mesogenic material MHPOBC, it is interesting to compare their behaviours with that of racemic MHPOBC, the chemical structure and transition temperatures of which are shown in Figure 4.80.
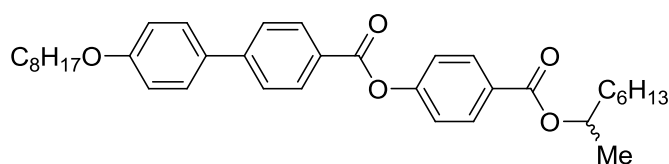
Cr 69 (SmI 65.5) SmC_A 110.8 SmC 121.1 SmA 148.9 Iso. Liq

Figure 4.80: The chemical structure and transition temperatures of racemic MHPOBC.

Racemic MHPOBC exhibits the same phase sequence as compound **11** and the two materials exhibit very similar transition temperatures, except the isotropization temperature and the SmC_A-SmI transition temperatures, which are higher for MHPOBC. If MHPOBC and compounds **11** and **12** are compared, it can be seen that all of the transition temperatures remain similar upon elongation of the terminal chain from C_8 to C_{11}, with the exception of the SmC_A-SmI transition temperature. Racemic MHPOBC has the highest thermal stability of the smectic I phase, it reduces upon elongation of the terminal chain to give compound **12** and compound **11** that do not exhibit a smectic I phase.

In order to explore whether chirality can be induced from racemic starting materials *via* the Mitsunobu reaction using the 'the reverse-twist disclination line

199

method', compounds **11** and **12**, were prepared by a number of different methods and their mixtures in E7 evaluated. From this point onwards the numbers **11** and **12** will be used to refer to these compound and a letter (**a**-**j**) will be used to refer to the different synthetic methodologies used to prepare them.

Initially, investigations were focused on a comparative study of the Mitsunobu and Steglich esterification reactions. Therefore the synthesis of compound **11** was undertaken using these two different methods, **11a** by the Mitsunobu reaction and **11b** by the Steglich esterification. The methodologies used to prepare **11a** (red arrows) and **11b** (blue arrows) are shown in Scheme 4.7. The source of 2-octanol used in the preparation of **11a** and **11b** was the same and was synthesised during the course of this work from the reduction of 2-octanone with sodium borohydride.[159] From this point onwards this batch of 2-octanol will be referred to using the abbreviation **Oct-1**.
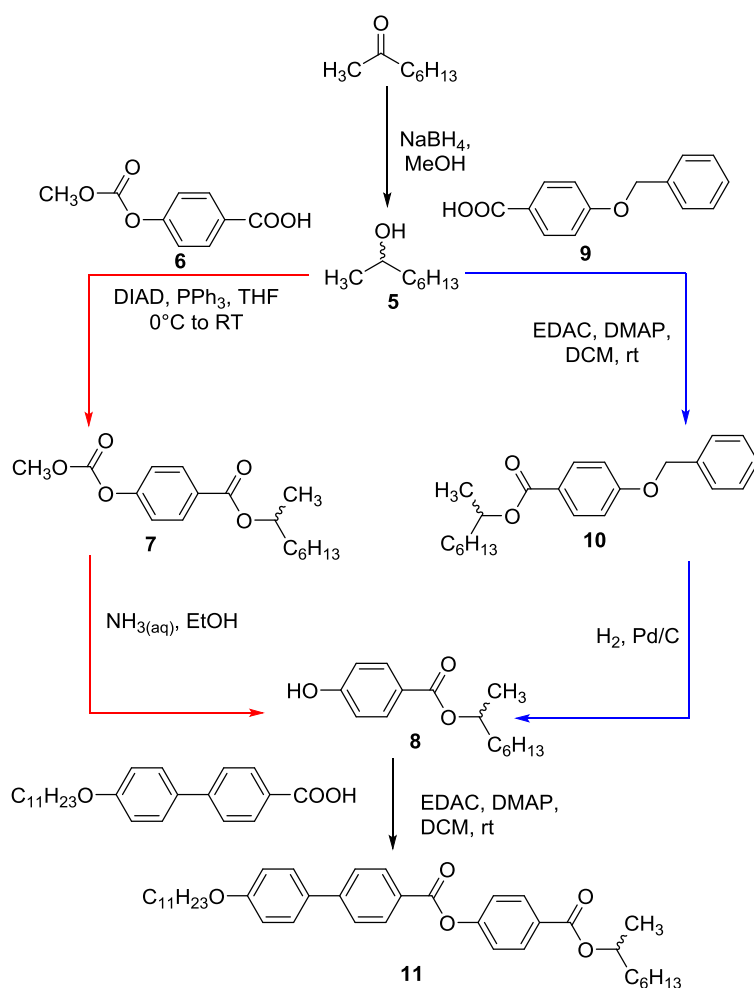
Scheme 4.7: The synthetic methodologies used to prepare **11a** (red arrows) and **11b** (blue arrows).

Despite their different preparations, the products **11a** and **11b** are structurally identical and, from the perspective of classical organic chemistry, it would be expected that they would show identical behaviours. However, when they were mixed with E7 and introduced into TN cell, compound **11a** showed significant curved disclination lines (radii of curvature is between 677 to 400 μm), which suggests compound **11a** is chiral, see Figure 4.81. Conversely, compound **11b** (radii of curvature is between 11838 to 19733 μm) behaved in an identical way to pure E7 (radii of curvature was between 3000 μm to infinity), which suggests compound **11b** is a non-chiral compound, see Figure 4.82. This result was expected because, as discussed previously, there is no mechanism by which the Steglich reaction can lead to the formation of a non-racemic product if the starting

materials are racemic. Since the same source of 2-octanol was used in both of these reactions, the result obtained for compound **11a** strongly suggests that the Mitsunobu reaction leads to the formation of a non-racemic, *i.e.* a chiral, product, thereby supporting the results reported by Cowling and co-authors.

(a)   (b)

(c)   (d)
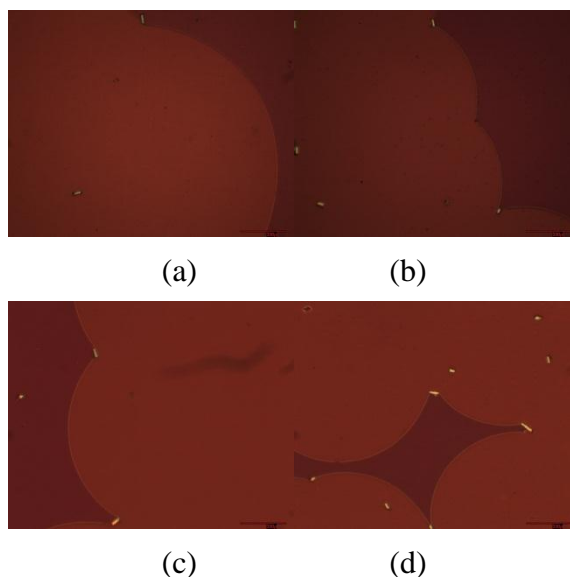
Figure 4.81: Photomicrographs (x50) showing the reverse-twist disclination lines of the mixtures of compound **11a** in E7 formed in 14.4 µm thickness TN cells at a concentration of (a) 1 wt%; (b) 2 wt%; (c) 3 wt% and (d) 5 wt%.

(a)   (b)
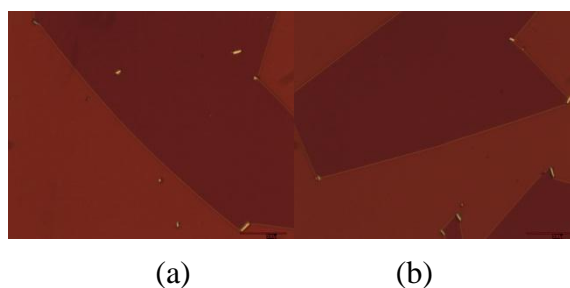
Figure 4.82: Photomicrographs (x50) showing the reverse-twist disclination lines of the mixtures of compound **11b** in E7 formed in 14.4 µm thickness TN cells at a concentration of (a) 2.5 wt% and (b) 5 wt%.

In order to investigate these results further, compounds **11c** and **11d** were synthesised. Like **11b**, both of these materials are structurally identical to **11a** as they are simply different batches of compound **11**. Since compound **11a** showed an enantiomeric excess, both **11c** and **11d** were prepared *via* an identical synthetic

pathway to **11a**, *i.e.* the same reaction types and the same reaction conditions were used. Furthermore, compound **11c** was prepared using the same bottles of starting materials and reagents as **11a** and is therefore an exact repeat of the synthesis of **11a**. Conversely, compound **11d** was prepared using a different source of 2-octanol, which was synthesized *via* the reduction of 2-octanone with sodium borohydride by Dr. S. Cowling (**Oct-2**). The syntheses of **11c** and **11d**, alongside the way in which the synthetic steps conform or differ from the synthetic steps used to prepare compound **11** are shown in Scheme 4.8.
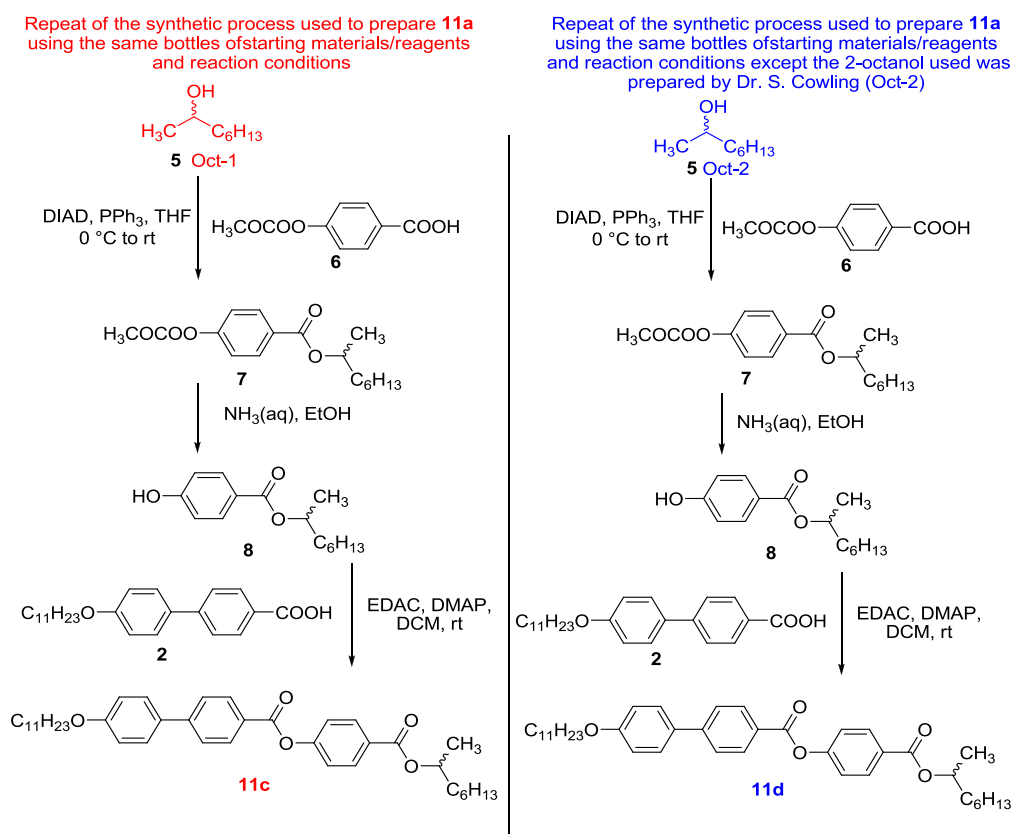
Scheme 4.8: The synthetic methodologies used to prepare **11c** (red) and **11d** (blue).

Interestingly, when examined *via* the reverse twist disclination line methods, all of the mixtures of compounds **11c** and **11d** in E7 did not show pronounced curved disclination lines. The radii of the disclination lines ranged for compounds **11c** and

11d in E7 between 3896 to 7528 μm and 3241 to 7213 μm, respectively. This is an unusual result as the methodology and materials used to prepare compound **11c**, which is achiral, are identical to those used to prepare **11a**, which shows and enantiomeric excess. Furthermore, **Oct-2** was prepared using the same methodology as **Oct-1,** which was prepared during this project, and it is therefore unusual that the behaviour of **11d** differs from that of **11a**. This is also an unusual result in the wider context as the materials reported by Cowling *et al*., which have been prepared numerous times by a number of different individuals have always been chiral, *i.e.* they always showed ferroelectric rather than dielectric switching. There are two possibilities to explain the observation made for **11c** and **11d**. Firstly, it is possible that **11c** and **11d** are only weakly chiral and therefore only induce a very slight bowing of the disclination lines that cannot be differentiated from the bowing of the disclination lines resulting from the pre-twist of the TN cell. Secondly, it could be that **11c** and **11d** are truly racemic. However, regardless of the explanation it is clear that the results obtained for these two materials are different from the results for **11a**. At first this seems very unusual. However, there are several previous reports of reactions that start from non-chiral or racemic starting materials and give chiral products. Moreover, in these previous studies it has often been observed that the formation of chiral products does not always occur. In some cases only racemic materials are formed and in some cases even when chiral materials are formed the *ee* can fluctuate markedly from reaction to reaction.[164] Clearly this could be the case here for **11c** and **11d**, *via* mechanisms that are out of the experimental chemists control, *e.g.* small fluctuations in temperature and concentration within the reaction vessel.

(a)   (b)   (c)

(d)   (e)   (f)
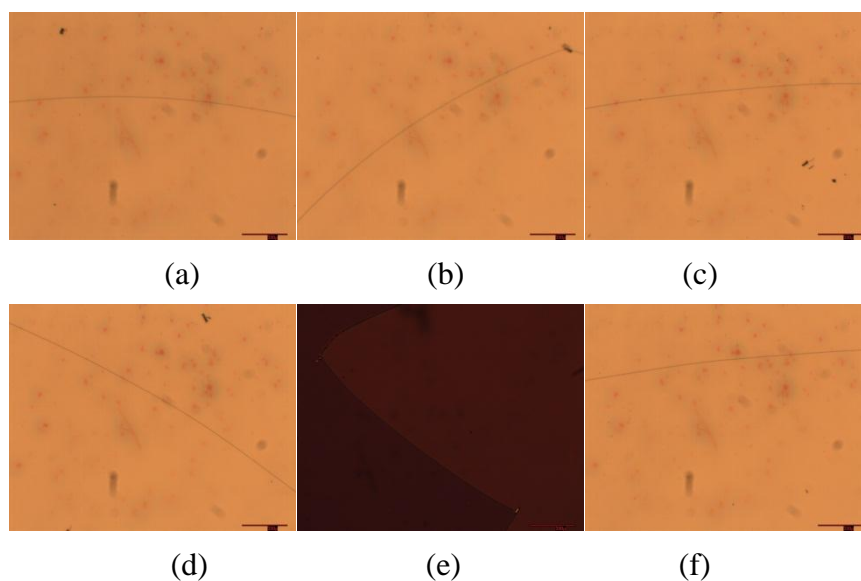
Figure 4.83: Photomicrographs (x50) showing the reverse-twist disclination lines of the mixtures of compound **11c** (a-c) and **11d** (d-f) in E7 formed in 14.4 μm thickness TN cells at a concentration of (a) 0.9 wt%; (b) 1.6 wt%; (c) 2.6 wt % (d) 1.3 wt%; (e) 3.2 wt%, and (f) 5.4 wt%.

In order to further investigate the impact of the reaction conditions on the properties of different batches of compound **11**, compounds **11e** and **11f** were prepared. These materials were prepared in the same way as compound **11a** and **11d**, *i.e.* using either **Oct-1** or **Oct-2**, with the exception that the Mitsunobu esterification was performed at room temperature, rather than starting the reaction at 0 °C and allowing it to warm to room temperature over time. The methodology used to prepare compounds **11e** and **11f** is shown in Scheme 4.9.
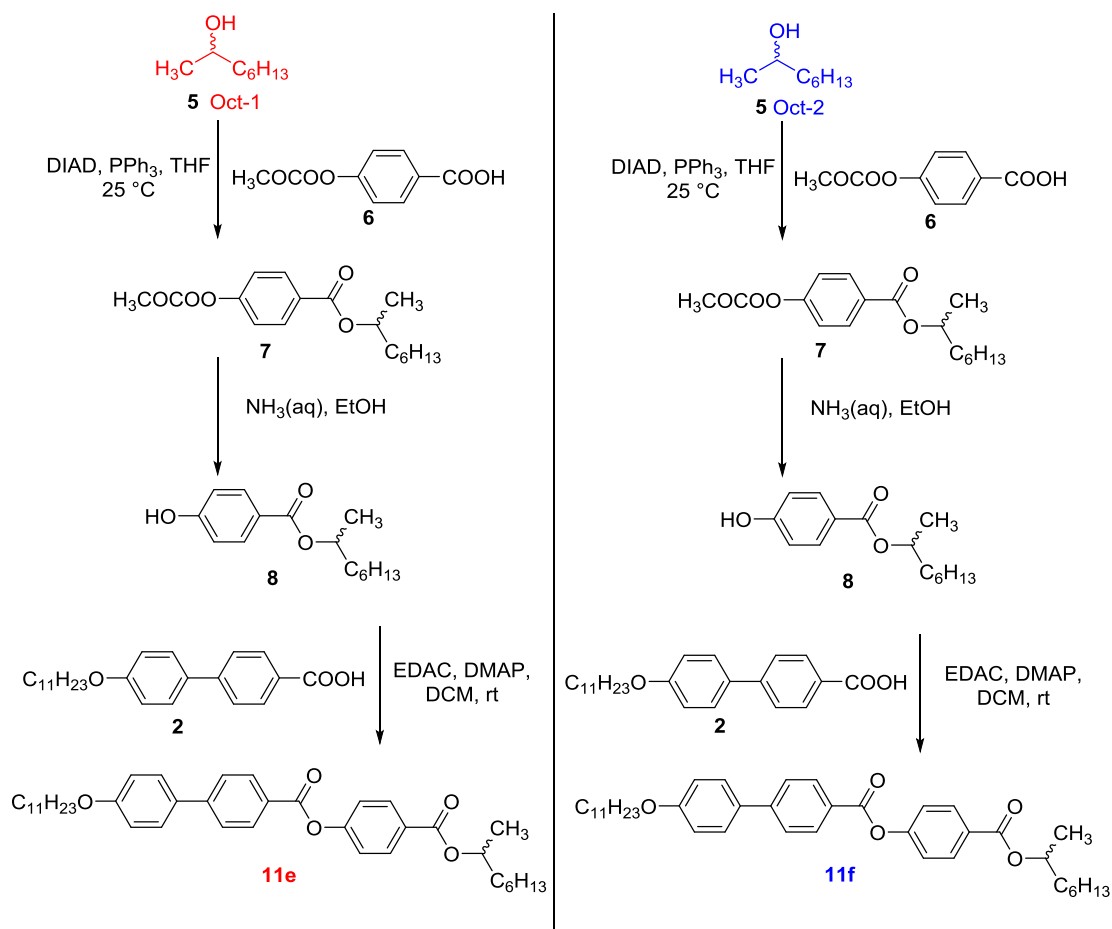
Scheme 4.9: The synthetic methodology used to prepare compounds **11e** and **11f**.

Interestingly, when analyzed using the reverse twist disclination line method, compound **11e** and **11f** behave in the same way as **11c** and **11d**. The radii of the disclination lines of compounds **11e** and **11f** in E7 is between 3331 to 6525 μm and 7213 to 8276 μm respectively (see Figure 4.84), which are still within the range of curvature observed for pure E7 as a result of the pretwist of the TN cells used. Thus, it is very difficult to conclude whether these two materials are weakly chiral or if they are racemic. However, the fact that they both clearly do not display the same degree of enantiomeric excess as compound **11a** lends some support to the idea that the temperature at which the reaction is conducted is important in the de-racimisation process of the Mitsunobu reaction.
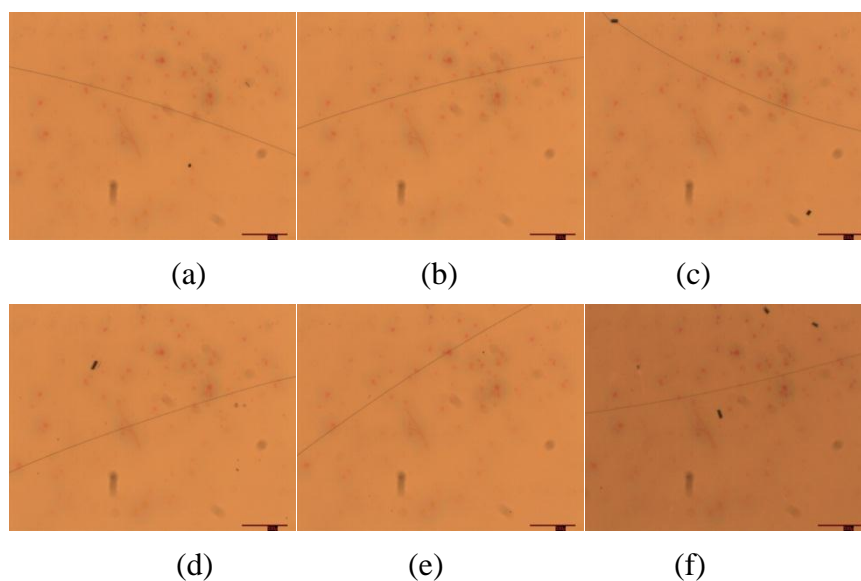
Figure 4.84: Photomicrographs (x50) showing the reverse-twist disclination lines of the mixtures of compound **11e** (a-c) and **11f** (d-f) in E7 formed in 14.4 μm thickness TN cells at a concentration of (a) 1.0 wt%;(b) 1.9 wt%;(c) 3.0 wt %;(d) 1.0 wt%;(e) 1.25 wt% and (f) 2.6 wt%.

In recent years the Mitsunobu reaction has become an extremely important reaction, not only in the development of liquid-crystalline materials, but also in the wider field of materials science and natural product chemistry.[46] There have, therefore, been many efforts to prepare new coupling agents that offer increased reactivity and substrate control in comparison to DIAD (diisopropylazodicarboxylate) or DEAD (diethylazodicarboxylate). In order to further investigate the impact of the Mitsunobu reaction on the potential enantiomeric excess of liquid-crystalline products, different batches of compound **12** were prepared using a variety of coupling reagents. In all cases the synthetic procedure was kept constant and only the coupling reagent used for the Mitsunobu reaction and the source of the 2-octanol (**Oct-1** or **Oct-2**) was varied. The synthetic procedure and materials used to prepare different batches of compound **12** are shown in Scheme 4.10.
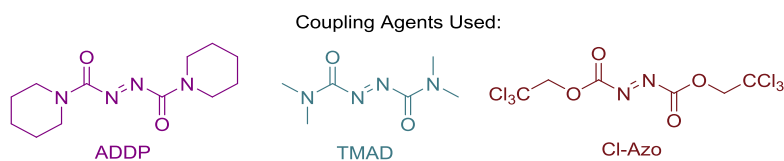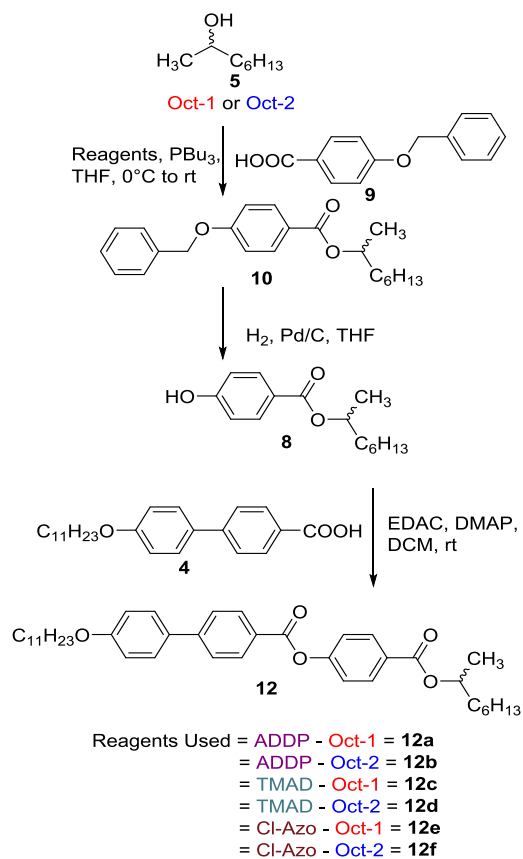
Scheme 4.10: The synthesis of **12a**-**12f** and the coupling agents used for the Mitsunobu esterification.

The chiral induction properties of compounds **12a-f** were tested by mixing them with E7 and putting the resulting mixtures into TN cells. As these compounds were all synthesed *via* Mitsunobu esterification using different coupling reagents and sources of 2-octanol (Oct-1 and Oct-2) these studies provide an insight into whether or not different coupling agents influence the properties of the final materials. The results of the analysis of mixtures of **12a-f** in E7 *via* the reverse twist disclination line method are shown in Figure 4.85.
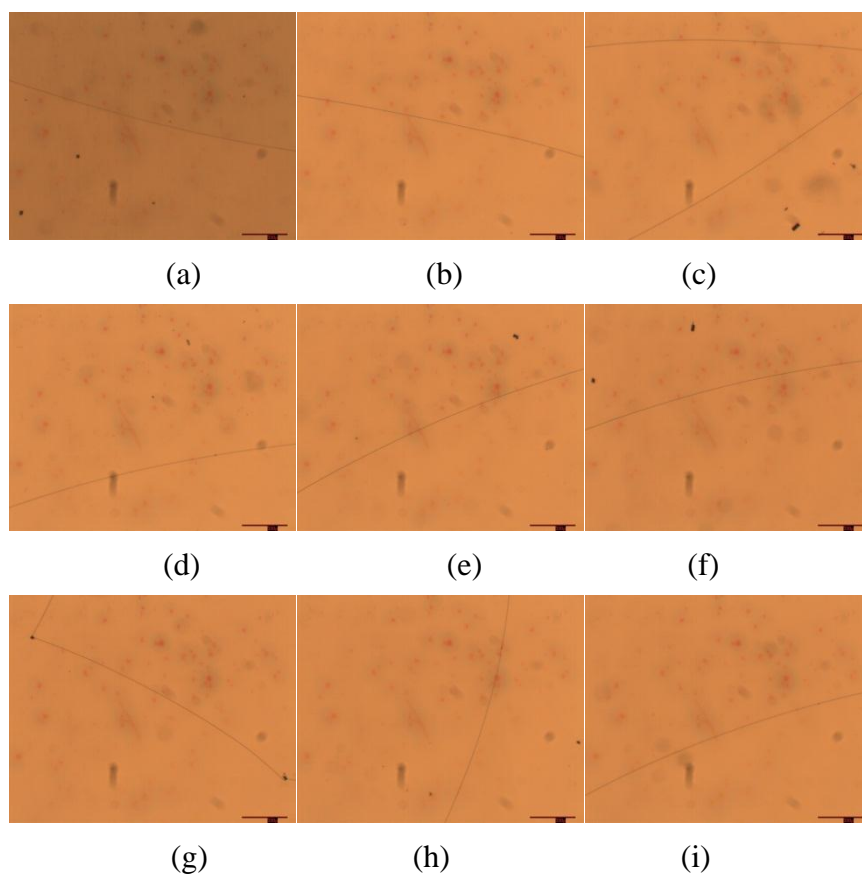
Figure 4.85: Photomicrographs (x50) showing the reverse-twist disclination lines of the mixtures of compound **12a** (a-c), **12b** (d-f), **12c** (g-i), **12d** (j-l), **12e** (m-o) and **12f** (p-r) in E7 formed in 14.4 μm thickness TN cells at a concentration of (a) 0.7 wt%; (b) 1.9 wt%; (c) 2.4 %; (d) 1.2 wt%;(e) 2.3 wt%;(f) 2.9 wt%; (g) 0.5 wt%; (h) 1.0 wt% and (i) 1.6 wt%

(j)　　　　　　　(k)　　　　　　　(l)

(m)　　　　　　　(n)　　　　　　　(o)

(p)　　　　　　　(q)　　　　　　　(r)
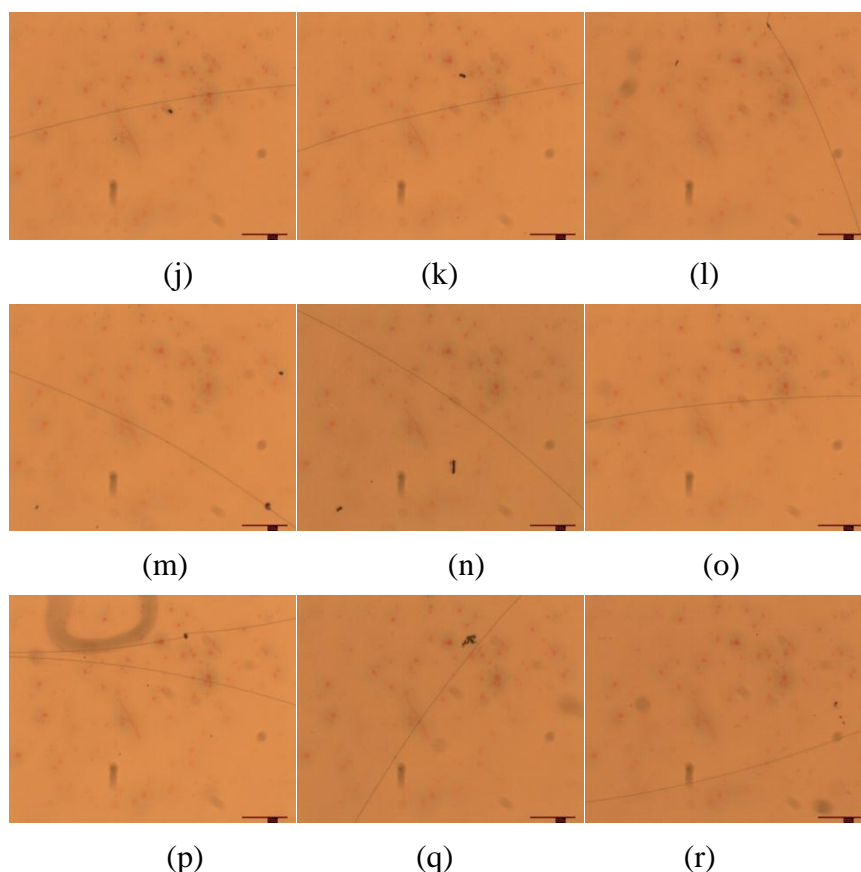
Figure 4.86: Photomicrographs (x50) showing the reverse-twist disclination lines of the mixtures of compound **12a** (a-c), **12b** (d-f), **12c** (g-i), **12d** (j-l), **12e** (m-o) and **12f** (p-r) in E7 formed in 14.4 μm thickness TN cells at a concentration of (j) 0.6 wt%;(k) 2.4 wt%; l) 3.0 wt%;(m) 2.2 wt%;(n) 3.2 wt%;(o) 3.4 wt%;(p) 0.7 wt%;(q) 2.0 wt% and (r) 3.8 wt%.

From all of the pictures above, it can be seen that none of the radii of curvature of the disclination lines are below 3000 μm. Thus, apart from compound **11a**, all the other compounds presented in this section exhibit similar behaviour to compounds **11c, 11d, 11e** and **11f** It is therefore very difficult to say for certain if they are only weakly chiral or racemic.

In summary, all the compounds were examined through 'the reverse-twist disclination method', only compound **11a** appeared to show a clear enantiomeric excess. Conversely, all of the other materials, including compound **11c** which was prepared *via* the exact same methodology, using the same reagents and starting materials, as compound **11a**, did not show a clear enantiomeric excess. In many

cases, mixtures of these materials in E7 did show slightly curved disclination lines but the radii of curvature of the disclination lines were found to be very large and of the order of those observed for pure E7. Two possibilities therefore arise for these batches of compound **11**. Firstly, these materials could be truly racemic or, alternatively, they could exhibit an enantiomeric excess that is too small to be measured definitively using the reverse twist discilination line method.

Overall, the results presented in this chapter clearly show that chiral materials can definitely be produced *via* the Mitsunobu reaction when a racemic alcohol is used. However, the results do not paint a clear picture of the origin of the enantiomeric excess that is observed in materials with structures similar to MHPOBC. However, for compound **11a** the result is clear in that it behaves as a non-racemic mixture, thereby confirming the observations of Cowling *et al.* The factors that give rise to this effect are not clear, although it is clear that for reactions conducted at room temperature or using coupling reagents other than DIAD, only weakly chiral or racemic products are formed. Furthermore, the results presented in this chapter strongly suggest that the ability of the Mitsunobu reaction to produce a measurable enantiomeric excess when racemic 2-octanol is used as the staring material is dependent upon conditions that are difficult for the synthetic chemist to control, *e.g.* very small fluctuations in temperature or concentration, small variations in concentration between reactions *etc*.

Chapter 5.   Conclusion

In the final section of this thesis, rather than enter into a lengthy discussion, much of which has been made in the various chapters, the important outcomes/highlights are simply listed as bullet points as follows:

- Initial studies on the helical twisting power of the commercially available CB15 confirmed the HTP value, with the result being comparable to those reported *via* other techniques. The important outcome being the level of sensitivity of the methodology, for example a gram of a chiral material in 100 kg of a non-chiral nematic host was detected, which applied to non-mesogenic chiral materials as well chiral ones. Another outcome was the helical pitch length of such as system could be measured in the millimetre range. Potentially the 'reverse-twist disclination' methodology has the possibility of measuring macromolecular pitch lengths to centimeters and beyond.

- The helical twisting power value of a given chiral dopant not only depends on the dopant itself, but also on the nematic host. Using the 'reverse-twist disclination method', it was shown that for a given chiral dopant different hosts can produce different HTP values. It appears that if the host's chemical structure is similar to that of the dopant, the HTP value can be enhanced, which gives a potentially useful structure-property correlation for the design of chiral dopants.

- The commercial, chiral dopants R1011 and S1011, as well as both enantiomers of the drug thalidomide achieved the highest HTP values of all of the dopants that were investigated. For thalidomide and R/S1011 the lowest energy conformation can be viewed as "propeller-shaped". The conclusion being that such "propeller-shaped" materials can attain higher HTP values than any other molecular shape of dopant, such as those presented by the

rod-like oxazoline dopants that were also studied. This hypothesis can also be extended to high HTP metal complex dopants in the literature.

- With respect to the drug thalidomide, the two enantiomers possessed different optical purities, which could be easily detected using the methodology. Thus, the reverse-twist disclination method could have the potential to be applied in quality control of pharmaceutical industry, due to its high level of sensitivity to chirality and its ability to test low sample quantities/concentrations. This was demonstrated with thalidomide, however this method may also be applicable to other enantiopure drugs such as penicillins or methorphan.

- One way to increase the helical twisting power of a dopant is through "mesogenic functionalization", where the original dopant is chemically modified to incorporate a number of mesogenic units. The sugar D-glucopyranose and a mesogen functionalised variant were studied and it was found that the HTP value was significantly higher when mesogenic units were incorporated, *i.e.,* the chirality of the central scaffold was transferred to the out-most parts of the dendritic structure. Furthermore, it appears that this also gave an increase in the solubility in nematic host.

- For the CDFBP based ferroelectric chiral dopants, a higher polarity functional group at the stereogenic centre appears to give larger values of HTP. Furthermore, when the stereogenic centre was appended to the core *via* a short aliphatic chain the resulting HTP values were higher than when using a longer aliphatic chain. This was related to rotational trapping of the asymmetric centre.

- Esterification *via* the Mitsunobu reaction can sometimes vary the enantiomeric excess in products by small amounts, and these were detected by the reverse-twist disclination method. Conversely, the Steglich esterification does not change the optical purity. This provides a fundamental method by which the mechanisms of related reactions can be compared.

Chapter 6. Experimental Annex

6.1 Experimental Details:

4'-(Undecyloxy)biphenyl-4-carbonitrile (1)

A mixture of 1-bromoundecane (21.42 g, 0.091 mol), 4'-hydroxybiphenyl-4-carbonitrile (16.60 g, 0.085 mol), potassium carbonate (24.41 g, 0.177 mol) and butanone (1 L) was heated to reflux for 24 hours. The reaction mixture was allowed to cool to room temperature, filtered and the solvent was removed in *vacuo.* Flash column chromatography (dichloromethane/hexane 10:1 over silica) followed by crystallisation from ethanol gave compound **1** (23.66 g, 80%) as a white powder.

^{1}H NMR (400MHz CDCl$_3$) δ_H 7.67 (4H, m, Ar), 7.53 (2H, d, J = 8.8 Hz, Ar), 6.99 (2H, d, J = 8.8 Hz, Ar), 4.0 (2H, t, J = 6.6 Hz, CH$_2$O), 1.90-1.76 (2H, m, CH_2CH$_2$O), 1.57-1.18 (16H, m, CH$_2 \times$8), 0.88 (3H, t, J = 6.8 Hz, CH$_3$).

4'-(Undecyloxy)biphenyl-4-carboxylic acid (2)

Compound **1** (5.00 g, 14.3 mmol) was dissolved in acetic acid (100 mL). The resulting mixture was heated to reflux before sulphuric acid (98% 10 mL) and water (10 mL) was added. The resulting mixture was then heated to reflux for 12 hours. The resulting solution was cooled to room temperature and water (500 mL) was added. The precipitate was filtered off and washed with water until it reached pH = 7. It was then dried in the oven, recrystallization in a mixture of solvents (ethanol : ethyl estate : terahydrofuran 10 :10 :1) gave acid **2** (5.10 g, 97%) as a white crystal.

^{1}H NMR (400MHz Acetone-D$_6$) δ_H 7.89 (2H, d, J = 8.5 Hz, Ar), 7.66 (2H, d, J = 8.5 Hz, Ar), 7.63 (2H, d, J = 8.8 Hz, Ar), 6.99 (2H, d, J = 8.8 Hz, Ar), 3.97 (2H, t,

$J = 6.5$ Hz, CH$_2$O), 1.73-1.65 (2H, m, CH$_2$CH$_2$O), 1.42-1.15 (16H, m, CH$_2 \times 8$), 0.82 (3H, t, $J = 7.0$ Hz, CH$_3$). COOH not observed.

IR v_{max} cm^{-1} 2916, 2848, 1683, 1602, 1582, 1529, 1500, 1275, 1254, 1129, 1000, 860, 835, 717, 695, 551, 491.

4'-(Decyloxy)biphenyl-4-carbonitrile (3)

Prepared *via* the same methodology as compound **1**. Quantities used: 1-bromodecane (24.33 g, 0.110 mol), 4'-hydroxybiphenyl-4-carbonitrile (20.00 g 0.102 mol), potassium carbonate (20.73 g, 0.150 mol) and butanone (1 L). Flash column chromatography (dichloromethane/hexane 10:1 over silica) followed by crystallisation from ethanol gave compound **3** (27.30 g, 79%) as a white powder.

^{1}H NMR (400MHz CDCl$_3$) δ_H 7.66 (4H, m, Ar), 7.52 (2H, d, $J = 8.8$ Hz, Ar), 6.99 (2H, d, $J = 8.8$ Hz, Ar), 4.0 (2H, t, $J = 7.0$ Hz, CH$_2$O), 1.86-1.76 (2H, m, CH$_2$CH$_2$O), 1.60-1.21 (14H, m, CH$_2 \times 7$), 0.88 (3H, t, $J = 7.0$ Hz, CH$_3$).

4'-(Decyloxy)biphenyl-4-carboxylic acid (4)

Prepared *via* the same methodology as compound **2**. Quantities used: compound **3** (5.00 g, 0.0148 mol), acetic acid (100 ml), water (10 ml) and sulphuric acid (10 ml) gave white crystals. Yield = 4.12 g (78%).

^{1}H NMR (400MHz Acetone-D$_6$) δ_H 7.86 (2H, d, $J = 8.5$ Hz, Ar), 7.64 (2H, d, $J = 8.5$ Hz, Ar), 7.55 (2H, d, $J = 8.8$ Hz, Ar), 6.98 (2H, d, $J = 8.8$ Hz, Ar), 4.00 (2H, t, $J = 6.6$ Hz, CH$_2$O), 1.85-1.76 (2H, m, CH$_2$CH$_2$O), 1.51-1.25 (14H, m, CH$_2 \times 7$), 0.88 (3H, t, $J = 7.0$ Hz, CH$_3$). COOH not observed.

IR v_{max} cm^{-1} 2918, 2880, 1685, 1602, 1431, 1291, 1253, 1201, 1029, 834, 772, 717, 553, 463.

2-Octanol (5)

2-Octanone (20.00 g, 0.156 mol) was dissolved in methanol before cooled to -5 ℃ under N_2. Then, sodium borohydride (2.9 g, 0.0766 mol) was added into the stirred solution generally with the temperature of the solution never exceeding 0 ℃. The resulting solution was stirred for 2 hours. Then, dilute hydrochloride acid (20%) was added until the solution reached pH = 7. Brine was added and the layers were separated. The aqueous layer was extracted with CH_2Cl_2 (3 $\times$ 20 mL) and the combined organic extracts were dried ($MgSO_4$) and evaporated under reduced pressure to give the alcohol **5** (20.21 g, 99%) as colourless oil. No further purification was required.

^{1}H NMR (400MHz $CDCl_3$) δ_H 3.77 (1H, m, CH), 1.40-1.35 (13H, m, CH_3, $CH_2 \times$ 5), 0.86 (3H, t, J = 7.0 Hz, CH_3CH_2).OH not observed.

IR v_{max} cm^{-1} 3348, 2924, 2854, 1458, 1373, 1265, 1111, 1033, 740, 624, 524.

4-Methoxycarbonyloxybenzoic acid (6)

4-Hydroxybenzoic acid (17.72 g, 0.128 mol) was added into a stirred solution of sodium hydroxide (15.00 g, 0.375 mol) in water (400 mL). The resulting solution was cooled down to -10 ℃. Methyl chloroformate (20.00 g, 0.212 mol) was then added slowly into the solution which maintained at -5 ℃. The solution was stirred for 4 hours before diluted hydrochloric acid (concentrate hydrochloric acid and water 1:1) was added into the solution until it reached pH 5. The precipitate was filtered off and recrystallized from ethanol gave acid **6** (23.27 g, 93%) as a white solid. Spectroscopic data consistent with those reported in the literature.[166]

^{1}H NMR (400MHz $CDCl_3$) δ_H 8.16 (2H, d, J = 8.0 Hz, Ar), 7.31(2H, d, J = 8.0 Hz, Ar), 3.94 (3H, s, CH_3). COOH not observed

^{13}C NMR (100MHz, CDCl$_3$) δ$_C$ 170.9 (C=O), 155.2 (C=OOH), 153.5 (*o*-Ar), 132.0 (Ar), 127.0 (*o*-Ar), 121.1 (Ar), 55.7 (OMe).

IR v_{max} cm^{-1} 2920, 1774, 1759, 1683, 1607, 1432, 1279, 1221, 1108, 1017, 940, 857, 845, 659, 550, 501.

HR-MS (ESI) (*m/z*) - Calculated: 219.0267 [M+Na]$^+$; Found: 219.0264 [M+Na]$^+$.

Octan-2-yl 4-(methoxycarbonyloxy)benzoate (7)

All glassware were dried in the oven prior to reaction. Compound **5** (1.00 g, 7.68 mmol), compound **6** (1.50 g, 7.68 mmol) and triphenyl phosphine (2.23 g, 8.50 mmol) were dissolved in dry THF (100 mL) in a three neck round bottomed flask under the N$_2$. The resulting mixture was cooled to 0 ℃. Then diisopropyl azodicarboxylate (1.54 g, 7.68 mmol) in dry THF (10 mL) was added slowly *via* a dropping funnel. The resulting solution was stirred under the N$_2$ for 12 hours. The solvent was reduced under pressure to give the crude product. Flash column chromatography (CH$_2$Cl$_2$: Hexane 10:1 over silica) gave compound **7a** (1.72 g, 73%) as a colourless oil. Spectroscopic data consistent with those reported in the literature.[166]

Compound **7c** prepared *via* the same methodology as compound **7a**. Quantities used: compound **5** Oct-1 (0.68 g, 5.25 mmol), compound **6** (1.02 g, 5.25 mmol), triphenylphosphine (1.45 g, 5.52 mmol) and diisopropyl azodicarboxylate (2.00 g, 5.25 mmol). Diisopropyl azodicarboxylate was added dropwise at 0 ℃ and reaction allowed to warm to room temperature to give colourless oil. Yield = 0.78 g (48%).

Compound **7d** prepared *via* the same methodology as compound **7a**. Quantities used: compound **5** Oct-2 (0.72 g, 5.53 mmol), compound **6** (1.08 g, 5.53 mmol), triphenylphosphine (1.60 g, 6.08 mmol) and diisopropyl azodicarboxylate (1.11 g, 5.53 mmol). Diisopropyl azodicarboxylate was added dropwise at 0 ℃ and reaction allowed to warm to room temperature to give colourless oil. Yield = 0.78 g (46%).

Compound **7e** prepared *via* the same methodology as compound **7a**. Quantities used: compound **5** Oct-1 (0.66 g, 5.07 mmol), compound **6** (1.0 g, 5.07 mmol), triphenylphosphine (1.46 g, 5.57 mmol) and diisopropyl azodicarboxylate (1.02 g, 5.07 mmol). Diisopropyl azodicarboxylate was added dropwise at 25 ℃ to give colourless oil. Yield = 0.86 g (55%).

Compound **7f** prepared *via* the same methodology as compound **7a**. Quantities used: compound **5** Oct-2 (0.56 g, 4.30 mmol), compound **6** (0.84 g, 4.30 mmol), triphenylphosphine (1.24 g, 4.73 mmol) and diisopropyl azodicarboxylate (0.86 g, 4.30 mmol). Diisopropyl azodicarboxylate was added dropwise at 25 ℃ to give colourless oil. Yield = 0.61 g (46%).

^{1}H NMR (400MHz CDCl$_3$) δ_H 8.08 (2H, d, J = 8.8 Hz, Ar), 7.25 (2H, d, J = 8.8 Hz, Ar), 5.14-5.08 (1H, m, CH), 3.92 (1H, s, CH$_3$O), 1.84-1.54 (13H, m, CH_3CH, CH$_2$ ×5), 0.87 (3H, t, J = 7.0 Hz, CH$_3$).

^{13}C NMR (100MHz, CDCl$_3$) δ_C 165.3 (C=O), 154.4 (C=OOH), 153.6 (*o*-Ar), 131.1 (Ar), 128.7 (*o*-Ar), 120.9 (Ar), 72.0 (OCH), 55.6 (OMe), 41.2 (CH$_2$), 36.0 (CH$_2$), 31.7 (CH$_2$), 29.1 (CH$_2$), 25.4 (CH$_2$), 20.0 (Me), 14.0 (Me).

IR v_{max} cm^{-1} 2956, 2930, 1767, 1713, 1606, 1505, 1440, 1414, 1379, 1253, 1231, 1163, 1104, 937, 857, 818, 772, 717, 685, 630, 504.

Octan-2-yl 4-hydroxybenzoate (8)

Ammonia (6.5 mL) was added dropwise into a stirred solution of compound **7** (1.50 g, 4.86 mmol) in ethanol (25 mL). The resulting mixture was stirred at room temperature for 12 hours. The solvent was reduced under pressure to give compound **8a** (1.19 g, 82%) as a colorless oil. No further purification was required.

Pd/C (10% wt on carbon, 0.10 g) was added to a stirred solution of the ester **10** (1.61 g, 4.73 mmol) in THF (50 mL) and ethanol (10 mL) at rt under N_2. The flask was evacuated and back-filled with N_2 three times and finally evacuated and back-filled with H_2. Then, the mixture was stirred at room temperature for 12 hours. Et_2O (10 mL) was added and the solids were removed by filtration through a pad of Celite® and the filter-cake was washed with Et_2O (3 × 10 mL). The combined organic washings were evaporated under reduced pressure to give ester **8b** (1.1 g, 93%) as a courless oil. No further purification was required.

^{1}H NMR (400MHz CDCl$_3$) δ_H 7.95 (2H, d, J = 8.8 Hz, Ar), 6.88 (2H, d, J = 8.8 Hz, Ar), 5.18-5.07 (1H, m, CH), 1.84-1.52 (13H, m, 13H, m, CH_3CH, CH$_2$ ×5), 0.86 (3H, t, J = 7.0 Hz, CH$_3$). OH not observed.

^{13}C NMR (100MHz, CDCl$_3$) δ_C 166.5 (C=O), 160.5 (*o*-Ar), 131.8 (Ar), 122.7 (*o*-Ar), 115.2 (Ar), 71.6 (OCH), 36.0 (CH$_2$), 31.7 (CH$_2$), 29.1 (CH$_2$), 25.4 (CH$_2$), 22.5 (CH$_2$), 20.0 (Me), 14.0 (Me).

IR v_{max} cm^{-1} 3318, 2930, 2858, 1682, 1608, 1591, 1514, 1449, 1355, 1229, 1271, 1164, 1107, 1079, 1050, 851, 772, 638, 618, 505.

4-Benzyloxy-benzonic acid (9)

Bromobenzene (109.12 g, 0.638 mol), 4-hydroxybenzoic acid (40.05 g, 0.290 mol) and potassium hydroxide (48.82 g, 0.870 mol) were dissolved in ethanol (500 mL). The resulting mixture was heated to reflux for 16 hours before cooled to room temperature. Hydrochloric acid solution (20%) was added into the mixtures until it reached pH = 7. Then, the precipitate was filtered off and recrystallized in ethanol gave acid **9** (62.81 g, 95%) as white crystals. Spectroscopic data consistent with those reported in the literature.[167]

^{1}H NMR (400MHz CDCl$_3$) δ_H 7.89 (2H, d, J = 8.0 Hz, Ar), 7.48-7.32 (5H, m, Ar), 7.10 (2H, d, J = 8.0 Hz, Ar), 5.18 (2H, s, CH$_2$). COOH not observed

^{13}C NMR (100MHz, CDCl$_3$) δ_C 167.3 (C=O), 166.3 (*o*-Ar), 137.8 (*o*-Ar), 132.6 (Ar), 132.4 (Ar), 129.4 (Ar), 128.9 (*o*-Ar), 128.6 (Ar), 115.6 (Ar), 70.8 (OCH$_2$).

IR v_{max} cm^{-1} 2964, 1695, 1604, 1510, 1373, 1241, 1168, 1107, 914, 857, 771, 755, 736, 690, 654, 551, 510.

HR-MS (ESI) (*m/z*) - Calculated: 251.0683 [M+Na]$^+$; Found: 251.0679 [M+Na]$^+$.

Octan-2-yl 4-(benzyloxy)benzoate (10)

Compound **10a** prepared *via* the same methodology as compound **7**. Quantities used: compound **5** Oct-1 (1.20 g, 9.21 mmol), compound **9** (2.10 g, 9.21 mmol), tributylphosphine (2.07 g, 10.13 mmol) and 1,1'–(azodicarbonyl)dipiperidine (2.32 g, 9.21 mmol) to give colourless oil. Yield = 1.54 g (49%). Spectroscopic data consistent with those reported in the literature.[168]

Compound **10b** prepared *via* the same methodology as compound **7**. Quantities used: compound **5** Oct-2 (1.20 g, 9.21 mmol), compound **9** (2.10 g, 9.21 mmol), tributylphosphine (2.07 g, 10.13 mmol) and 1,1'–(azodicarbonyl)dipiperidine (2.32 g, 7.67 mmol) to give colourless oil. Yield = 1.29 g (52%).

Compound **10c** prepared *via* the same methodology as compound **7**. Quantities used: compound **5** Oct-1 (1 g, 7.67 mmol), compound **9** (1.75 g, 7.67 mmol), triphenylphosphine (2.03 g, 7.67 mmol) and tetramethlazodicarboxamide (1.32 g, 7.67 mmol) to give colourless oil. Yield = 1.07 g (41%).

Compound **10d** prepared *via* the same methodology as compound **7**. Quantities used: compound **5** Oct-2 (1.25 g, 9.60 mmol), compound **9** (2.19 g, 9.60 mmol), triphenylphosphine (2.16 g, 10.56 mmol) and tetramethlazodicarboxamide (1.65 g, 9.60 mmol) to give colourless oil. Yield = 1.01 g (31%).

Compound **10e** prepared *via* the same methodology as compound **7**. Quantities used: compound **5** Oct-1 (0.68 g, 5.22 mmol), compound **9** (1.19 g, 5.22 mmol), triphenylphosphine (1.17 g, 5.74 mmol) and bis(2,2,2, trichlorethyl) azodicarboxylate (1.98 g, 5.22 mmol) to give colourless oil. Yield = 1.44 g (81%).

Compound **10f** prepared *via* the same methodology as compound **7**. Quantities used: compound **5** Oct-2 (0.68 g, 5.22 mmol), compound **9** (1.19 g, 5.22 mmol), triphenylphosphine (1.17 g, 5.74 mmol) and bis(2,2,2, trichlorethyl) azodicarboxylate (1.98 g, 5.22 mmol) to give colourless oil. Yield = 1.10 g (62%).

^{1}H NMR (400MHz CDCl$_3$) δ_H 7.99 (2H, d, J = 8.9 Hz, Ar), 7.38 (5H, d, J = 8.9 Hz, Ar), 6.99 (2H, d, J = 8.9 Hz, Ar), 5.12 (2H, s, ArCH_2O), 5.14-5.08 (1H, m, CH), 1.76-1.20 (13H, m, CH_3CH, CH$_2$ $\times$ 5), 0.87 (3H, t, J = 6.8 Hz, CH$_3$).

^{13}C NMR (100MHz, CDCl$_3$) δ_C 166.0 (C=O), 162.3 (o-Ar), 136.3 (Ar), 131.5 (o-Ar), 128.6 (Ar), 128.1 (Ar), 127.4 (Ar), 123.5 (o-Ar), 114.3 (Ar), 71.4 (OCH), 70.0 (OCH$_2$), 36.0 (CH$_2$), 31.7 (CH$_2$), 29.1 (CH$_2$), 25.4 (CH$_2$), 22.5 (CH$_2$), 20.1 (Me), 14.0 (Me).

IR ν_{max} cm^{-1} 2929, 2957, 1708, 1604, 1582, 1508, 1455, 1420, 1379, 1354, 1311, 1271, 1248, 1165, 1101, 1079, 1025, 1010, 918, 846, 769, 733, 656, 633, 617.

4-((Octan-2-yloxy)carbonyl)phenyl 4'-(undecyloxy)biphenyl-4-carboxylate (11)

4-(Dimethylamino) pyridine (0.10 g, 0.82 mmol) was added into a stirred mixture of compound **8** (0.50 g, 2.00 mmol), N-(3-dimethylaminopropyl)-N'-ethylcarbodiimide hydrochloride (0.43 g, 2.20 mmol) and compound **2** (0.74 g, 2.00 mmol) in dry CH$_2$Cl$_2$ (30mL). The resulting mixture was stirred at room temperature for 12 hours. The solvent was reduced under pressure to give the crude product. Purification by flash column chromatography with (CH$_2$Cl$_2$:Hexane 10:1 over silica) gave ester **11** (0.73 g, 61%) as a white solid.

^{1}H NMR (400MHz CDCl$_3$) δ_H 8.24 (2H, d, J = 8.4 Hz, Ar), 8.11 (2H, d, J = 8.7 Hz, Ar), 7.70 (2H, d, J = 8.4 Hz, Ar), 7.60 (2H, d, J = 8.7 Hz, Ar), 7.31 (2H, d, J = 8.7 Hz, Ar), 7.01 (2H, d, J = 8.7 Hz, Ar), 5.23-5.11(1H, m, CH), 3.97 (2H, t, J = 6.6 Hz, CH$_2$O), 1.87-1.20 (31H, m, CH$_2$ $\times$ 14, CH$_3$), 0.88 (6H, t, J = 7.0 Hz, CH$_3$ $\times$ 2).

^{13}C NMR (100MHz, CDCl$_3$) (two CH$_2$ signal not resolved) δ$_C$ 165.5 (C=O), 164.7 (*o*-Ar or C=O), 159.7 (*o*-Ar or C=O), 154.5 (*o*-Ar or C=O), 146.3 (*o*-Ar or C=O), 131.8 (*o*-Ar), 131.1 (Ar), 130.8 (Ar), 128.5 (*o*-Ar), 128.4 (Ar), 127.0 (*o*-Ar), 126.6 (Ar), 121.7 (Ar), 115.0 (Ar), 71.9 (OCH), 68.2 (OCH$_2$), 36.0 (CH$_2$), 31.9 (CH$_2$), 31.7 (CH$_2$), 29.6 (CH$_2$), 29.4 (CH$_2$), 29.3 (CH$_2$), 29.2 (CH$_2$), 29.1 (CH$_2$), 26.0 (CH$_2$), 25.4 (CH$_2$), 22.7 (CH$_2$), 22.6 (CH$_2$), 20.1 (Me), 14.1 (Me), 14.0 (Me).

IR v_{max} cm^{-1} 2957, 2918, 2850, 1735, 1717, 1601, 1580, 1530, 1504, 1467, 1400, 1280, 1262, 1213, 1111, 1075, 1014, 1030, 1000, 923, 858, 733, 720, 645, 495.

HR-MS (ESI) (*m/z*) - Calculated: 623.3700 [M+Na]$^+$; Found: 623.3707[M+Na]$^+$.

Assay (HPLC 100% CH$_3$CN, 250 nm): >99.5 %.

4-((1-methylheptyloxy)carbonyl)phenyl 4'-(decyloxy)-[1,1'-biphenyl]-4-carboxylate (12a)

Compound **12** prepared *via* the same methodology as compound **11**. Quantities used: 4-(dimethylamino)pydridine (500 mg, 4.09 mmol), compound **8** (2.56 g, 10.23 mmol), *N*-(3-dimethylaminopropyl)-*N*'-ethylcarbodiimide hydrochloride (1.75 g, 11.25 mmol) and compound **4** (3.65 g, 10.23 mmol) to give white powder. Yield = 4.42 g (72%).

^{1}H NMR (400MHz CDCl$_3$) δ$_H$ 8.24 (2H, d, *J* = 8.0 Hz, Ar), 8.13 (2H, d, *J* = 8.0 Hz, Ar), 7.70 (2H, d, *J* = 8.0 Hz, Ar), 7.60 (2H, d, *J* = 8.0 Hz, Ar), 7.31 (2H, d, *J* = 8.0 Hz, Ar), 7.01 (2H, d, *J* = 8.0 Hz, Ar), 5.20-5.12(1H, m, CH), 4.02 (2H, t, *J* = 7.0 Hz, CH$_2$O), 1.85-1.29 (29H, m, CH$_2$ × 13, CH$_3$), 0.89 (6H, t, *J* = 7.0 Hz, CH$_3$ × 2).

^{13}C NMR (100MHz, CDCl$_3$) (one CH$_2$ signal not resolved) δ$_C$ 165.5 (C=O), 164.6 (*o*-Ar or C=O), 159.6 (*o*-Ar or C=O), 154.5 (*o*-Ar or C=O), 146.2 (*o*-Ar or C=O), 131.8 (*o*-Ar), 131.1 (Ar), 130.8 (Ar), 128.5 (*o*-Ar), 128.4 (Ar), 127.0 (*o*-Ar), 126.6 (Ar), 121.7 (Ar), 115.0 (Ar), 71.9 (OCH), 68.1 (OCH$_2$), 36.0 (CH$_2$), 31.9 (CH$_2$), 31.7 (CH$_2$), 29.6 (CH$_2$), 29.5 (CH$_2$), 29.4 (CH$_2$), 29.3 (CH$_2$), 29.2 (CH$_2$), 29.1 (CH$_2$), 26.0 (CH$_2$), 25.4 (CH$_2$), 22.7 (CH$_2$), 22.6 (CH$_2$), 20.1 (Me), 14.1 (Me), 14.0 (Me).

IR v_{max} cm^{-1} 2957, 2918, 2850, 1735, 1716, 1735, 1601, 1582, 1530, 1504, 1467, 1411, 1280, 1213, 1111, 1014, 1030, 1000, 924, 858, 733, 688cb, 645, 495.

Assay (HPLC 100% CH$_3$CN, 250 nm): >99.5 %.

HR-MS (ESI) (*m/z*) - Calculated: 587.3723 [M]$^+$; Found: 587.3731[M]$^+$.

Cpd. 12	Cpd. 8	Cpd. 4	4-(dimethyl-amino)pydridine	*N*-(3-dimethylamino propyl)-*N'*-ethylcar-bodiimide hydrochloride	Yield / g (%)
12b	2.56 g, 10.23 mmol	1.75 g, 11.25 mmol	0.10 g, 0.82 mmol	1.75 g, 11.25 mmol	4.13g (67%)
12c	2.56 g, 10.23 mmol	1.75 g, 11.25 mmol	0.10 g, 0.82 mmol	1.75 g, 11.25 mmol	3.76g (61%)
12d	2.56 g, 10.23 mmol	1.75 g, 11.25 mmol	0.10 g, 0.82 mmol	1.75 g, 11.25 mmol	4.47g (73%)
12e	2.56 g, 10.23 mmol	1.75 g, 11.25 mmol)	0.10 g, 0.82 mmol	1.75 g, 11.25 mmol	4.56g (74%)
12f	2.56 g, 10.23 mmol	1.75 g, 11.25 mmol	0.10 g, 0.82 mmol	1.75 g, 11.25 mmol	4.03g (66%)

Table 6.1 Quantity of used for preparing compound **12b**-**12f**

6.2 Photomicrographs Obtained from TN Device Studies

The sections that follow contain further examples of the photomicrographs of mixtures of the chiral dopants, detailed in Chapter 4, in the nematic hosts (BL036, PCH7 and ZLI559) were filled into TN devices. Each section details the chemical structure of the dopant and the corresponding photomicrographs obtained for mixtures of this dopant.

6.2.1   AE8 in BL036, PCH7 and ZLI559

AE8

(a)   (b)   (c)

(d)
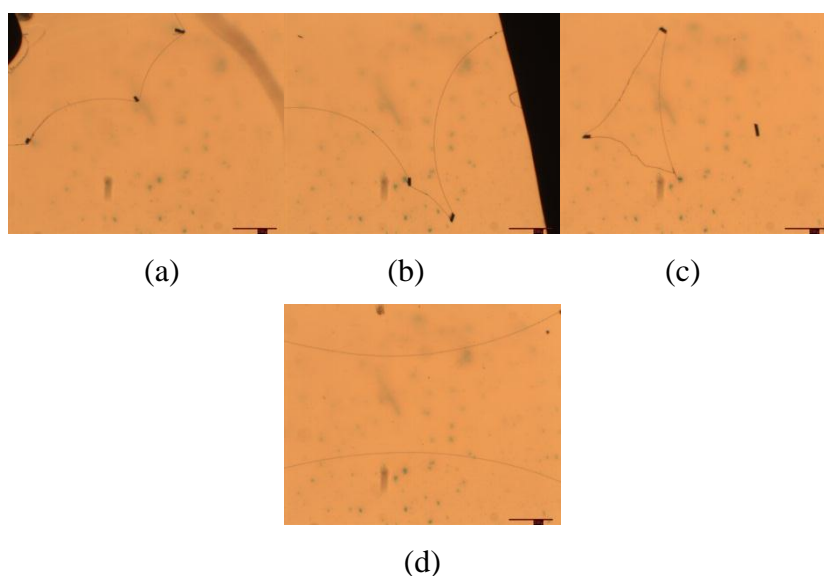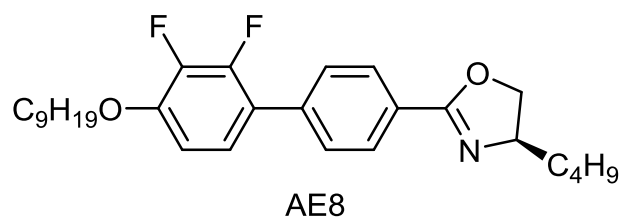
Figure 6.1: Photomicrographs (x50) showing the reverse-twist disclination lines of the mixtures of AE8 in BL036 formed in 14.4 μm thickness TN cells at a concentration of of (a) 0.02205 wt%;(b) 0.01639 wt%;(c) 0.01095 wt% and (d) 0.005408 wt%.

(a)   (b)   (c)

(d)   (e)
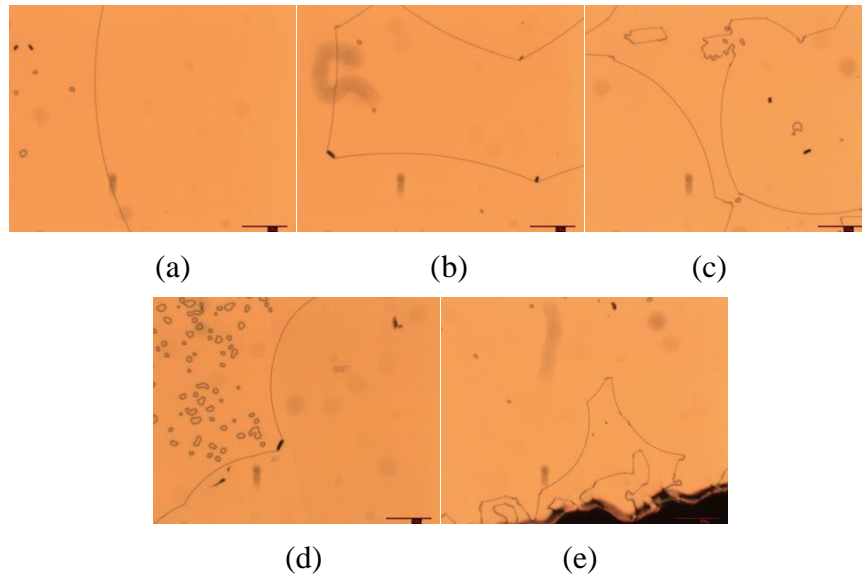
Figure 6.2: Photomicrographs (x50) showing the reverse-twist disclination lines of the mixtures of AE8 in PCH7 formed in 14.4 μm thickness TN cells at a concentration of (a) 0.008378wt%;(d) 0.01100wt%;(g) 0.02188wt%;(j) 0.03252 wt% and (m) 0.04364wt%.

(a)   (b)   (c)

(d   (e)
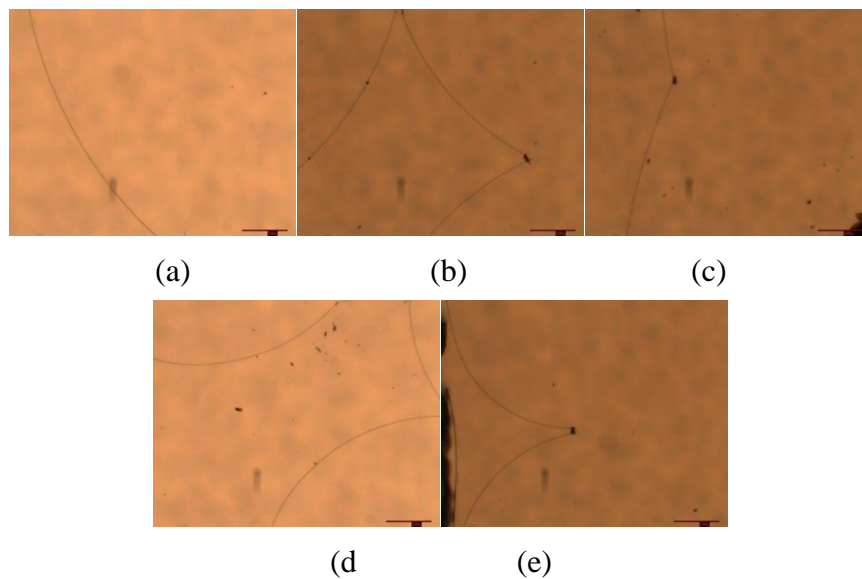
Figure 6.3: Photomicrographs (x50) showing the reverse-twist disclination lines of the mixtures of AE8 in ZLI559 formed in 14.4 μm thickness TN cells at a concentration of (a) 0.006604wt%;(d) 0.008700wt%;(g) 0.01305wt%;(j) 0.01761wt% and (l) 0.01901 wt%.

6.2.2   AE14   in BL036, PCH7 and ZLI559

AE 14

(a)   (b)   (c)

(d)   (e)

Figure 6.4: Photomicrographs (x50) showing the reverse-twist disclination lines of the mixtures of AE14 in BL036 formed in 14.4 μm thickness TN cells at a concentration of (a) 0.01028 wt% ;(b) 0.02062 wt% ;(c) 0.03127 wt% (d) 0.04186 wt% and (e) 0.006209 wt%.

(a)   (b)   (c)

(d)   (e)

Figure 6.5: Photomicrographs (x50) showing the reverse-twist disclination lines of the mixtures of AE14 in PCH7 formed in 14.4 μm thickness TN cells at a concentration of (a) 0.03103wt%;(b) 0.04129wt%;(c) 0.05160wt%;(d) 0.06254 wt% and (e) 0.07309wt%.

(a)   (b)   (c)

(d)   (e)

Figure 6.6: Photomicrographs (x50) showing the reverse-twist disclination lines of the mixtures of AE14 in ZLI559 formed in 14.4 μm thickness TN cells at a concentration of (a) 0.01036 wt%;(b) 0.02085 wt%;(c) 0.03089 wt%;(d) 0.04152 wt% and (e) 0.05192 wt%.

6.2.3 AGML74 in BL036, PCH7 and ZLI559

AGML 74

(a) (b) (c)

(d) (e)

Figure 6.7: Photomicrographs (x50) showing the reverse-twist disclination lines of the mixtures of AGML74 in BL036 formed in 14.4 μm thickness TN cells at a concentration of (a) 0.02087 wt%;(b) 0.04096 wt%;(c) 0.06121 wt%;(d) 0.08112 wt% and (e) 0.1295 wt%.
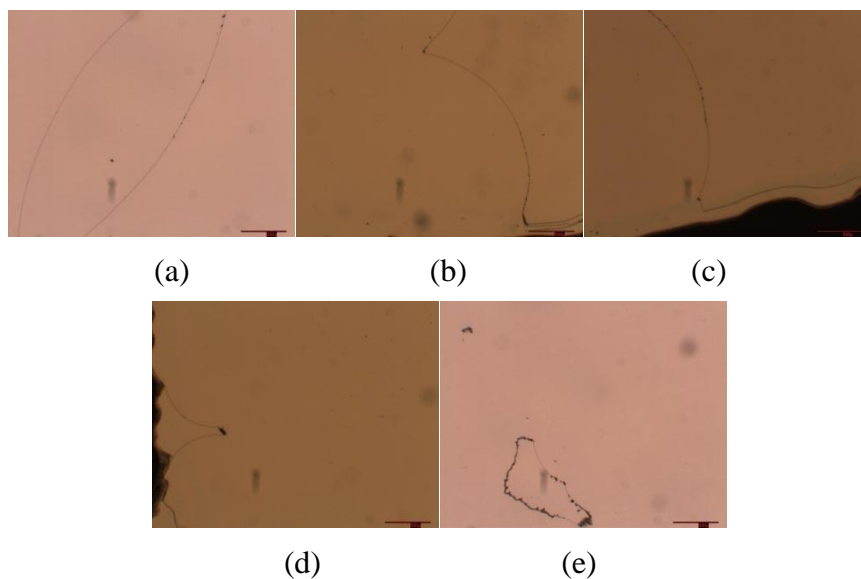

(a) (b) (c)

Figure 6.8: Photomicrographs (x50) showing the reverse-twist disclination lines of the mixtures of AGML74 in PCH7 formed in 14.4 μm thickness TN cells at a concentration of (a) 0.05298wt%;(b) 0.07310wt%;(c) 0.09451wt%.
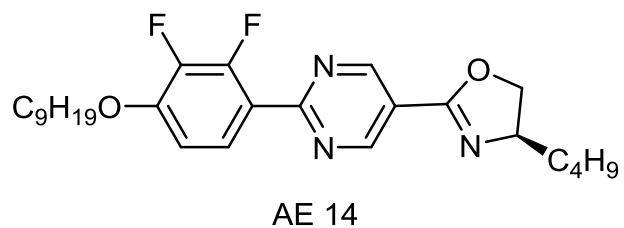
(a)　　　　　　　　(b)　　　　　　　　(c)

(d)　　　　　　　　(e)

Figure 6.9: Photomicrographs (x50) showing the reverse-twist disclination lines of the mixtures of AGML74 in ZLI559 formed in 14.4 μm thickness TN cells at a concentration of (a) 0.04258 wt%;(b) 0.08363 wt%;(c) 0.1283 wt% (d) 0.1718 wt% and (e) 0.2058 wt%.

6.2.4 R1011 in BL036, PCH7 and ZLI559

R1011

(a)　　　　　　　(b)　　　　　　　(c)

(d)　　　　　　　(e)
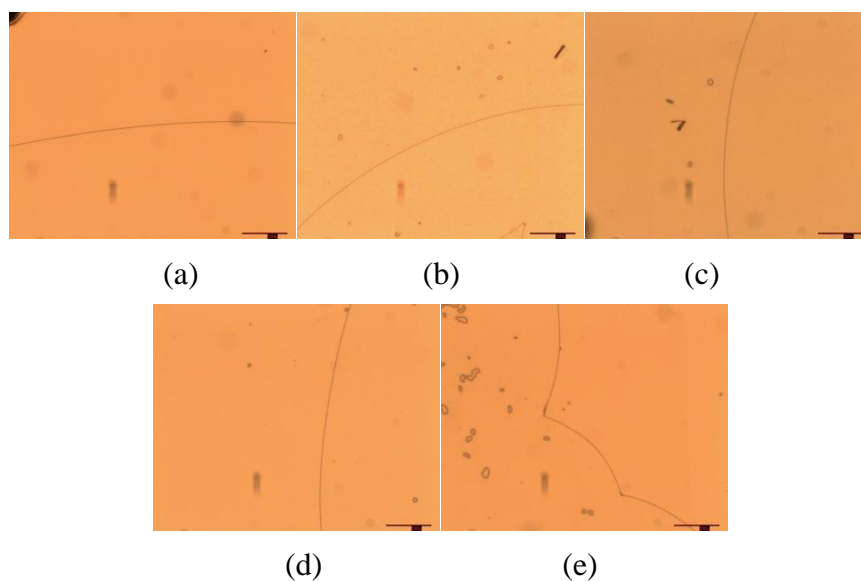
Figure 6.10: Photomicrographs (x50) showing the reverse-twist disclination lines of the mixtures of R1011 in BL036 formed in 14.4 μm thickness TN cells at a concentration of (a) 0.0003312 wt%;(b) 0.0008976 wt%;(c) 0.001225 wt%;(d) 0.001555 wt% and (e) 0.001780 wt%.

Figure 6.11: Photomicrographs (x50) showing the reverse-twist disclination lines of the mixtures of R1011 in PCH7 formed in 14.4 μm thickness TN cells at a concentration of (a) 0.001186 wt%;(b) 0.001769 wt%;(c) 0.002367 wt%;(d) 0.002943 wt% and (e) 0.003544 wt%.

Figure 6.12: Photomicrographs (x50) showing the reverse-twist disclination lines of the mixtures of R1011 in ZLI559 formed in 14.4 μm thickness TN cells at a concentration of (a) 0.0005685 wt%;(b) 0.001116 wt%;(c) 0.001333 wt% (d) 0.001567 wt% and (e) 0.001773 wt%.

6.2.5   S1011   in BL036, PCH7 and ZLI559

R1011

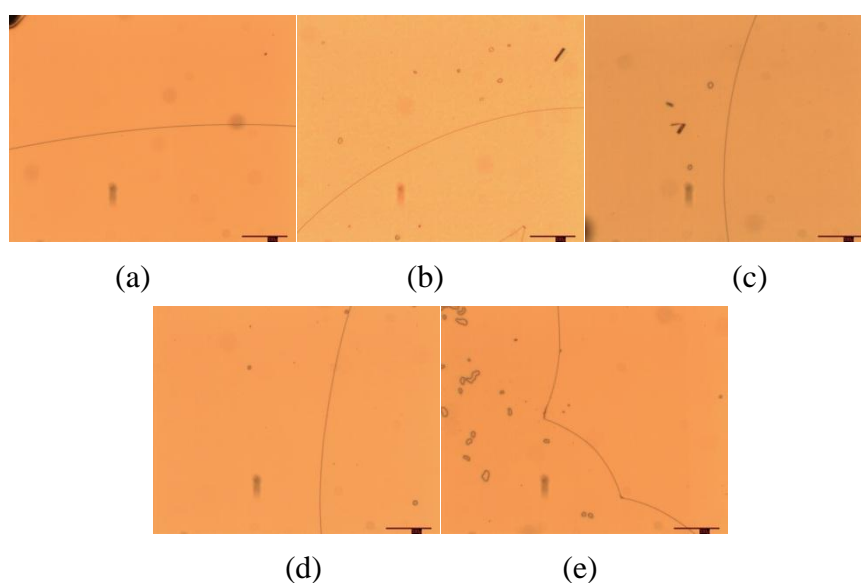(a)   (b)   (c)

(d)   (e)
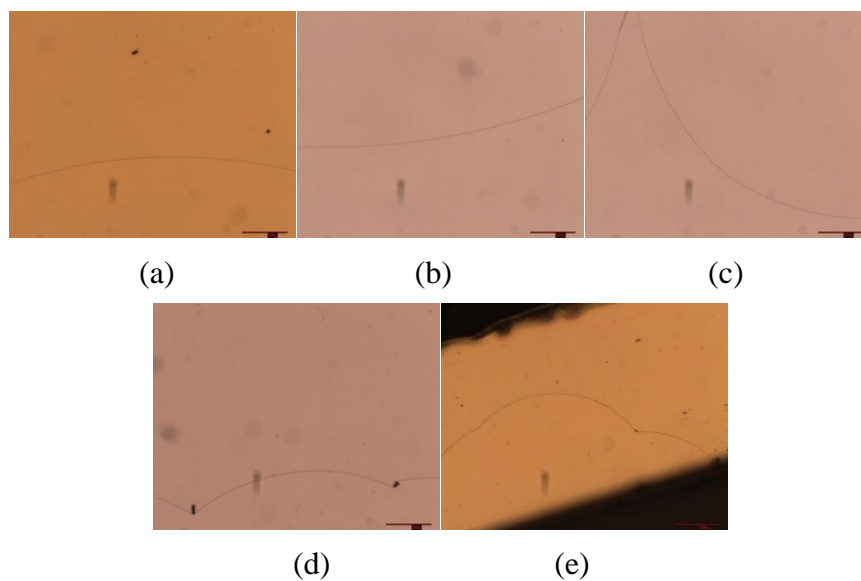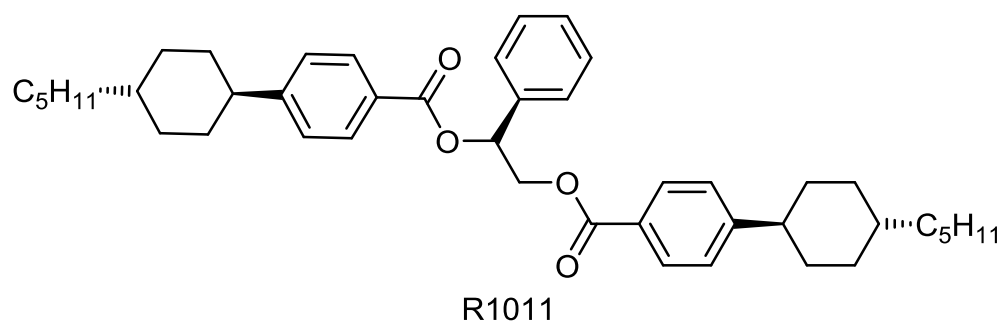
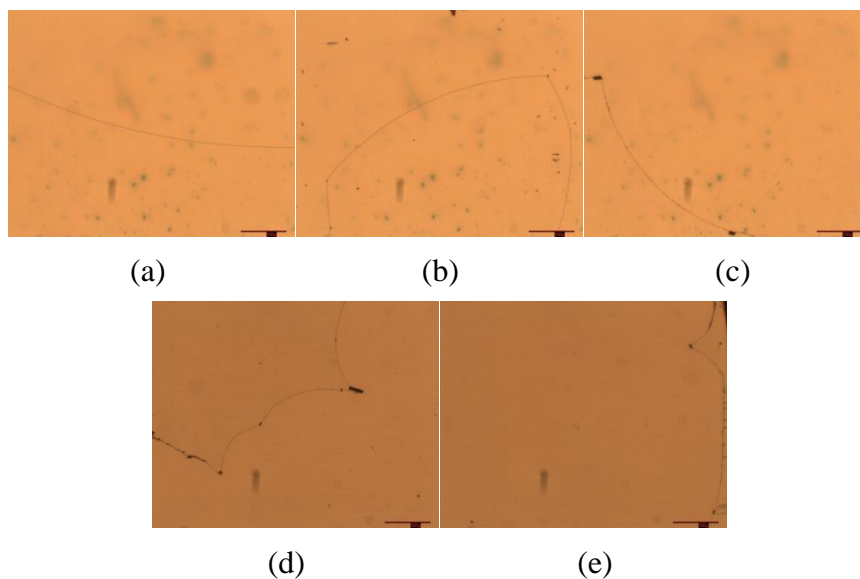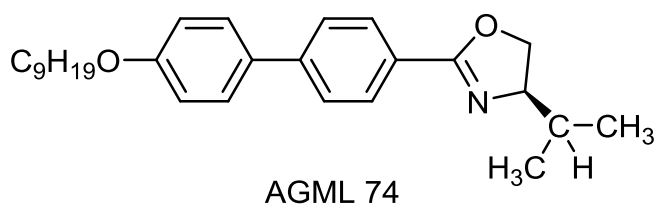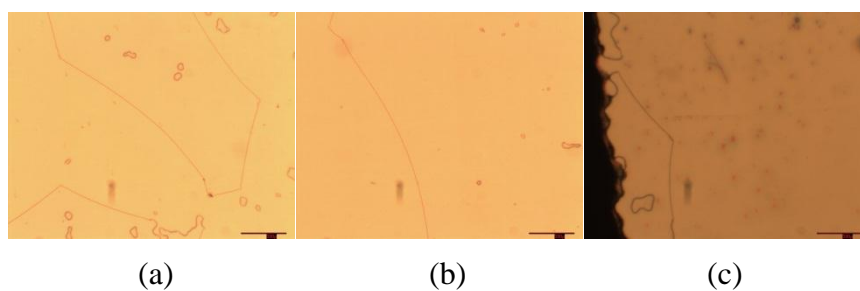**Figure 6.13**: Photomicrographs (x50) showing the reverse-twist disclination lines of the mixtures of S1011 in BL036 formed in 14.4 μm thickness TN cells at a concentration of (a) 0.0005602 wt%;(b) 0.001065 wt%;(c) 0.001603 wt%;(d) 0.002110 wt% and (e)   0.002269 wt%.

(a)   (b)   (c)

(d)
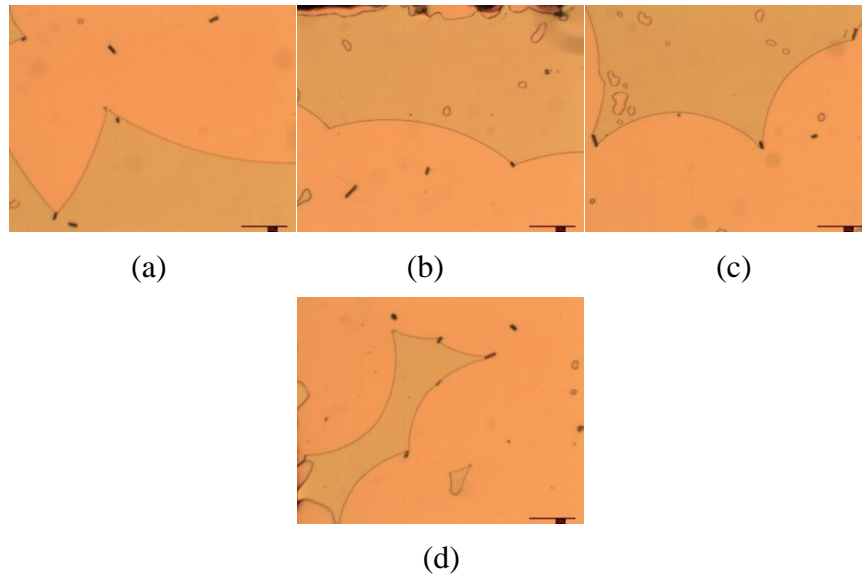
Figure 6.14: Photomicrographs (x50) showing the reverse-twist disclination lines of the mixtures of S1011 in PCH7 formed in 14.4 μm thickness TN cells at a concentration of (a) 0.001143 wt%;(b) 0.001711 wt%;(c) 0.02293 wt%;(d) 0.002862 wt%.

(a)   (b)   (c)

(d)   (e)
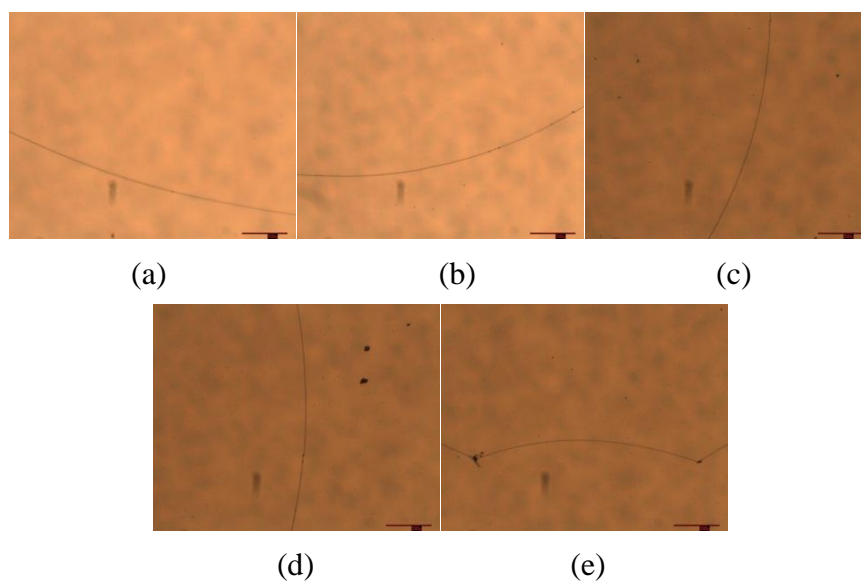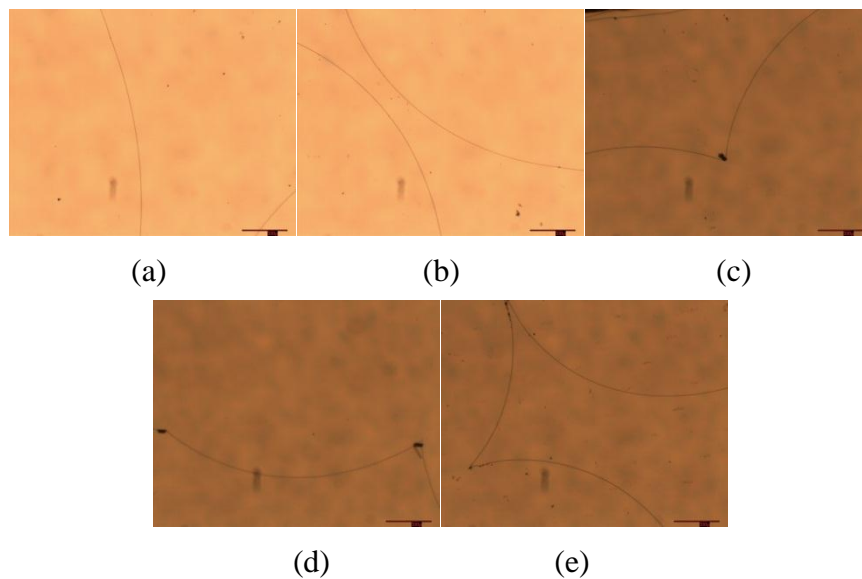
Figure 6.15: Photomicrographs (x50) showing the reverse-twist disclination lines of the mixtures of S1011 in ZLI559 formed in 14.4 μm thickness TN cells at a concentration of (a) 0.0008484 wt%;(b) 0.001371 wt%;(c) 0.001586 wt% (d) 0.001807 wt% and (e) 0.002004 wt%.

6.2.6   (*R*)-(+)-Thalidomide in BL036, PCH7 and ZLI559

(*R*)–(+)-Thalidomide

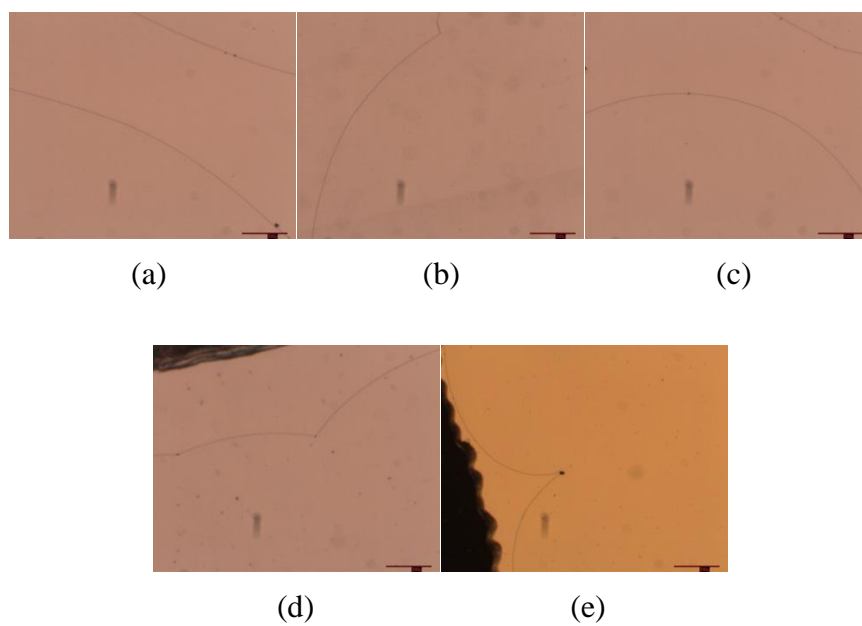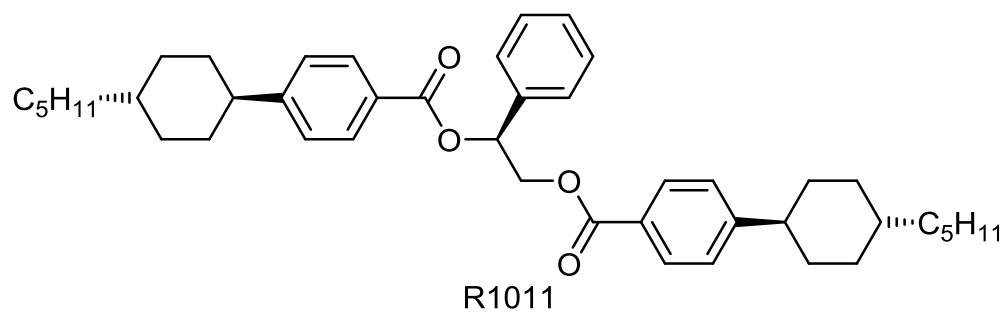(a)   (b)   (c)

(d)   (e)

Figure 6.16 Photomicrographs (x50) showing the reverse-twist disclination lines of the mixtures of (*R*)-(+)-Thalidomide in BL036 formed in 14.4 μm thickness TN cells at a concentration of (a) 0.04258 wt%;(b) 0.08363 wt%;(c) 0.1283 wt% (d)   0.1718 wt% and (e) 0.2058 wt%.

(a)   (b)   (c)

(d   (e)
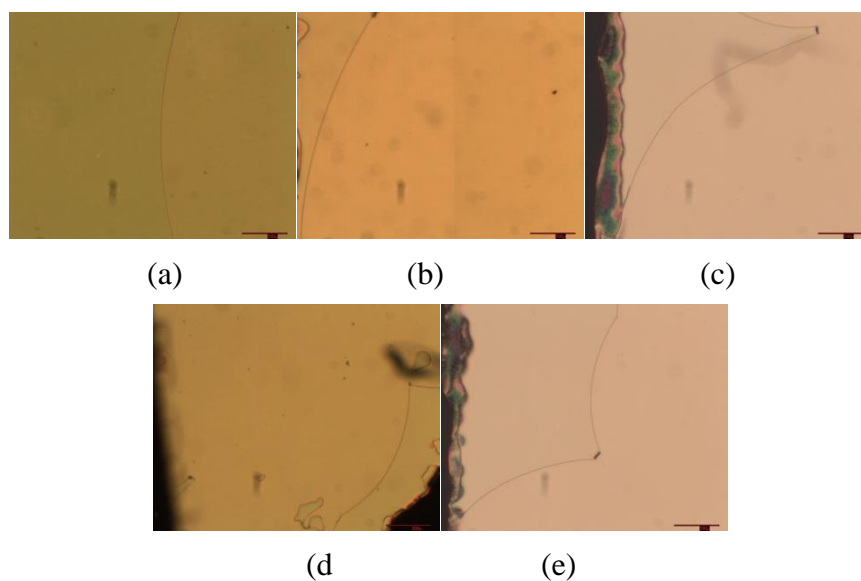
Figure 6.17: Photomicrographs (x50) showing the reverse-twist disclination lines of the mixtures of (*R*)-(+)-Thalidomide in PCH7 formed in 14.4 μm thickness TN cells at a concentration of (a) 0.001418 wt%;(d) 0.001931 wt%;(g) 0.002408 wt% (j)-(l) 0.002889 wt% and (m) 0.003285 wt%.

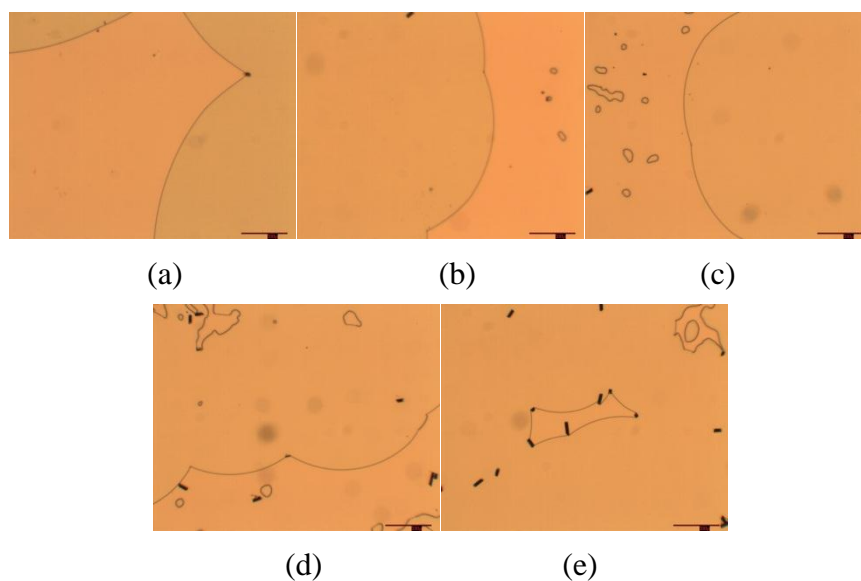(a)   (b)   (c)

(d)   (e)
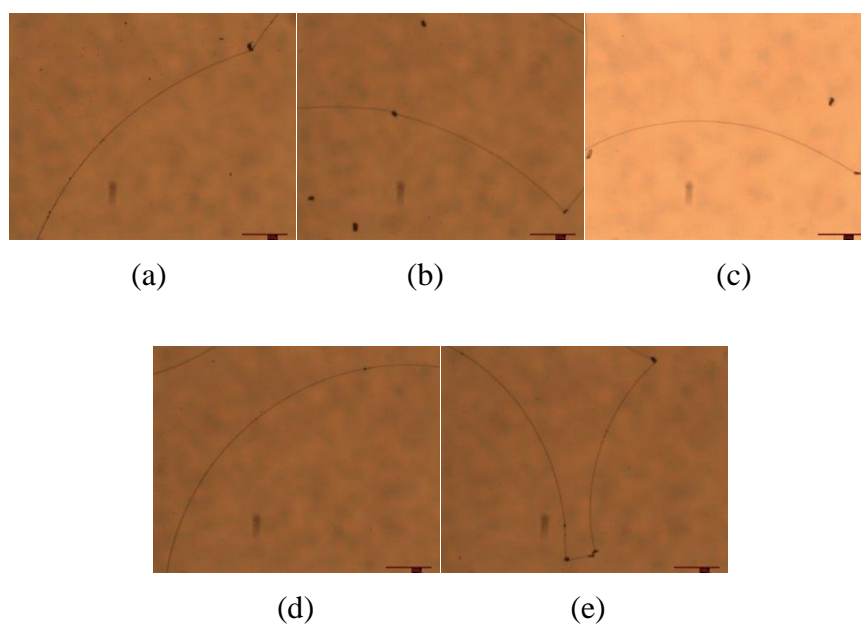
Figure 6.18: Photomicrographs (x50) showing the reverse-twist disclination lines of the mixtures of (*R*)-(+)-Thalidomide in ZLI559 formed in 14.4 μm thickness TN cells at a concentration of (a) 0.001922 wt%;(d) 0.002128 wt%;(g) 0.002419 wt%;(j) 0.002427 wt% and (m) 0.002838 wt%.

6.2.7 (*S*)-(-)-Thalidomide in BL036, PCH7 and ZLI559

(*S*)–(+)-Thalidomide

(a)   (b)   (c)

(d)   (e)

Figure 6.19: Photomicrographs (x50) showing the reverse-twist disclination lines of the mixtures of (*S*)-(‾)-Thalidomide in BL036 formed in 14.4 μm thickness TN cells at a concentration of (a) 0.04258 wt%;(b) 0.08363 wt%;(c) 0.1283 wt%;(d) 0.1718 wt% and (e) 0.2058 wt%.
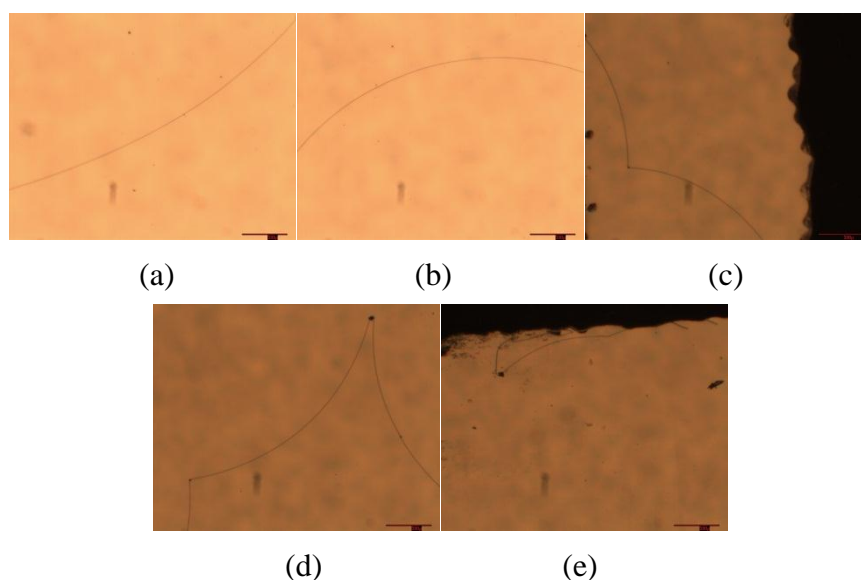
(a)　　　　　　　(b)　　　　　　　(c)

(d)　　　　　　　(e)
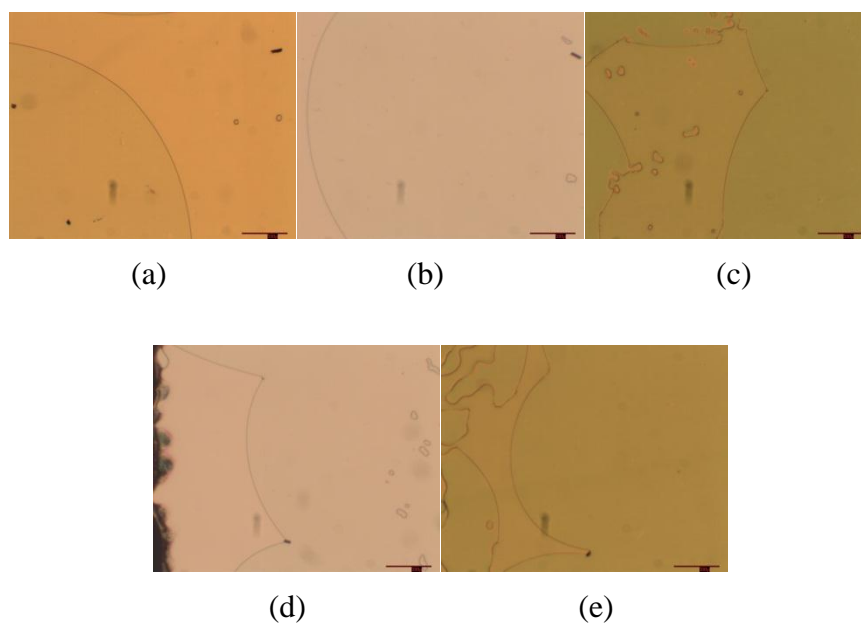
Figure 6.20: Photomicrographs (x50) showing the reverse-twist disclination lines of the mixtures of (*S*)-(⁻)-Thalidomide in PCH7 formed in 14.4 μm thickness TN cells at a concentration of (a) 0.001488wt%;(d) 0.001792 wt%;(g) 0.002107 wt%;(j) 0.002639 wt% and (m) 0.002987 wt%.

(a)　　　　　　　(b)　　　　　　　(c)

(d)　　　　　　　(e)

Figure 6.21: Photomicrographs (x50) showing the reverse-twist disclination lines of the mixtures of (*S*)-(⁻)-Thalidomide in ZLI559 formed in 14.4 μm thickness TN cells at a concentration of (a) 0.001785 wt%;(b) 0.002689 wt%;(c) 0.002955 wt%;(d) 0.003292 wt% and (e) 0.003652 wt%.

6.2.8   RAL1568 in BL036, PCH7 and BL036

RAL1568

(a)   (b)   (c)

(d) n   (e)

Figure 6.22: Photomicrographs (x50) showing the reverse-twist disclination lines of the mixtures of RAL1568 in BL036 formed in 14.4 μm thickness TN cells at a concentration of (a) 0.003257 wt%;(b) 0.004346 wt%;(c) 0.05457 wt%;(d) 0. 03131 wt% and (e) 0.04323 wt%.
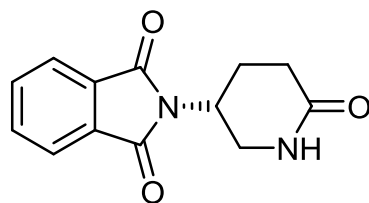
(a)   (b)   (c)

(d)

Figure 6.23: Photomicrographs (x50) showing the reverse-twist disclination lines of the mixtures of RAL1568 in PCH7 formed in 14.4 μm thickness TN cells at a concentration of (a) 0.005496 wt%;(b) 0.008206 wt%;(c) 0.01105 wt% and (d) 0.01370 wt%.
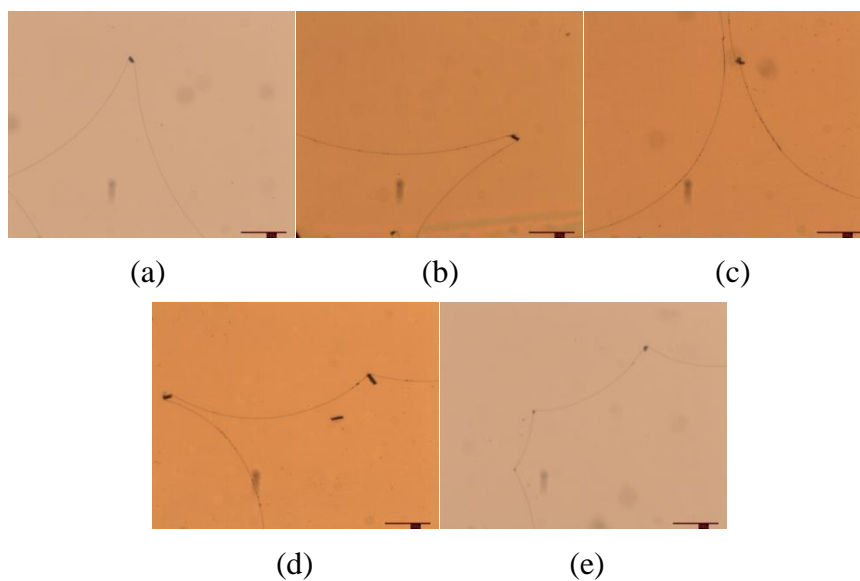

(a)   (b)   (c)

(d)   (e)
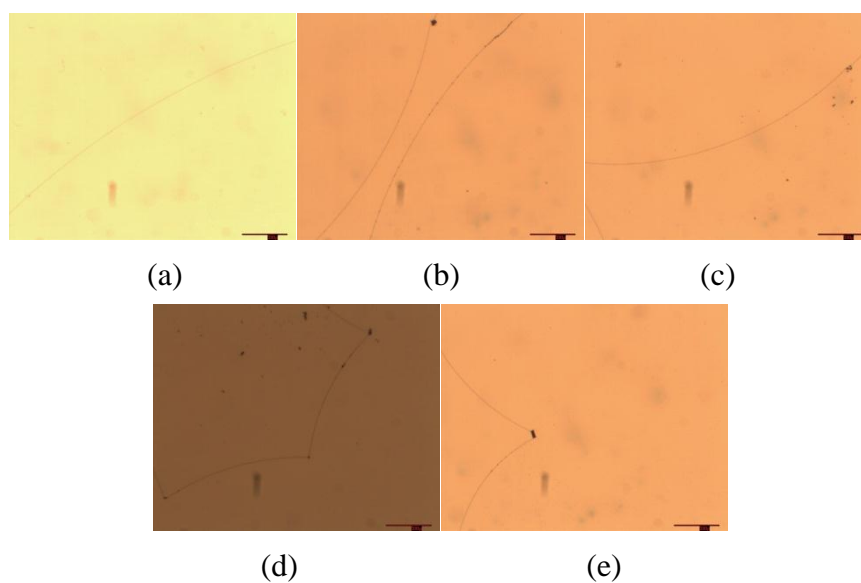
Figure 6.24: Photomicrographs (x50) showing the reverse-twist disclination lines of the mixtures of RAL1568 in ZLI559 formed in 14.4 μm thickness TN cells at a concentration of (a) 0.002744 wt%;(b) 0.005462 wt%;(c) 0.08237 wt%;(d) 0.01104 wt% and (e) 0.02161 wt%.

6.2.9 RAL1569 in BL036, PCH7 and BL036

RAL1569

(a)   (b)   (c)

(d)   (e)

Figure 6.25: Photomicrographs (x50) showing the reverse-twist disclination lines of the mixtures of RAL1569 in BL036 formed in 14.4 μm thickness TN cells at a concentration of (a) 0.003281 wt%;(b) 0.003946 wt%;(c) 0.007529 wt%;(d) 0.01191 wt% and (e) 0.01518 wt%.

Figure 6.26: Photomicrographs (x50) showing the reverse-twist disclination lines of the mixtures of RAL1569 in PCH7 formed in 14.4 μm thickness TN cells at a concentration of (a) 0.003944 wt%;(b) 0.007840 wt%;(c) 0.01191 wt%;(d) 0.01579 wt% and (e) 0.01982 wt%.
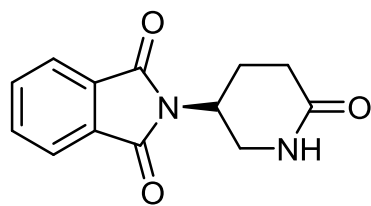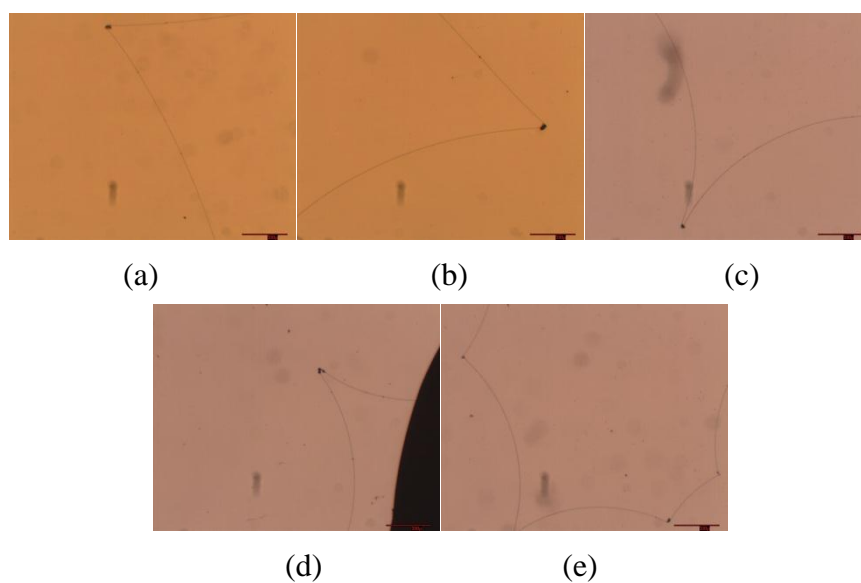

Figure 6.27: Photomicrographs (x50) showing the reverse-twist disclination lines of the mixtures of RAL1569 in ZLI559 formed in 14.4 μm thickness TN cells at a concentration of (a) 0.007590 wt%;(b) 0.01497 wt%;(c) 0.01967 wt%;(d) 0.02385 wt% and (e) 0.02767 wt%.

6.2.10   RAL1608 in BL036, PCH7 and BL036

RAL1608

(a)   (b)   (c)

(d)   (e)
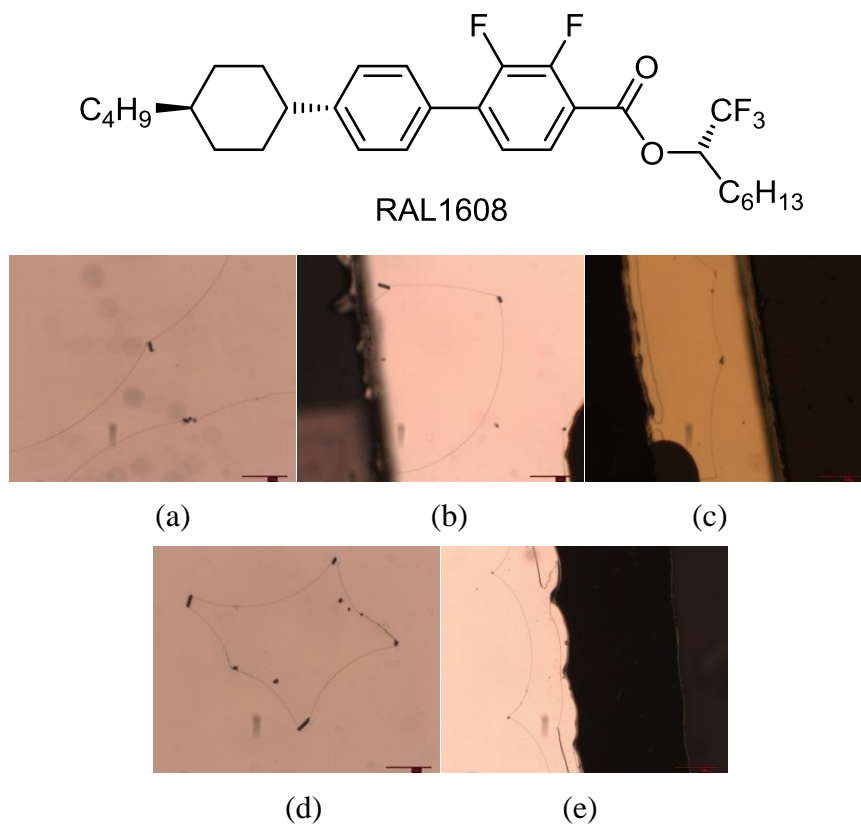
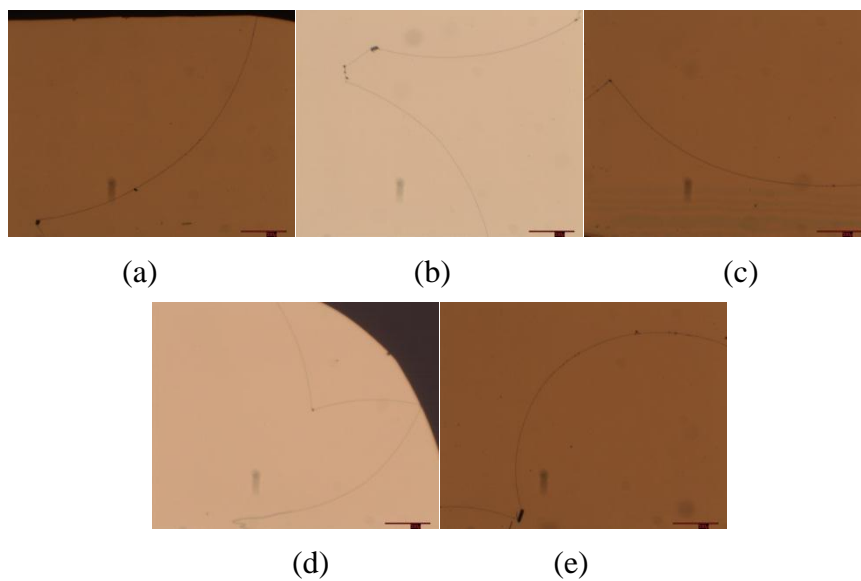**Figure 6.28**: Photomicrographs (x50) showing the reverse-twist disclination lines of the mixtures of RAL1608 in BL036 formed in 14.4 μm thickness TN cells at a concentration of (a) 0.003292 wt%;(b) 0.005234 wt%;(c) 0. 06788 wt%;(d) 0.07882 wt% and (e) 0.1039 wt% .

(a)   (b)   (c)
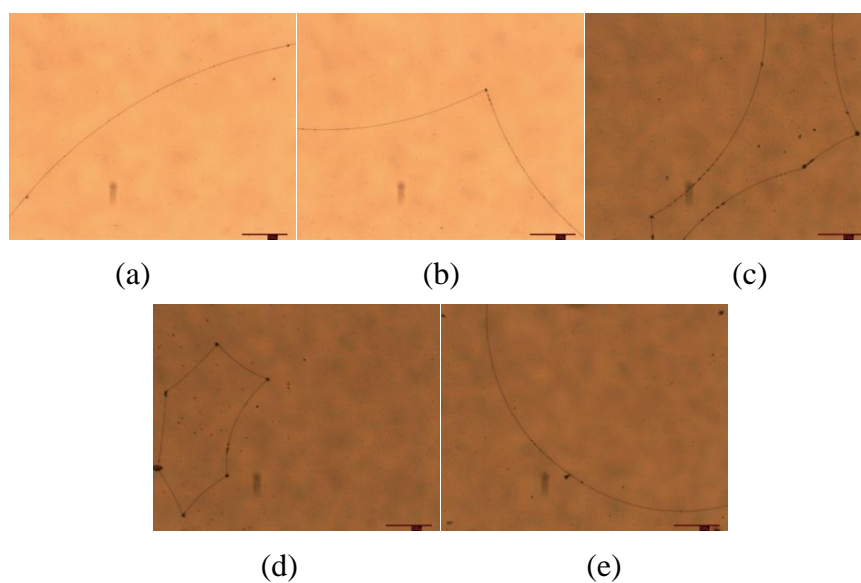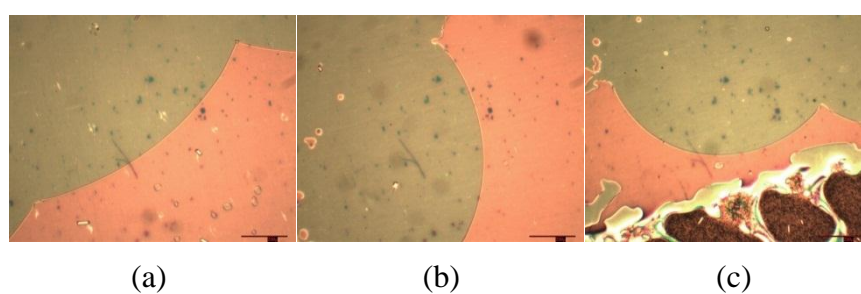
Figure 6.29: Photomicrographs (x50) showing the reverse-twist disclination lines of the mixtures of RAL1608 in PCH7 formed in 14.4 μm thickness TN cells at a concentration of (a) 0.003289 wt%;(b) 0.006519 wt% and (c) 0.009851 wt%.

(a)   (b)   (c)

(d)   (e)
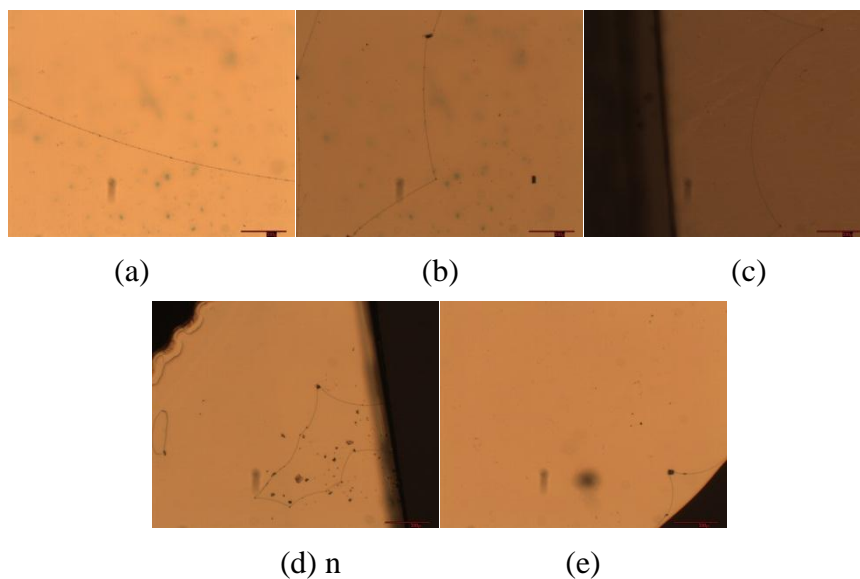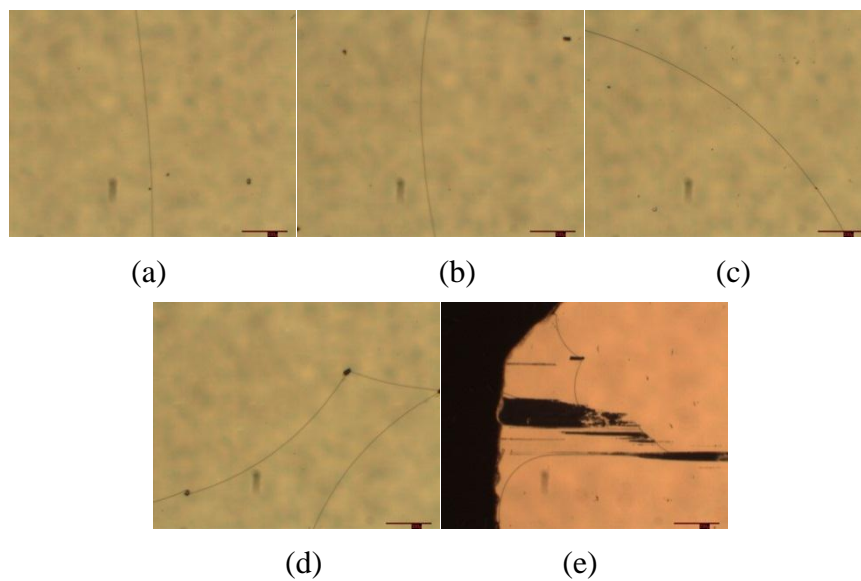
Figure 6.30: Photomicrographs (x50) showing the reverse-twist disclination lines of the mixtures of RAL1608 in ZLI559 formed in 14.4 μm thickness TN cells at a concentration of (a) 0.001072 wt%;(b) 0.001279 wt%;(c) 0.002571 wt%;(d) 0.003882 wt% and (e) 0.005188 wt%.

6.2.11 RAL1636 in BL036, PCH7 and BL036

RAL1636

(a)   (b)   (c)

(d)   (e)
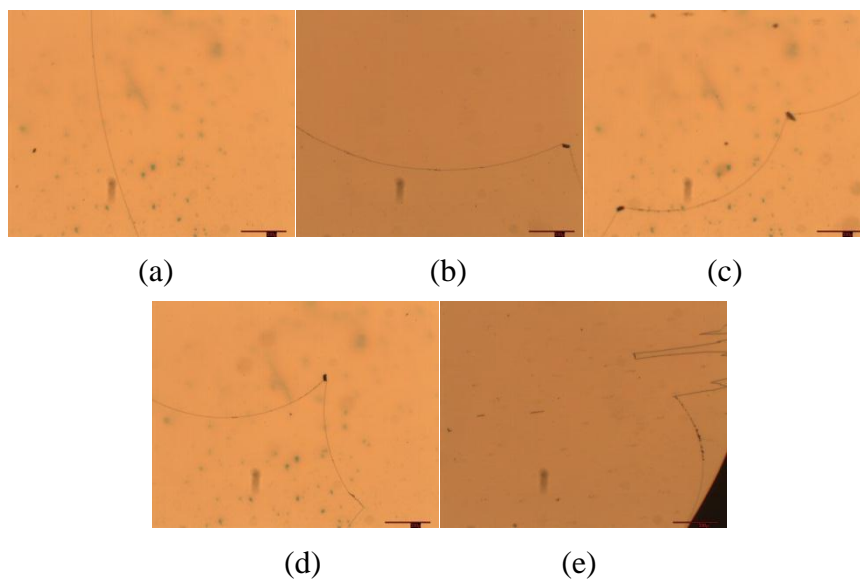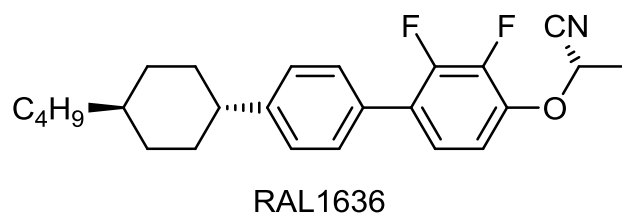
Figure 6.31: Photomicrographs (x50) showing the reverse-twist disclination lines of the mixtures of RAL1636 in BL036 formed in 14.4 μm thickness TN cells at a concentration of (a) 0.003930 wt%;(b) 0.007772 wt%;(c) 0.01190 wt%;(d) 0.01419 wt% and (e) 0.01961 wt%.

(a)   (b)   (c)

(d)
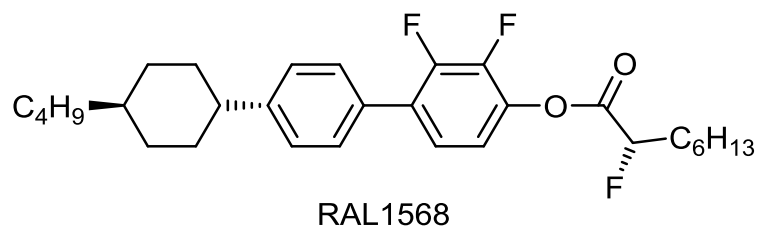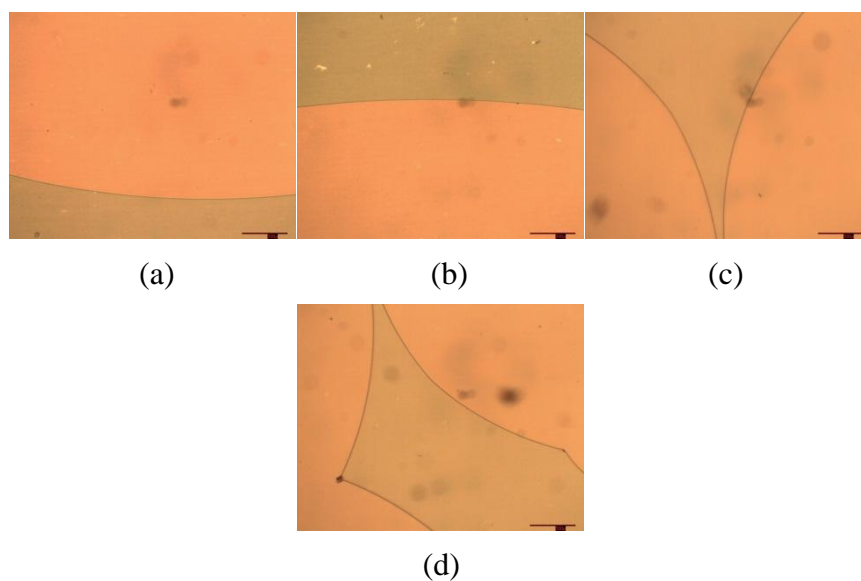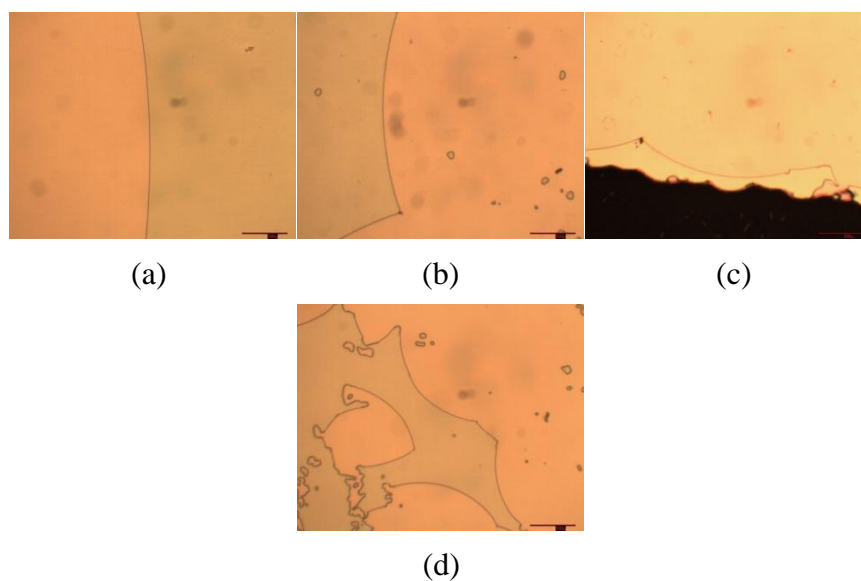
Figure 6.32: Photomicrographs (x50) showing the reverse-twist disclination lines of the mixtures of RAL1636 in PCH7 formed in 14.4 μm thickness TN cells at a concentration of (a) 0.003949 wt%;(b) 0.007975 wt%;(c) 0.01728 wt% and;(d) 0.01970 wt%.

(a)   (b)   (c)

(d)   (e)
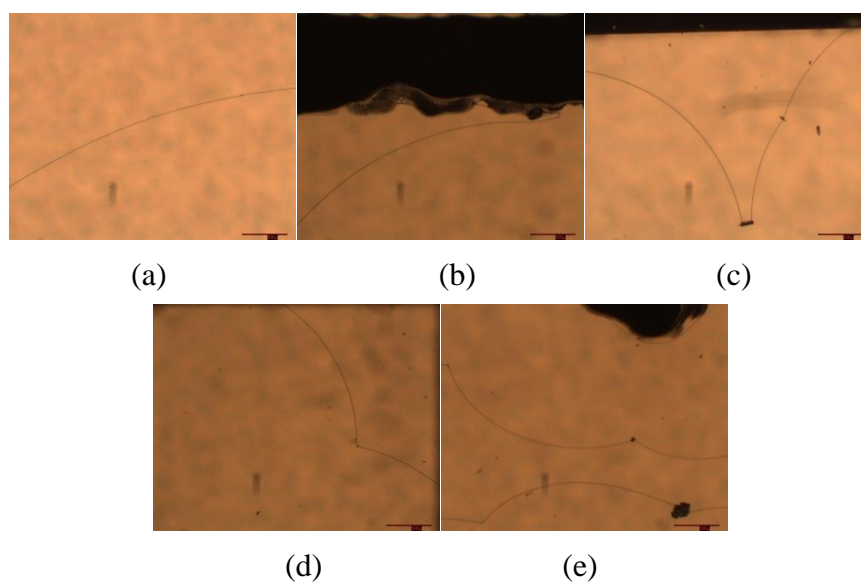
Figure 6.33: Photomicrographs (x50) showing the reverse-twist disclination lines of the mixtures of RAL1636 in ZLI559 formed in 14.4 μm thickness TN cells at a concentration of (a) 0.003972 wt%;(b) 0.007916 wt% (c) 0.01118 wt%;(d) 0.01358 wt% and (e) 0.01500 wt%.

6.2.12 CB15 in BL036, PCH7 and BL036
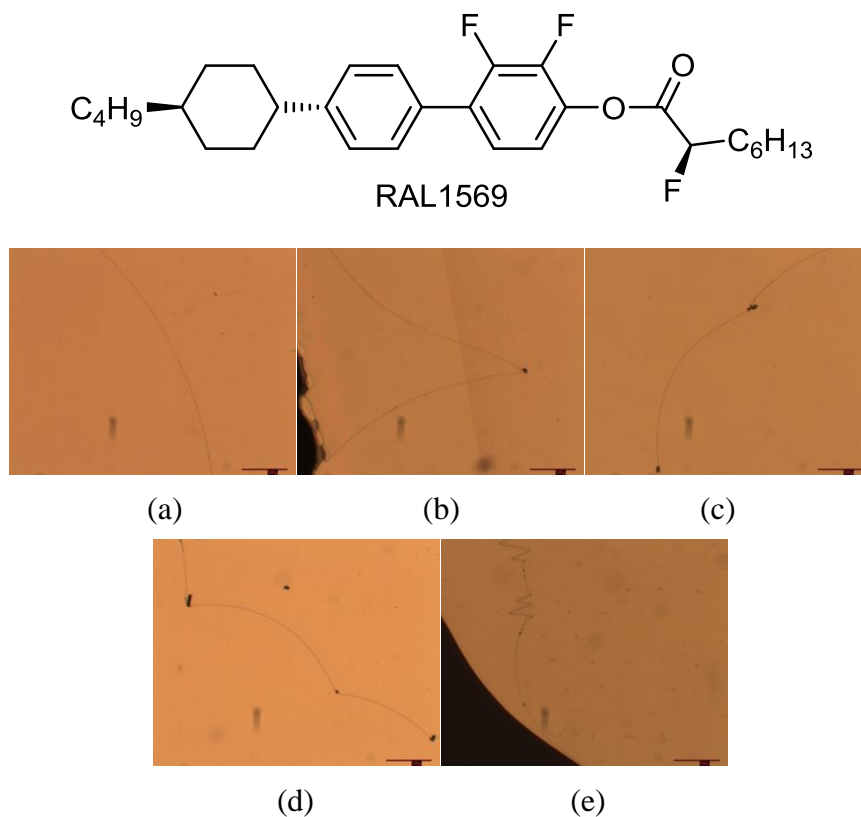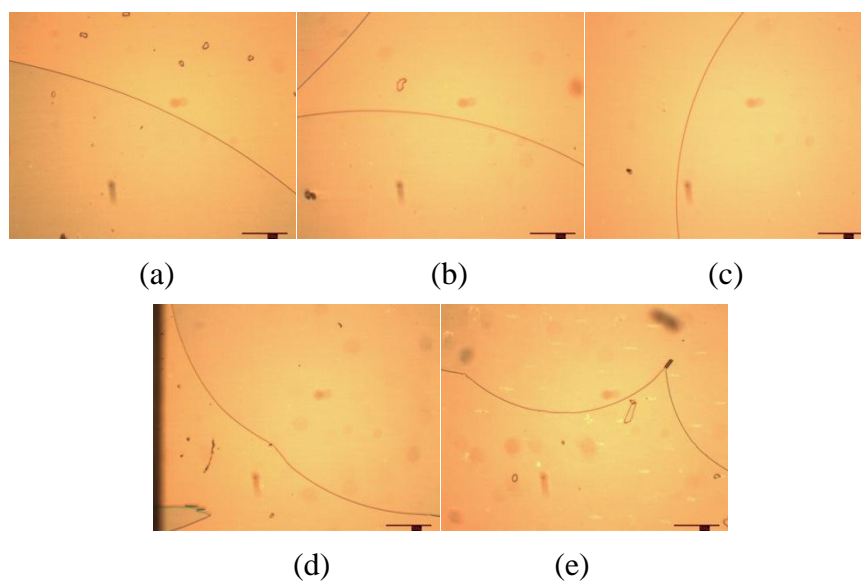

(a)   (b)   (c)

(d)   (e)
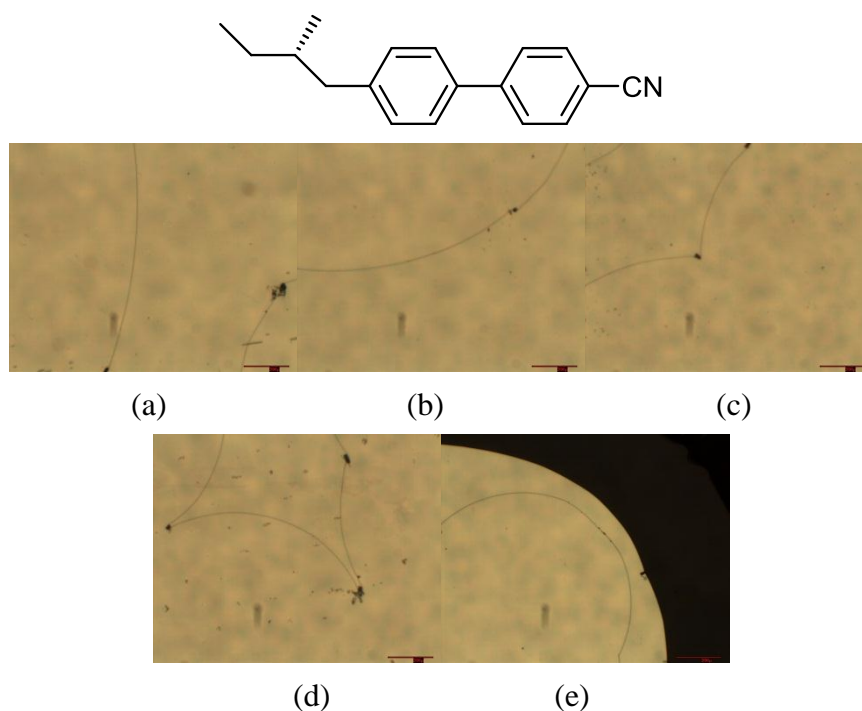
Figure 6.34: Photomicrographs (x50) showing the reverse-twist disclination lines of the mixtures of CB15 in BL036 formed in 14.4 μm thickness TN cells at a concentration of (a) 0.002464 wt%;(b) 0.004898 wt%;(c) 0.007383 wt%;(d) 0.009770 wt% and (e) 0.01231 wt%.

(a)   (b)   (c)

(d)   (e)
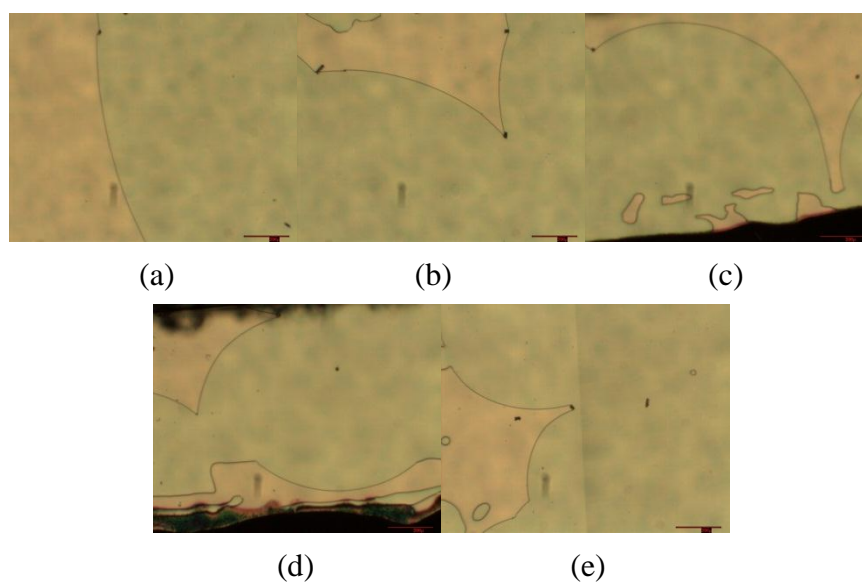
Figure 6.35: Photomicrographs (x50) showing the reverse-twist disclination lines of the mixtures of CB15 in PCH7 formed in 14.4 μm thickness TN cells at a concentration of (a) 0.002467 wt%;;(b) 0.004903 wt%;(c) 0.007325 wt%;(d) 0.009708wt% and (e) 0.01228 wt%.

(a)   (b)   (c)

(d)   (e)
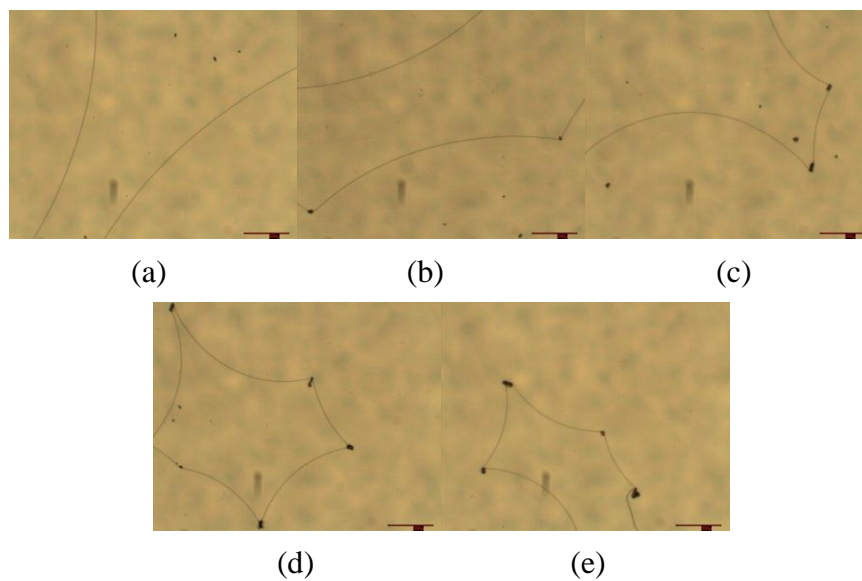
Figure 6.36: Photomicrographs (x50) showing the reverse-twist disclination lines of the mixtures of CB15 in PCH7 formed in 14.4 μm thickness TN cells at a concentration of (a) 0.002446 wt%;(b) 0.004927 wt%;(c) 0.007408 wt%;(d) 0.009827 wt% and (e) 0.01233 wt%.

# Chapter 7.   References

1. E. Davis and J.W. Goodby, in *"The Handbook of Liquid Crystals Volume 1: Fundamentals of Liquid Crystals"*, Eds. J.W. Goodby, P.J. Collings, T. Kato, C. Tschierske, H.F. Gleeson and P. Raynes, Wiley-VCH, Weinheim, 2014, pp 197-230.

2. M. Schadt, W. Helfrich. *Appl. Phys. Lett.*, 1971, **18**, 127-128.

3. R. Hasegawa in *"Alignment Technologies and Applications of Liquid Crystal Devices"*, Eds. G.W.Gray, J.W. Goodby and A. Fukuda, Taylor and Francis, Oxford, 2005, pp. 99-110.

4. E.P. Raynes. *Rev. de Phys. Appl.*, 1975, **10**, 117-120.

5. E.P. Raynes, *Liq. Cryst.*, 2006, **33**, 1215-1218.

6. J.W. Goodby, I.M. Saez, S.J. Cowling, V. Görtz, M. Draper, A.W. Hall, S. Sia, G. Cosquer, S.-E. Lee and E.P. Raynes, *Angew. Chem. Int. Ed.*, 2008, **47**, 2754-2787.

7. E.P. Raynes, S.J. Cowling and J.W. Goodby, *Anal. Methods,* 2009, **1**, 88-92.

8. E.L. Eliel, *Stereochemisty of Carbon Compounds*, 1962, McGraw-Hill, New York.

9. A.D. Buckingham, G.P. Ceasar and M.B. Dunn, *Chem. Phys. Lett.*, 1969, **3**, 540–541.

10. S. Pieraccini, S. Masiero, A. Ferrarini and G.P. Spada, *Chem. Soc. Rev.*, 2011, **40**, 258-271.

11. J. B. Biot, *Memoires de la classe des sciences mathematiques et physiques de I'Institut imperial de France*, 1812, **1**, 1-372.

12. A. Fresnel, *Imprimerie Imperiale (Paris)*, 1866, **1**, 731-767.

13. A. Fresnel, *Imprimerie Imperiale (Paris)*, 1866, **2**, 479-498.

14. L. Pasteur, *Ann. Chim. Phys.*, 1850, **28**, 56-99.

15. W.T. Kelvin, *J. Oxford Univ. Junior Sci. Club*, 1894, **18**, 3-57.

16. J.H. Van't Hoff, *Arch. Neerl. Sci. Exact. Nat.,* 1874, **9**, 445-454.

17. J.A. Le Bel, *Bull. Soc. Chim. Fr.*, 1874, **22**, 337-347.

18. H. Kolbe, *J. Prackt. Chem.*, 1877, **15**, 473-477.

19. M. Born, *Z. Physik*, 1915, **16**, 251-258.

20. C.W. Oseen, *Ann. Phys. (Berlin)*, 1915, **48**, 1-56.

21. F. Gray, *Phys. Rev.,* 1916, **7**, 472-488.

22. J. Applequist, *Acc. Chem. Rev.*, 1977, **10**, 79-85.

23. A. Cotton, *C.r. hebd. Seanc. Acad. Sci. (Paris)*, 1895, **120**, 989-991.

24. G. Snatzke in*"Circular Dichroism: Principles and Applications, 2nd Edition"*, Eds. N. Berova, K. Nakanishi and R.W. Woody, Wiley-VCH, Weinheim, 2000, pp 1-28.

25. R.S. Cahn and C.K. Ingold, *J. Chem. Soc.*, 1951, **1**, 612-622.

26. R.S. Cahn, C.K. Ingold, and V. Prelog, *Experientia*, 1956, **12**, 81-94.

27. J.W. Goodby in *"The Handbook of Liquid Crystals Vol. 1: Fundamentals"*, Eds. D. Demus, J.W. Goodby, G.W. Gray, H.-W. Spiess and V. Vill, Wiley-VCH, Weinhein, 1998, pp 115-132.

28. J.W. Goodby, *Lecture Notes on Stereochemistry*, University of Hull.

29. P. Hubera, S. Bratovanova, S. Bienza, C. Syldatkb and M. Pietzschb, *Tetrahedron: Asymmetry*, 1996, **7**, 69-78.

30. J. McMurray, *"Organic Chemistry with Biological Applications"*, CENGAGE Learning Custom Publishing, Stamford, 2014.

31. J.W. Goodby, *Proc. R. Soc. A*, 2012, **468**, 1521-1542.

32. M.D. McCreary, D.W. Lewis, D.L. Wernick and G.M. Whitesides, *J. Am. Chem. Soc.*, 1974, **96**, 1038-1054.

33. G.W. Gray and P.A. Winsor, *"Liquid Crystals and Plastic Crystals Vol. 1"*, Ellis Horwood, Chichester, 1974.

34. S. Singh, *"Liquid Crystals: Fundamentals"*, World Scientific, London, 2002.

35. E.B. Priestley in *"Introduction to Liquid Crystals"*, Eds. E.B. Priestley, P.J.

Wojtowicz and P. Sheng, Plenum Press, New York, 1976, pp 1-12.

36. P.J Collings and M. Hird, *"Introduction to Liquid Crystals",* Taylor and Francis, London, 1997.

37. D. Coates and G.W. Gray, *Phys. Lett. A*, 1973, **45**, 115-116.

38. P.G. de Gennes, *Solid State Commun.*, 1972, **10**, 753-756.

39. S.R. Renn and T.C. Lubensky, Phys. Rev. A, 1988, **38**, 2132-2147.

40. J.W. Goodby, M.A. Waugh, S.M. Stein, E. Chin, R. Pindak and J.S. Patel, *J. Am. Chem. Soc.,* 1989, **111**, 8119-8125.

41. J.W. Goodby, M.A. Waugh, S.M. Stein, E. Chin, R. Pindak and J.S. Patel, *Nature,* 1989, **337**, 449-452.

42. J.W. Goodby in *"Ferroelectric Liquid Crystals: Principles, Properties and Applications",* Gordon and Breach, Philadelphia, 1991, pp. 99-241.

43. M. A. Osipov and H.-G. Kuball, *Eur. Phys. J. E.*, 2001, **5**, 589-598.

44. R. Eelkma and B. L. Feringa, *J. Am. Chem. Soc.*, 2005, **127**, 13480-13481.

45. H. Taniguchi, M. Ozaki, K. Nakao and K. Yoshino, *Mol. Cryst. Liq. Cryst.*, 1989, **167**, 191-197.

46. J.W. Goodby, J.S. Patel and E. Chin, *J. Am. Chem. Soc.*, 1987, 91, 5151-5152.

47. J.W. Goodby in *"The Handbook of Visual Display Technology"*, Eds ,J. Chen, W. Cranton, and M. Fihn, Springer-Verlag, Berlin Heidelberg, 2012, pp 1290-1314.

48. M. J. Stephen and J. P. Straley, *Rev. Mod. Phys*, 1974, **46**, 617-704.

49. F. M. Lesley in "The Handbook of Liquid Crystals Vol. 1: Fundamentals", Eds. D. Demus, J.W. Goodby, G. W. Gray, H. –W. Spiess and V. Vill, Wiley-VCH, Weinhein, 1998, 25-39.

50. S.T. Largerwall, *Ferroelectrics,* 2004, **301**, 15-45.

51. PG. de Gennes, *"The Physics of Liquid Crystals"*, Clarendon Press, Oxford, 1974.

52. I. Sage, *Liquid Crystals*, 2011, **38**, 1551-1561.

53. T. Harada and P. Crooker, *Liq. Cryst.*, 1975, **30**, 79-86.

54. F.D. Saeva, *Mol. Cryst. Liq. Cryst.*, 1973, **23**, 171-177.

55. M. Leclerq, J. Billard and J. Jacques, *Mol. Cryst. Liq. Cryst.*, 1969, 8, 367-387.

56. I. Dierking, *"Textures of Liquid Crystals"*, Wiley-VCH, Weinheim, 2003.

57. M. Glogarova, L. Lejek, J. Pavel, U. Janovec and F. Fousek, *Mol. Cryst. Liq. Cryst.*, 1983, 91, 309-325.

58. R. Cano. *Bull. Soc. Fr. Miner. Cristallogr.*, 1967, **90**, 333.

59. T. Nakagiri, H. Kodama, and K. K. Kobayashi, *Phys. Rev. Lett.*, 1971, **27**, 564-567.

60. A. Saupe, *Angew. Chem. Int. Ed.*, 1968, **7**, 97-112.

61. E.P. Raynes, *Liq. Cryst.*, 2007, **34**, 697-699.

62. E.P. Raynes in *"The Optics of Theremotropic Liquid Crystals"*, Eds. S. Elston and R. Sambles, Taylor and Fraincis, London, 1998, pp 289-305.

63. E.P. Raynes, *Personal Communication.*

64. P. Kirsch and M. Bremer, *Angew. Chem. Int. Ed.*, 2000, **39**, 4216-4235.

65. I. Sage in *"Thermotropic Liquid Crystals"*, Critical Reports on Applied Chemistry Ed. G.W. Gray, Wiley, Chichester, 1987, pp 64-98.

66. E.P. Raynes in *"The Handbook of Liquid Crystals Volume 1: Fundamentals of Liquid Crystals"*, Eds. J.W. Goodby, P.J. Collings, T. Kato, C. Tschierske, H.F. Gleeson and P. Raynes, Wiley-VCH, Weinheim, 2014, pp 351-364.

67. K.J. Toyne in *"Thermotropic Liquid Crystals"*, Critical Reports on Applied Chemistry Ed. G.W. Gray, Wiley, Chichester, 1987, pp 28-63.

68. See, for example, J.W. Goodby, *Liq. Cryst.*, 2011, **38**, 1363-1387.

69. U. Maschke, M. Benmouna, X. Coqueret, *Macromol. Rapid. Commun.*, 2002, **23**, 159.

70. S. Pieraccini1, A. Ferrarini, and G.P Spada, *Chirality*, 2008, **20**, 749-759.

71. G.W. Gray and D.G. McDonnel, *Mol. Cryst. Liq. Cryst.*, 1977, **34**, 211-217.

72. R. Eelkema and B.L. Feringa, *Org. Biomol. Chem.*, 2006, **4**, 3729-3745.

73. R.A. van Delden and B.L. Feringa, *Angew. Chem., Int. Ed.,* 2001, **40**, 3198-3200.

74. J. Yoshida, H. Sato, A. Yamagishi and N. Hoshino, *J. Am. Chem. Soc.*, 2005, **127**, 8453-8456.

75. N. Hoshino, Y. Matsuoka, K. Okamoto and A. Yamagishi, *J. Am. Chem. Soc.*, 2003, **125**, 1718-1719.

76. H.-G. Kuball, B. Weiss, A. K. Beck and D. Seebach, *Helv. Chim. Acta*, 1997, **80**, 2507-2514.

77. R. Eelkema and B. L. Feringa, *J. Am. Chem. Soc.*, 2005, **127**, 13480-13481.

78. R. Eelkema and B. L. Feringa, *Org. Lett.*, 2006, **8**, 1331-1334.

79. G. Gottarelli, G. P. Spada, R. Bartsch, G. Solladie and R. G. Zimmermann, *J. Org. Chem.,* 1986, **51**, 589-592.

80. G. Gottarelli, M. Hibert, B. Samori, G. Solladie, G. P. Spada and R. Zimmermann, *J. Am. Chem. Soc.*, 1983, 105, 7318-7321.

81. H.-G. Kuball and T. Höfer in *"Chirality in Liquid Crystals"*, Eds. H.S. Kitzrow and C. Bahr, Springer, New York, 2001, pp 67-100.

82. M.P. Neal, M. Solymosi1 M.R. Wilson and D.J. Earl, *J. Chem. Phys.*, 2003, **119**, 2567-2573.

83. M.J. Cook and M.R. Wilson, *J. Chem. Phys.*, 2000, **112**, 1560-1564.

84. D.J. Earl and M.R. Wilson, *J. Chem. Phys.*, 2003, **119**, 10280-10288.

85. M.R. Wilson and D.J. Earl, *J. Mater. Chem.*, 2001, **11**, 2672-2677.

86. A. Ferrarini, P.L. Nordio, P. V. Shibaev and V.P. Shibaev, *Liq. Cryst.*, 1998, **24**, 219-227.

87. G. Proni and G.P. Spada, *J. Org. Chem.*, 2000, **65**, 5522-5527.

88. J. Yoshida, H. Sato, A. Yamagishi and Naomi Hoshino, *J. Am. Chem. Soc.*, 2005, **127**, 8453-8456.

89. A.J. Leadbetter in *"Thermotropic Liquid Crystals"*, Critical Reports on Applied Chemistry Ed. G.W. Gray, Wiley, Chichester, 1987, pp 1-27.

90. S.T. Lagerwall in *"The Handbook of Liquid Crystals Vol. 2B"*, Eds. D.

Demus, J.W. Goodby, G.W. Gray, H.-W. Spiess and V. Vill, Wiley-VCH, Weinhein, 1998, pp 515-692.

91. J.W. Goodby, in the *"Handbook of Liquid Crystals Vol 4: Smectic and Columnar Liquid Crystals",* Eds. J.W. Goodby, P.J. Collings, T. Kato, C. Tschierske, H.F. Gleeson and P. Raynes, Wiley-VCH, Weinheim, 2014, pp 43-68

92. S. Dumrongrattana and C.C. Huang, *Phys. Rev. Lett.,* 1986, **56**, 464-467.

93. S. Dumrongrattana, S. Nounesisand and C.C. Huang, *Phys. Rev. A*, **33**, 2181-2183.

94. G.W. Gray and J.W. Goodby, "*Smectic Liquid Crystals: Textures and Structures*", Leonard Hill, Glasgow, 1985.

95. See, for example, J.W. Goodby, R. Blinc, N.A. Clark, S.T. Lagerwall, M.A. Osipov, S.A. Pikin, T. Sakurai, K. Yoshino, B. Zeks, *Ferroelectric Liquid Crystals: Principles, Properties and Applications,* Ferroelectricity and Related Phenomena Vol 7, Gordon and Breach, Philadelphia,1991, p 99 – 123.

96. R.B. Meyer, L. Li ébert, L. Strzelecki and P. Keller, *J. Phys (Paris)*, 1975, **36**, L69-L71.

97. R.B. Meyer, *Mol. Cryst. Liq. Cryst.,* 1977, **40**, 33-48.

98. H.R. Brand, P.E. Cladis, and P.L. Finn, *Phys. Rev. A*, 1985, **31**, 361-365.

99. N.A. Clark and S.T. Lagerwall, *Appl. Phys. Lett.*, 1980, **36**, 899-901.

100. J.W. Goodby, E. Chin, T.M. Leslie, J.M. Geary and J.S. Patel, *J. Am. Chem. Soc.*, 1986, **108**, 4729-4735.

101. J.W. Goodby and E. Chin, *J. Am. Chem. Soc.*, 1986, **108**, 4736-4742.

102. S.J. Cowling, A.W. Hall and J.W. Goodby, *Chem. Commun.,* 2005, 1546-1548.

103. S.J. Cowling, A.W. Hall and J.W. Goodby, *Adv. Mater.*, 2005, **17**, 1077-1080.

104. E. Davis and J.W. Goodby, in "*The Handbook of Liquid Crystals Volume 1:*

Fundamentals of Liquid Crystals", Eds. J.W. Goodby, P.J. Collings, T. Kato, C. Tschierske, H.F. Gleeson and P. Raynes, Wiley-VCH, Weinheim, 2014, pp 27-58.

105.   S. Garoff and R.B. Meyer, *Phys. Rev. A*, 1979, **19**, 338-347.

106.   D.M. Walba, L. Eshdat, E. Korblova, R. Shao and N.A. Clark, *Angew. Chem. Int. Ed.*, 2007, **46**, 1473 –1475.

107.   D. Demus and L. Richter *"Textures of Liquid Crystals"*, Verlag Chemie, Weinheim, 1978.

108.   P. Oswald and P. Pieranski, *"Nematic and Cholesteric Liquid Crystals: Concepts and Physical Properties Illustrated by Experiments"*, Taylor and Francis, New York, 2006.

109.   T. Ohzono, T. Yamamoto and J.-I. Fukuda, *Nat. Commun.*, 2014, **5**, 3735-3741.

110.   K. Ariga, G.J. Richards, S. Ishihara, H. Izawa and J.P. Hill, *Sensors*, 2010, **10**, 6796-6820.

111.   K. Maeda , Y. Takeyama, K. Sakajiri and Eiji Yashima, *J. Am. Chem. Soc.*, 2004, **126**, 16284-16285.

112.   G. Solladie and G. Gottarelli, *Tetrahedron*, 1987, **43**, 1425-1437.

113.   A.G.M. Lamb, A.J. Eastwood, S.M. Kelly and J.W. Goodby, *Ferroelectrics*, 1998, **212**, 317-324.

114.   J.W. Goodby, *Mol. Cryst. Liq. Cryst.*, 1997, **292**, 245-263.

115.   O. Parry, P. Nolan, L. Farrand and A.L. May, UK Patent GB2329636, 1999.

116.   S.J. Cowling and R.A. Lewis, *Unpublished Results*.

117.   C.C. Dong, P. Styring, J.W. Goodby and L.K.M. Chan, *J. Mater. Chem.*, 1999, **9**, 1669-1677.

118.   M. Hird and K.J Toyne, *J. Mater. Chem.*, 1995, **5**, 2239-2245.

119.   M. Hird, K.J. Toyne, A.J. Slaney and J.W. Goodby, *J. Mater. Chem.*, 1995, **5**, 423-430.

120. J.H. Kim and A.R. Scialli, *Toxicol. Sci.*, 2011, **122**, 1-6.

121. A. Belaissaoui, S.J. Cowling, I.M. Saez and J.W. Goodby, *Soft Matter*, 2010, **6**, 1958-1963.

122. O. Mitsunobu, *Synthesis*, **1981**, 1-28.

123. B. Neises and W. Steglich, *Angew. Chem. Int. Ed.*, 1978, **17**, 522-524.

124. S-W. Ko, S-H. Huang, A. Y-G. Fuh and T-H. Lin, *Opt. Express*, 17, 2009, 15926-15931.

125. G. P. Crawford and S. Zumer, *"Liquid Crystals in Complex Geomertries: Formed by Polymer and Porus Networks"*, CRC Press, 1996, Florida, pp 131-171.

126. A. G. M. Lamb, M. Hird, S. M. Kelly and J. W. Goodby, *Mol. Cryst. Liq. Cryst.*, 1997, **303**, 279-284.

127. G. W. Gray and D. G. McDonnel, *Mol. Cryst. Liq. Cryst.*, 1977, **34**, 211-217.

128. G. Solladi é, R. G. Zimmerman, *Angew. Chem. Int. Ed*. 1984, **23**, 348-362.

129. Gaussian 09, Revision D.01, M. J. Frisch, G. W. Trucks, H. B. Schlegel, G. E. Scuseria, M. A. Robb, J. R. Cheeseman, G. Scalmani, V. Barone, B. Mennucci, G. A. Petersson, H. Nakatsuji, M. Caricato, X. Li, H. P. Hratchian, A. F. Izmaylov, J. Bloino, G. Zheng, J. L. Sonnenberg, M. Hada, M. Ehara, K. Toyota, R. Fukuda, J. Hasegawa, M. Ishida, T. Nakajima, Y. Honda, O. Kitao, H. Nakai, T. Vreven, J. A. Montgomery, Jr., J. E. Peralta, F. Ogliaro, M. Bearpark, J. J. Heyd, E. Brothers, K. N. Kudin, V. N. Staroverov, R. Kobayashi, J. Normand, K. Raghavachari, A. Rendell, J. C. Burant, S. S. Iyengar, J. Tomasi, M. Cossi, N. Rega, J. M. Millam, M. Klene, J. E. Knox, J. B. Cross, V. Bakken, C. Adamo, J. Jaramillo, R. Gomperts, R. E. Stratmann, O. Yazyev, A. J. Austin, R. Cammi, C. Pomelli, J. W. Ochterski, R. L. Martin, K. Morokuma, V. G. Zakrzewski, G. A. Voth, P. Salvador, J. J. Dannenberg, S. Dapprich, A. D. Daniels, Ö. Farkas, J. B. Foresman, J. V. Ortiz, J. Cioslowski, and D. J. Fox, Gaussian, Inc.,

Wallingford CT, 2009.

130. K. Kishikawa, S. Aikyo, S. Akiyama, T. Inoue, M. Takahashi, S. Yagai, H. Aonuma and S. Kohmoto, *Soft Matter*, 2011, **7**, 5176-5187.

131. A. G. M. Lamb, A. J. Estwood, S. M. Kelly and J. W. Goodby, *Ferroelectrics*, 1998, **212**, 317-324.

132. H. Jeong, S. Aya, S. Kang, F. Araoka, K. Ishikawa and H. Takezoe, *Liq. Cryst.*, 2013, 7, 951-958.

133. A. J. Hutt, *CNS Spectr,* 2002, **7**, 14-22.

134. P. Wolkenstein, J. Latarjet, J. C. Roujeanu, C. Duguet, S. Boudeau, L. Vaillant, M. Maigan, M. H. Schuhmacher, B. Milpied, A. Pilorget, H. Bocquet, C. Brun-Bussion and J. Revuz, *Lancet*, 1998, **352**, 1586-1589.

135. R. J. D'amato, M. S. Loughnan, E. Flynn and J. Folkman, *PNAS*, 1994, **91**, 4082-4085.

136. M. E. Franks, G.R. Macpherson and W. D. Figg., *Lancet*, 2004, **363**, 1802-1811.

137. G. W. Mellin and M. Katzenstein, *New Eng. J. Med.*, 1962, **267**, 1184-1193.

138. S. K. Teo, K. E. Resztak, M. A. Scheffer, K. A. Kook, J. B. Zeldis, D. I. Stirling and S. D. Thomas, *Microbes Infect.*, 2002, **4**, 1193-1202.

139. W. Lenz, *Teratology*, 1988, **38**, 203-215.

140. R. C. Frederickson, I. H. Slater, W. E. Dusenberry, C. R. Hewes, G. T. Jones and R. A. Moore, *J. Pharmacol. Exp. Ther.*, 1977, **203**, 240-251.

141. S. Singal, J. Mehta, R. Desikan, D. Ayers, P. Roberson, P. Eddlemon, N. Munshi, E. Anaissie, C. Wilson, M. Dhodapkar, J. Zeldis D. Siegel, J. Crowley and B. Barlogie, "Antitumour Activity of Thalidomide in Refractory Multiple Myeloma", *New Eng. J. Med.*, 1999, **341**, 1565-1571.

142. R. Silverman, *Pediatrics*, 2002, **110**, 404-406.

143. R. Eelkema and B. L. Feringa, *Org. Biomol. Chem.*, 2006, **4**, 3729-3745.

144. G. Gottarelli, G. P. Spada, G. Solladié, *New   J. Chem.* 1986, **10**, 691-700.

145. N. Hoshino, Y. Matsuoka, K. Okamoto and A. Yamagishi, *J. Am. Chem,*

Soc., 2003, **125**, 1718-1719.

146. B. Ringstrand, P. Kaszynaski, A. Januszko and V. G. Young, *J. Matter. Chem*, 2009, **19**, 9204-9212.

147. K. Takatoh, A. Harima, Y. Kaname, K. Shinobara and M. Akimoto, *Liq. Cryst.*, 2012, **39**, 715-720.

148. N. Anzai, S. Machida and K. Horie, *Liq. Cryst.*, 2003, **30**, 359-366.

149. Heppke, G., Lötzsch, D. and Oestreicher, F. Z., *Naturforsch. A: Phys. Sci.* 1986, **41**, 1214-1218.

150. J. A. Rego, J. A. A. Harvey, A. L. Mackinno and E. Gatdula, *Liquid Crytsals*, 2010, **37**, 37-43.

151. Kayni, Z. N, Lewis, R. A and Nassem, S. *J. Mol. Liq.*, 2013, **180**, 74-78.

152. G. Proni, G. P. Spada, P. Lustenberger, R. Welti, F. Diederich, *J. Org. Chem.* 2000, **65**, 5522-5527

153. H. G. Kuball, H. Brüning, T. Müller, O. Türk, A. Schönhofer, *J. Mater. Chem.* 1995, **5**, 2167-2174.

154. H. G. Kuball and H. Brüning, *Chirality*, 1997, **9**, 407-423.

155. R. Bhargavi, G. G. Nair, S. K. Prasad, N. Kumar and A. Sundaresan, *Soft Matter*, 2011, **7**, 10151-10161.

156. D. J. Earl and M. R. Wilson, *J. Chem. Phys.* 2004, **120**, 9679-9683.

157. B. I. Outram and S. J Elston, *Liquid Crystals*, 2012, **39**, 149-156.

158. H-G. Kuball and T. Höffer, *"Chirality in Liquid Crystals"*, Springer-Verlag, 2001, New York, (Page)

159. S. J. Cowling, A. W. Hall and J. W. Goodby, *Chem. Commun*, 2005, 1546-1548.

160. S. J. Cowling, A. W. Hall and J. W. Goodby, *Adv. Mater.*, 2005, 17, 1077-1080.

161. A. D. L. Chandani, T. Hagiwara, Y-I. Suzuki, Y. Ouchi, H. Takezoe and A. Fukuda, *Jpn. J. Appl. Phys.* 1998, **27**, L729-L732.

162. J. Clayden, N. Greeves, S. Warren, P. Wothers, *Organic Chemsitry*, 2008,

Oxford University Press.

163.   J.W. Goodby, *Proc. R. Soc. A*, 2012, **468**, 1521-1542.

164.   G. Valero, J. M Ribó and A. Moyano, *Chem. Eur. J.*, 2014, **20**, 1-7.

165.   K. C. K. Swamy, N. N. B. Kumar, E. Balaraman and K. V. P. P. Kumar, *Chem. Rev*, 2009, **109**, 2551-2651.

166.   Y. Yu, T. Maeda, J. Mamiya, and T. Ikeda, *Angew. Chem. Int. Ed*. 2007, **46**, 881-883.

167.   M. F. Oldfield, L. Chen, N. P. Botting, *Tetrahedron*, 2004 , **60**, 1887-1893.

168.   D. L. de Murillas, R. Piñol, M. Blanca Ros, J. L. Serrano, T. Sierraa and M. Rosario de la Fuente, *J. Mater. Chem*., 2004, **14**, 1117-1127